1993

AN INVESTIGATION OF THE THERMOPHYSICAL PROPERTIES OF HYDROFLUOROALKANES, AND THE CONTRIBUTION OF HALOCARBONS TO THE CHLORINE/BROMINE LOADING OF THE ATMOSPHERE

DAVID CHRISTIAN DOWDELL

PHD

AN INVESTIGATION OF THE THERMOPHYSICAL PROPERTIES OF HYDROFLUOROALKANES, AND THE CONTRIBUTION OF HALOCARBONS TO THE CHLORINE/BROMINE LOADING OF THE ATMOSPHERE

DOWDELL, DAVID CHRISTIAN

Award date:
1993

Awarding institution:
University of Plymouth

AN INVESTIGATION OF THE THERMOPHYSICAL PROPERTIES OF HYDROFLUOROALKANES, AND THE CONTRIBUTION OF HALOCARBONS TO THE CHLORINE/BROMINE LOADING OF THE ATMOSPHERE

by

DAVID CHRISTIAN DOWDELL

A thesis submitted to the University of Plymouth

in partial fulfilment for the degree of

DOCTOR OF PHILOSOPHY

Department of Environmental Sciences

Faculty of Science

In collaboration with

The National Engineering Laboratory

East Kilbride

Glasgow

December 1993

An Investigation of the Thermophysical Properties of Hydrofluoroalkanes, and the Contribution of Halocarbons to the Chlorine/Bromine Loading of the Atmosphere

by

David Christian Dowdell

Abstract

A capillary flow gas viscometer has been used to measure the shear viscosities of the hydrofluoroalkanes HFC 134a, HCFC 123, HCFC 124 and the ternary blend MP 39, at pressures up to 0.1 MPa relative to a nitrogen standard. Having applied small correction factors to the measured flow time data, the resultant viscosities are compared to those obtained by other workers (where possible) using alternative techniques. We calculate self diffusion coefficients and hard sphere collision diameters for the molecules within the rigorous Chapman-Enskog kinetic theory of gases, and calculate optimum well depths of the intermolecular interactions using the Extended Law of Corresponding States. The use of a Stockmayer potential energy function by other workers is discussed and within this, the Mason-Monchick approximation is applied to calculate the percentage effect of the dipole moment on the collision integral.

In order to assess the affect to the atmospheric chlorine loading of the hydrochlorofluorocarbons measured above (HCFC 123, HCFC 124 and HCFC 22 in MP 39) as well as other halocarbons currently in use, two globally averaged mass balance models have been developed on a workstation spreadsheet to assess the future chlorine and bromine levels in the atmosphere and the sensitivity of those loadings to possible forcing factors. These models use production, growth, lifetime and concentration data for fourteen chlorocarbons and three bromocarbons and allow for characteristic emission profiles according to the use to which the halocarbon is applied. Current international agreement, ie. Montreal Protocol 3, is used as a reference level (in most cases), and the models have been used to assess those scenarios which most influence the peak level of chlorine and bromine attained, when that peak occurs and the period of time before 'safe' levels are reached.

List of Contents

List of Tables

Chapter 5

Chapter 6

loading model.

Chapter 7

Chapter 8

List of Figures

Figure 7.14 The sensitivity of the total chlorine loading to an error in HCFC lifetime.

Figure 7.15 The sensitivity of the total chlorine loading to uncertainty in halocarbon lifetime.

Figure 7.16 The sensitivity of the total chlorine loading to calibration error in determination of halocarbon concentrations in the atmosphere.

Figure 7.17 The sensitivity of the total chlorine loading to errors in production data used in the model.

Figure 7.18 The sensitivity of the total chlorine loading to use of growth factors from WMO 1991.

Figure 7.19 The sensitivity of the total chlorine loading to patterns of changing use.

Figure 7.20 The sensitivity of the total chlorine loading to the stepped phase out assumption.

Figure 7.21 The sensitivity of the total chlorine loading to use of delay coefficients.

Figure 7.22 Comparison of total and free chlorine.

Figure 7.23 Comparison of the total chlorine loading under Montreal Protocols 1, 2 and 3.

Figure 7.24 The sensitivity of the total chlorine loading to a tightening and loosening of the Montreal Protocol 3 requirements.

Figure 7.25 The sensitivity of the total chlorine loading to possible production of halocarbons by non-reporting companies.

Figure 7.26 The sensitivity of the total chlorine loading to release of fugitive emissions of halocarbon.

Figure 7.27 The sensitivity of the total chlorine loading to level of chlorine imparted to the atmosphere by HCFCs.

Figure 7.28 The sensitivity of the total chlorine loading to future use of HCFC 124.

Figure 7.29 The sensitivity of the total chlorine loading to future use of HCFC 141b.

bromocarbons.

Figure 8.4 The sensitivity of the bromine loading to uncertainty in bromocarbon lifetime.

Figure 8.5 The sensitivity of the bromine loading to a calibration error in determination of halon concentrations in the atmosphere.

Figure 8.6 The sensitivity of the bromine loading to errors in production data used in the model.

Figure 8.7 The sensitivity of the bromine loading to the use of growth factors from WMO 1991.

Figure 8.8 The sensitivity of the bromine loading to the use of delay coefficients.

Figure 8.9 Comparison of the bromine loading under Montreal Protocol's 1,2 and 3.

Figure 8.10 The sensitivity of the bromine loading to an accelerated phase out schedule for man-made methyl bromide production.

Figure 8.11 The sensitivity of the bromine loading to the proportion of the total production of halons emitted in the year of production.

Figure 8.12 The sensitivity of the bromine loading to the period of emission after the year of production.

Figure 8.13 The sensitivity of the bromine loading to recycling of halons.

Figure 8.14 The sensitivity of the bromine loading to extended use of halons.

Figure 8.15 The sensitivity of the total chlorine loading to the combined effects of bromine- and chlorine-catalysed ozone destruction.

Figure 8.16 The sensitivity of the total chlorine loading to uncertainty in the conversion factor used to convert the bromine-catalysed chemistry into a chlorine equivalent.

Appendix 3

Figure A3a Slip flow correction plot for HFC 134a at 323.15 K.

Figure A3b Slip flow correction plot for HFC 134a at 383.15 K.

Figure A3c Slip flow correction plot for HCFC 123 at 308.15 K.

Figure A3d Slip flow correction plot for HCFC 123 at 323.15 K.

Figure A3e Slip flow correction plot for HCFC 124 at 343.15 K.

Figure A3f Slip flow correction plot for HFC 124 at 383.15 K.

Figure A3g Slip flow correction plot for MP 39 at 323.15 K.

Figure A3h Slip flow correction plot for MP 39 at 343.15 K.

Acknowledgements

I would like to take this opportunity to sincerely thank my supervisor, Dr Peter Matthews, for his unfaltering enthusiasm and advice in awkward moments throughout this project. I would also like to extend this gratitude to my industrial supervisor, Dr Alan Scott of the National Engineering Laboratory, for his help and the loan of the platinum resistance thermometer.

Maurice Perrenoud of Du Pont de Nemours International SA in Switzerland is also thanked for his interest and the supply of the refrigerants used in this work as well as Dr MacFarland and Mr Vogelsberg of E I Du Pont Freons Products Division in the USA, for their advice and help with the model. I am also grateful to the Physical Chemistry Laboratory at Oxford University for the loan of their capillary flow gas viscometer and to John Ryan of UniPress Software for his problem solving concerning eXclaim!. Other names which should be mentioned for their informal and helpful conversation are Dr Sandra Cayless and Mr David Warrilow of the United Kingdom Stratospheric Ozone Review Group, Professor Bill Wakeham, Mr Archie McCulloch, Dr Peter Brimblecombe and Professor F Sherwood Rowland. I am grateful to the Science and Engineering Research Council for sponsoring this work.

My thanks must also go to the many technical staff who have aided and advised me. These include Roger Bowers for his excellent glass blowing, Brian and co-workers at Mechanical Technical Services, Ian at Electrical Technical Services, Nigel in the Library and Ian, Andy and Andrew in the 5th Floor Prep Room.

I would also like to thank my project students for trusting me with the outcome of their degrees, particularly Ian Wells for his excellent contribution to this thesis, Kate/Kathryn Lamble and John Puddicombe. I wish Ian and Kate/Kathryn well with their fledgling Doctorates.

Finally, I must mention a few of the people who have made my time in Plymouth the unforgettable experience it has been. These include Adam for his philosophical discussions, Cathy J, Bob and Cath for the help, AM, Jen and the Ladysmith crew.

Author's Declaration

At no time during the registration for the degree of Doctor of Philosophy has the author been registered for any other University award.

This study was financed with the aid of a studentship from the Science and Engineering Research Council, and carried out in collaboration with the National Engineering Laboratory in East Kilbride, Scotland.

A programme of advanced study was undertaken, which included supervised instruction on use of advanced vacuum line techniques and supervised workstation instruction.

Relevant scientific seminars and conferences were regularly attended at which work was often presented; external institutions were visited for consultation purposes, and several papers prepared for publication.

Publications (or presentation of other forms of creative work):

'Gas Viscosities and Intermolecular Interactions of Replacement Refrigerants HCFC 123 (2,2-dichloro-1,1,1-trifluoroethane), HCFC 124 (2-chloro-1,1,1,2-tetrafluoroethane and HFC 134a (1,1,1,2-tetrafluoroethane)' by D C Dowdell and G P Matthews, *Journal of the Chemical Society, Faraday Transactions* **89 (19)**, 1993, 3545-3552.

'Use of a Computer Model to Investigate the Sensitivity of the Atmospheric Chlorine Loading' by D C Dowdell and G P Matthews, *Proceedings of the 1st International Conference on Air Pollution*, Computational Mechanics Publications (Southampton and Boston) co-published with Elsevier (London and New York), ISBN 1-85166-836-5, 355-362, 1993.

'Experimental Measurement of Gas Viscosities of HFC 134a, HCFC 123 and HCFC 124, and Intermolecular Potential Parameters for HCFC 123' by D C Dowdell and G P Matthews, *Proceedings of the PROTECT Workshop on Thermophysical Properties of Environmentally Acceptable Refrigerants*, in press, 1993.

'An Investigation into the Sensitivity of the Atmospheric Chlorine and Bromine Loading using a Spreadsheet based Computer Model' by D C Dowdell, G P Matthews and I Wells, submitted to *Atmospheric Environment*, 1993.

'Measurement and Estimation of the Low Pressure Gas Viscosity of Replacement Refrigerant MP-39 (52% chlorodifluoromethane, HCFC 22; 15% 1,1-difluoromethane, HFC 152a; 33% 2-chloro-1,1,1,2-tetrafluoroethane, HCFC 124' by D C Dowdell, G P Matthews and I Wells, submitted to *Journal of the Chemical Society, Faraday Transactions*, 1993.

Presentations and Conferences Attended:

'Ozone Depletion: An Investigation into the Sensitivity of the Total Chlorine Loading in the Atmosphere' by D C Dowdell and G P Matthews; Air Pollution 1993; Monterrey, Mexico; February 1993, (oral presentation).

'Measurement of the Viscosities of HFC 134a, HCFC 123 and HCFC 124 in the Gaseous Phase at Pressures up to 0.1 MPa' by D C Dowdell and G P Matthews; PROTECT Workshop on Thermophysical Properties of Environmentally Acceptable Refrigerants; Lisbon, Portugal; November 1992, (poster presentation).

'Antarctica and Environmental Change'; Royal Society discussion meeting; London, UK; May 1992, (attended).

'World Summit Preview'; United Nations Conference on Environment and Development; Plymouth, UK; March 1992 (helped chair a workshop on global climatic change with G P Matthews).

'Modelling the Changes in Atmospheric Chlorine Loading due to Halocarbon Emissions' by D C Dowdell and G P Matthews; Informatik für den Umweltschutz (Computer Science for Environmental Protection); Munich, Germany; December 1991, (poster presentation).

'Spectroscopy in Environmental Science - Atmospheric Chemistry - The Stratospheric Ozone Layer and the Greenhouse Effect'; RSC Autumn Meeting; York, UK; September 1991, (attended).

'CFCs and Ozone: Progress on Alternatives'; RSC Industrial Division Symposium; London, UK; May 1990, (attended).

External Contacts:

Dr Alan Scott, Energy and Environment Centre, National Engineering Laboratory, East Kilbride, Glasgow, G75 0QU.

Maurice Perrenoud, Du Pont International SA, 2 Chemin de Pavillion, PO Box 50, CH1218, Switzerland.

Dr M MacFarland/Mr F A Vogelsberg, E I Du Pont Freons Products Division, 10 and Market Street, Wilmington, Delaware 19898, USA.

Dr Sandra Cayless, Room B246, Romney House, 43 Marsham Street, London. SW1P 3PY.

John Ryan, UniPress Software, 59/60 Derby Square, Douglas, Isle of Man.

Archie McCulloch, ICI Chemicals & Polymers Ltd, Environment Department, Runcorn, Cheshire WA7 4QD.

Bob Miller (Technical Director), Refrigerant Reclaim Ltd, Unit 1, Sandalheath Industrial Estate, Fordingbridge, Hampshire.

Northampton Refrigeration Company Ltd, Victory House, Somers Road North, Portsmouth, Hampshire.

Signed..... D. C. Dandell .....

Date..... 2nd December, 1993 .....

Chapter 1

Ozone Depletion

1.1 Introduction

The ozone layer is found in the stratosphere (strato = layered), a section of the atmosphere which is so called because it exhibits a temperature inversion. Although vertical motion is slow due to the inherent stability of the stratosphere, horizontal motion is rapid owing to the presence of strong winds which circulate around an anticyclone in the summer pole and a cyclonic vortex in the winter pole.

The temperature inversion in the stratosphere is due to the natural formation and destruction reactions of ozone, some of which are exothermic.[1-3]

$$O_2 + h\nu \rightarrow O + O \qquad (1.1)$$

$$O + O_2 + M \rightarrow O_3 + M \qquad (1.2)$$
$$\Delta H = -100 \text{ kJ mol}^{-1}$$

Here M is a third species (usually nitrogen) which is required to carry away excess energy.

Alternatively the atomic oxygen formed by Equation 1.1 may combine in the presence of M to reform molecular oxygen.

$$O + O + M \rightarrow O_2 + M \qquad (1.3)$$
$$\Delta H = -493 \text{ kJ mol}^{-1}$$

Ozone is then destroyed by either Equation 1.4 or 1.5.

$$O_3 + h\nu \rightarrow O + O_2 \qquad (1.4)$$

$$O + O_3 \rightarrow 2O_2 \qquad (1.5)$$
$$\Delta H = -390 \text{ kJ mol}^{-1}$$

As a result of these reactions, the ozone concentration is in a state of constant dynamic equilibrium.

The altitude at which the ozone layer is found represents a compromise between the availability of oxygen molecules and ultraviolet light, both of which are essential to

its production. At higher altitudes there is more ultraviolet light but less molecular oxygen as the air is thin whereas at lower altitudes there is more oxygen but less ultraviolet light (mainly due to its absorption by ozone at higher altitudes).

Thus, just as the concentration of ozone within the ozone layer is a balance of the reactions in Equations 1.1 to 1.5, so its very position in the atmosphere is a balance between the two essential requirements for its production.

Other processes also influence the rate of ozone removal through catalytic reactions. The primary catalysts in these reactions are hydroxyl radicals (OH), nitric oxide (NO), chlorine atoms (Cl) and bromine atoms (Br). The basic reactions which occur are;

$$X + O_3 \rightarrow XO + O_2 \qquad (1.6)$$

$$XO + O \rightarrow X + O_2 \qquad (1.7)$$

Here X represents OH, NO, Cl and Br and XO represents their oxides, ie. HO_2, NO_2, ClO and BrO.[4] Many of these reactions are also exothermic, contributing to the stratospheric temperature inversion.

Ozone is mainly formed at the Equator due to the greater incidence of ultraviolet light and then distributed poleward in the stratospheric circulation.

1.2 The Ozone Hole

Traditional measurements of ozone have been made using Dobson spectrophotometers, which measure the ratio of UVB to UVA light penetrating the atmosphere. The ozone layer absorbs the shorter wavelength (less than 293 nm), more harmful UVB light whilst allowing more UVA light (more than 293 nm) to pass through. Therefore, an increase in the ratio UVB/UVA indicates a decrease in the ozone concentration.[5]

By 1984, a British Antarctic Survey team based at Halley Bay, Antarctica, thought they had been witnessing a decline in the springtime ozone concentration since 1977. The

average springtime concentration of ozone appeared to have dropped from 300 Dobson Units (DU) in the early 1970's, to about 180 DU by 1984.[6] A Dobson Unit is equivalent to 1 part per billion by volume (ppbv) of ozone[7] or an amount of ozone in a vertical column of the atmosphere equivalent to a 0.01 mm thick layer of ozone at standard temperature and pressure. Since these findings, the ozone hole has deepened, reaching 121 DU, 124 DU and 125 DU in 1987, 1989 and 1990 respectively.

In 1991, normal springtime ozone loss was observed over Antarctica between 12 and 20 km, but with an additional ozone loss of about 50% in the upper and lower stratosphere. Part of this additional ozone depletion was believed to be due to an aerosol produced by the eruption of Mount Hudson in Chile in August of that year.[8] As a result, an October low of 108 DU was recorded.[9]

By 1992, the aerosol from another eruption in June 1991 (Mount Pinatubo in the Philippines), was fully distributed in the stratosphere and contributed to a record low of 105 DU in the South Pole.[10]

The ozone 'hole' is in fact a thinning of various layers, the greatest depletion occurring at lower altitudes where removal of up to 80-98% has been found. The area of depletion is vast, being larger than the size of the USA and as deep as Mount Everest is tall.

1.2.1 The Mechanism of Ozone Depletion over the Antarctic

During the southern hemisphere winter a stable cyclonic vortex forms over the Antarctic and effectively seals off the air within from the air outside. It is only with the return of springtime incident radiation and an associated rise in temperature, that the winds weaken and the vortex breaks down.

Within the vortex, temperatures can become very cold (less than 193 K) and allow the formation of 'polar stratospheric clouds' (PSCs) upon which heterogeneous processes

have important consequences for Antarctic ozone.[3,4,11-14] The clouds consist of two particle sizes. Type I PSCs consist of particle sizes of about 1 μm in diameter and condense at around 190-193 K. They are composed of nitric acid trihydrate (NAT).[15] Larger particles of about 10 μm diameter (termed type II PSCs) condense at temperatures 4-5 K lower than the type I PSCs. They are composed mainly of water ice with large amounts of nitric acid dissolved in them. Most importantly, they are large enough to gravitationally settle out of the stratosphere, thereby denitrifying and dehydrating the Antarctic stratosphere within the vortex.

Most chlorine in the atmosphere is bound up in reservoir compounds such as hydrogen chloride (HCl) and chlorine nitrate ($ClONO_2$),[16] but in the presence of PSCs, these reservoir compounds react together to release chlorine:

$$ClONO_2 + HCl \rightarrow Cl_2 + HNO_3 \qquad (1.8)$$

The molecular chlorine released by this mechanism remains within the polar vortex during the dark polar winter, whereas the nitric acid is removed in the PSCs.

With the onset of Spring, the incident light splits the chlorine molecule into chlorine atoms, making it available for ozone depletion. Another important reaction involving chlorine monoxide and bromine monoxide, aids the rejuvenation of chlorine and bromine atoms for attack on ozone; thus elevated levels of each (which are present in the Antarctic vortex), further enhance ozone depletion:[4]

$$ClO + BrO \rightarrow Cl + Br + O_2 \qquad (1.9)$$

As the vortex finally breaks down in November, the ozone depleted air mixes into the rest of the stratosphere, contributing to the ongoing global depletion of ozone.

1.2.2 The Causes of Ozone Depletion

Natural sources of atmospheric chlorine and bromine include an ocean source of methyl chloride and methyl bromide respectively. Volcanic activity can also contribute

a significant source of chlorine in the form of hydrogen chloride through direct injection of aerosols from explosive eruptions.[17,18] These sources are intermittent but can be significant.

However the major sources of ozone depleting chlorine and bromine in the stratosphere are the man-made halocarbons, of which the major contributors are the chlorofluorocarbons (CFCs). CFCs were primarily designed as refrigerants in the late 1920's, for which they had ideal properties; low boiling points, specific heats and heats of vaporization, non-toxic, non-flammable and very stable. However, it is because of their stability that they pose such a threat to the ozone layer, as they are not removed by any natural tropospheric removal mechanism such as attack by hydroxyl radicals (OH) or removal to the oceanic sink before reaching the stratosphere. It is only in the stratosphere that they are removed through photochemical decomposition and thereby release active chlorine.

1.3 The Dangers of Ozone Depletion

A decline in the ozone layer allows more harmful short wave ultraviolet radiation to penetrate the Earth's atmosphere and reach its surface. This is particularly acute in the Antarctic where such large levels of depletion are evident. Already there is evidence to show that the production of Antarctic plankton has decreased by a minimum of 6-12% due to UVB inhibition of photosynthesis. The situation is made worse by the timing of the springtime depletion occurring at the same time as the spring bloom of Antarctic plankton, which form the basis for the whole Antarctic food chain.[19] This problem also highlights another area of concern in terms of species vulnerability. Different organisms have different abilities to protect themselves against UVB radiation. There are two types of phytoplankton found around the seas of Antarctica, these being *Phaeocystis* and diatoms. *Phaeocystis* is dominant, but its growth is slowed due to exposure to UVB. However the

diatoms are less affected which could therefore bring about a change in the role of the different types of plankton, upsetting the balance of the community. There may be further effects on organisms higher up in the food chain, depending on how selective they are on the species they graze on.

The effects on mankind include an increase in skin cancer, particularly the fatal melanoma type which is the one most likely to increase due to UVB exposure.[20,21] It has been predicted that a 1% decline in the ozone layer can lead to an extra 70 000 cases of skin cancer worldwide. So far, we have seen an overall decrease in ozone of around 5-6%.[22] Other effects include an increase in the incidence of eye cataracts and other eye problems as well as suppression of the body's immune system,[21] leading to greater susceptibility to disease and longer recovery times. These problems will also occur in both domestic and wild animals to varying degrees, depending on a species ability to cope with more UVB.

Another problem is the effect on plant life.[23] In particular, agricultural productivity is likely to suffer as food crops, trees and grasses are all vulnerable. Of 200 species tested, around two-thirds showed an adverse reaction to increased UVB such as reduced growth, reduced photosynthetic activity and flowering.

Another major worry is the effect of ozone depletion on the climate. The global depletion in ozone may reduce the flux of exothermic chemical reactions such as Equations 1.3 and 1.5, thus causing the stratosphere to cool, allowing PSCs to form more readily and further increasing ozone depletion rates. This is a positive feedback mechanism which could have potentially disastrous consequences for the stratospheric circulation.

1.4 The Answer to the Problem

A large body of research has been undertaken on the issue of ozone depletion and

related issues, covering many disciplines. Replacements for the ozone depleting CFCs have been found in the form of hydrofluoroalkanes (HFAs), which can be subdivided into hydrofluorocarbons (HFCs) and hydrochlorofluorocarbons (HCFCs). These molecules contain hydrogen, making them vulnerable to attack by hydroxyl radicals in the troposphere, so that less reach the stratosphere. HCFCs contain chlorine and therefore are ozone depleting to a limited extent whereas HFCs are totally ozone benign as they contain no chlorine. As these new compounds are produced, they have to undergo a number of stages in development before achieving commercial acceptance (Figure 1.1).[24] One of these stages involves gathering data on their transport properties which is part of the work undertaken by the author (Chapters 2 to 5).

As well as the drive to find suitable HFAs and other ozone benign technologies, it is imperative that we find some kind of international agreement on the removal of the most ozone depleting halocarbons. In March 1985, representatives from a number of countries signed the Vienna Convention for the Protection of the Ozone Layer. This set a precedent, as the countries involved agreed that action must be taken against CFC use, before there was any conclusive scientific proof that CFCs were the cause of ozone depletion in the Antarctic.

In September 1987, at a meeting of parties contracting to the Montreal Protocol on Substances that Deplete the Ozone Layer, a schedule was drawn up detailing limited use of CFCs and halons (Montreal Protocol 1 in Table 1.1). However after this agreement was made, scientific evidence showed that it was largely useless in reducing atmospheric chlorine levels. There was therefore a call for tighter controls which were finally agreed for Montreal Protocol 2 held in London in April 1990. Under the terms of this agreement, CFCs and halons were to be removed by 2000. In addition, it was agreed that carbon tetrachloride and methyl chloroform should be phased out by 2000 and 2005 respectively (Table 1.1). There was also an acknowledgement that HCFC use should be limited and

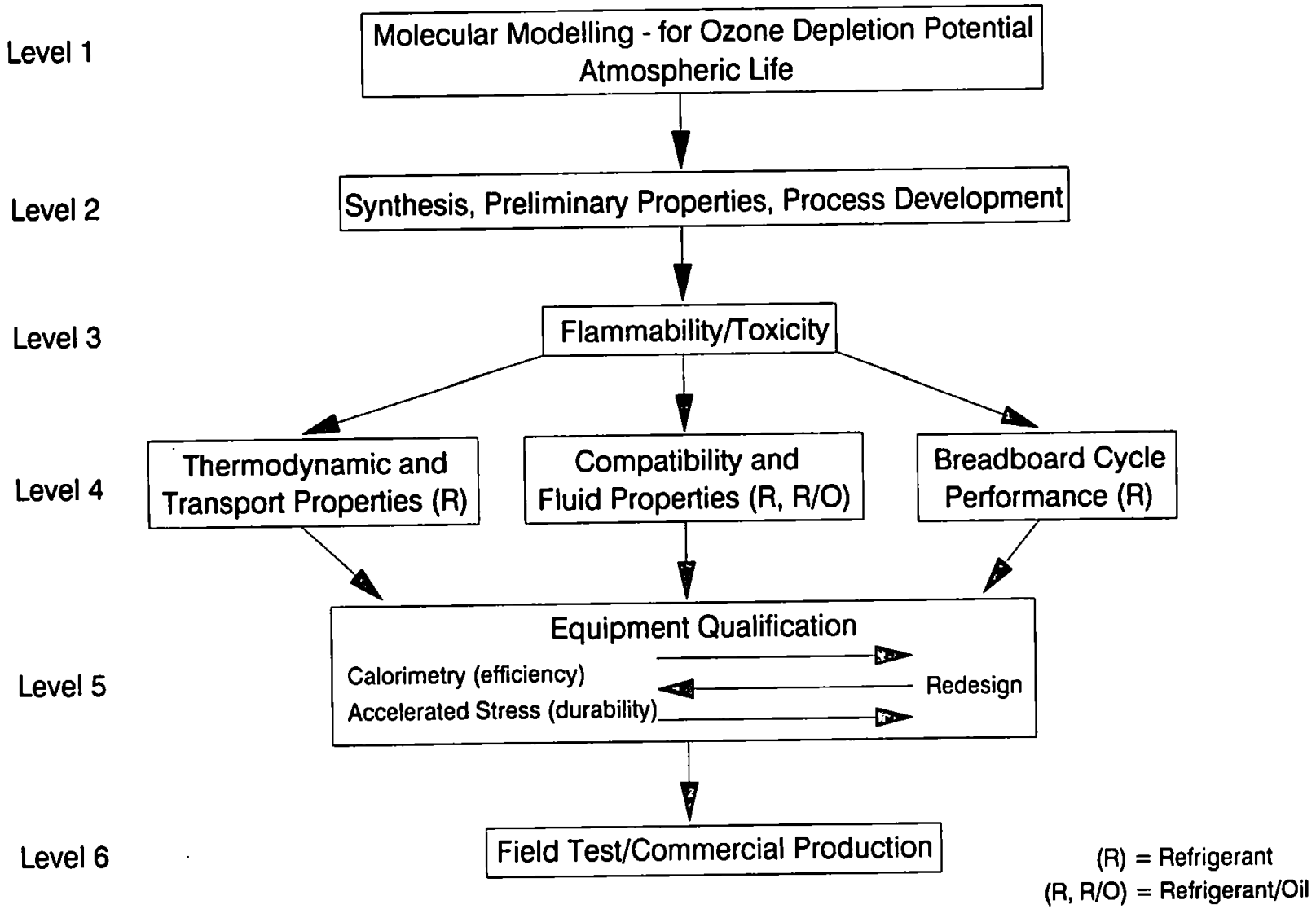

Figure 1.1 The refrigerant development process.[24]

Table 1.1 The requirements for consumption under the terms of Montreal Protocol.

Montreal Protocol	Halocarbon	Consumption relative to 1986* (* unless otherwise stated)
1	CFCs 11, 12, 113, 114, 115	1989 = 100% 1993 = 80% 1998 = 50%
	Halons 1211, 1301, 2402	1992 = 100%
2	CFCs 11, 12, 113, 114, 115	1995 = 50% 1997 = 15% 2000 = 0%
	Halons 1211, 1301, 2402	1995 = 50% 2000 = 0%
	Carbon Tetrachloride	1995 = 15% 2000 = 0%
	Methyl Chloroform	2000 = 70% 2005 = 0%
	HCFCs	Must be used wisely, with a planned phase out between 2020-2040.
3	CFCs 11, 12, 113, 114, 115	1994 = 25% 1996 = 0%
	Halons 1211, 1301, 2402	1994 = 0%
	Carbon Tetrachloride	1995 = 15% 1996 = 0%
	Methyl Chloroform	1994 = 50% 1996 = 0% (relative to 1989)
	HCFCs	Freeze by 1996, at no more than 3.1% of the sum of 1989 CFCs and HCFCs. Then with a 1996 baseline; 2004 = 65% 2010 = 35% 2015 = 10% 2020 = 0.5% 2030 = 0%
	Methyl Bromide	Freeze by 1995 at 1991 level. Phase down to be decided before 1995.

eventually removed. Importantly, it was decided to set up a fund to be administered by the World Bank, the UN Environment Programme and the UN Development Programme to help transfer of the replacement refrigerant technology to developing countries. Developing countries were also allowed to delay the conditions of Montreal Protocol 2 by ten years, provided that their per capita consumption of chlorofluorocarbons is less than 0.3 kg.

Finally in November 1992, Montreal Protocol 3 was held in Copenhagen. It called for a complete phase out of halons by 1994 and CFCs, carbon tetrachloride and methyl chloroform by 1996, as well as a removal of the HCFCs by 2030. Methyl bromide was also added to the Protocol although no definite dates have been made for its removal (Table 1.1). In the light of such decisions, it is useful and important to assess the effect this will have on the atmospheric chlorine and bromine loading.

There are many factors which have the potential to affect the chlorine and bromine loading of the atmosphere, such as the effectiveness of recycling halocarbons and use by developing countries and it is important to assess the implications for the atmosphere of these effects. One way of doing this is to use a computer model to predict future chlorine and bromine loadings and determine their relative sensitivity to actual or possible forcing factors. This is an area of work which has been covered by the author using a model which fulfils a need expressed in WMO 1991[25] (Chapters 6 to 8).

Chapter 2

The Study and Determination of Intermolecular Forces

2.1 Introduction to Intermolecular Forces

An early attempt to explain deviations in gaseous behaviour from the perfect gas equation was made by J D van der Waals:

$$\left(P + \frac{a}{\bar{V}^2}\right)(\bar{V}-b) = RT \qquad (2.1)$$

Here P is pressure, $\bar{V}$ is the molar volume, R is the universal gas constant and T is the temperature. The retardation of molecular motion due to attractive forces between molecules is described as a reduced pressure a and the repulsive forces are accounted for by the volume occupied by the molecules themselves, b. The equation is important because it makes a connection between macroscopic properties and forces between molecules.[1,2]

Of the four types of forces between molecules (gravitational, electromagnetic, strong and weak nuclear), gravitational forces are some 10^{30} times weaker than electromagnetic forces, and nuclear forces exert an influence over too short a range to affect intermolecular interactions. Therefore it is the electromagnetic forces which produce the short range repulsive forces and long range attractive forces which van der Waals described in Equation 2.1.

At short ranges these electromagnetic forces are repulsive as the shells of electrons of neighbouring molecules are restricted from occupying the overlap region. Therefore, the positively charged nuclei are less shielded from each other and a repulsive force results.

At longer distances four types of attractive force exist:

1) due to species carrying a net opposite electrical charge;

2) due to electrostatic energy between polar molecules which exhibit permanent dipoles/quadropoles. The charge about these molecules is unevenly distributed and consequently interactions can occur between the positively charged nucleus of one molecule and the negatively charged electrons of the other molecule. The charge distribution amongst such molecules can be described by a multipole moment. Interactions of molecules depend on this multipole moment, as well as the separation and orientation of the molecules;

3) due to an induced charge on a non-polar molecule because of the presence of a neighbouring polar molecule, which induces a temporary dipole;

4) due to the formation of instantaneous dipoles within non-polar molecules because of random fluctuations in the charge distribution. This is termed dispersion energy and is a net force of attraction.

2.2 A Representation of the Pair Potential Energy Function

In a simple system where spherically symmetric molecules are at low pressure (the dilute gas phase region) and binary collisions are assumed to be dominant, the intermolecular forces are a function of separation r. The average energy between molecules is defined as $U(r)$ and is called the intermolecular pair potential energy function.[3]

At an infinite separation of two molecules a and b the energy E of the system is the sum of their individual energies;

$$E_{tot(\infty)} = E_a + E_b \tag{2.2}$$

At a closer separation r, an additional energy due to the interaction of the molecules (Section 2.1) contributes to the system, ie;

$$E_{tot(r)} = E_a + E_b + U(r) \tag{2.3}$$

By combination of Equations 2.2 and 2.3;

$$U(r) = E_{tot(r)} - E_{tot(\infty)} \tag{2.4}$$

Thus the pair potential energy function represents the deviation in energy of the system when the molecules are at infinite separation. This deviation can be considered as the work done in bringing the molecules from infinite separation (∞) to a finite separation (r).

$$U(r) = \int_{r}^{\infty} F(r)dr \tag{2.5}$$

Here $F(r)$ is the force acting upon molecules a and b and can be equated to;

$$F(r) = -\frac{dU}{dr} \tag{2.6}$$

The general forms of Equations 2.5 and 2.6 are shown in Figure 2.1[3] which illustrates two important parameters. ε is the well depth or minimum energy where the attraction between molecules is greatest and σ is the collision diameter where the energy of interaction is zero.

It is the convention in discussion of potential energy functions to use 'reduced' quantities (marked by an asterisk) which are dimensionless and dependent on ε and σ. For example the reduced temperature T^* is defined as $T^* = kT/\varepsilon$.

2.2.1 Potentials for Spherical, Non-Polar Systems

Many functional forms of varying complexity and accuracy have been suggested which attempt to describe the shape of the potential function in Figure 2.1.

The simplest of these is the hard sphere potential which assumes that molecules are hard spheres of diameter d.

$$U(r) = \infty, \quad r \leq d \tag{2.7}$$

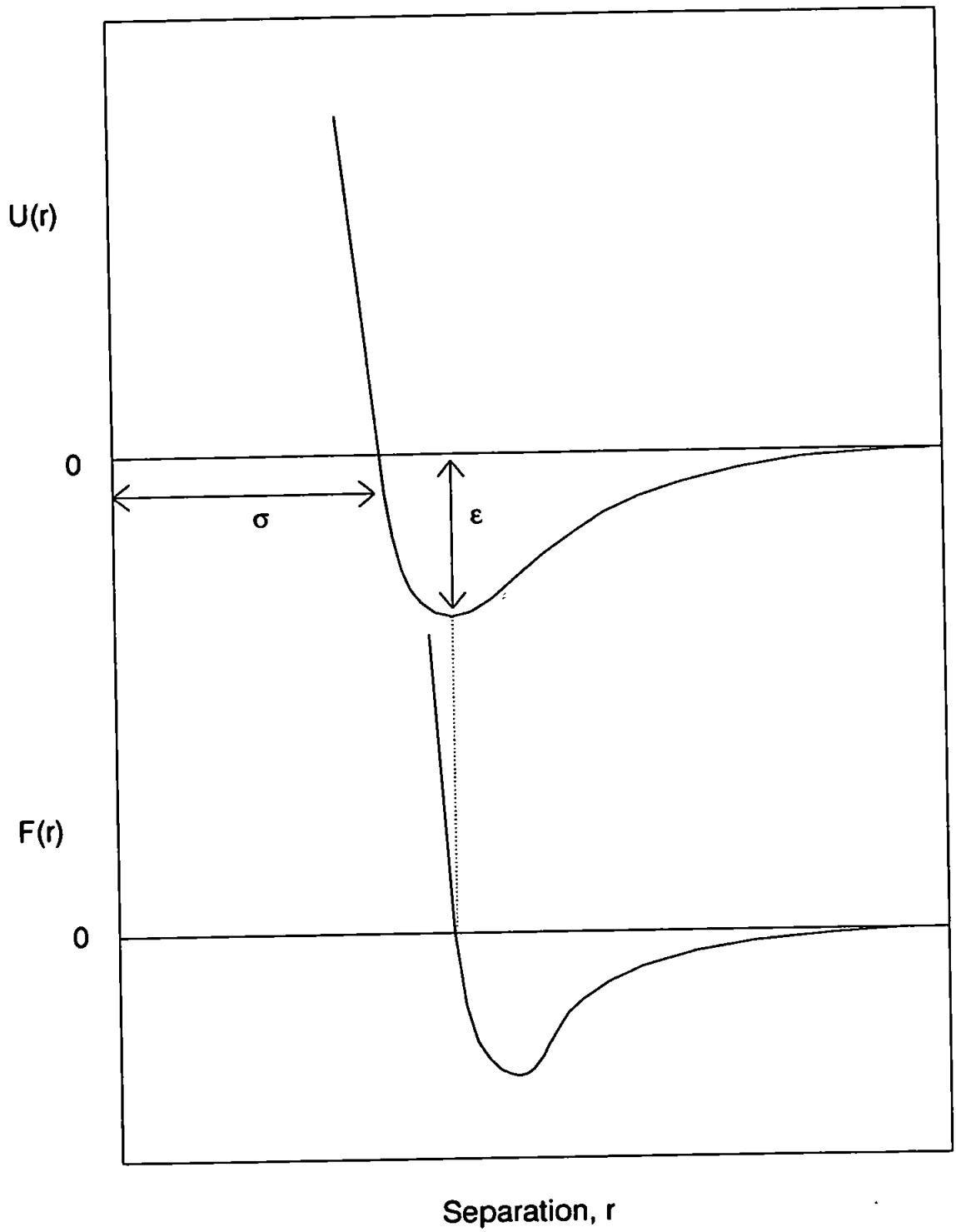

Figure 2.1 The general form of an intermolecular pair potential energy function.

$$U(r) = 0, \quad r>d \tag{2.8}$$

Another simple model is the square well intermolecular potential model which describes a well region consisting of right angles and straight sides (Figure 2.2).[3] Although crude, it has been used by workers in the study of the refrigerants HFC 134a,[4] HCFC 123[5] and HCFC 123a.[5] Its application to the non-spherical, polar refrigerants is discussed in Section 5.4.2.

The Lennard-Jones (LJ) model potential is the best known, of which the most widely used version is the LJ (12-6) potential function;

$$U(r) = 4\,\varepsilon\left[\left(\frac{\sigma}{r}\right)^{12} - \left(\frac{\sigma}{r}\right)^{6}\right] \tag{2.9}$$

This function features a long range attractive region (due to dispersion energy) and a short range repulsive region (although the form this takes has no theoretical justification). The advantage of this function is that it has just two adjustable parameters, namely the well depth and collision diameter. However, in practice, the (12-6) potential function does not give a reliable representation of any molecules. Its widespread use stems from its mathematical simplicity.[6]

Several functions have been proposed since the Lennard-Jones model was proposed. These include the Buckingham potential[7] and the n(r*-6) potential of Maitland and Smith.[8] Further developments have produced more complex potential functions (though with no guarantee of being nearer 'reality') such as the Hartree-Fock dispersion function (HFD), the Barker-Pompe potential (which contains eleven parameters)[3] and the Barker-Bobetic-Maitland-Smith (BBMS) potential (which modifies the Barker-Pompe potential to bring it more into line with spectroscopic data). The BBMS potential in particular has proved to be an important potential for argon-argon interactions.[3]

Rather than developing new potential functions, other workers have 'fine-tuned' functions that already exist, such as work done by Aziz and Chen[3] for argon using a

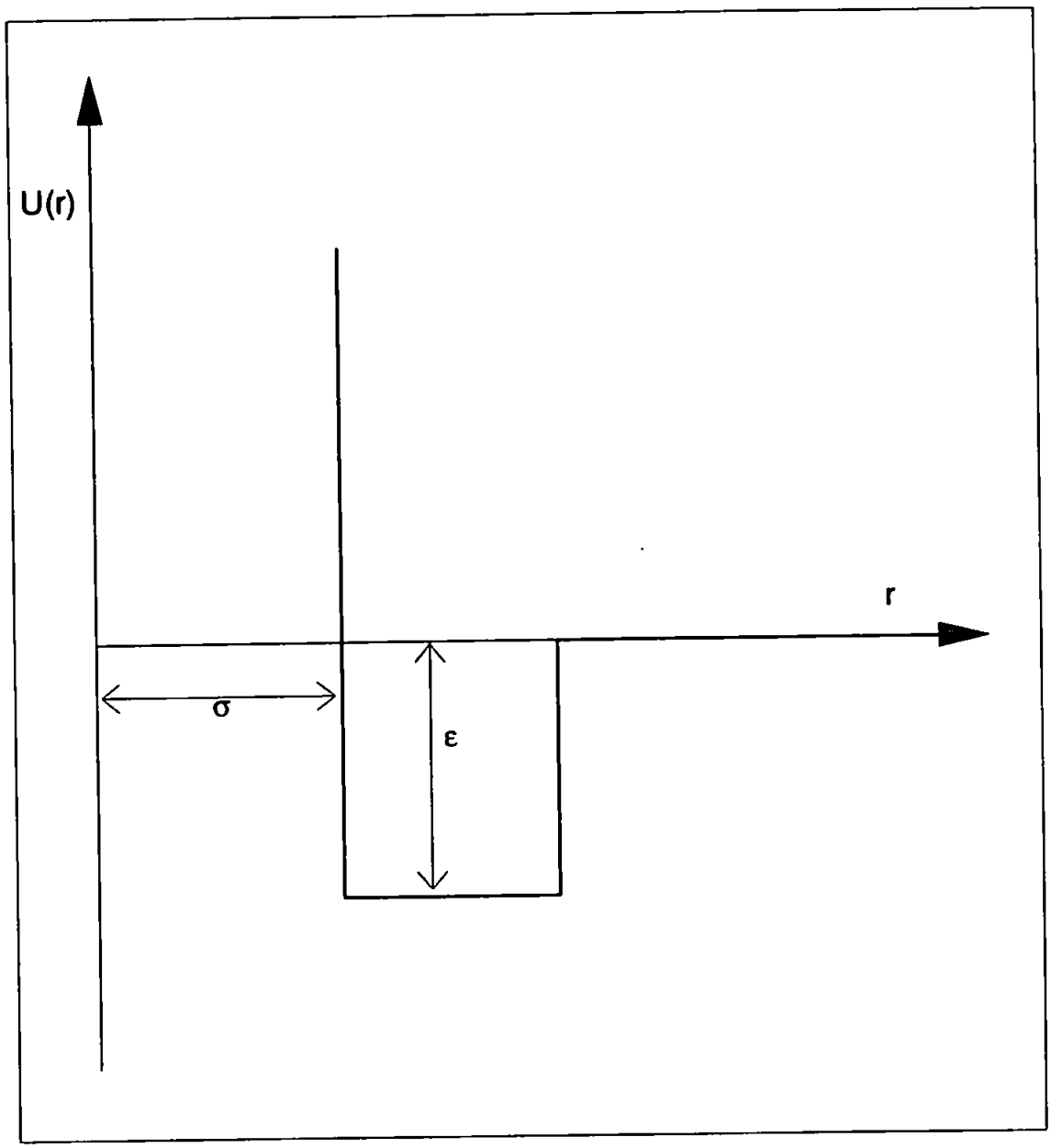

Figure 2.2 The general form of a square well intermolecular potential.

modified HFD function.

2.2.2 Potentials for Non-Spherical, Polar Molecules

When considering non-spherical molecules, the relative orientation between molecules becomes of additional importance to the separation of the molecules. To account for this, Stockmayer[9] incorporated a long-range electrostatic contribution into a LJ (12-6) potential function;

$$U(r) = 4\varepsilon\left\{\left(\frac{\sigma}{r}\right)^{12} - \left(\frac{\sigma}{r}\right)^{6}\right\} - \frac{\mu^2}{4\pi\varepsilon_0 r^3}\zeta(\theta_1,\theta_2,\phi) \qquad (2.10)$$

This equation describes the interaction of two polyatomic linear molecules of dipole moment μ with an orientation function described by $\zeta(\theta_1, \theta_2, \phi)$. This type of function has been favoured by Schramm and his co-workers[10] in their calculation of second virial coefficients for CFC 114, HFC 134a, HFC 142b and HFC 152a for comparison with their own measurements of second virial coefficients.

Other more complex equations describing the interaction of non-spherical, polar molecules have been developed but their description is beyond the scope of this work.

2.2.3 Inversion Methods

Inversion is the name adopted for obtaining potential energy functions from transport data such as viscosity measurements. For instance, the viscosity coefficient η can be related to the collision integral $\Omega^{*(2,2)}(T)$ by;

$$\eta = \frac{5}{16}\left[\frac{MkT}{\pi N}\right]^{1/2}\frac{\delta\eta}{\Omega^{*(2,2)}(T)} \qquad (2.11)$$

By knowing that $\bar{r} = [\Omega^{*(2,2)}(T)]^{1/2}$ where $\bar{r}$ is the hard sphere collision diameter,

substitution into Equation 2.11 and rearrangement allows $\bar{r}$ to be estimated from measurements of viscosity by;[11]

$$\bar{r} = 0.5166 \left[\frac{(MT)^{1/2}}{\eta} \right]^{1/2} \delta_\eta \qquad (2.12)$$

This type of analysis has been used in this work and is discussed in more detail in Section 5.3.

The characteristic separation of two adjacent molecules is dependent on the temperature. At higher temperatures the molecules will smash into each other with greater penetration, meaning $\bar{r}$ will be smaller. At lower temperatures, $\bar{r}$ will be longer because the molecules gently collide and are then repelled away.

If an initial estimate of the potential function $U_0(r)$ is known together with corresponding values of $\bar{r}$, then they can be approximated to $G_0(T^*)$. Using Equation 2.13, a new potential function $U_1(r_1)$ can be obtained and by further iterations, a 'true' potential function can be converged upon.[12] Such a method is inappropriate for the refrigerants used in this work, because they represent complicated systems in which the energy functions depend further upon internal energy states and the relative orientation of the molecules.

$$U(r) = G(T^*)kT \qquad (2.13)$$

2.2.4 The Principle of Corresponding States

Useful additional information can be obtained from viscosity measurements and other experimental data without any knowledge of the intermolecular potential, using the Principle of Corresponding States.[13] Potentials for many systems can be characterised by;

$$U(r) = \varepsilon_c \, F\left(\frac{r}{\sigma_c}\right) \qquad (2.14)$$

Here F is a universal shape function and ε_c and σ_c are scaling parameters which are

dependant on a specific interaction. The principle is based on the approximation that the potential functions for different systems are conformal (ie, they have the same shape *F*) with different scaling parameters. This idea has been extended by Kestin and co-workers[14,15] to some polar molecules such as HCFC 22 ($CHClF_2$) and provides a powerful tool for predicting and correlating the properties of gases.

2.3 The Investigation of Intermolecular Forces

Four areas of study have been of the most value in obtaining information about molecular forces. These are gas imperfections, molecular beams, atomic spectra and transport properties. Detailed discussion of these techniques (except the study of transport properties) is not warranted as it is outside the scope of this work. However brief descriptions are given. Investigation of solid properties is another method but is less revealing than the other four techniques and is not dealt with further.

2.3.1 Gas Imperfection

The ideal gas equation can be extended to account for non-ideal gas behaviour by means of the van der Waals equation described earlier (Equation 2.1). Alternatively, deviations from ideality can be expressed in the form of a virial expansion;[1-3]

$$\frac{P\bar{V}}{RT} = 1 + \frac{B(T)}{\bar{V}} + \frac{C(T)}{\bar{V}^2} + \ldots \qquad (2.15)$$

Here *B(T)* and *C(T)* are second and third virial coefficients respectively, where the second virial coefficient represents the effect of interactions between pairs of molecules and the third virial coefficient represents the interaction of three molecules, and so on.

The traditional method for measuring virial coefficients is the Burnett expansion method where a test gas is used to fill a sample vessel to a high pressure, and then allowed to flow to a previously evacuated expansion vessel until the pressures equalise.

Second virial coefficients are calculated from measurements of the pressure of the gas at successive stages of this type.[16-18] Another method uses two vessels of equal volume, one filled with a reference gas and the other with a test gas. After beginning at the same temperature and pressure, the temperature of the vessels is raised, and the pressure difference between the vessels is noted. The difference in the second virial coefficients is obtained from the pressure difference, and therefore, knowing the second virial coefficient of the reference gas, the second virial coefficient of the test gas is obtained.[10]

Second virial coefficient data can be 'inverted' to give the intermolecular separation and the width of the potential energy function, as has been shown by Clancy et al. for krypton.[11]

2.3.2 Molecular Beams

Monoenergetic supersonic beams of molecules can be used to study the effect of bimolecular collisions and the resulting scattering which they cause. The two methods used in the study of molecular beam scattering can be related to the potential energy function, and are briefly described below.[1-3]

1) Integral scattering cross sections are a measure of the total scattering of molecules in all directions from an incident molecular beam after collision with target molecules. Integral scattering produces oscillations in the beams due to both attractive and repulsive regions of the potential energy function. Thus, the spacing between the oscillations is sensitive to the shape of the potential energy well. Scattering is favoured by lower energies as at higher energies, the colliding particles are less influenced by the intermolecular potential energy function and therefore scattering decreases.

2) Differential scattering cross sections are a measure of the fraction of molecules of an incident energy beam which are scattered through measured deflection angles. Differential scattering cross-sections provide more detailed information about the intermolecular

potential energy function in the low energy repulsive region and the well.

2.3.3 Atomic Spectra

Atoms or molecules which do not combine as chemically bound molecules can be made to form physically bound, two molecule systems called van der Waals dimers under appropriate conditions.

In a low energy three molecule system, one molecule may remove energy from the other two, leaving them trapped as a dimer in the potential well. By observation of absorption bands, the entire potential energy function in the well region can be attained whilst the dissociation energy of the dimer yields the potential energy well depth.[1-3]

2.3.4 Transport Properties

The measurement of viscosity, thermal conductivity and diffusion coefficients has proved to be an important source of information on intermolecular forces. Each represents the transport of momentum, energy and mass along gradients of velocity, heat and concentration respectively. In a low density gas, the transport of these properties is related to the intermolecular forces between colliding molecules and the potential energy function. As viscosity is the property measured in this work, it will be discussed in more detail.

2.4 Viscosity and the Kinetic Theory of Gases

When there is a flux J in a direction x due to the existence of a gradient X, then the transport process can be described by Equation 2.16, where K represents a transport coefficient (viscosity η, thermal conductivity λ or diffusivity D).

$$J=-K\frac{dX}{dx} \tag{2.16}$$

It is the movement of molecules which provides the medium for the transport process, and therefore the rate of that transport or flux must be governed by the number of collisions occurring. Likewise, the outcome of these collisions will depend on the pair potential energy function. The kinetic theory of gases attempts to provide the connection between macroscopic properties such as viscosity, and the microscopic intermolecular interactions.

Simple kinetic theory provides an understanding of the principles involved, whereas rigorous kinetic theory attempts to go a stage further, and account precisely for the non-ideality of gases.

2.4.1 Simple Kinetic Theory and its Application to Viscosity

This theory considers a low density gas to consist of identical hard spheres which are in continuous random motion and exert no influence on each other except on impact.

In order to evaluate the properties of a gas using this theory, three quantities are required.

The first is the mean molecular speed ($\bar{C}$) which, from a consideration of equipartition factor, is given by;

$$\bar{C} = \left(\frac{8kT}{\pi m}\right)^{1/2} \tag{2.17}$$

where m is the molecular mass and k is the Boltzmann constant.

Secondly the flux of molecules moving in a given Cartesian direction is required. Six directions in space are taken (±x, ±y, ±z) and it is assumed that 1/6 of the molecules will be moving in any one of these directions at any particular time, ie. the flux is equal to $n\bar{C}/6$, where n is the number of molecules per unit volume.

Lastly, the distance a molecule travels between collisions is required (termed the mean free path length l). In unit time a molecule with speed C and diameter d, passes through a cylinder of volume $\pi d^2\bar{C}$. If the number density of molecules is n, then the

number of collisions with molecules in unit time is $\pi d^2 \bar{C} n$. It follows that the mean free path length is the speed of the molecule divided by the number of collisions in unit time;

$$l = \frac{\bar{C}}{\pi d^2 \bar{C} n} = \frac{1}{\pi d^2 n} \tag{2.18}$$

Inspection of Figure 2.3 shows a reference layer B with a velocity u moving in the x direction. This layer is bounded by an upper layer A and a lower layer C each separated from layer B by the mean free path length l, which thus have velocities $u+(du/dz).l$ and $u-(du/dz).l$ respectively, where du/dz is the velocity gradient across the reference layer. Molecules in one layer collide with those in another, and transfer momentum. The slower moving (lower) layer thus exerts a drag on the upper layer. In order to overcome this drag and maintain the velocity gradient, a force must be applied to the upper layers. Newton's law of viscosity defines the coefficient of shear viscosity η as a function of the viscous force F on an area A with a velocity gradient du/dz acting across it;

$$F = -\eta A \frac{du}{dz} \tag{2.19}$$

Molecules reaching layer B from layers A and C will have travelled an average distance l since their last collisions and will transfer x directional momentum in unit time, according to the respective expressions below.

$$\frac{1}{6} n \bar{C} m \left\{ u + \left(\frac{du}{dz} \right) l \right\} \tag{2.20}$$

$$\frac{1}{6} n \bar{C} m \left\{ u - \left(\frac{du}{dz} \right) l \right\} \tag{2.21}$$

Combining these, the force applied to layer B due to the net transfer of momentum per unit time from layers A and C can be obtained from Equation 2.22, where F is the frictional force acting on the reference layer B in the x direction.

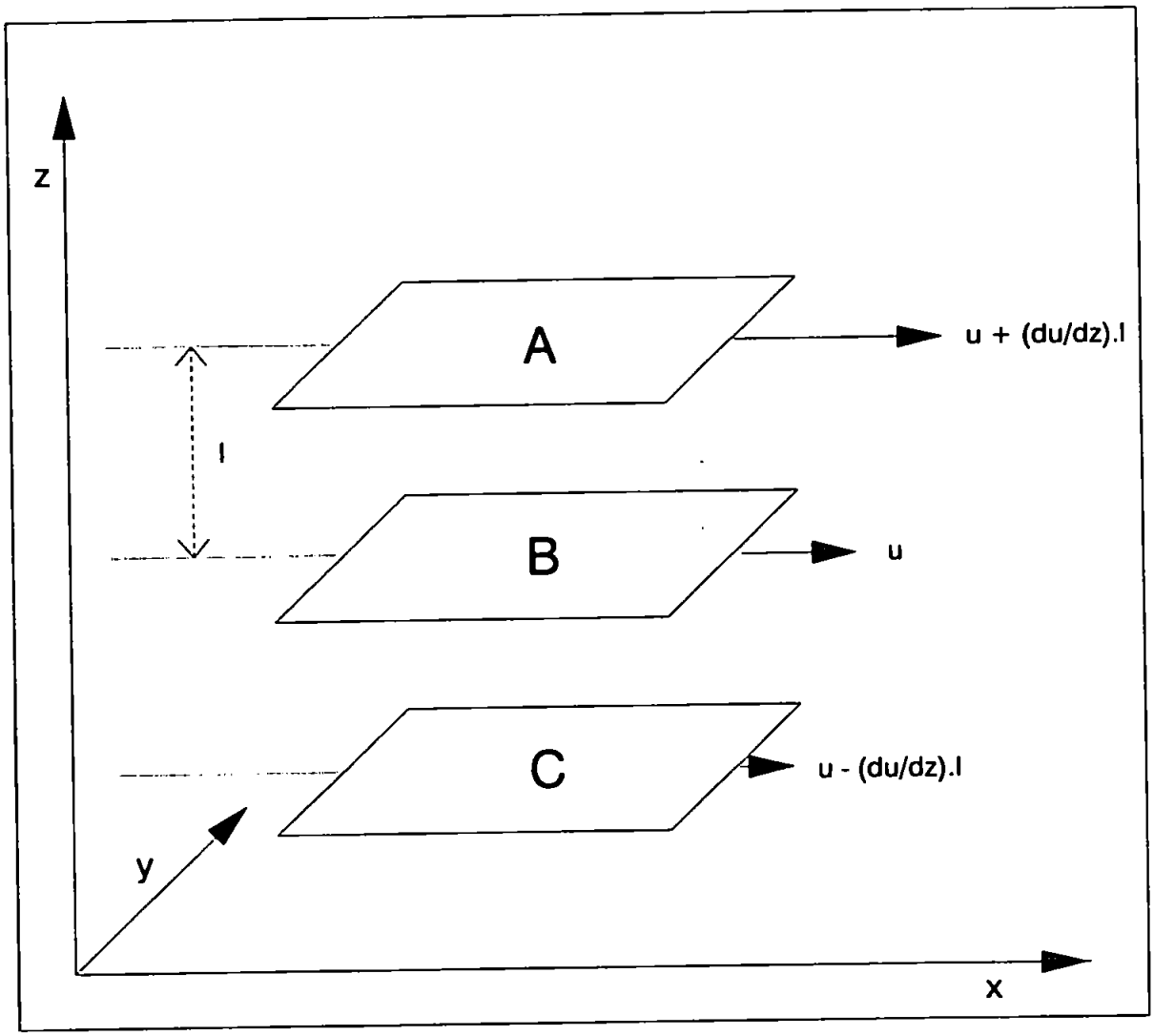

Figure 2.3 A representation of the movement of layers of a gas within a Cartesian co-ordinate framework.

$$F = -\frac{1}{3} n m \bar{C} \left(\frac{du}{dz}\right) l \qquad (2.22)$$

Knowing that η is the frictional force per unit area for a unit velocity gradient (Equation 2.19), Equation 2.22 can be rewritten;

$$\eta = \frac{1}{3} n m \bar{C} l = \frac{1}{3} \rho \bar{C} l \qquad (2.23)$$

Finally, substitution of the terms in Equations 2.17 and 2.18, gives;

$$\eta = \frac{1}{3} \frac{m\bar{C}}{\pi d^2} = \frac{1}{3} \frac{m}{\pi d^2} \left(\frac{8kT}{\pi m}\right)^{1/2} \qquad (2.24)$$

This equation predicts that the viscosity of a dilute gas consisting of hard spheres, is independent of density. To a good approximation, this has been found to be true by measurement of gases at moderate densities. The reason for this is that in a denser gas more molecules move between layers, producing a greater number of collisions, but the mean free path length is less so that for each collision, the amount of momentum transferred by each molecule is less.

It also predicts that viscosity varies by $T^{1/2}$, although for real gases the viscosity varies more rapidly with temperature than this.

2.4.2 Rigorous Kinetic Theory

The rigorous kinetic theory still assumes that a gas comprises of hard sphere molecules but incorporates a number of developments of the simple kinetic theory.

1) It is inaccurate to regard all molecules except the reference layer as stationary. The average 'relative' molecular speed is better expressed as $\sqrt{2}\bar{C}$, so the mean free path length becomes:

$$l = \frac{1}{\sqrt{2}\pi d^2 n} \tag{2.25}$$

2) The assumption of a flux of molecules in each orthogonal Cartesian direction of $n\bar{C}/6$, as used in the simple kinetic theory, is too simplistic as all directions are possible. Therefore an angular average of the velocities of all the molecules is required. For example, in the z direction, the mean velocity $\bar{C}_z$ is;

$$\bar{C}_z = \overline{C\cos\theta} = \overline{\bar{C}\cos\theta} = \frac{\bar{C}}{2} \tag{2.26}$$

The number of molecules crossing an xy plane per unit time with velocity $\bar{C}_z$ will be half the total number of molecules in the column $\bar{C}_z$ (as half will be travelling in the opposite direction). Hence the collision rate per unit area is;

$$\textit{Collision rate per unit area} = n\bar{C}_z/2 = n\bar{C}/4 \tag{2.27}$$

3) It is inaccurate to assume that a molecule moving to a reference layer, from either above or below, will acquire the characteristics of that layer after only one collision.

Inclusion of these modifications into the equation for viscosity gives;

$$\eta = \frac{5}{16}(\pi mkT)^{1/2}\frac{1}{\bar{\Omega}(T)} \tag{2.28}$$

Here $\bar{\Omega}(T)$ is a collision integral which acts as a correction for the non-ideality of the temperature dependence of viscosity, and is more commonly expressed as;

$$\bar{\Omega}(T) = \pi d^2 \Omega^*(T) \tag{2.29}$$

Here $\Omega^*(T)$ is the reduced collision integral and reflects how the hard sphere molecular cross section (πd^2) needs modifying to account for temperature effects on intermolecular forces. The mathematical derivation of the collision integrals is beyond the scope of this work.

2.4.3 Application of Kinetic Theory to Polyatomic Molecules

The rigorous kinetic theory of gases has proved successful for spherically symmetric species. However application to both polar and non-polar polyatomic molecules is more difficult because the potential function is angular dependent and collisions involve the exchange of both rotational and internal energy as well as translational energy.

Kestin, Ro and Wakeham[13] have proposed the following empirical expression for the calculation of omega integrals for a range of dilute gases;

$$\Omega^{(2,2)*}(T^*) = \exp[0.45667 - 0.53955(\ln T^*) + 0.187265(\ln T^*)^2 - 0.03629(\ln T^*)^3 + 0.00241(\ln T^*)^4] \qquad (2.30)$$
$$1 < T^* < 90$$

The viscosity can then be obtained from the Chapman Enskog expression;

$$\eta = \frac{5}{16}\left(\frac{mkT}{\pi}\right)^{1/2} \frac{1}{\sigma^2\,\Omega^{(2,2)*}(T^*)} \qquad (2.31)$$

A similar result can also be obtained for diffusion coefficients in polyatomic systems which are used in Chapter 5.

If these equations are used for polyatomic gases, then it has to be assumed that the value of $\Omega^{(2,2)*}$ is not affected by inelastic collisions, and that it is a meaningful average of the angle-averaged angle-dependent omega integrals, ie. that;

$$\Omega^{(2,2)*} = \langle\Omega^{(2,2)*}(\theta)\rangle \qquad (2.32)$$

Mason and Monchick[19,20] have made a more precise approximation, which is that molecules do not rotate with respect to their centre-of-mass co-ordinates during a collision. We do not have any angle-dependent data for our molecules which would allow us to use this approximation. However we do briefly discuss it with respect to the Stockmayer potential function in Section 5.5.1.

2.5 The Measurement of Viscosity

Viscosity measurements can be divided into both absolute and relative methods. Absolute methods require no external viscosity data to calculate results whereas relative methods require external data to calibrate the apparatus and ultimately any data which is obtained is compared to a standard at room temperature.[21] Absolute methods include rotating cylinders,[21] oscillating discs[22,23] and some capillary flow methods.[24] Relative methods include capillary flow[25,26] and oscillating disc techniques[27] and for experiments at higher densities, piezoelectric quartz crystal viscometers are used.[28]

Most measurements of dilute gas viscosities of the refrigerants have been made using oscillating disc viscometers.[29-31] These consist of a quartz disc suspended in a gas-tight chamber between two horizontal plates by a quartz torsion wire. The gaseous medium between the disc and plates contributes to the damping effect on the period and amplitude of oscillation. A mirror attached to the torsion wire turns with the oscillations and reflects an incident light beam. The angular displacement of the reflected beam is used to monitor the period and amplitude of oscillation. Edge corrections are required in order to account for the finite width of the quartz disc.

The viscosity measurements made in this work use the relative capillary flow technique and it is the explanation of this which will now be discussed.

2.5.1 Capillary Flow Viscometry

Capillary flow viscometers measure the laminar flow of a gas from one vessel (the front vessel V_f) via a capillary tube to a second vessel (the back vessel V_b). The rate of flow is proportional to the fourth power of the radius of the capillary tube which limits the accuracy of absolute capillary flow techniques for viscosity determination.

Relative capillary flow methods are well developed[25,26] and generally produce accuracies of better than ±1%. By making measurements over a wide range of

temperatures, data useful for the determination of pair potential energy functions can be obtained, through the application of inversion methods.[25,26]

2.6 The Theory of Capillary Flow

The type of flow experienced by a gas flowing through a capillary tube will depend on the pressure conditions and dimensions of the capillary. Flow may be one of four types.

2.6.1 Laminar or Poiseuillian Flow

This type of flow is the optimum for capillary flow viscometry. It is streamlined such that flow is symmetrically distributed about the central axis of the capillary with a parabolic velocity profile (to zero velocity at the walls). The flow rate is described by Poiseuille's equation and can be assigned a value known as the Knudsen number (K);

$$K = l/d \tag{2.33}$$

Here l is the mean free path and d is the diameter of the capillary. Flow is laminar when K is of the order of 10^{-5}.

2.6.2 Turbulent Flow

As the velocity of the fluid flow increases, flow becomes irregular and full of eddies. This is termed turbulent flow and the point at which it is reached can be determined by calculating a critical parameter called the Reynolds number (Re).[32] The Reynolds number is found using Equations 2.34 or 2.35.

$$Re = 2r\rho v_{av}/\eta \tag{2.34}$$

$$Re = \frac{r^3 M(\bar{P}_f^2 - \bar{P}_b^2)}{8\eta^2 R T_c L} \tag{2.35}$$

Here r is the capillary radius, ρ is the gas density, v_{av} is the average velocity, M is the

relative molecular mass, $\bar{P}_f$ and $\bar{P}_b$ are the mean front and back vessel pressures, R is the universal gas constant and T_c and L are the temperature and length of the capillary respectively. The Reynolds number is usually of the order of 2300-4000 being near 2000 for a straight capillary and increasing to 4000 for curved pipes. Values less than 500 are generally considered on the threshold for laminar flow. Reynolds numbers in this work were all less than 100, meaning flow was not turbulent.

2.6.3 Slip Flow

This type of flow exists when the velocity of the gas at the wall of the capillary is not zero and occurs when the gas pressure in the capillary is such that the mean free path length l is between 1-10% of the capillary diameter d. The Knudsen number is of the order of 10^{-2} to 10^{-1}. The fluid velocity at the walls must be corrected for, and the method used is explained in Section 2.8.5.

2.6.4 Free Molecular Flow

This type of flow occurs at very low pressures, when $K \geq 5$. Here the rate of flow is governed by molecule-wall collisions rather than molecule-molecule collisions.

2.7 Poiseuille's Equation For Laminar Flow

It is this equation which forms the basis of the relationship between viscosity and flow rate through a capillary. It has five requirements;

1) Flow must be laminar.

2) Flow must be steady.

3) The velocity at the walls must be zero.

4) The fluid must be incompressible, ie. for gas flow the solution must be modified.

5) The fluid must be Newtonian, ie. it will flow when subjected to the smallest shearing

force; the velocity gradient being directly proportional to the shearing force.

The volume flow rate dV/dt can thus be expressed as;

$$\frac{dV}{dt} = \frac{\Delta P_c \pi r^4}{8\eta L} \tag{2.36}$$

Here ΔP_c is the pressure difference $(P_f - P_b)$ across the capillary tube.

For a compressible fluid, the molar flow rate dn/dt can be expressed by Meyer's equation, which underpins capillary flow viscometry;

$$\frac{dn}{dt} = \frac{\pi r^4 (\bar{P}_f^2 - \bar{P}_b^2)}{16\eta R T_c L} \tag{2.37}$$

The molar flow rate can be related to the pressure drop in the front vessel by;

$$\frac{dP_f}{dt}\left[\frac{V_f}{T_f} + \frac{V_c}{T_c}\right] = \frac{dn}{dt}R \tag{2.38}$$

Here V_f and V_c are the volumes of the front vessel and capillary respectively and T_f and T_c are the temperatures of the front vessel and capillary respectively. Provided that the apparatus is of such a construction that $V_f >> V_c$ and the conditions of operation are such that $T_c > T_f$ or near equal, then V_c/T_c can be neglected and Equation 2.37 substituted into Equation 2.38, to give;

$$\frac{dP_f}{dt} = \frac{\pi r^4}{16\eta L T_c}(\bar{P}_f^2 - \bar{P}_b^2)\frac{T_f}{V_f} \tag{2.39}$$

Hence, for a pressure drop from P_f^0 to P_f^t where t is the time of flow, integration gives;

$$\int_{P_f^0}^{P_f^t} \frac{V_f}{(P_f^2 - P_b^2)} dP_f = \frac{t\pi r^4 T_f}{16\eta L T_c} \tag{2.40}$$

If identical pressure conditions are employed for two gases A and B then the

equation can be used in a comparative sense and the viscosity ratio can be related to the respective flow times of the two gases by;

$$\frac{t_A}{t_B} = \frac{\eta_A}{\eta_B} \tag{2.41}$$

2.8 Corrections to Poiseuille's Equation

Before Equation 2.41 can be used, the flow time measurements must be corrected for the effects of temperature drift, slip flow, kinetic energy, gas imperfection and curved pipe flow.

2.8.1 Temperature Corrections

Temperatures may drift between successive experiments, and a correction is therefore necessary to bring the experimental temperature T_{exp} to the nominal temperature T_{nom}, with a corresponding adjustment to the experimental flow time t_{exp} to bring it to the flow time at the nominal temperature t_{nom}. This correction is performed by applying Equation 2.42.

$$\frac{t_{\exp}}{t_{nom}} = \frac{T_{\exp}^{A}}{T_{nom}^{A}} \tag{2.42}$$

Here A is a coefficient describing how the viscosity changes with temperature and is based on a value for nitrogen, any differences between it and the sample gases being considered small.

2.8.2 Curved Pipe Flow

The capillary tube used for this work was coiled into a helix in order to minimise the effect of temperature differences over the length of the capillary. Within a helix, the fluid at the centre of the capillary is forced to the walls, so that any portion of the fluid

moves in an elongated spiral motion down the capillary. The Dean number (D) is a dimensionless parameter which can be calculated to ascertain the value of this deviation in flow. If the Dean number is 6 or less, then the effects of curved pipe flow are negligible, requiring no correction to the flow time. The Dean number is calculated by Equations 2.43 or 2.44.[32]

$$D = \frac{r^3 M(\bar{P}_f^2 - \bar{P}_b^2)}{8\eta^2 R T_c L}\left(\frac{r}{R_c}\right)^{1/2} \tag{2.43}$$

$$D = Re\left[\frac{r}{R_c}\right]^{1/2} \tag{2.44}$$

Here r is the radius of the capillary, R_c is the radius of the capillary helix and Re is the Reynolds number (Section 2.6.2). All calculated Dean numbers in this work were less than 6, meaning no correction for curved pipe flow was necessary.

2.8.3 Hagenbach (Kinetic Energy) Correction

When a gas enters a capillary, a finite pressure difference is required to accelerate it from a rest state to the parabolic velocity profile assumed in the Poiseuille equation (Equation 2.36). The kinetic energy required to do this is dissipated as heat in the reservoir at the end of the capillary tube. The result is an observed initial resistance to flow, which is corrected by applying Equation 2.45.[33]

$$K_h = 1 - \frac{1.1\ M\ \Delta P_f\ V_f}{8\ \pi\ \eta\ L\ R\ T_f\ t_{exp}} \tag{2.45}$$

Here K_h is the Hagenbach correction and ΔP_f is the change in pressure in the front vessel.

2.8.4 Gas Imperfection

In order to correct for non-ideality of the gas, the virial equation of state is applied

up to the second virial coefficient to give the following correction term.

$$K_b = \left(1 + \frac{2P_f B(T_f)}{R(T_f)}\right)\left(1 - \frac{2B(T_c)}{3R(T_c)}\frac{(P_f^3 - P_b^3)}{(P_f^2 - P_b^2)}\right) \tag{2.46}$$

Here $B(T_f)$ and $B(T_c)$ are the second virial coefficients of the gas at the front vessel and capillary temperatures respectively.

2.8.5 Slip Flow

Poiseuille's equation assumes that the velocity of flow at the walls of the capillary is zero. However, only at infinite pressures when the mean free path of the molecules is zero, is the velocity of the gas at the capillary walls zero.

Looking at Equation 2.41, the flow time ratio t_A/t_B must be found at infinite pressure, so as to remove the effects of slip flow. In order to achieve this, t_A/t_B is plotted against the inverse mean capillary pressure $1/\bar{P}_c$ where $\bar{P}_c$ is $(\bar{P}_f - \bar{P}_b)/2$. By extrapolation to the y axis ($1/\bar{P}_c = 0$) the flow time ratio at infinite pressure is attained and the effects of slip flow are removed.

Chapter 3

Description and Use of the Apparatus

3.1 Introduction

It was originally intended to use a capillary flow gas viscometer built by A Townsend[1] for the measurement of shear viscosities in this work. However the viscometer had previously been used to measure the viscosity of corrosive gases such as hydrogen chloride which, amongst other problems highlighted below, contributed to the decision not to use this viscometer.

1) Many parts of the internal surfaces of the gas lines were showing signs of corrosion, due to the combination of water vapour and hydrogen chloride.

2) Examination of the broken stainless steel capillary using a microscope linked to an image analyzer showed that the internal surfaces of the capillary were roughened and pitted. The capillary in this form would be unusable as laminar flow of the gas could not be guaranteed.

3) The gas lines of the viscometer had many joins which allowed ample scope for leaking of air into the viscometer when evacuating.

4) There was no mechanism for independently thermostatically controlling the temperature of the gas lines. Such a feature was necessary as one of the hydrochlorofluorocarbons (HCFC 123) has a boiling point of 301 K meaning it is a liquid at room temperature. In order to admit it to the viscometer and maintain it in the vapour phase, the temperature in all the gas lines needed to be elevated above 301 K.

A second viscometer was therefore used for this work, which was built by I N Hunter[2] and originally used for the measurement of atom-polyatomic molecule systems such as argon-hydrogen and argon-carbon dioxide.[3] A brief description of this viscometer is offered in the subsequent sections but for more detailed specifications, the reader is

referred to the PhD thesis of I N Hunter.[2]

3.2 Principle of the Apparatus

The capillary flow gas viscometer measures the time for the flow of a gas from a vessel of higher pressure (the 'front' vessel (V_f)) to another vessel of lower pressure (the 'back' vessel (V_b)) via a coiled capillary tube of accurately known and controlled temperature. The flow time of a test gas through the capillary is measured using an automated mercury manometer and compared to a standard gas (nitrogen) through the capillary tube at the same temperature.

3.2.1 The Mercury Manometer

The manometer stands 760 mm high, is of glass construction and contains approximately 300 ml of double distilled mercury. It is connected to the gas lines via Jencons glass-metal seals with flange fittings. Along the manometer arm are fourteen pointers, each sealed through the glass wall of the manometer, and aligned vertically within the manometer arm at arbitrary distances between 60 mm and 700 mm from the base of the manometer. Each points downward and is tapered to a fine tip to prevent the mercury column sticking. At the base of the manometer arm are two tungsten rods which allow a small AC current through the mercury to the pointers. The manometer arm measures the time it takes for the pressure to drop in the front vessel due to flow of the gas from the front vessel to the back vessel via the capillary.

In order to identify the particular pressure regime of an experimental run, the pressure code adopted by Townsend[1] has been used in this work. For FVx/BVy, 'x' represents the pointer on the manometer arm to which the front vessel pressure has initially been set and 'y' represents the pointer for the back vessel pressure which is initially set.

The manometer sits on a brass table with cork cushioning in order to provide support, and is held in a 0.1 m^3 tank containing a light paraffin oil, chosen to prevent bacterial growth, discolouring and corrosion of metal parts. The paraffin tank also contains a 3.0 litre back vessel, a heater and a stirrer blade. A rheostat is used to fine tune any temperature oscillations in the tank and maintain the temperature of the oil at 305.15 K while the stirrer keeps the oil circulating around the tank.

During initial testing, a fungus of the genus *Cladosporium sp.* was observed growing in the oil, which has been known to grow in aviation fuel. The paraffin tank was emptied and its internal walls cleaned with hot water and bleach in an effort to remove fungal spores. Once the tank and its contents were replaced, fresh paraffin oil was used to refill it, together with 200 ml of a biocide (Kathon FP 1.5%) supplied by Rohm & Haas Limited. No repeat growth has since been observed.

3.2.2 The Vacuum Lines (Figure 3.1)

The lines to the pumps are constructed of Edwards KF10 (10 mm internal diameter) pipe and Edwards 10 mm 'speedivalves' in order to aid evacuation, as the pumping rate is roughly proportional to the fourth power of the radii of the lines. Between the capillary and front and back vessels, copper pipe of 5 mm internal diameter and Edwards 5 mm 'speedivalves' are used to reduce dead space volume. The viscometer was originally used at temperatures as low as 118 K which meant it featured a cold trap between taps L and R, which consisted of a U-shaped section of gas line surrounded by a glass dewar flask. When the dewar flask was filled with a coolant such as liquid nitrogen or solid carbon dioxide, it would form the coldest part of the gas line and due to its position before the capillary, would cause mercury vapour to condense harmlessly at this point rather than in the capillary which it would block. Only one set of low temperature measurements (283.15 K) have been undertaken as part of this work for

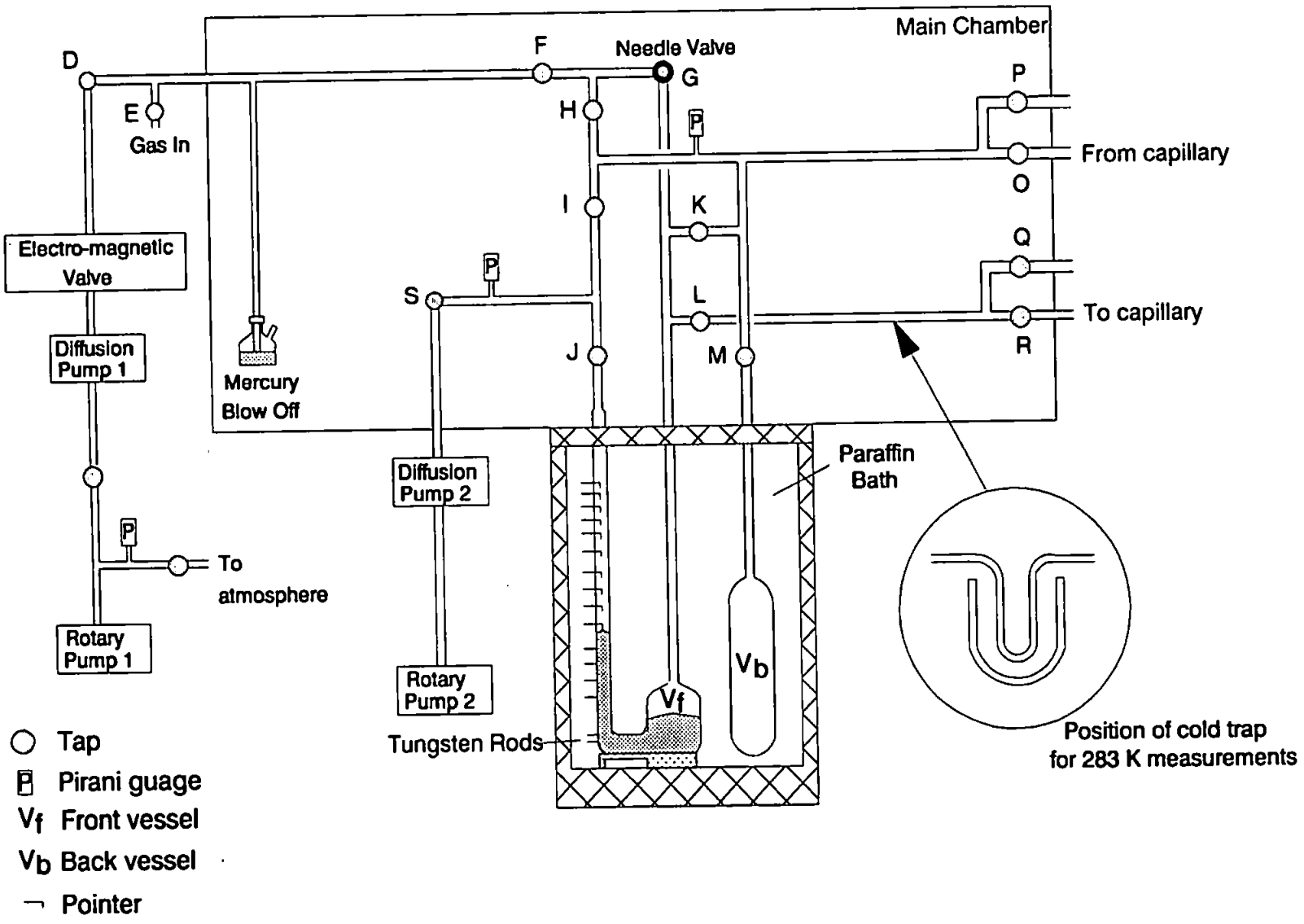

Figure 3.1 Schematic diagram of the gas lines in the capillary flow viscometer used for this work.

which the cold trap was necessary. For these experiments, it was sufficient to fill the glass dewar flask with ice to provide the necessary cooling. All other experiments were undertaken at capillary temperatures higher than the 305.15 K temperature of the front vessel, for which the U-shaped gas line and dewar flask were replaced by a smaller section of tube which was kept at the same temperature as the rest of the gas lines.

All of the lines surrounded by the box in Figure 3.1 are enclosed within a thermostatically controlled chamber, fronted by a metal panel through which the valve taps protrude, and upon which a schematic representation of the configuration of the gas lines behind is marked. A temperature controller built by Electrical Technical Services switches current to a 250 watt infra red lamp, the heat from which is circulated around the chamber by a 150 mm diameter fan. Temperatures have been maintained at approximately 305.15 K for this work.

Two one-stage rotary pumps back two 25 mm air-cooled diffusion pumps and are sufficient to evacuate the vacuum lines to less than 5×10^{-3} mbar. An electromagnetic valve situated between tap D and diffusion pump 1 provides a safety feature in case of power failure, by preventing oil sucking back from the rotary pump into the vacuum lines. Rotary pump 2 incorporates an automatic air bleed in case of power failure. During an experimental run, rotary and diffusion pump 2 are used to maintain a good vacuum in the manometer arm, which is necessary for accurate flow time determination using the experimental method adopted for this work.

The vacuum is measured by two pirani gauges at the positions marked in Figure 3.1, which provide a readout on two Edwards 1101 pirani gauge controllers. There is also an independent pirani gauge reading the roughing vacuum between diffusion pump 1 and rotary pump 1, which is also shown in Figure 3.1.

The lead tubes from the thermostatted main chamber to the oil bath containing the capillary have to be separately thermostatted. This is achieved using a thermostatted

water bath with a pump. Warm water is pumped from the water bath via thin walled rubber tubing supplied by Altec, which coils around the lead tubes from the chamber wall to the top of the oil bath. The water bath is insulated by polystyrene foam. Three thermometers at points around the lead tubes monitor the temperature as 307±2 K. This variation in temperature is not considered a source of error as it is the stability of the temperature at the capillary which is most important.

3.2.3 Gas Input

The samples of HFC 134a, HCFC 124 and MP 39, as well as the nitrogen standard, are admitted to the viscometer from cylinders attached to tap E (Figure 3.1).

Due to the HCFC 123 boiling point of 301 K, a method of introduction to the viscometer was developed enabling the liquid HCFC 123 to be admitted as a gas. The apparatus designed for this purpose is shown in Figure 3.2 and the following procedure was followed.

1) Before introduction of the HCFC 123, the line from the viscometer to tap 1 is evacuated, taps 1 and 4 being closed.

2) Tap 2 is closed to maintain the vacuum in the U-tube.

3) Tap 5 is closed and tap 4 opened, so that the line between tap 5 and tap 2 is brought up to atmospheric pressure.

4) The U-tube is removed from the apparatus and placed in a fume cupboard.

5) The Introduction Vessel is attached via a Quickfit adaptor to the inlet tube. Using a funnel, liquid HCFC 123 is poured in so that it fills the tube from tap 1 to midway up the Introduction Vessel.

6) Tap 1 is opened causing the vacuum to suck the liquid HCFC 123 into the U-tube as far as tap 2. Tap 2 is then opened slightly to allow the liquid level to rise past it after which, it is screwed down into the liquid ensuring that no air is trapped behind the tap.

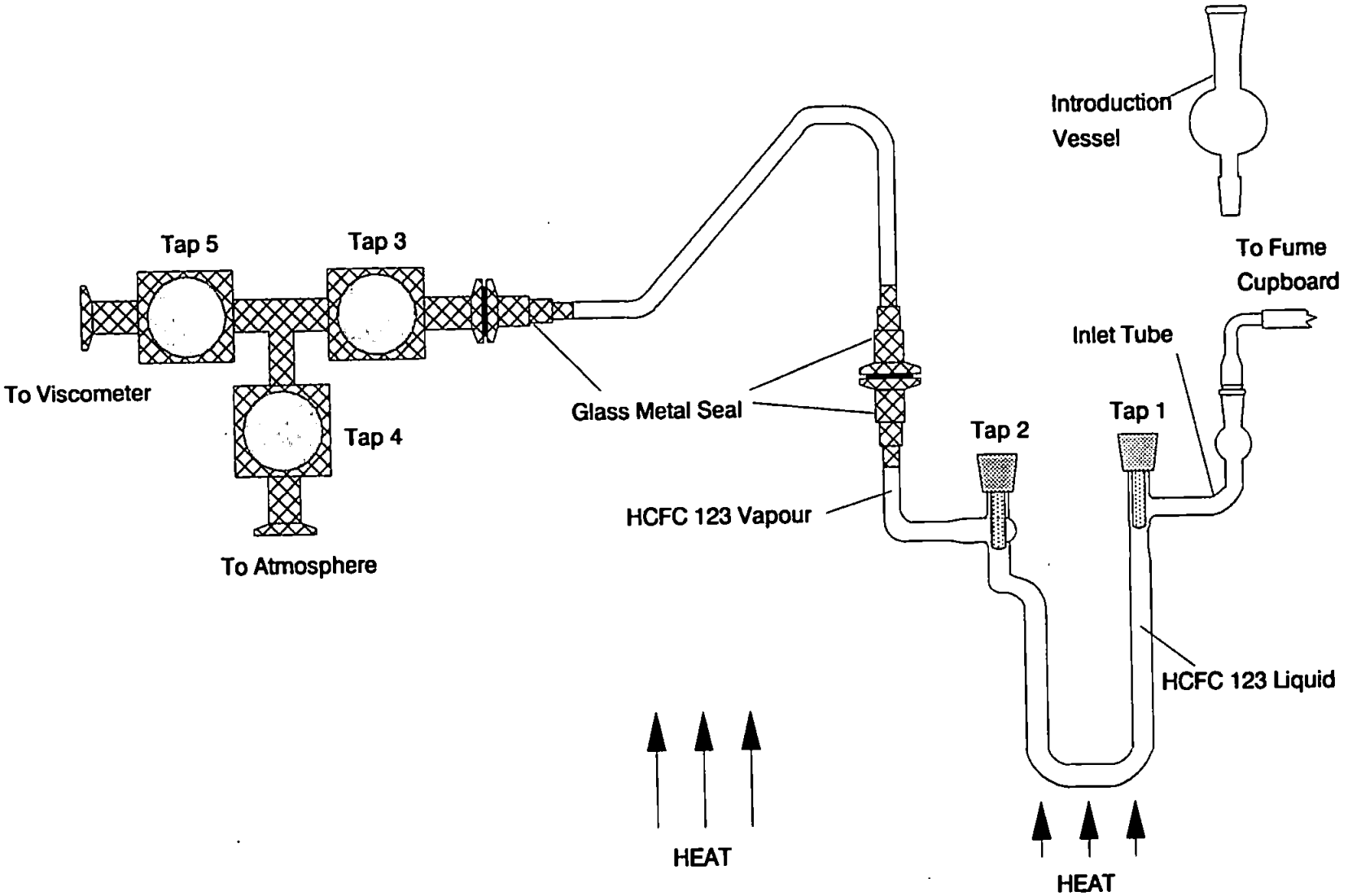

Figure 3.2 Diagram of the introductory device used to admit liquid HCFC 123 to the viscometer in the vapour phase.

7) The Introduction Vessel is removed from the inlet tube. A glass stopper is placed in the Quickfit adaptor of the inlet tube, the U-tube re-attached to the viscometer and the stopper replaced by a link to the fume cupboard.

8) Tap 4 is closed, tap 5 opened and the section between taps 2 and 5 allowed to evacuate for 10 minutes. Any liquid HCFC 123 in the U-tube which vaporises during this time could escape via tap 1 to the fume cupboard.

9) Once the section is evacuated, tap 1 is screwed down into the HCFC 123 liquid, tap 2 is opened and the area warmed to encourage a gentle vaporisation of the HCFC 123 using a fan heater.

10) Once enough gas has been admitted to the viscometer, taps 2 and 5 are closed, tap 4 opened and the U-tube removed so that any remaining HCFC 123 liquid in the U-tube can be poured into a bottle in the fume cupboard.

11) The U-tube is re-attached to the viscometer and evacuated to tap 1, ready for the next experiment.

3.2.4 The Capillary Tube

The pyrex capillary tube is 2 m in length and at each end opens out into tubes of 6 mm internal diameter and 120 mm length which are connected to the lead tubes via glass metal seals and flange fittings. The capillary tube has a precision bore of nominal radius 0.15 mm and is coiled into a helix of average radius 37.5 mm and 5 mm pitch.

3.2.5 The Oil Bath

The oil bath was taken from the Townsend viscometer and is described in more detail elsewhere.[1] It consists of an insulated metallic box of 0.03 m^3 volume which contains the capillary, heating coils, a cooling coil, stirrer, independent temperature sensor and platinum resistance thermometer, all immersed in Dow Corning silicon oil (Figure

3.3).

The heating coils are connected to a Eurotherm 3-parameter temperature controller type 810 and Eurocube thyristor which monitors the heating profile in the oil bath and adjusts the heating rate so that the required set-point temperature is attained. The temperature probe connected to the Eurotherm controller is used for thermostatting the oil bath and not for determining the exact temperature.

The cooling coil is connected to a cold water tap and a steady flow of water constantly maintained. It acts as a heat sink and improves control of the temperature in the oil bath. For the experiments taken at 283.15 K, cooling water and antifreeze (in the ratio 3:1) were pumped from an insulated tank containing a refrigeration coil from a chiller unit (CC 15) supplied by Grant Instruments. The water pumped from this tank fed through insulated rubber pipes to the cooling coils in the oil bath and then returned to the tank. A thermometer read the temperature in the tank as consistently 275.15 K.

Accurate temperature determination is made using the independent temperature sensor which is connected to a digital volt meter and lineariser, and has been calibrated against reliable standards by Townsend.[1]

The readout from the independent temperature sensor is adjusted to the ITS-90 scale[4] using a platinum resistance thermometer calibrated by the National Physical Laboratory and accurate to ±0.05 K.

Any fumes from the silicon oil are vented to a fume cupboard via an exhaust pipe.

3.2.6 Time Measurement

Electrical wires are attached to each of the fourteen pointers and the tungsten rods in the manometer arm, which lead out of the paraffin tank to a bank of four timers. These can be adjusted using a bank of switches of which there are two to every timer and two lights (one green and one red). The green light is on when the timers are on but not

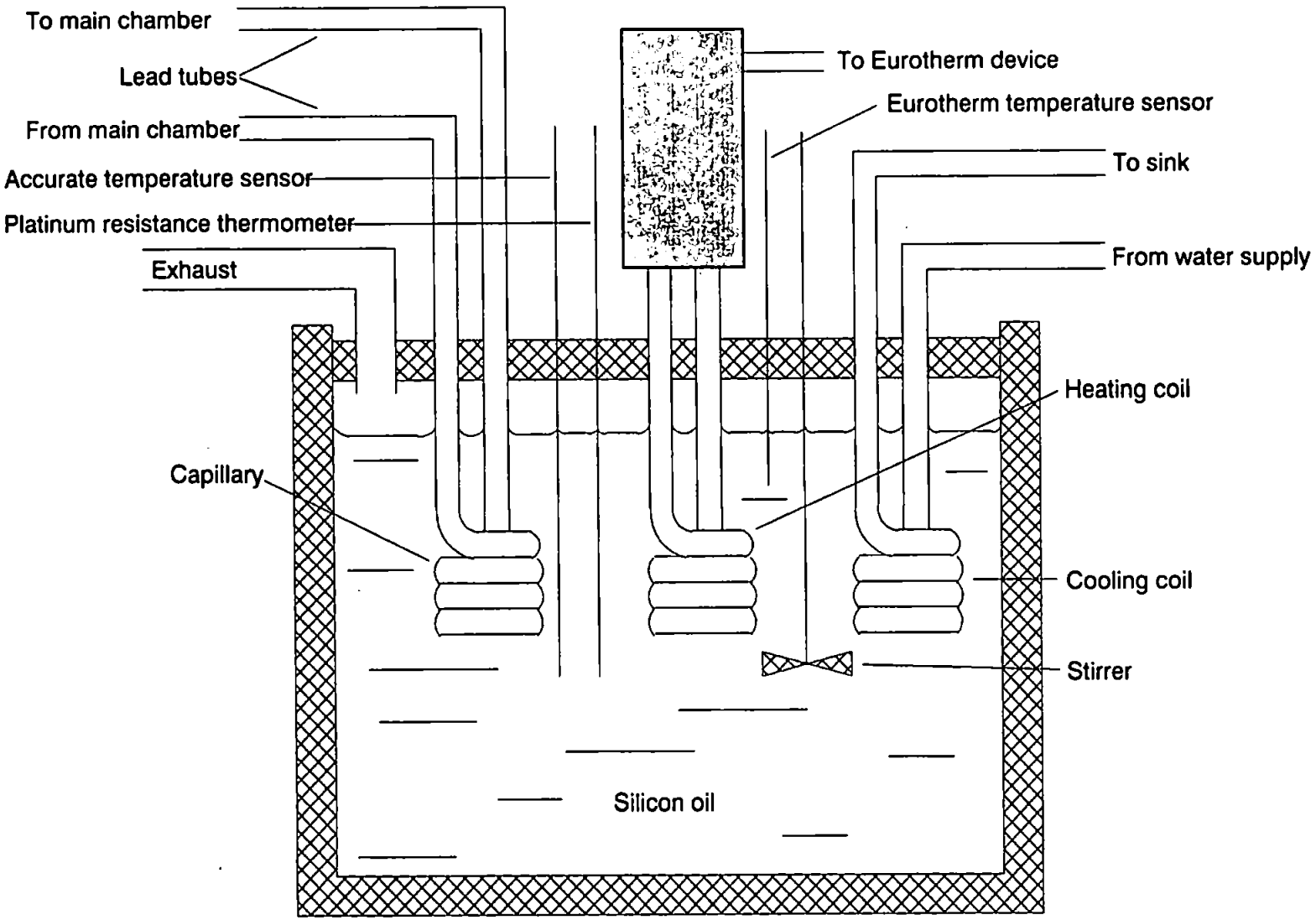

Figure 3.3 Detailed diagram of the oil bath containing the capillary.

timing and the red light shows when a particular timer is timing. Using the switches any combination of up to four pointers can be selected for timing. The timer gives a liquid crystal display in hundredths of a second with a quoted accuracy of ±0.055 s in 1 hour which was verified using the U.K.'s broadcast time standard before experimentation was undertaken.

3.2.7 Pointer Pressure Determination and Volume Testing

In order to undertake accurate capillary flow measurements, the capillary pressure ($\bar{P}_c$) must be known. The Dean number[5] (D) is also required in order to verify that the effects of curved pipe flow (due to the coiled capillary) are negligible. For both of these quantities, the front and back vessel pressures must be known. To do this, nitrogen was admitted to the front vessel while the manometer arm remained under vacuum until the mercury column was above the uppermost pointer (pointer 1). By careful adjustment of the needle valve G, the gas was evacuated until the top of the mercury meniscus was just touching the tip of pointer 1. The heights of the mercury column and mercury reservoir were measured using a cathetometer, accurate to ±0.05 mmHg. The difference between the column height and the reservoir height provides the pressure at that pointer and is shown in Table 3.1. The capillary pressure can be attained by;

$$\bar{P}_c = (\bar{P}_f + \bar{P}_b)/2 \tag{3.1}$$

where $\bar{P}_f$ and $\bar{P}_b$ are the mean front and back vessel pressures respectively, from;

$$\bar{P}_f = (P_{f(x)} + P_{f(x+1)})/2 \tag{3.2}$$

$$\bar{P}_b = (P_{b(x)} + P_{b(x+1)})/2 \tag{3.3}$$

where x represents a pointer from 1 to 13.

However during a run only the front vessel pressures can be monitored by the

Table 3.1 Pressures associated with pointers in the manometer column.

Pointer	Pointer Pressure /mmHg
1	590.09
2	558.01
3	516.06
4	486.21
5	454.78
6	434.28
7	396.28
8	344.86
9	312.22
10	282.64
11	199.53
12	119.80
13	59.52
14	37.96

manometer. Therefore, the back vessel pressures must be calculated, which requires the determination of the volumes of the front and back vessels and the gas lines.

The volume of the front vessel was determined using the method of Hunter.[2] The volume of other parts of the viscometer were determined as follows;

1) A standard volume is attached to tap E and a nitrogen cylinder to tap P (Figure 3.1).

2) All the gas lines and the standard volume are evacuated. Tap P is closed.

3) Taps D and S are closed to isolate the pumps.

4) The height of the mercury in the manometer arm and reservoir are measured using a cathetometer, accurate to ±0.05 mmHg. If they are not level, a correction is applied to successive measurements based on the discrepancy.

5) Tap J is closed to maintain a vacuum in the manometer arm. Nitrogen is introduced from the cylinder through tap P to an arbitrary pressure, causing the mercury in the manometer arm to rise.

6) The height of the mercury column and reservoir are remeasured.

7) The tap to the standard volume is opened, causing a drop in the height of the mercury column. The mercury column and reservoir are measured again.

8) Temperatures in the paraffin tank (*pt*), main chamber (*mc*), standard volume (*sv*) and capillary (*c*) were noted, so that corrections for differences in temperature could be applied to subsequent calculations.

The procedure was repeated for different combinations of open and closed taps, so that successively more sections of the gas lines were open to the nitrogen. The pressures before and after the standard volume is opened are entered into Equation 3.4 with corrections for temperature.

$$P_1\left[(V_{mc})+\frac{T_{mc}}{T_{pt}}(V_{pt})+\frac{T_{mc}}{T_c}(V_c)\right] = P_2\left[(V_{mc})+\frac{T_{mc}}{T_{pt}}(V_{pt})+\frac{T_{mc}}{T_c}(V_c)\right]+\frac{T_{mc}}{T_{sv}}.P_2.V_{sv} \qquad (3.4)$$

Here P_1 and P_2 are the pressures before and after the standard volume is opened, as measured by the cathetometer, T is the temperature (K) and V the volume (cm^3). Equation 3.4 simplifies to Equation 3.5 as the terms within the large brackets are constant and equal to V_{total}.

$$P_1 V_{total} = P_2 V_{total} + \frac{T_{mc}}{T_{sv}} P_2 V_{sv} \tag{3.5}$$

The volumes for the sections of the apparatus bounded by the relevant closed taps (Figure 3.1) are given in Table 3.2.

3.2.8 Calibration of the Eurotherm Device

A more detailed explanation of the calibration of the Eurotherm device is offered by Townsend[1] and the Eurotherm reference manual.[6] The variable parameters governing the heating profile were proportional band (Pb %), integral time (t_i), derivative time (t_d), maximum power (HL %), approach (AP) and the setpoint temperature which is the required nominal temperature. Optimum parameters for the required setpoint temperatures are given in Table 3.3.

3.3 Experimental Procedure

Before any experiments could be performed, the paraffin tank, main chamber and lead tubes were checked to ensure that they were at their respective required temperatures. The oil bath was set to the required setpoint temperature and the entire apparatus evacuated to less than 5×10^{-3} mbar. Initially taps E, I, J, P, Q and needle valve G are closed (Figure 3.1). Dean numbers (D) and Reynolds numbers (Re) were calculated prior to an experiment to determine the correct pressure conditions at each temperature. The chosen conditions were such that the values of D and Re were always below 6 and 500 respectively, thus ensuring that the effects of curved pipe flow were negligible and flow was non-turbulent respectively.

Table 3.2 Volumes of sections of the apparatus - the letters refer to volume boundaries at the taps shown in Figure 3.1.

Section	Volume /cm^3
$V_f \rightarrow$GKL (mercury surfaces level)	709.0
$V_b \rightarrow$M	3171.9
Manometer arm$\rightarrow$J (mercury surfaces level)	209.1
POMKHI	170.0
IJS	91.6
O$\rightarrow$capillary$\rightarrow$R	72.5
LR (without cold trap)	18.1
(with cold trap)	26.2
One capillary lead tube	36.2

Table 3.3 Optimum parameter values for the Eurotherm device to thermostat the oil bath.

	Temperature / °C						
Parameters	10	35	50	70	90	110	130
Pb	3	3	3	3	3	2	2
t_i	200	200	200	150	150	120	120
t_d	20	20	20	20	20	20	20
HL	100	100	100	100	100	100	100
Hc	0.3	0.3	0.3	0.3	0.3	0.3	0.3
AP	1	1	1	1	1	1	1
Water cooling	ON (from chiller)	ON	ON	ON	OFF	OFF	OFF

The procedure for carrying out a run is set out in detail below for an example pressure code of FV_2BV_7;

1) Tap J is opened, followed by tap I so that both pumps can evacuate the gas lines.

2) Tap D is closed in order to prevent further evacuation by rotary pump 1, and diffusion pump 1 is switched off, to allow it to cool. The apparatus is left for 5 minutes in this state, with the gas lines being evacuated by rotary and diffusion pump 2.

3) During these 5 minutes, a number of procedures are carried out;

a) The timers are switched on, and the bank of switches adjusted for the pointer relating to the desired back vessel pressure and the pointers above and below it. In this example, the switches for the timers would be set for 6, 7 and 8.

b) The gas canister tap is opened (for nitrogen, HCFC 124 and MP 39). In the case of HCFC 123, parts 1 to 8 of Section 3.2.3 would have been performed before part 1 of this section, while part 9 would be performed at this stage.

c) Taps L, K and H are closed in readiness for the first filling. This is the determination of the back vessel pressure using the front vessel and the pointers in the manometer arm.

4) Tap E is opened and adjusted in order to provide a steady flow of gas. Excess gas is observed to bubble through the mercury blow off and is vented to the fume cupboard via a rubber hose. Once the desired flow rate is attained, the gas is left to bubble off for about 15 seconds so that any air that might be present is displaced.

5) The needle valve G is opened slowly so that the gas is admitted to the front vessel and as a result, the mercury column is observed to move up the manometer arm. Valve G is closed when the mercury column reaches the desired height, where electrical contact is just being made with pointer 7. This would be seen as a flickering of the red timing lights between pointers 6 to 7 and 7 to 8 on the bank of timers. The flickering is caused by a small amount of vibration in the mercury column from the rotary pumps but is not

major. To ensure the mercury was steady at this height, it was left in this state for 15 seconds and after this time, the lights on the timers were checked again to ensure that both the red lights were flickering. If not, minor adjustments were made using needle valve G (see part 6 below) until the mercury column was steady after a further 15 second period.

6) If the level of mercury in the manometer arm is too low (seen as a red light for pointers 7 to 8 and a green light for pointers 6 to 7), the needle valve G is opened slightly to allow more gas into the front vessel until the required mercury column height is obtained. However if the mercury is too high (seen as a red light for pointers 6 to 7 and a green light for pointers 7 to 8) the following procedure is adopted;

a) Tap E is closed to prevent any further gas entering the gas line.

b) Tap D is opened to allow partial evacuation of the line DG. Needle valve G is opened in order to allow some of the gas in the front vessel to be evacuated, thereby reducing the mercury column height. Once the desired height is attained (seen by flickering of the red lights 6 to 7 and 7 to 8), needle valve G is closed, tap D is closed and tap E is reopened and a steady flow of the gas through the mercury blow off is reattained.

7) Tap I is closed in order to maintain the vacuum in the manometer arm which is constantly evacuated by rotary and diffusion pumps 2 throughout the experiment.

8) Taps L and K are opened, allowing the gas to disperse from the front vessel into the capillary, back vessel and throughout the gas lines bounded by taps H, I, P and Q. The height of the mercury column decreases and once steady, the system is left for one minute in order to allow the gas to disperse equally around the gas lines.

9) During the one minute period, the switches on the bank of timers are set for the pointer representing the desired front vessel pressure and the pointers above and below it. In this example, the switches are set to 1, 2 and 3. This is for the second filling which is for the

setting of the front vessel pressure.

10) Taps L and K are closed.

11) The procedure in steps 5 and 6 is repeated so that the mercury column is steady at pointer 2, in this example.

12) Tap L is opened, allowing the gas to flow from the higher pressure front vessel to the lower pressure capillary and back vessel. Initially a rapid drop in the mercury column is observed as the gas initially occupies the wider bore gas line from L, through R to the lead tubes before the capillary. The switches are altered to reflect the pointers over which the fall in the mercury column are to be timed. Care is taken to choose pointers which are below the column of mercury after its initial large drop. Thus the timers connected to the following pointers will reflect the time it takes the gas to flow through the capillary tube, not through the lead tubes. The timers are zeroed ready for the first timing.

13) The temperature of the capillary according to the independent temperature sensor is taken together with a measurement with the platinum resistance thermometer. The temperatures of the lead tubes and main chamber are also noted in order to check their long term consistency.

14) Tap E is closed and for nitrogen, HCFC 124 and MP 39 the cylinder taps are also closed. For HCFC 123 parts 10 and 11 of Section 3.2.3 are performed at this time.

After a run has been completed, ie. the timers have timed the fall of the mercury column past the relevant pointers, the following procedure is adopted;

1) The times between the relevant pointers are noted, as are the temperatures for the capillary, main chamber and lead tubes.

2) The timers are switched off and zeroed.

3) Taps D, H and K are opened in order to allow the gas lines to be evacuated by rotary pump and diffusion pump 1. For HCFC 123, tap P is opened slightly to allow air to circulate through the gas lines and out via rotary pump 1, thereby aiding the removal of

residual HCFC 123 which is harder to evacuate due to possible adsorption effects suggested by the high boiling point of the sample. After approximately 3 hours in this state, tap P is closed and the apparatus allowed to evacuate normally.

4) Once a vacuum had been roughed out to approximately 0.3 mbar by rotary pump 1, diffusion pump 1 is switched on.

5) Whilst leaving the equipment evacuating overnight, taps I and J are closed so that in the event of a power failure during the night, air from the automatic air bleed on rotary pump 2 could not enter the manometer arm whilst the mercury reservoir was evacuated, possibly resulting in damage to the manometer.

It should be noted that for HFC 134a, which was the first gas tested, the method of Hunter[2] was adopted which did not require the manometer arm to be evacuated but was actually occupied by gas after the first filling. However this does rely on the manometer arm being initially evacuated so that relevant back vessel pressures can be calculated, which worked well for his work and the HFC 134a results of this work. However, due to the adsorption problems associated with the HCFC 123, complete evacuation from the manometer arm overnight could not be guaranteed, so the method described in parts 1 to 14 above was adopted for the HCFC 123 samples out of necessity and the HCFC 124 and MP 39 samples through choice. Results for nitrogen were taken using both methods.

Chapter 4

Viscosity Measurements and Results

4.1 Introduction

Four replacement refrigerants have been tested on the capillary flow gas viscometer described in Chapter 3. These are HFC 134a (1,1,1,2-tetrafluoroethane, CH_2FCF_3), HCFC 123 (2,2-dichloro-1,1,1-trifluoroethane, $CHCl_2CF_3$), HCFC 124 (2-chloro-1,1,1,2-tetrafluoroethane, $CHClFCF_3$) and the ternary blend MP 39 which consists of 52% HCFC 22 (chlorodifluoromethane, $CHClF_2$), 33% HCFC 124 and 15% HFC 152a (1,1-difluoroethane, CH_3CHF_2) by weight.

HFC 134a is intended as a replacement for chlorofluorocarbon (CFC) 12 in household and commercial refrigeration in addition to blowing agent applications. MP 39 is also intended as a replacement for CFC 12 in home applications.

HCFC 123 was a potential substitute for CFC 11 in many of its applications such as refrigeration, blowing agent and propellant uses, but since the discovery of benign tumours in rats at prolonged low exposure levels as part of the Programme for Alternative Fluorocarbon Toxicity Testing (PAFT),[1] it may now be limited to refrigeration applications only.

HCFC 124 is a component of ternary blends such as MP 39 but is also a potential replacement for CFC 114 in applications such as water and brine chillers.

Flow times for each of the sample gases were measured over a range of pressures between their respective boiling points and decomposition points. All of the samples were obtained through Du Pont de Nemours International SA, Geneva, Switzerland. HFC 134a, at a stated purity of 99.95% and a production sample of MP 39 were measured at 308.15 K, 323.15 K, 343.15 K, 363.15 K, 383.15 K and 403.15 K. A production sample of HCFC 124 was measured at 283.15 K in addition to the temperatures at which HFC 134a

and MP 39 were measured. A production sample of HCFC 123 was measured at 308.15 K, 323.15 K, 343.15 K and 363.15 K.

Before any measurements were undertaken the accuracy of the viscometer had to be assessed.

4.2 Testing the Accuracy of the Viscometer

The viscosities of nitrogen and argon have been well documented elsewhere.[2-6] The nitrogen standards used for this work are those of Gough et al.[4] below 300 K and those of Maitland and Smith[5] above 300 K (Table 4.1). Maitland and Smith fitted eight sets of viscosity measurements over a temperature range of 90 - 2150 K using least squares regression analysis, to a function of the form in Equation 4.1.[7]

$$\ln(\eta/S)=A\ln T + B/T+C/T^2+D \qquad (4.1)$$

Here T is the temperature in Kelvins and S is in μPa s. A data set[8] used by Maitland and Smith between 90 - 300 K was subsequently shown to deviate systematically from accepted values, and therefore the correlation for the viscosity of nitrogen below 300 K has since been revised.[4] The fitting curves of both works join almost perfectly at 300 K and agree well to work by Vogel.[2]

The coefficients for the fitting curve (Equation 4.1) of argon between 120 - 1700 K are taken from Barr et al.[3] and are shown in Table 4.1.

Using the coefficients in Table 4.1, the viscosities of both nitrogen and argon can be calculated within the range of temperatures given, and thus, the ratio of their viscosities $\eta_{argon}/\eta_{nitrogen}$ can be obtained.

Flow time measurements were carried out over a range of pressures using nitrogen and argon at a capillary temperature of 301.15 K. A correction for slip flow was applied to this data, using the method in Section 2.8.5, to give a ratio of the corrected flow times ($t_{argon}/t_{nitrogen}$) which can be compared to the viscosity ratio by Equation 4.2.

Table 4.1 Coefficients of the Curve $ln(\eta/S)=AlnT+B/T+C/T^2+D$ for argon and the nitrogen standard.

Gas	Temperature /K	A	B/K	C/K^2	D	S/μPa s
Nitrogen	<300	0.556994	-72.1361	1365.89	2.234	0.1
Nitrogen	>300	0.600970	-57.0050	1029.10	-3.232	17.57
Argon	<300	0.583152	-96.1924	2923.99	2.390	0.1
Argon	>300	0.599369	-57.5041	-3118.53	2.236	0.1

$$\frac{t_{argon}}{t_{nitrogen}} = \frac{\eta_{argon}}{\eta_{nitrogen}} \tag{4.2}$$

The measured flow time ratio was found to be within 0.1% of the calculated viscosity ratio ($\eta_{argon}/\eta_{nitrogen}$) of 1.2747 at 301.15 K, and indicates that the viscometer is operating to a satisfactory level.

4.3 Correction of Raw Flow Time Data

A Supercalc 5.0 spreadsheet has been used to aid the processing of flow time data. Flow time measurements were repeated under the same pressure and nominal temperature conditions and the results for the standard and sample gases stored on spreadsheet files on disk, which can be found at the back of this thesis, with an explanation of the file names in Appendix 1. The Dean and Reynolds numbers for the flow conditions of an experimental run are also calculated, as has previously been described in Sections 2.6.2 and 2.8.2 respectively. The maximum Reynolds numbers (*Re*) and Dean numbers (*D*) for experiments undertaken at each temperature are shown in Table 4.2 for each of the sample gases.

Using the pointer pressures and volume determinations (Tables 3.1 and 3.2) the front vessel, back vessel and mean capillary pressures are calculated for both the experimental methods used in this work.

The spreadsheet file has also been set up to apply correction terms to the raw flow time data. The capillary temperature varied slightly between successive flow time measurements and was brought up to the nominal temperature using the method described in Section 2.8.1. The flow time at the nominal temperature must then be corrected for non-ideality of the gas at the capillary temperature (K_b) and front and back vessel temperatures (K_{b1}) as well as kinetic energy using the Hagenbach correction (K_h). The method used to correct for gas imperfection (Section 2.8.4) requires the second virial

Table 4.2 Maximum Reynolds and Dean numbers for experimental conditions.

Temperature	HFC 134a		HCFC 123		HCFC 124		MP 39	
/K	*Re*	*D*	*Re*	*D*	*Re*	*D*	*Re*	*D*
283.15					92.26	5.84		
308.15	73.97	4.68	88.69	5.61	79.17	5.01	57.94	3.66
323.15	79.91	5.05	78.67	4.98	70.23	4.44	51.40	3.25
343.15	71.62	4.53	85.46	5.40	76.29	4.83	55.84	3.53
363.15	75.67	4.79	84.61	5.35	75.53	4.78	55.28	3.50
383.15	54.45	3.44			83.16	5.26	60.85	3.85
403.15	73.05	4.62			73.34	4.64	53.67	3.39

coefficient (B) to be calculated for the gas at the capillary temperature and the front and back vessel temperature. As second virial coefficient data was unavailable for the HCFC 124 and MP 39 sample gases at the time of developing the flow correction spreadsheet files, other molecules were chosen from Dymond and Smith[9] as an approximation for the test gases in this work. They were chosen on the basis that they were structurally similar to the sample gases and second virial coefficient data (in cm^3mol^{-1}) for them was available over a similar range of temperatures as our intended viscosity experiments. With the ternary blend, MP 39, a molecule was chosen with a similar molecular weight which contained chlorine, fluorine and carbon as second virial coefficient data for a ternary compound of a similar structure to MP 39 could not be found. The gases chosen to represent the sample gases are shown in Table 4.3. Measured second virial coefficients of Schramm et al.[10] and Tillner-Roth and Baehr[11] were used for HFC 134a, whilst those of Weber[12] and Goodwin and Moldover[13] were adopted for HCFC 123. Corrections for non-ideality and kinetic energy can have an effect of up to 3.3% on the flow time and examples are given for each of the sample gases in Appendix 2.

The corrected flow times for each gas were printed out and the flow times for each gas under the same temperature and pressure conditions were averaged. A criterion of repeatability was adopted in which experiments were performed until three to four runs had a combined deviation of no more than 0.3% and was attained except for five results (HCFC 123 at 343.15 K, FV_7BV_{13} [0.31%], at 363.15 K, FV_7BV_{14} [0.35%], HCFC 124 at 308.15 K, FV_1BV_5 [0.42%], MP 39 at 383.15 K, FV_1BV_2 [0.31%] and at 403.15 K, FV_1BV_2 [0.52%]). It is acknowledged that even if results are repeatable it does not necessarily mean that they are accurate. However if results are not repeatable then it is reasonable to assume that most will be wrong. From these averaged flow times, the flow time ratio between the sample gas and the nitrogen standard $t_{sample} / t_{standard}$ was calculated, where t is the corrected flow time.

Table 4.3 Approximations used in the absence of second virial coefficient data for the sample gases (required for correction terms applied to raw flow time data).

Sample Gas	Formula	Molecular Weight	Approximation	Formula	Molecular Weight
HCFC 124	$CHClFCF_3$	136.5	1,2-dichloro-1,1,2,2-tetrafluoroethane	$CClF_2CClF_2$	170.1
MP 39	$CHClF_2$ $CHClFCF_3$ CH_3CHF_2	99.9	Chlorotrifluoromethane	$CClF_3$	104.1

Low pressure conditions reduce the effects of curved pipe flow and gas imperfection, but increase the correction necessary due to slip flow (Section 2.8.5). It is corrected by plotting the flow time ratio against the inverse mean capillary pressure for the nominal temperature at which measurements were taken. The intercept of the least squares regression line on the vertical axis provides the flow time ratio at infinite pressure ($1/\bar{P}_c=0$) which is a hypothetical condition at which there is no slip effect. Examples of the slip flow correction plots for each of the sample gases are given in Appendix 3. The graphs in Appendix 3 also display the standard error in the y-intercept which provides an indication of the level of uncertainty in the value of the flow time ratio which can be translated into uncertainty in the viscosity derived from Equation 4.3. The standard error of the y-intercept in the slip flow correction plots for each of the sample gases is shown in Table 4.4.

Having applied all the necessary corrections to the raw flow time data, the viscosity of the sample gas at each nominal temperature can be found from Equation 4.3.

$$\frac{t_{sample}}{t_{standard}} = \frac{\eta_{sample}}{\eta_{standard}} \tag{4.3}$$

Nitrogen standard viscosities calculated from Equation 4.1 and subsequently used in Equation 4.3, are given in Table 4.1.

4.3.1 The Sample Gas HFC 134a

Appendix 4a shows the averaged flow time results for the HFC 134a and nitrogen standard experimental runs. The fourth column gives the mean capillary pressure, being the average of the front and back vessel pressures in columns two and three. Column seven provides the flow time ratio ($t_{HFC\ 134a}$ / $t_{nitrogen}$) based on the flow times given in columns five and six. By plotting a least squares regression line of the inverse of the mean capillary pressures against the flow time ratio, slip flow correction plots such as

Table 4.4 Standard errors for slip flow correction plots.

Temperature	Standard Error /%			
/K	HFC 134a	HCFC 123	HCFC 124	MP 39
283.15			0.26	
308.15	0.29	1.91	0.53	0.43
323.15	0.13	2.09	0.46	0.30
343.15	0.17	2.32	0.37	0.29
363.15	0.18	2.07	0.28	0.64
383.15	0.09		0.29	0.30
403.15	0.09		0.37	0.26

those in Appendix 3 are obtained and the flow time ratio without the effects of slip can be obtained (Table 4.5). 73% of experimental runs for HFC 134a were accepted and used in the calculation of the shear viscosity of HFC 134a. Employing the flow time ratio without slip effects (Table 4.5) and the standard viscosities of nitrogen calculated from Table 4.1 at each nominal temperature, in Equation 4.3, the shear viscosity of HFC 134a is obtained (Table 4.5).

4.3.2 The Sample Gas HCFC 123

Appendix 4b for HCFC 123 is of the same format as Appendix 4a for HFC 134a. Here 56% of experimental runs for HCFC 123 were accepted. The flow time ratio $t_{HCFC\ 123} / t_{nitrogen}$ without slip effects and the shear viscosity of HCFC 123 are shown in Table 4.6.

4.3.3 The Sample Gas HCFC 124

Appendix 4c gives the average flow time data for the HCFC 124 and nitrogen experimental runs, which have been used to calculate the flow time ratio without slip effects and the shear viscosity of HCFC 124 in Table 4.7. For HCFC 124, 88% of experimental runs were accepted.

4.3.4 The Ternary Blend MP 39

Appendix 4d gives the average flow time data for the ternary blend MP 39 and the nitrogen standard which are used to calculate the flow time ratio without slip effects and the shear viscosity shown in Table 4.8. Here, 68% of experimental runs for MP 39 were accepted.

Table 4.5 Flow time ratio without slip effects and shear viscosity for HFC 134a.

Temperature /K	Flow time ratio	Viscosity /μPa s
308.15	0.6717	12.253
323.15	0.6785	12.833
343.15	0.6888	13.631
363.15	0.6911	14.267
383.15	0.6995	15.024
403.15	0.7070	15.762

Table 4.6 Flow time ratio without slip effects and shear viscosity for HCFC 123.

Temperature /K	Flow time ratio	Viscosity /μPa s
308.15	0.6094	11.117
323.15	0.6179	11.687
343.15	0.6136	12.143
363.15	0.6284	12.973

Table 4.7 Flow time ratio without slip effects and shear viscosity for HCFC 124.

Temperature /K	Flow time ratio	Viscosity /μPa s
283.15	0.6659	11.380
308.15	0.6659	12.148
323.15	0.6759	12.784
343.15	0.6766	13.390
363.15	0.6895	14.234
383.15	0.6874	14.764
403.15	0.6990	15.584

Table 4.8 Flow time ratio without slip effects and shear viscosity for MP 39.

Temperature /K	Flow time ratio	Viscosity /μPa s
308.15	0.7134	13.014
323.15	0.7121	13.469
343.15	0.7184	14.217
363.15	0.7383	15.241
383.15	0.7368	15.610
403.15	0.7461	16.634

4.4 A Consideration of Errors

Errors in the final shear viscosity results can arise from uncertainties in the many measurements carried out as part of this work. The magnitudes of these possible errors have been evaluated and the findings summarised.

4.4.1 Timing Errors

Errors arising from the timers are considered to be negligible, being less than 0.002% as shown in Section 3.2.6.

4.4.2 Temperature Errors

Errors arising from inaccuracies in the measurement of the capillary temperature are of more importance. Flow time ratios for HFC 134a, HCFC 123, HCFC 124 and MP 39 changed by 0.05%, 0.05%, 0.04% and 0.05% in 1 K respectively. However errors of these magnitudes in the temperature would alter the viscosity by up to 5.3%, 5.1%, 3.4% and 4.2% respectively as the wrong value of the standard viscosity would be used. The platinum resistance thermometer used to measure temperature has a quoted accuracy of ±0.05 K which represents an error of 0.02% at 308.15 K and 0.01% at 403.15 K. Hence the maximum errors associated with temperature uncertainties for HFC 134a, HCFC 123, HCFC 124 and MP 39 are negligible (0.1% or less).

4.4.3 Sample Gas Composition

The composition of the sample gases has been a problem as it has been difficult to ascertain the purity of the samples used. We have been told by Du Pont de Nemours International SA in Geneva, Switzerland (who supplied our gas samples), that the purity of HFC 134a is 99.95% and, despite repeated requests, have been unable to find out the purity of the other samples used (HCFC 123, HCFC 124 and MP 39). This remains an

area in which the associated errors cannot be estimated but are probably negligible.

4.4.4 Secondary Corrections

Other quantities, such as the pointer pressure and volume determinations, were used for the calculation of correction terms, which are around 1% or less except for the correction term for non-ideality at the front and back vessel temperatures (K_{bl}) which reaches a maximum of 3.3%. If the three correction terms for non-ideality at the capillary temperature (K_b), front and back vessel temperature (K_{bl}) and kinetic energy are considered together (Appendix 2), then the overall correction is around 3% or less. Part of any error in this correction term will be due to the use of a substitute gas to represent the sample gas (for HCFC 124 and MP 39 only, Table 4.3) in the calculation of second virial coefficients used for these correction terms. The magnitude of this source of error cannot be estimated as second virial coefficient data has not been found at temperatures and pressures used in this work for these sample gases.

Errors in pressure readings are considered to be less than 0.1%. An absolute error in pressure of ±0.1 mmHg corresponds to 0.0133 kPa and will have the largest effect at the lowest pressure experimental runs ie. FV_7BV_{14}.

Errors arising from the method used to determine the volume of sections of the apparatus (Table 3.2) explained in Section 3.2.7 produce a negligible error in the mean capillary pressure of less than 0.1%.

4.4.5 Slip Flow Correction Plots

The standard error evident in the slip flow correction plots (Table 4.4 and Appendix 3) represents the largest source of error. However using a least squares regression line to find the flow time ratio at infinite pressure will compensate for a degree of random scatter. The length of the extrapolation of the regression line from the data set

to the y-axis relative to the pressure range over which the data set extends has the largest effect on the extent of the standard error in the slip flow correction plots. A suggestion as to the cause of the magnitude of the standard error in the slip flow correction plots is the problem of adsorption of the gas in the gas lines, particularly around the rubber O-rings joining adjacent sections of gas line. The degree of adsorption and desorption will depend on the temperature in the gas lines and the previous pressures to which the front and back vessels have been set. These processes will serve to alter the pressures set in the apparatus for experimental purposes. HCFC 123, with the highest boiling point (301 K), shows the largest standard error (Table 4.4), and problems of evacuating the apparatus were very evident with this sample. Similarly HCFC 124, with a boiling point of 262 K has a smaller degree of scatter and HFC 134a the smallest, with a boiling point of 247 K. The magnitude of the adsorption effect is difficult to quantify because it depends on the temperature and pressure conditions in the viscometer, and effects may be cumulative over successive experiments.

4.4.6 Total Error

Having estimated the individual errors in the various measurements, the total error for HFC 134a, HCFC 123, HCFC 124 and MP 39 are estimated to be ±0.4%, ±2.3%, ±0.6% and ±0.7% respectively, excluding those errors which cannot be quantified as highlighted above.

4.5 Fitting Functions for the Sample Gases

Coefficients which best fit the measured viscosities of each of the sample gases of this work (Tables 4.5 to 4.8) have been derived using a Minitab statistics package, and are shown in Table 4.9 and Figures 4.1 to 4.4. The data points on these diagrams represent the 'measured' points from this work and the 'fitted' line represents the best fit

Table 4.9 Coefficients of the curve $ln(\eta/S) = A lnT + B/T + C/T^2 + D$ for HFC 134a, HCFC 123, HCFC 124 and MP 39.

Gas	Temperature /K	A	B /K	D	S /μPa s
HFC 134a	308-403	0.6937	-83.0	-1.200	1
HCFC 123	308-363	0.6238	-93.9	-0.861	1
HCFC 124	283-403	1.1532	88.2	-4.392	1
MP 39	308-403	1.2840	131.2	-2.918	0.1

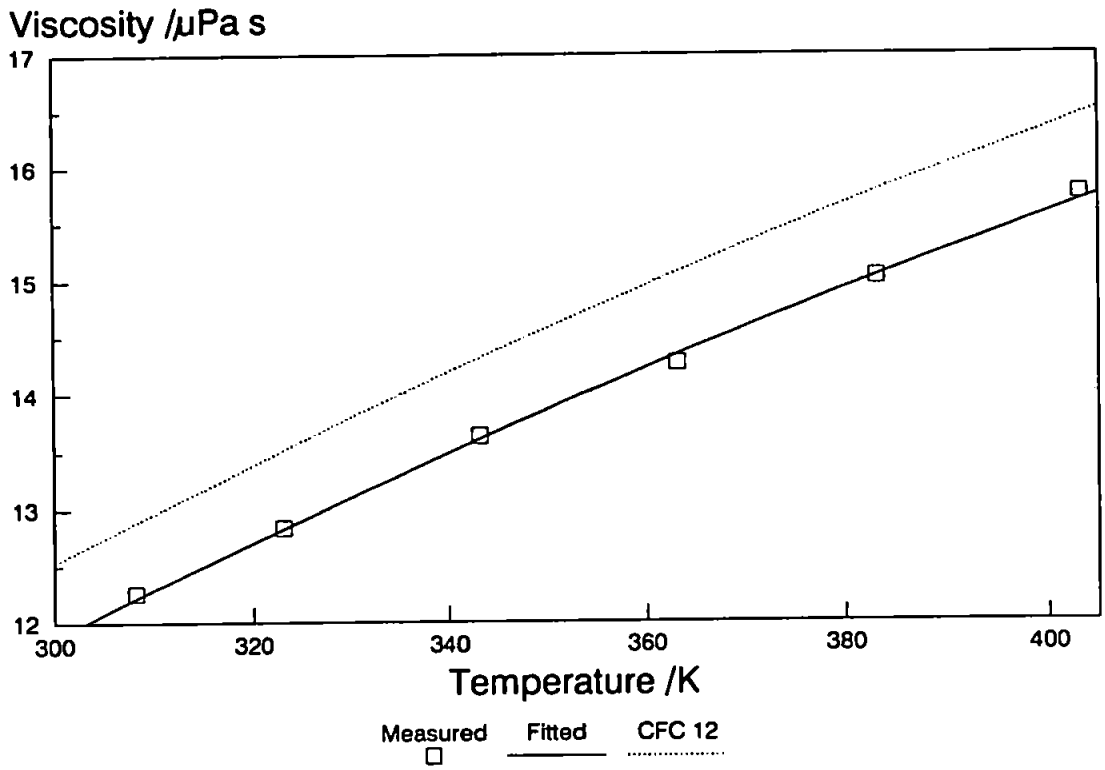

Figure 4.1 Measured and fitted viscosities for HFC 134a and a comparison with CFC 12 which it is intended to replace.

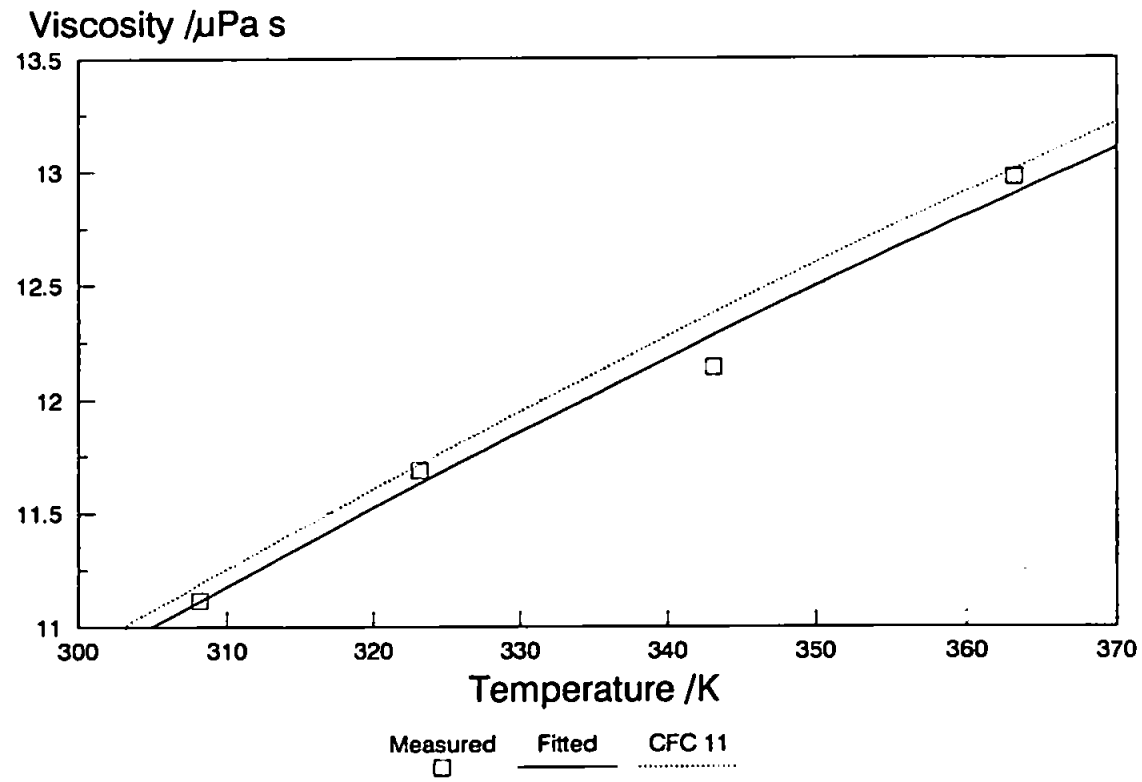

Figure 4.2 Measured and fitted viscosities for HCFC 123 and a comparison with CFC 11 which it is intended to replace.

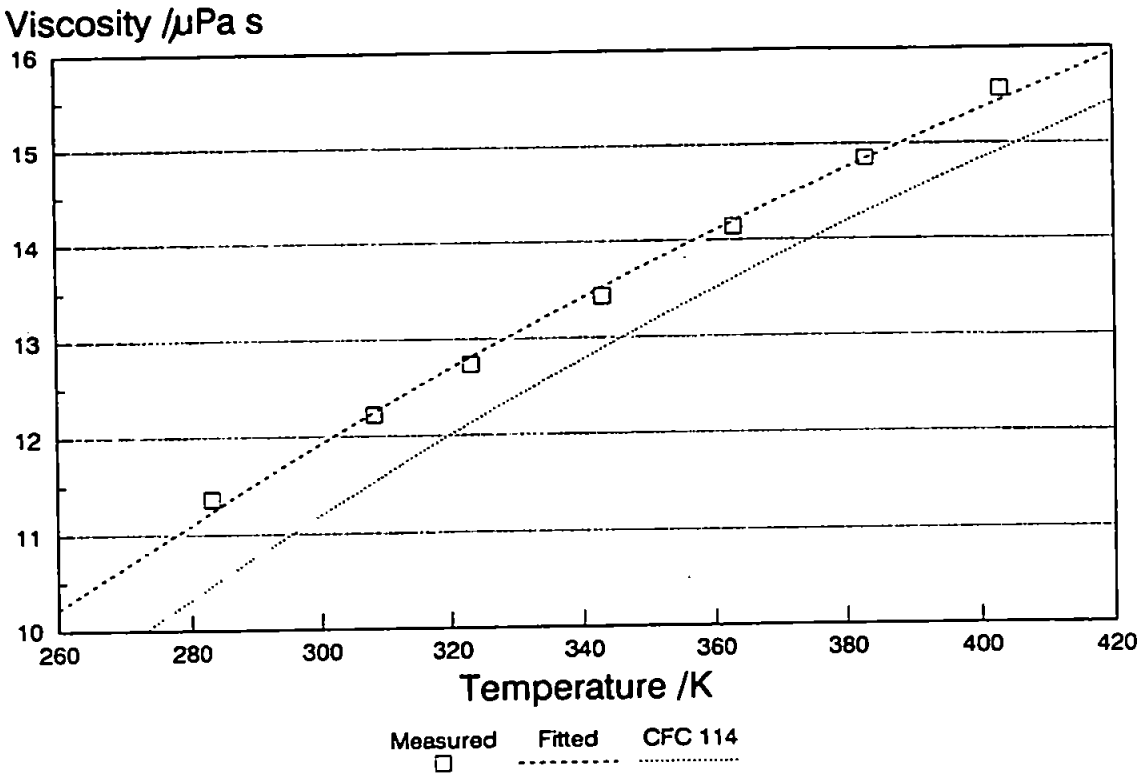

Figure 4.3 Measured and fitted viscosities for HCFC 124 and a comparison with CFC 114 which it is intended to replace.

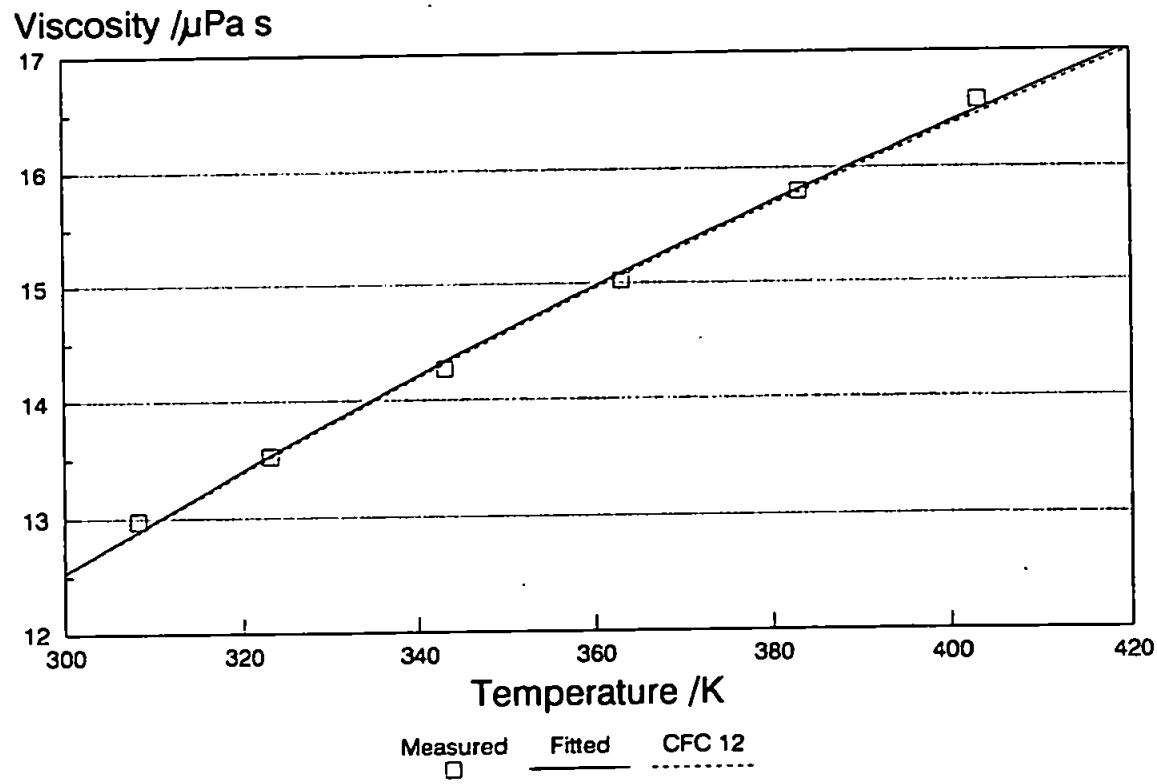

Figure 4.4 Measured and fitted viscosities for MP 39 and a comparison with CFC 12 which it is intended to replace.

line for the data points. Statistically, the coefficient C is highly correlated with coefficient B and its inclusion does not significantly improve the fit of the points over the experimental temperature range. In the case of HCFC 123, the number of statistical degrees of freedom was too small to justify an independent value of the temperature exponent coefficient A, and this was therefore equated to a value of A obtained from a fit to the measured viscosities of other workers.[14] The coefficients B and D were then independently optimised.

4.6 Comparison of the Sample Gases with the CFCs they are Replacing

It is hoped that the replacement refrigerants will have properties close to those they are intended to replace, so that they may be exchanged for the original CFCs without any major changes in the apparatus using them (so called 'drop-in replacements'). The following section offers a comparison in terms of dilute gas viscosity, between the original CFCs and the refrigerants intended to replace them.

4.6.1 HFC 134a v CFC 12

Figure 4.1 shows our fitting curve for HFC 134a (Table 4.9) and the fitting curve for CFC 12[15] of the form in Equation 4.4.

$$\eta = \frac{\sqrt{T}}{0.75309 + \frac{188.969}{T} - \frac{803.786}{T^2}} \qquad (4.4)$$

CFC 12 has a 4.5% to 5.5% higher viscosity than HFC 134a over the temperature range 308.15 K to 403.15 K.

4.6.2 HCFC 123 v CFC 11

Figure 4.2 shows the fitting curve of HCFC 123, derived from Table 4.9 and the fitting curve for CFC 11[15] of the form in Equation 4.5.

$$\eta = \frac{\sqrt{T}}{0.43547 + \frac{511.161}{T} - \frac{50128}{T^2}} \qquad (4.5)$$

The measured viscosities for HCFC 123 of this work are much closer to the viscosities of CFC 11 than the comparison between HFC 134a and CFC 12. The CFC 11 viscosities are between 0.62% and 0.93% higher than the HCFC 123 viscosities.

4.6.3 HCFC 124 v CFC 114

Figure 4.3 shows the fitting curves of HCFC 124 (Table 4.9) and CFC 114.[16] The fitting curve of CFC 114, within the temperature range 303 K to 473 K, is of the form in Equation 4.6.

$$\eta = \frac{13.70\sqrt{T} - 125.31}{10} \qquad (4.6)$$

Within the true temperature range of the fitting equation of Nabizadeh and Mayinger[16] for CFC 114 (shown by the unbroken part of the curve in Figure 4.3), the viscosity of gaseous HCFC 124 is between 3.9% and 6.1% higher than the viscosity of CFC 114.

4.6.4 MP 39 v CFC 12

The gaseous viscosity of MP 39 is very close to CFC 12 which it is intended to replace. Figure 4.4 offers a comparison between the fitting functions of MP 39 (Table 4.9) and CFC 12[15] and shows that the viscosity of MP 39 is between 0.1% and 0.5% higher than the viscosity of CFC 12.

4.7 Comparison with Other Workers' Results

The dilute gas viscosities of this work have been measured on a capillary flow gas

viscometer. Other workers have made viscosity measurements using oscillating disc viscometers[14, 17, 18] and a rolling ball type viscometer.[19] The following sections offer a comparison between the results of this work and those of other workers (where possible) for each of the sample gases.

4.7.1 HFC 134a

Figure 4.5 shows the percentage deviation of our viscosity measurements of HFC 134a and the measurements and calculations of other workers from our fitting curve (Table 4.9). Note that our experimental temperature range for this gas is 308.15 K to 403.15 K, shown as a solid horizontal line at 0% deviation. The comparison is extended beyond this range for interest, but is less reliable. The graph shows the deviations of the experimental results of Nabizadeh and Mayinger[14] and Takahashi et al.,[17] measured on oscillating disc viscometers. Tanaka and Matsuo[19] have also measured the viscosity of gaseous HFC 134a on a rolling ball type viscometer, but comparison with our results is difficult because we have only found their data published as a small-scale graph in a secondary source. Krauss and Stephan[20] correlated existing viscosity measurements, mainly based on those of Nabizadeh and Mayinger.[14] The gaseous viscosities of Schramm et al.[10] are calculated from measurements of second virial coefficients using the Stockmayer intermolecular potential model.

On calculation of the deviations shown in Figure 4.5, a problem becomes apparent, namely that the results of other workers deviate from our results by more than the sum of our experimental uncertainty and theirs. We quote an accuracy of ±0.4%, and Nabizadeh and Mayinger[14] quote an accuracy in their measurements of ±0.5%. However within the range of our experimental data, the two sets of results only agree at the lowest temperatures of our measurements and those of Nabizadeh and Mayinger.[14] Above 308.15 K the measurements of Nabizadeh and Mayinger are between 1.0% and 1.5% higher than

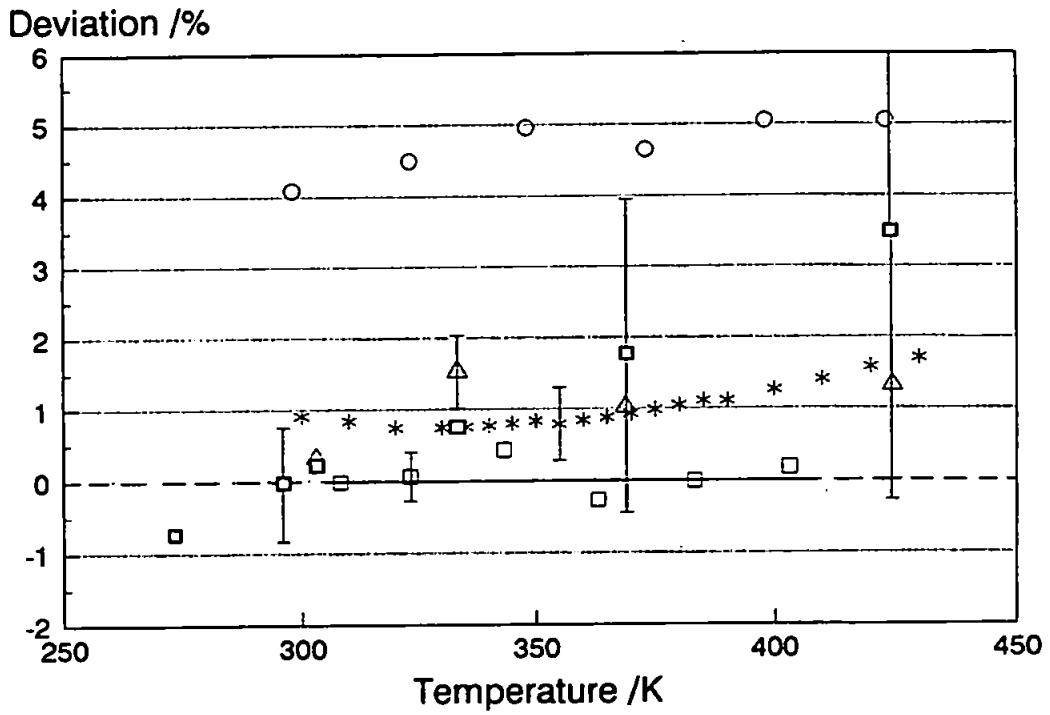

Figure 4.5 Deviation of measured and calculated viscosities of HFC 134a from a curve fitted to the present experimental results, Table 4.9. □, this work; Δ, ref. 14; ○, ref. 17; ✳, ref. 20; □, ref. 10. Error bars as described in text.

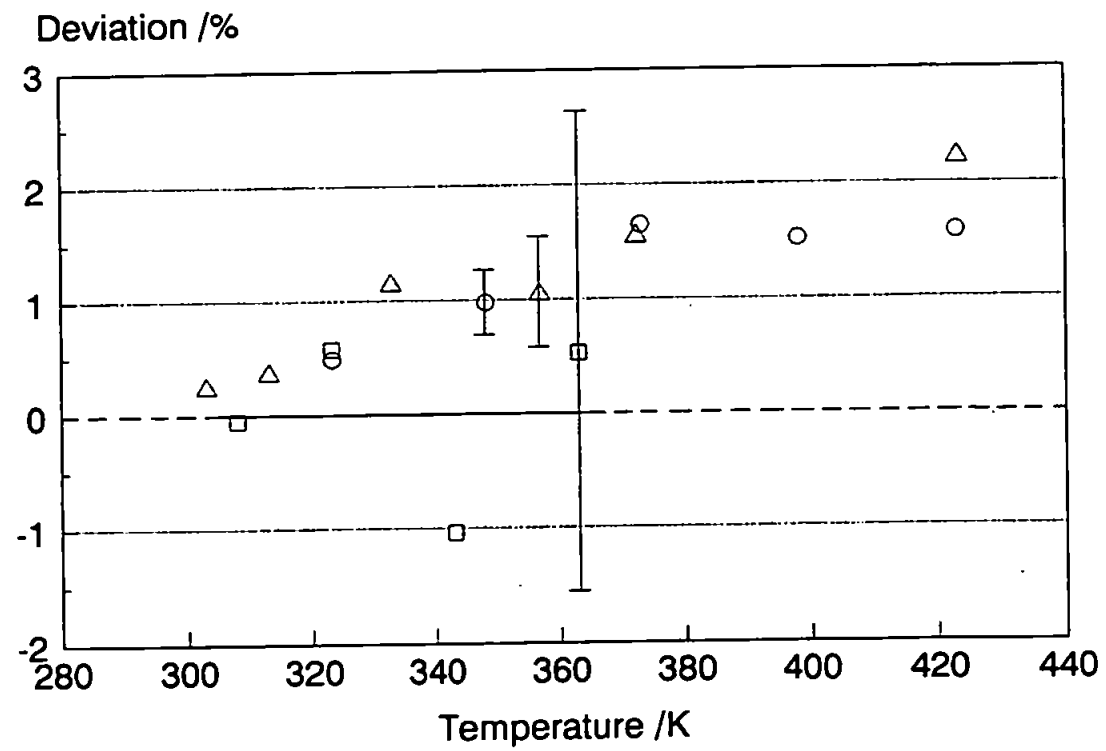

Figure 4.6 Deviation of measured and calculated viscosities of HCFC 123 from a curve fitted to the present experimental results, Table 4.9. □, this work; Δ, ref. 14; ○, ref. 18. Error bars show workers' own estimates of error over the whole temperature range.

the measurements of this work. We do not know the quoted accuracy of the Takahashi et al.[17] data but if differs from our results by 4.1% to 5.0% and from the measurements of Nabizadeh and Mayinger data by 3.1% to 3.5%. Krauss and Stephan's[20] correlation is primarily based on the Nabizadeh and Mayinger[14] data set, hence its similarity to their measurements. The correlation is within combined 'experimental' error of the fitting curve of our measurements up to a temperature of 360 K. Schramm et al.[10] state that the lower temperature results of Nabizadeh and Mayinger are within experimental error of their calculated viscosities, but have omitted the level of that error. They make no comparison with the results of Takahashi et al.[17] However the second virial coefficient measurements of Schramm et al.[10] show a trend of increasing experimental uncertainty from ±0.79% at 296.15 K, through 2.20% at 353.15 K, 3.76% at 413.15 K, up to 6.08% at 473.15 K. If these experimental uncertainties in the virial coefficients transpose into corresponding uncertainties in the calculated viscosities, the results of Schramm et al.[10] agree with ours to within the combined experimental uncertainty. On this assumption, Nabizadeh and Mayinger's[14] results also agree with the Schramm et al.[10] calculations within the respective combined experimental uncertainties.

4.7.2 HCFC 123

Figure 4.6 shows the deviation of our measured viscosities of HCFC 123 and those of Nabizadeh and Mayinger[14] and Takahashi et al.[18] from our fitting curve (Table 4.9). Our experimental uncertainty for this gas is ±2.3%. Nabizadeh and Mayinger[14] quote an accuracy of ±0.5%, and Takahashi et al.[18] ±0.3%, and therefore both sets of results agree with our results to within the combined experimental uncertainty. The deviation of these data sets from each other within our measured temperature range is +0.5% to -0.2%, and therefore agree with each other to within their own quoted accuracies.

It is suggested that the level of error associated with the oscillating disc

experiments is less than the error of our capillary flow experiments, because using our technique, the sample gas must flow through long lengths of gas line containing valves and rubber O-rings, which provide a greater surface upon which adsorption can take place. The oscillating disc method avoids this problem.

4.7.3 HCFC 124 and MP 39

To date, no other dilute gas measurements of HCFC 124 and MP 39 at temperatures within the range 283.15 K to 403.15 K have been found for comparison. Therefore Figures 4.7 and 4.8 simply show the deviation of our own measurements from the respective fitting curves of Table 4.9.

4.7.4 MP 39 and its Components

Figure 4.9 compares the measured viscosity of MP 39 from this work with the viscosities of its three components, ie. HCFC 22, HFC 152a and HCFC 124. The fitting function for HCFC 124 is taken from this work (Table 4.9) whereas the fitting functions for the viscosities of HFC 152a[21] and HCFC 22[15] are given in Equations 4.7 and 4.8 respectively.

$$\eta = (3.38791 \times 10^{-2} T) + (2.32458 \times 10^{-6} T^2) \tag{4.7}$$

$$\eta = \frac{\sqrt{T}}{\left(0.61943 + \frac{239.551}{T} - \frac{7605.74}{T^2}\right)} \tag{4.8}$$

Unlike some mixtures, MP 39 does not exhibit a viscosity maximum when compared to its components. Viscosity maximums tend to occur in polar-non polar mixtures where the pure component viscosities are not greatly different, such as in ammonia-hydrogen mixtures for example.[1] Clearly, MP 39 does not fulfil these criteria as all the components are polar and their viscosities are very different.

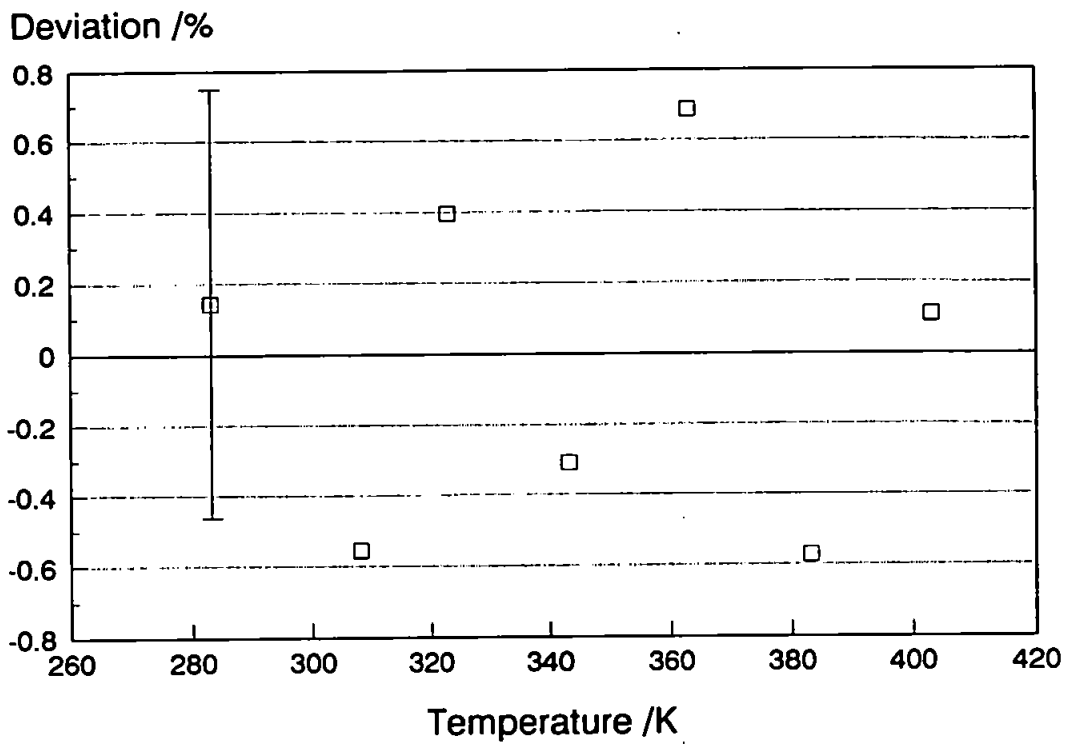

Figure 4.7 Deviation of the measured viscosities of HCFC 124 presented in this work (□) from the fitting curve, Table 4.9. Error bar corresponds to our experimental uncertainty over the whole temperature range.

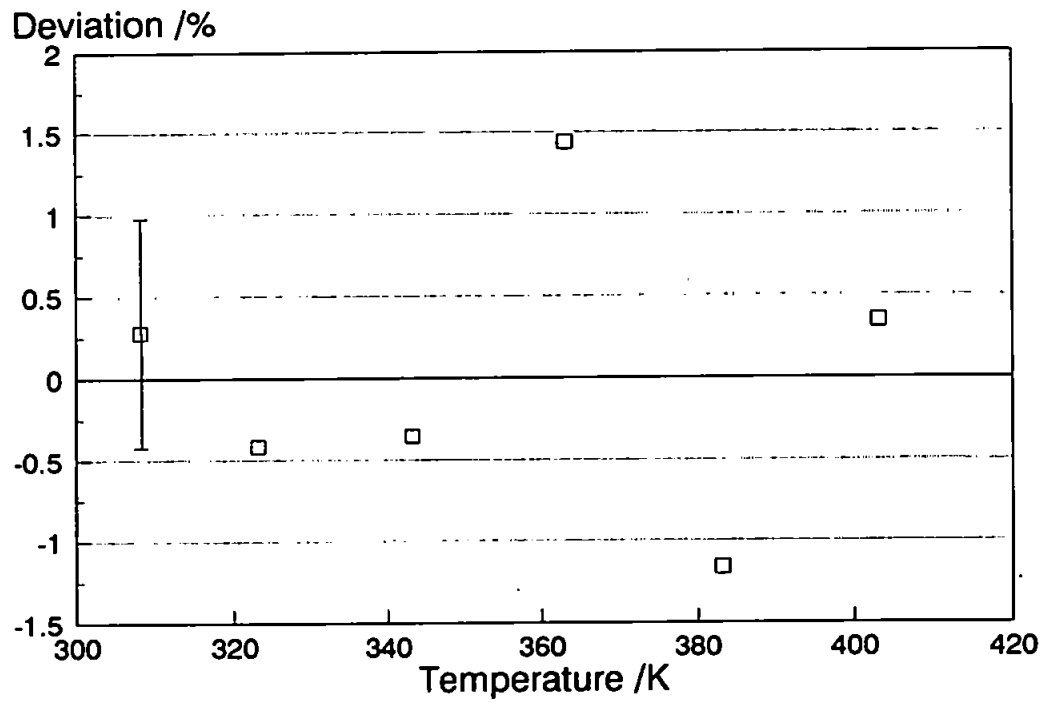

Figure 4.8 Deviation of the measured viscosities of MP 39 presented in this work (□) from the fitting curve, Table 4.9. Error bar corresponds to our experimental uncertainty over the whole temperature range.

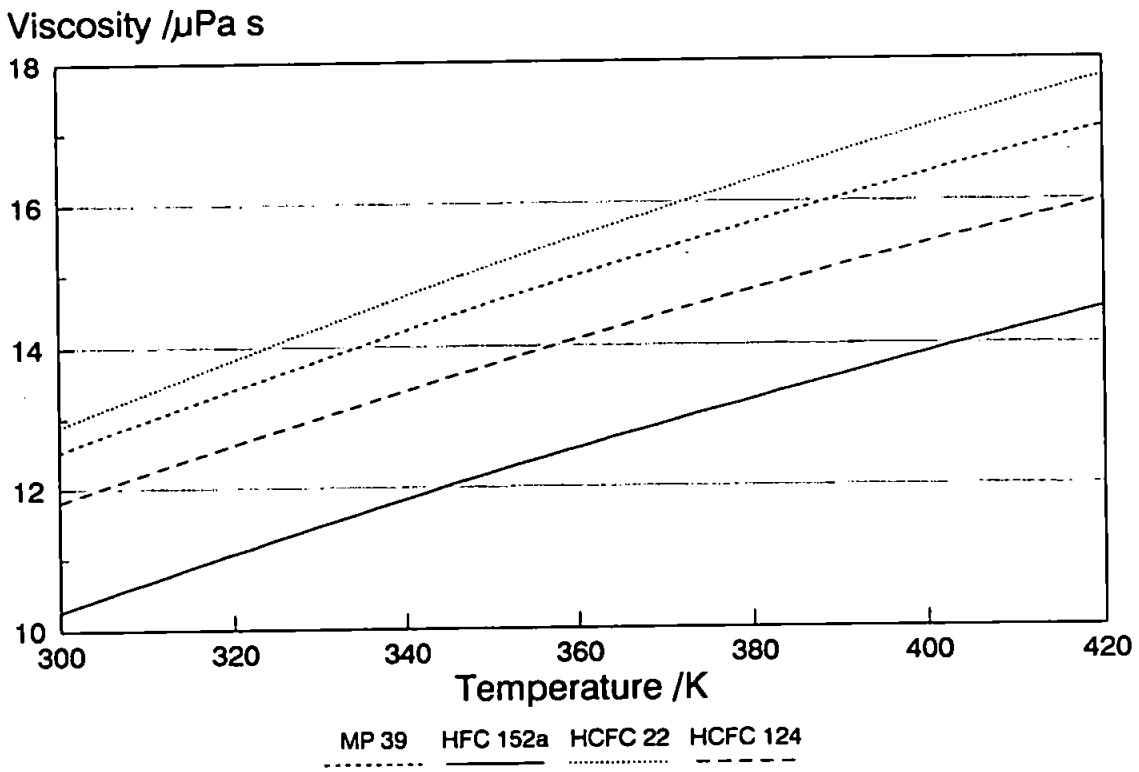

Figure 4.9 Comparison of the measured viscosity of MP 39 with the viscosities of its components.

Chapter 5

Calculations within the Chapman Enskog Approximation and Analysis of Results

5.1 Introduction

Measurements of shear viscosity can be used to calculate other physical properties such as thermal conductivity (the transport of kinetic energy along a temperature gradient) and diffusivity (the transport of mass along a concentration gradient). However, the theory proposed by Chapman and Enskog has four important assumptions[1] which are;

1) the gas is sufficiently dilute for only binary collisions to occur.

2) the motion of the molecules during a collision can be described by classical mechanics.

3) only elastic collisions occur.

4) the intermolecular forces act only between fixed centres of the molecules, ie. the molecules are spherically symmetrical.

Within the limitations set by these assumptions, the theory should only be applicable to low pressure, high temperature monatomic gases. Its application to polyatomic gases can be useful for viscosity and diffusivity, but is inappropriate for thermal conductivity for the gases studied here because of storage and transfer of energy into and from internal modes.

The viscosity data measured for this work and presented in Chapter 4 has therefore only been used to calculate self diffusion coefficients for each of the sample gases. For interest, the collision diameter for each of the sample gases has also been calculated, assuming that the molecules consist of hard spheres.

We apply the Extended Law of Corresponding States to the Chapman Enskog equation to;

1) Optimise the well depth of HFC 134a and HCFC 123 for a fit to our viscosity data

(Tables 4.5 and 4.6) using a fixed collision diameter obtained from published sources.[2]

2) Calculate viscosities for HFC 134a and HCFC 123 using the optimum well depth and comparing them to our measured viscosities.

3) Calculate an optimum well depth for a fit to both viscosity and bulk second virial coefficients for HFC 134a and HCFC 123. We also show that Corresponding States acoustic second virial coefficients are incompatible with a fit to viscosity and bulk second virial coefficients.

4) Estimate a well depth and collision diameter for HCFC 124.

The use of the Stockmayer potential energy function by Schramm et al.[3] is discussed and the effect of the dipole on the viscosity of HFC 134a estimated using the Mason Monchick approximation.

Finally, equations based on the Chapman Enskog theory are employed to estimate the mixture viscosity of the ternary blend MP 39 and the results are compared to the measured viscosities of this work.

5.2 Self Diffusion Coefficients

As mentioned previously (Section 2.4.3), self diffusion is a measure of the diffusion of a dilute gas into itself which, in practice, is measured by the diffusion of one isotope of the gas into another. This property is virtually independent of the inelasticity of collisions, and it is therefore valid to calculate it by means of the Chapman Enskog theory, which itself assumes an absence of inelastic collisions.[4]

$$\eta = \frac{5}{16}\left(\frac{mkT}{\pi}\right)^{1/2} \cdot \frac{1}{\sigma^2\,\Omega^{(2,2)*}(T^*)} \tag{5.1}$$

Here m is the mass of a molecule, k is the Boltzmann constant, σ is the collision diameter (distance at which the interaction energy passes through zero) and T^* is the reduced

temperature $= kT/\varepsilon$, where ε is the well depth (maximum attractive energy). (Note that throughout this discussion, we divide the value of the well depth ε by the Boltzmann constant k to give ε/k with units of Kelvins). Values for the self diffusion coefficient D may be calculated from experimental shear viscosities using the Chapman Enskog relation below.

$$pD = \frac{6}{5} \frac{A^* \eta RT}{M} \tag{5.2}$$

The self diffusion coefficients D are usually expressed as the product pD, where p is the pressure in Nm^{-2}, and pD has units of Ns^{-1}. M is the relative molecular mass, T the thermodynamic temperature in Kelvins, R the gas constant and A^* is the following ratio of collision integrals:

$$A^* = \frac{\Omega^{(2,2)*}(T^*)}{\Omega^{(1,1)*}(T^*)} \tag{5.3}$$

Values of A^* are relatively insensitive to the potential function used to generate them; we have adopted the average of the A^* values calculated from the Lennard-Jones 12-6 and Lennard-Jones 9-6 potential functions, these A^* values differing from each other by only 0.7%. Although Equation 5.2 is accurate only for gases within the Chapman Enskog approximation with no internal degrees of freedom, the diffusion of a polyatomic gas is not highly sensitive to the exchange of energy into and from internal modes, and Equation 5.2 therefore provides a useful approximation. The results of our calculations are given in Table 5.1.

The calculation of a self diffusion coefficient for MP 39 is very approximate, because in order to obtain a reduced temperature (for the calculation of A^*), the geometric mean of the well depths of the three components (HCFC 22, HFC 152a and HCFC 124) was calculated in line with the common combining rules of Lorentz-Berthelot.[4] The well

Table 5.1 Calculated self diffusion coefficients for HFC 134a, HCFC 123, HCFC 124 and MP 39. Units explained in text.

Temperature /K	HFC 134a pD /Ns^{-1}	HCFC 123 pD /Ns^{-1}	HCFC 124 pD /Ns^{-1}	MP 39 pD /Ns^{-1}
283.15			0.262	
308.15	0.410	0.248	0.304	0.443
323.15	0.450	0.273	0.335	0.481
343.15	0.507	0.301	0.372	0.538
363.15	0.561	0.340	0.418	0.610
383.15	0.622		0.457	0.658
403.15	0.686		0.507	0.737

depths used were 307.3 K[5], 177.6 K[3] and 275.8 K[6] respectively. If only the well depths are known and not the shape of the potential function, then this is the best estimate which can be obtained.[7] The use of these well depths is discussed later (Section 5.6.4).

5.3 Calculation of the Hard Sphere Collision Diameter

It is of interest to calculate the collision diameter $\bar{r}$ for hard sphere molecules having the same viscosity (and hence collision integral) as the real molecule at a particular temperature. The collision integral $\Omega^{(2,2)*}(T^*)$ may be regarded as the correction term which converts σ^2 to $\bar{r}^2$. Thus:

$$\bar{r}^2 = \sigma^2 \Omega^{(2,2)*}(T^*) = \Omega^{+(2,2)}(T) \tag{5.4}$$

The term $\Omega^{+(2,2)}(T)$ has been used by Clancy et al.[8] to produce the following rearrangement and simplification of Equation 5.1:

$$\bar{r} = 0.5166 \left[\frac{(MT)^{1/2}}{\eta} \right]^{1/2} \delta_\eta \tag{5.5}$$

Here $\bar{r}$ is in nm, M is in g mol^{-1}, T is in K and η is in 10^{-7} kg m^{-1} s^{-1}. δ_η is a factor in the range 1.000-1.008 which we assume to be unity.

The calculated hard sphere collision diameters for each of the hydrofluoroalkanes at our experimental temperatures are given in Table 5.2.

5.4 The Extended Law of Corresponding States

The application of the Extended Law of Corresponding States to shear viscosities uses Equation 5.1. Kestin, Ro and Wakeham[9] have developed the following empirical expression for $\Omega^{(2,2)*}(T^*)$, which is an averaged value for a range of simple gases;

Table 5.2 Calculated temperature-dependent hard-sphere collision diameters for HFC 134a, HCFC 123, HCFC 124 and MP 39.

Temperature /K	HFC 134a $\bar{r}$ /nm	HCFC 123 $\bar{r}$ /nm	HCFC 124 $\bar{r}$ /nm	MP 39 $\bar{r}$ /nm
283.15			0.679	
308.15	0.621	0.722	0.671	0.600
323.15	0.614	0.712	0.662	0.597
343.15	0.605	0.710	0.657	0.590
363.15	0.600	0.696	0.646	0.577
383.15	0.593		0.643	0.578
403.15	0.586		0.634	0.567

$$\Omega^{(2,2)*}(T^*) = \exp[0.45667 - 0.53955(\ln T^*) + 0.187265(\ln T^*)^2 - 0.03629(\ln T^*)^3 + 0.00241(\ln T^*)^4] \qquad 1 < T^* < 90 \tag{5.6}$$

The gases covered by this equation were mainly non-polar, but included some polar gases such as HCFC 22 ($CHClF_2$). This gas has a dipole moment parameter $\delta_{max} = 0.25$, where;

$$\delta_{max} = \frac{\mu^2}{8\pi\varepsilon_0\varepsilon\sigma^3} \tag{5.7}$$

Here μ is the dipole moment in units of Debyes and ε_0 is the permittivity of free space.[4,5] Using the collision diameter and well depth of HCFC 22,[5] this corresponds to a dipole moment μ of 1.42 D.

The Extended Law of Corresponding States is an extension to all gases of the Corresponding States principle for spherical, non-polar gases. The validity of the equation may therefore decrease with increasing dipole moment unless additional correlation parameters are included. The dipole moment of HCFC 123 is 1.356 ± 0.019 D,[10] and that of HCFC 124 is 1.469 ±0.012 D.[11] These dipole moments are both similar to that of HCFC 22. However HFC 134a has a dipole moment of 2.058 ± 0.01 D.[11] This dipole moment is considerably greater than that of HCFC 22, and thus the Extended Law of Corresponding States correlation may be less valid.

5.4.1 Corresponding States fit to Viscosity Only

Within the framework of these approximations, a spreadsheet file has been developed for HFC 134a, HCFC 123 and HCFC 124 which calculates shear viscosities based on Equations 5.1 and 5.6. (MP 39 is a different case which is explained in Section 5.6). Viscosity is calculated at each of our nominal temperatures for each of the sample gases and compared with measured viscosities[2,6,12] to obtain an rms deviation. In order

to calculate an rms deviation for the measured viscosities of other workers[2,12] at our nominal temperatures, a fitting curve must be employed. Nabizadeh and Mayinger[2] fail to provide a fitting function in their paper for both HFC 134a and HCFC 123, so we have deduced them both (Table 5.3) for a fitting curve of the form in Equation 4.1, using the Minitab statistics package we have employed to produce the fitting curve for our viscosity data. Takahashi et al.[12,13] provide fitting functions for their measurements of HFC 134a and HCFC 123 viscosities, which are shown in Equations 5.8 and 5.9 respectively.

$$\eta = 4.366\times10^{-2}T - 6.832\times10^{-6}T^2 \tag{5.8}$$

$$\eta = 3.904\times10^{-2}T - 8.548\times10^{-6}T^2 \tag{5.9}$$

Here, T is in Kelvins and η is in μPa s.[14]

Inspection of Equation 5.1 and the definition of its terms shows that to relate the Corresponding States correlation to experimental viscosities both the well depth and collision diameter are required. We do not have experimental measurements over a sufficient range to allow independent fitting of these two parameters. We have therefore used Nabizadeh and Mayinger's collision diameters for HFC 134a and HCFC 123, and by adjusting the value of the well depth on the spreadsheet, have been able to optimise the well depth to generate Extended Corresponding States viscosities which best fit our measured viscosities for these gases. The optimum fit for both HFC 134a and HCFC 123 is taken as the minimum rms deviation between the calculated viscosities and our measured viscosities on the spreadsheet. The optimisation graphs for HFC 134a and HCFC 123 are shown in Figures 5.1 and 5.2 respectively. 'Deviation /%' is the rms deviation for measured viscosities over our experimental range. The well depths which are derived from the optimisations of Figures 5.1 and 5.2 are 283 K for HFC 134a and 279 K for HCFC 123, also listed in Table 5.4. Figures 5.1 and 5.2 also show optimisations using other workers' measured viscosities. When the viscosities of Nabizadeh and Mayinger[2] are used, we obtain well depths within 1 K of their

Table 5.3 Coefficients of the Curve $ln(\eta/S)=AlnT+B/T+C/T^2+D$ for the HFC 134a and HCFC 123 viscosity measurements of Nabizadeh and Mayinger.[2]

Gas	Temperature /K	A	B/K	D	S/μPa s
HFC 134a	302-425	0.3679	-207.20	1.076	1
HCFC 123	303-424	0.6238	-114.37	-0.791	1

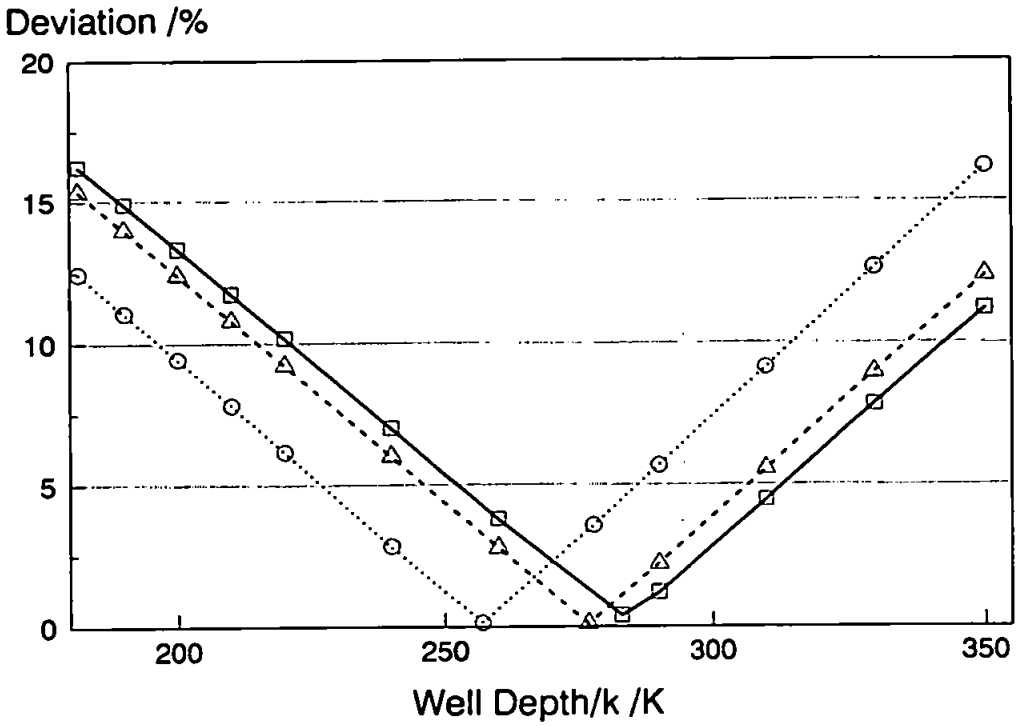

Figure 5.1 Optimisation of the HFC 134a well depth for a fit to viscosity using Nabizadeh and Mayinger's collision diameter of 0.5067 nm. □, this work; Δ, ref. 2; O, ref. 12.

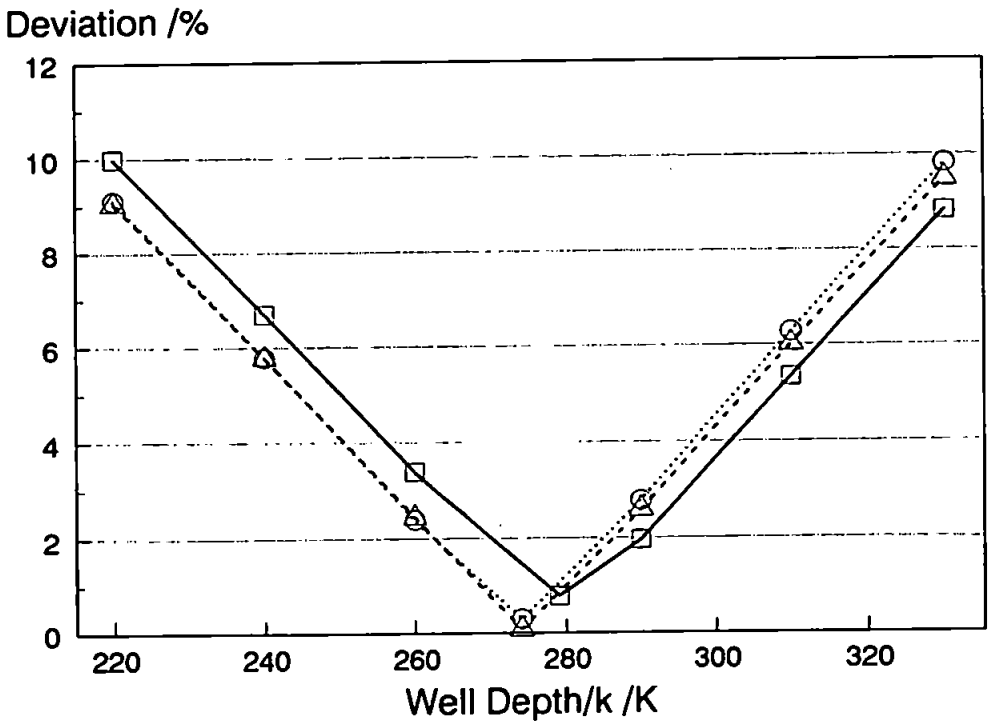

Figure 5.2 Optimisation of the HCFC 123 well depth for a fit to viscosity using Nabizadeh and Mayinger's collision diameter of 0.5909 nm. □, this work; Δ, ref. 2; O, ref. 13.

Table 5.4 ε/k and σ values for HFC 134a, HCFC 123 and HCFC 124.

Gas	Workers	Method of Analysis	Properties	Well Depth ε/k /K	Collision Diameter σ /nm
HFC 134a	This work	Corresponding states	Viscosity	283	0.5067
	This work	Corresponding states	Viscosity, bulk 2nd virial coefficients	350	0.5067
	Nabizadeh and Mayinger[2]	Corresponding states	Viscosity	277.74	0.5067
	Schramm et al.[3]	Stockmayer potential function	Bulk 2nd virial coefficients	181.5	0.4455
	Schramm et al.[3]	Stockmayer potential function	Viscosity, bulk 2nd virial coefficients	156.0	0.4868
	Goodwin and Moldover[19]	Square well potential function	Acoustic 2nd virial coefficients	629.5	0.373
	Goodwin and Moldover[19]	Square well potential function	Bulk and acoustic 2nd virial coefficients	601.6	0.399
HCFC 123	This work	Corresponding states	Viscosity	279	0.5909
	Dowdell and Matthews[6]	Corresponding states	Viscosity, bulk 2nd virial coefficients	380	0.5909
	This work	Corresponding states	Viscosity, bulk 2nd virial coefficients	420	0.56
	Nabizadeh and Mayinger[2]	Corresponding states	Viscosity	275.16	0.5909
	Takahashi et al.[13]	Not known by the present authors	Viscosity	340	0.56
	Goodwin and Moldover[20]	Square well potential function	Bulk and acoustic 2nd virial coefficients	605	0.475
HCFC 124	This work	Corresponding states	Viscosity	275.8	0.550

recommended values of 277.74 K and 275.16 K for HFC 134a and HCFC 123 respectively, as expected. The measured viscosities of Takahashi et al. give a lower well depth for HFC 134a[12] of 257 K, Figure 5.1, but the same well depth as Nabizadeh and Mayinger for HCFC 123,[13] Figure 5.2. Overall the spread of well depths in Figure 5.1 is generated by the spread of experimental results shown in Figure 4.5, and correspondingly the greater agreement in the HCFC 123 results, Figure 4.6, generates closer estimates of the well depth in Figure 5.2.

Using the optimised well depths for HFC 134a and HCFC 123 derived above, the maximum deviation of the calculated viscosities from our measured data is 0.5% and 1.3% respectively.

5.4.2 Corresponding States Fit to Viscosity, Bulk Second Virial Coefficients and Acoustic Second Virial Coefficients

We also attempt simultaneously to optimise the fit to both shear viscosities and bulk second virial coefficients for HFC 134a and HCFC 123. The Corresponding States principle is thus extended to non-spherical, polar gases for both viscosities and bulk second virial coefficients, and a further level of approximation is introduced.

Bulk second virial coefficients are calculated on our spreadsheet file using the Corresponding States correlation in Equation 5.10.[15]

$$B(T)=b_0 B(T^*) \tag{5.10}$$

Here b_0 is $1261.3\sigma^3$ for σ in nm and b_0 in cm^3mol^{-1}. The reduced second virial coefficient ($B(T^*)$) can be found from;[15]

$$B(T^*) = (T^*)^{1/2} - 0.7175 + 0.2377 lnT^* + 0.50172(\ln T^*)^2 - 0.1026(\ln T^*)^3 + 0.0068(\ln T^*)^4 \exp\left(\frac{1.0582}{T^*}\right) \tag{5.11}$$

$$0.5 < T^* < 130$$

The calculated values for the second virial coefficients at our nominal temperatures are then compared with published second virial coefficients for HFC 134a and HCFC 123. In order to obtain a comparison at our nominal temperatures, fitting functions are used to calculate published second virial coefficients at each of our measured temperatures.

Tillner-Roth and Baehr[16] made pressure, density and temperature measurements of HFC 134a with a Burnett apparatus and obtained values of HFC 134a second virial coefficients from isothermally fitted truncated virial expansions. They provide a fitting function of the form in Equation 5.12 to describe the change in second virial coefficient with temperature.

$$B(\tau)/B_0 = b_1\tau^{0.25} + b_2\tau^{1.75} + b_3.\exp(\alpha\tau) \qquad (5.12)$$

Here B_0 is 1 cm^3mol^{-1} and τ is equivalent to T_c/T with T_c being the critical temperature. The parameters b_1, b_2, b_3 and α are 120.32, -376.30, -0.14126 and 4.7539 respectively with a value for T_c of 374.18 K.

In the absence of a fitting function for the measured second virial coefficients of Schramm et al.,[3] a function of the form in Equation 5.12 was adopted using the Minitab statistics package to obtain a fitting curve with 0% deviation from the actual data points of Schramm et al. In this case the coefficients b_1, b_2, b_3 and α were 22.4248, -330.214, -0.226964 and 4.7539.

Weber has made vapour pressure and gas phase measurements of HFC 134a[17] and HCFC 123[18] on a Burnett apparatus. For HFC 134a, a fitting function of the form in Equation 5.13 is given to describe the change in second virial coefficient with temperature.

$$B(T) = 1000\left(B_0 + B_1\exp(520/T)\right) \qquad (5.13)$$

Here T is in Kelvins and $B(T)$ is in cm^3mol^{-1}. The coefficients B_0 and B_1 are 0.242848 and -0.128252 respectively. For HCFC 123, a fitting function of the form in Equation 5.14 is given.

$$B(T) = B_0 + B_1\tau + B_2\tau^2 + B_3\tau^3 \qquad (5.14)$$

Here τ is $T^{0.5}$, B_0 is 2.47362, B_1 is -1.80284 x 10^2, B_2 is 4.62679 x 10^3 and B_3 is -4.41843 x 10^4. However, this fitting function is valid between 358 K and 453 K, and thus only one of our data points falls within this range (363.15 K).

Goodwin and Moldover have taken speed of sound measurements using a spherical acoustic resonator to obtain calculated acoustic second virial coefficients from which bulk second virial coefficients have been estimated for HFC 134a[19] and HCFC 123.[20] In order to represent the bulk second virial coefficients, they used a square-well model intermolecular potential (Equation 5.15).

$$B(T) = b_0 \left[1 - (r^3 - 1)\Delta \right] \qquad (5.15)$$

Here b_0 is the co-volume, r is the ratio of the radius of the well to the radius of the hard core and Δ can be found by;

$$\Delta = \exp\left(\frac{\varepsilon}{k}/T\right) - 1 \qquad (5.16)$$

Parameters for HFC 134a, suggested by Goodwin and Moldover, which best fit their own calculations of second virial coefficients plus the measurements of Weber[17] are b_0 = 79.95 cm^3mol^{-1}, r = 1.2807 and the well depth ε/k is 601.6 K (Table 5.4).

For HCFC 123, the parameters adopted by Goodwin and Moldover for Equations 5.15 and 5.16 are b_0 = 135.189 cm^3mol^{-1}, r = 1.32437 and ε/k is 605 K (Table 5.4).

Having calculated other workers' second virial coefficients at our nominal temperatures, an rms deviation can be obtained between our calculated values for the second virial coefficient and their values. Taking Nabizadeh and Mayinger's collision diameter of 0.5067 nm for HFC 134a, the deviations of the calculated properties minimise as shown in Figure 5.3. The viscosities and second virial coefficients together suggest a well depth of around 350 K, also shown in Table 5.4. Hence a fit to both viscosity and

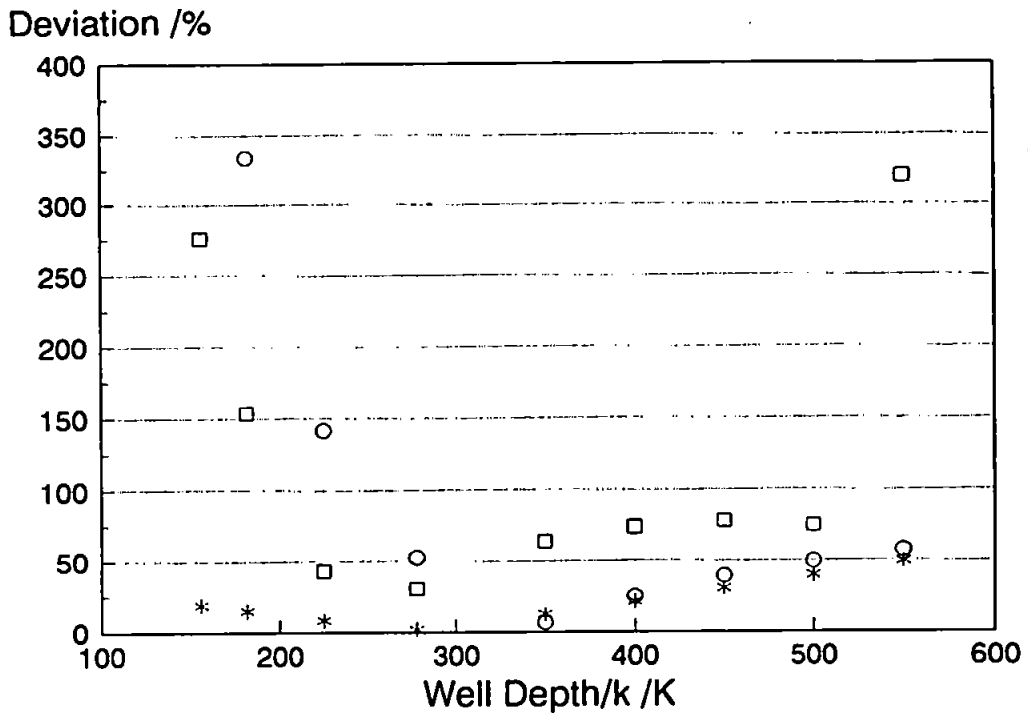

Figure 5.3 Optimisation of the HFC 134a well depth for a fit to viscosity and second virial coefficients using Nabizadeh and Mayinger's collision diameter of 0.5067 nm. ✳, viscosity[2, 6, 12]; ○, second virial coefficient[3, 16, 17, 19]; □, acoustic second virial coefficient[19].

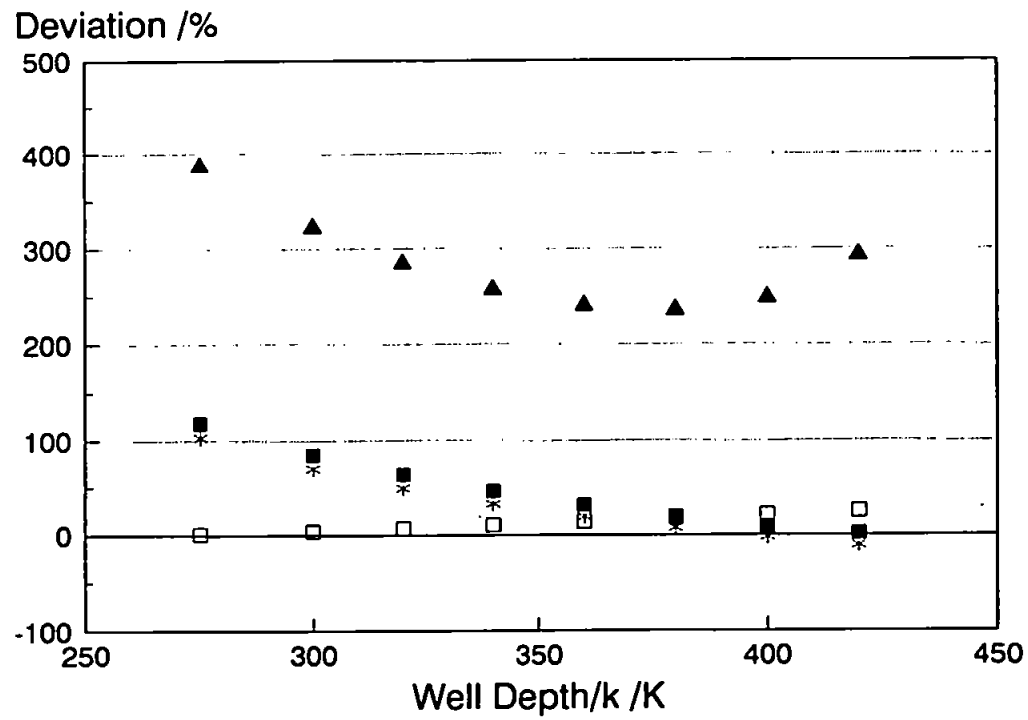

Figure 5.4 Optimisation of the HCFC 123 well depth for a fit to viscosity and second virial coefficients using Nabizadeh and Mayinger's collision diameter of 0.5909 nm. □, viscosity[2, 6, 13]; ✳[18], ■[20], second virial coefficient; ▲, acoustic second virial coefficient[20].

second virial coefficients increases the optimum well depth when compared to a fit to viscosities only, which produced an optimum well depth of 283 K to our data and 277.74 K to Nabizadeh and Mayinger's.

The same procedure as used for HFC 134a has been adopted for HCFC 123. Nabizadeh & Mayinger use an effective well depth ε/k of 275.16 K and collision diameter σ of 0.5909 nm (Table 5.4). We have used these values of ε/k and σ to calculate bulk second virial coefficients, and have compared the calculated values to measurements made by Weber[18] and Goodwin & Moldover,[20] as well as other HCFC 123 viscosity measurements made by Nabizadeh and Mayinger[2] and Takahashi et al.[13] (Figure 5.4). Only one bulk second virial coefficient of Weber[18] is in our experimental range, and the absolute percentage deviation of this point is therefore plotted. Figure 5.4 shows that a fit to both viscosities and second virial coefficients optimises at around 380 K.

Another literature value of σ was then tested by the same procedure. Takahashi et al.[13] have made viscosity measurements using an oscillating disc viscometer, and suggest σ = 0.560 nm (Table 5.4), Figure 5.5. As with the HFC 134a results both Figures 5.4 and 5.5 suggest that when second virial coefficients are taken into account, a higher well depth is appropriate than that implied by fitting to viscosity only. The optimum value for σ = 0.5909 nm is 380 K, Figure 5.4, in contrast to 275.16 K for viscosity only[2] (Table 5.4), and for σ = 0.560 nm the optimum is 420 K in contrast to 340 K for viscosity only[13] (Table 5.4).

As well as fitting Corresponding States viscosities and bulk second virial coefficients, Figures 5.3 to 5.5 demonstrate the incompatibility of fitting acoustic virial coefficients, which have been calculated on our spreadsheet file using the equations of Goodwin and Moldover (Equations 5.17 to 5.19).[19, 20] Perfect gas heat capacities for HFC 134a and HCFC 123 may be calculated using Equations 5.17 and 5.18 respectively below;

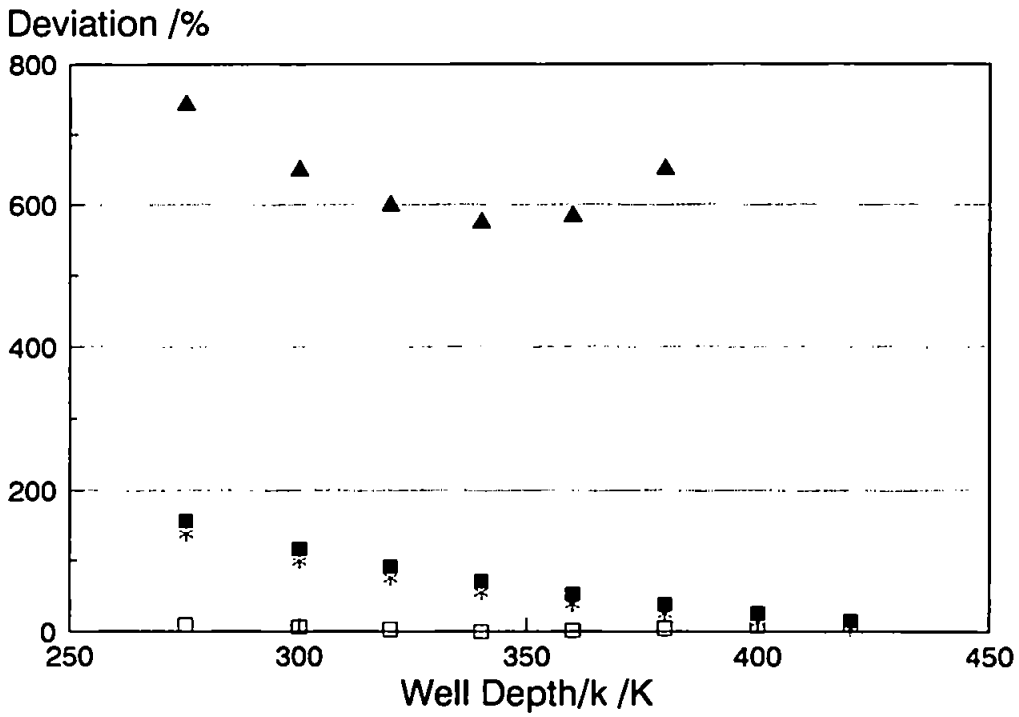

Figure 5.5 Variation of deviation of HCFC 123 with well depth for Takahashi et al.'s collision diameter of 0.56 nm. □, viscosity[2, 6, 13]; ✳[18], ■[20], second virial coefficient; ▲, acoustic second virial coefficient[20].

$$C_{p,m}^{pg} / R = 2.2540 + 0.0317(T) - 16.8 \times 10^{-6}(T)^2 \quad (5.17)$$

$$C_{p,m}^{pg} /R = 1.531 + 0.04963(T) - 4.474 \times 10^{-5}(T)^2 \quad (5.18)$$

The zero pressure limit of the heat capacity ratio γ_0 is then found using;

$$C_{p,m}^{pg}/R = \gamma_0/(\gamma_0-1) \quad (5.19)$$

Finally, using second virial coefficients ($B(T)$) calculated from our viscosity measurements (Equation 5.10), the acoustic second virial coefficient (β_a) can be obtained from Equation 5.20.

$$\beta_0=2B(T)+2(\gamma_0-1)T\frac{dB(T)}{dT}+\frac{(\gamma_0-1)^2}{\gamma_0}T^2\frac{d^2B(T)}{dT^2} \quad (5.20)$$

The values of the acoustic second virial coefficients obtained from this expression were compared to the values of Goodwin and Moldover[19,20] to obtain an rms deviation.

Figure 5.3 for HFC 134a and Figures 5.4 and 5.5 for HCFC 123 suggest that the acoustic virial coefficients of Goodwin and Moldover cannot be accommodated by interaction parameters in these ranges. For HCFC 123, Goodwin and Moldover themselves analyzed their data using a square well potential function (Equations 5.15 and 5.16) with σ = 0.475 nm and ε/k = 605 K (Table 5.4). If their value of σ = 0.475 nm is used in an Extended Law of Corresponding States correlation, then the acoustic virial coefficients remain incompatible, and bulk second virial coefficients and viscosities optimise around 580 K, Figure 5.6. It is of interest to note that the calculation methods of Goodwin and Moldover, which are obviously incompatible with our own Corresponding States calculations, yield smaller collision diameters and very much higher well depths than any other calculation method.

Even with more than one property being used in the determination of interaction

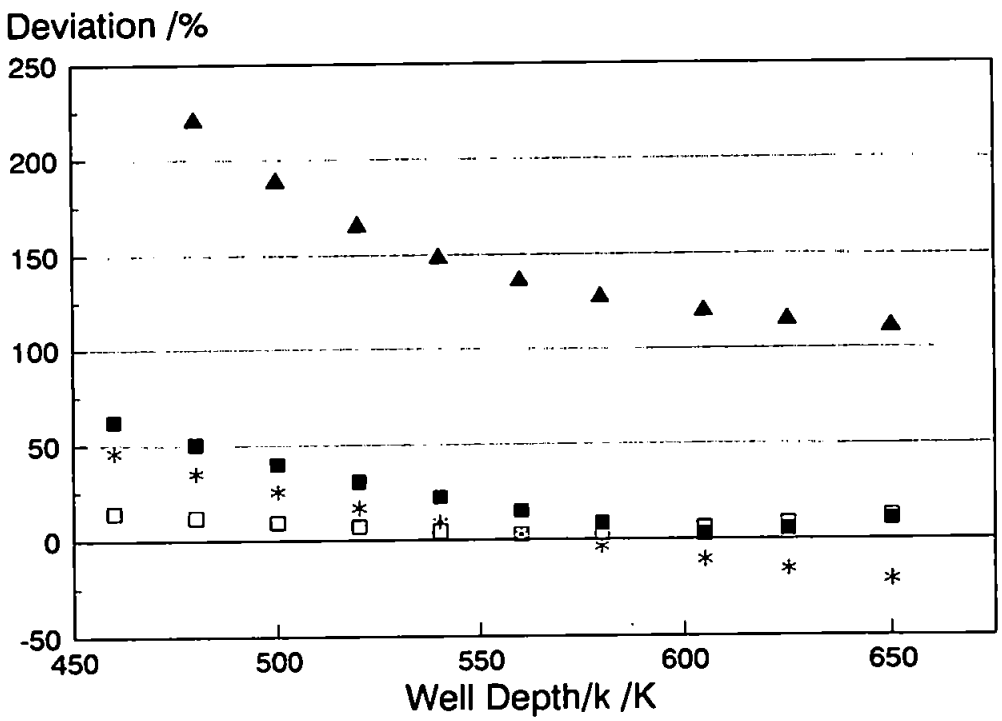

Figure 5.6 Variation of deviation of HCFC 123 with well depth for Goodwin and Moldover's collision diameter of 0.475 nm. □, viscosity[2, 6, 13]; ✳[18], ■[20], second virial coefficient; ▲, acoustic second virial coefficient[20].

parameters, it is difficult independently to derive optimum values of both the well depth and collision diameter.

5.4.3 Corresponding States Optimisation of HCFC 124 Potential Parameters

No other workers have estimated the collision diameter of HCFC 124. The structure of HCFC 124 is intermediate between that of HFC 134a and HCFC 123. We therefore took three equally spaced values between the well depths of HFC 134a and HCFC 123, and optimised the collision diameter for each well depth. All three resulting collision diameters were 0.550 nm. The optimum fit to viscosities, ranging from an rms deviation of 1.05% - 1.07%, was insensitive to the initial choice of well depth. The well depth of 275.8 K listed in Table 5.4 is that which gave the lowest rms deviation of 1.05% (Figure 5.7).

5.5 The Stockmayer Potential Function

The difference in the collision diameter and well depth used by Schramm et al.[3] and Nabizadeh and Mayinger,[2] is due to the choice of pair potential energy function utilised by the two groups of workers. Nabizadeh and Mayinger[2] opted for the averaged function shape with no dipole moment, implicit in the Extended Law of Corresponding States. However Schramm et al.[3] used the Stockmayer potential to calculate viscosities:

$$U(r) = 4\varepsilon\left\{\left(\frac{\sigma}{r}\right)^{12} - \left(\frac{\sigma}{r}\right)^{6}\right\} - \frac{\mu^2}{4\pi\varepsilon_0 r^3}\,\zeta(\theta_1,\theta_2,\phi) \qquad (5.21)$$

This equation describes the interaction of two point dipoles with dipole moment μ. Here r is the distance between the centres of mass of the two molecules, and ζ a function of the relative orientation of the molecules described by the angles θ_1, θ_2 and ϕ.[4] Schramm et al.[3] found that in order to obtain a good fit to experimental viscosities, a smaller well

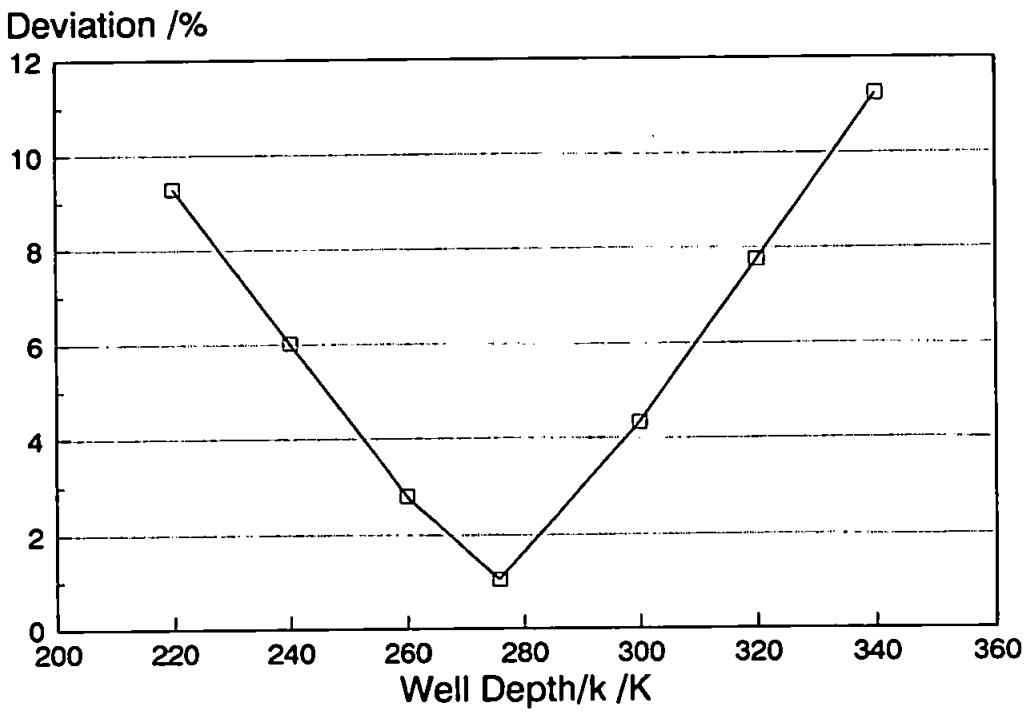

Figure 5.7 Optimisation of the HCFC 124 well depth based on a collision diameter of 0.550 nm.

depth and a larger collision diameter were required than when fitted to measured second virial coefficients only (Table 5.4). The well depth of 181.5 K and collision diameter 0.4455 nm were derived by the fitting of Stockmayer second virial coefficients to their own experimental second virial coefficients. The second set ε/k = 156.0 K and σ = 0.4868 nm was obtained by simultaneously fitting Stockmayer second virial coefficients to their own experimental virial coefficients and Stockmayer viscosities to Nabizadeh and Mayinger's experimental viscosities. The Lennard-Jones 12-6 potential function, which describes the non-polar interaction within the Stockmayer function, is generally inexact for spherical molecules,[4] and is obviously inexact for non-spherical molecules. Furthermore the dipole moment does not in fact act from a point at the centre of mass of each molecule, as the Stockmayer function assumes. Schramm and his co-workers themselves note the inflexibility of the Stockmayer potential function.[3] They also confirm that the shape as well as the dipole moment must be taken into account in a "real three-dimensional molecule", and they therefore use the reduced dipole moment as a fitting parameter rather than an experimental parameter. The reduced dipole moment t^* is defined as:

$$t^* = \frac{\mu^2}{\sqrt{8}\,\varepsilon\,\sigma^3\,(4\pi\varepsilon_0)} = \frac{\delta_{max}}{\sqrt{2}} \qquad (5.22)$$

Schramm et al.[3] use t^* = 1.4 for HFC 134a for a fit to second virial coefficients and viscosities, which corresponds to a dipole moment μ of 3.136 D. This contrasts to the experimental dipole moment, mentioned earlier, of 2.058 D.[11]

5.5.1 Effect of the Dipole Moment on Viscosity

Mason and Monchick have calculated omega integrals $\Omega^{(2,2)^*}(T^*)$ for the Stockmayer potential energy function for a range of values of the dipole moment parameter δ_{max} (Equation 5.7) from 0 to 2.0. (δ_{max} = 0 represents the Lennard Jones 12-6 potential

function for non-polar gases). They assumed that each binary collision takes place at a single relative orientation of the molecules.[4] The collision integrals $\Omega^{(l,s)^*}(T^*)$ are defined as equally weighted averages for each fixed orientation θ, so that:

$$\Omega^{(l,s)^*}(T^*) = \langle \Omega^{(l,s)^*}(T^*,\theta) \rangle = \frac{1}{2} \int_{-1}^{+1} \Omega^{(l,s)^*}(T^*,\theta)\, d(\cos\theta) \qquad (5.23)$$

Here l and s are the small integers determining the type of integral required for each particular transport property. The calculations of Mason and Monchick, shown in Figure 5.8,[4] allow us to gain an idea of the relative effect of the dipole moment on viscosity.

The dipole moment of HFC 134a is 2.058 D,[11] as mentioned previously. Its well depth is 156.0 K and collision diameter is 0.4868 nm from a fit of the Stockmayer potential function to both bulk second virial coefficients and viscosities,[3] Table 5.4. Insertion of these various parameters into Equation 5.7 gives $\delta_{max} = 0.85$. The reduced temperature range of the calculations of Schramm et al., using their recommended well depth, is $T^* = 1.5$ to 3.8. Using Figure 5.8, we find that over this range, the δ_{max} value increases $\Omega^{(2,2)^*}(T^*)$ by approximately 9%. This change in $\Omega^{(2,2)^*}(T^*)$ gives an idea of the magnitude of the effect of the dipole moment on viscosity. However this magnitude will not be 9%, because other parameters in Equation 5.1 will change on moving from a hypothetical non-polar to the real polar molecule.

Finally we recollect the use of t^* as a fitting parameter by Schramm et al.,[3] which corresponds to $\mu = 3.136$ D for HFC 134a, rather than the experimental value of 2.058 D. If the dipole moment of the molecule really was this high, then δ_{max} would be 2.0 (Equation 5.7), and $\Omega^{(2,2)^*}(T^*)$ would be approximately 50% higher.

5.6 Calculation of Low Pressure Gas Viscosity of the Ternary Blend MP 39

The rigorous kinetic theory of Chapman and Enskog (Equation 5.1) can be extended to calculate the low pressure gas viscosities of multi-component blends such as

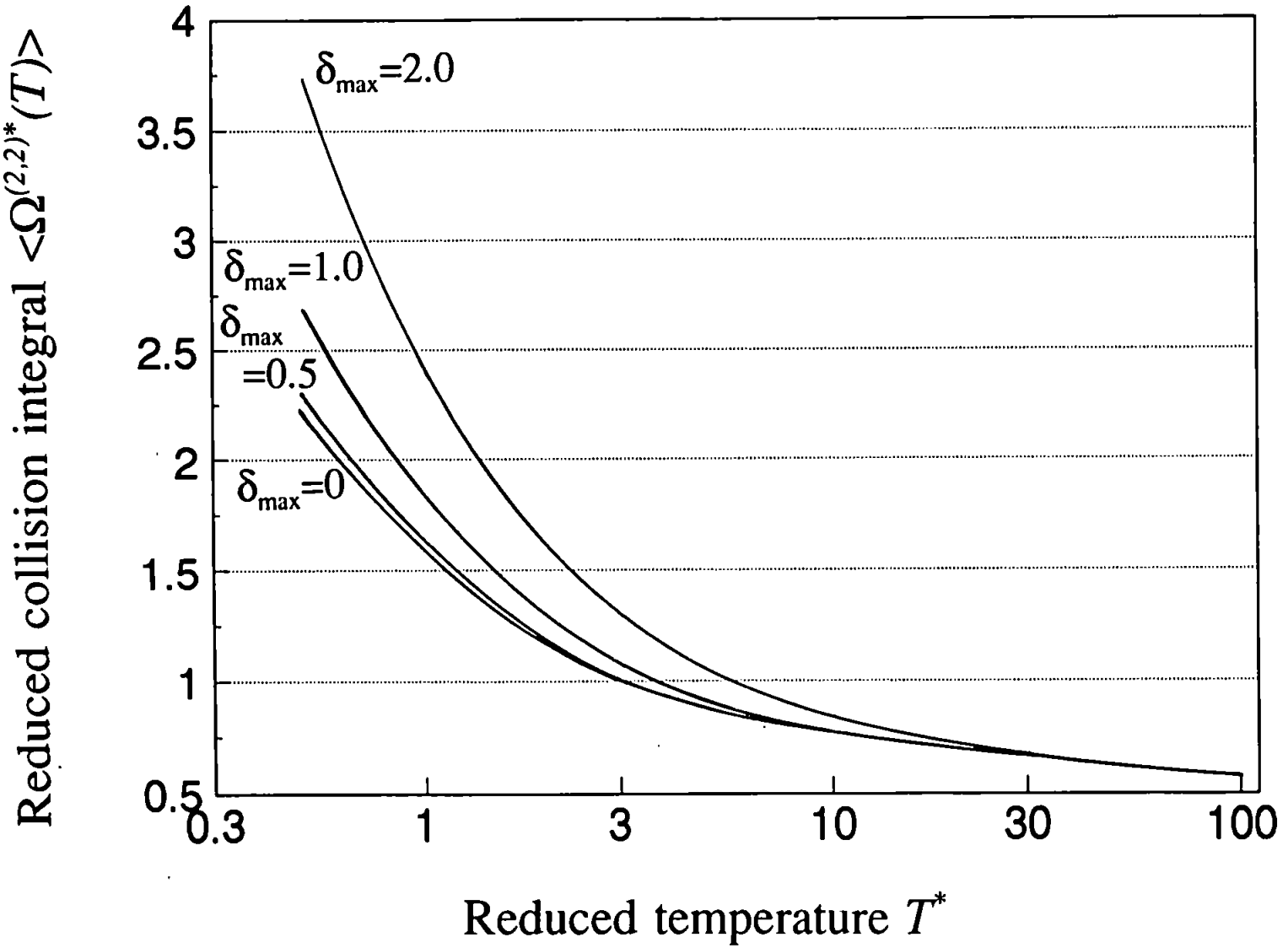

Figure 5.8 The reduced collision integral $<\Omega^{(2,2)*}(T^*)>$ for a Stockmayer potential.

MP 39. The resulting expression gives a ratio of two determinants containing variables including mole fractions, molecular weights, pure component viscosities and temperature. If second order effects are neglected the solution can be approximated in a series as;[1]

$$\eta_m = \sum_{i=1}^{n} \frac{y_i \eta_i}{\sum_{j=1}^{n} y_j \phi_{ij}} \tag{5.24}$$

Here η_m is the viscosity of the mixture, y_i and y_j are mole fractions of two components, and ϕ_{ij} is a parameter used to describe the interaction between two components in a multi-component gas. For a three component gas mixture (such as MP 39), Equation 5.24 expands to;

$$\eta_m = \frac{y_1 \eta_1}{y_1 + y_2 \phi_{12} + y_3 \phi_{13}} + \frac{y_2 \eta_2}{y_2 + y_1 \phi_{21} + y_3 \phi_{23}} + \frac{y_3 \eta_3}{y_3 + y_1 \phi_{31} + y_2 \phi_{32}} \tag{5.25}$$

Here η_1, η_2 and η_3 are the viscosities of each of the pure components and y_1, y_2 and y_3 are the mole fractions of each of those components. Viscosities of the pure components HCFC 22 and HFC 152a were obtained from the fitting functions of other workers (Section 4.7.4).[20, 21] HCFC 124 viscosities were obtained from the fitting curve of our own measurements (Table 4.9). There are three methods available for estimating ϕ_{ij}, each of which is discussed below.

5.6.1 Wilke's Approximation of ϕ_{ij}

Wilke[1] used Sutherland's kinetic theory in order to obtain the expression in Equation 5.26.

$$\phi_{ij} = \frac{[1 + (\eta_i/\eta_j)^{1/2} (M_j/M_i)^{1/4}]^2}{[8(1 + M_i/M_j)]^{1/2}} \tag{5.26}$$

In order to obtain ϕ_{ji}, the subscripts in Equation 5.26 can be interchanged, or the following equation can be used, where M is the relative molecular mass.

$$\phi_{ji}=\frac{\eta_j}{\eta_i}\frac{M_i}{M_j}\phi_{ij} \tag{5.27}$$

5.6.2 Herning and Zipperer Approximation of ϕ_{ij}

Herning and Zipperer proposed the following approximate expression for calculating ϕ_{ij}.[1]

$$\phi_{ij} = \left(\frac{M_j}{M_i}\right)^{1/2} = \frac{1}{\phi_{ji}} \tag{5.28}$$

5.6.3 Brokaw Approximation of ϕ_{ij}

Brokaw suggested that ϕ_{ij} may be obtained from the expression;[1]

$$\phi_{ij} = \left(\frac{\eta_i}{\eta_j}\right)^{1/2} S_{ij}\, A_{ij} \tag{5.29}$$

ϕ_{ji} can be determined by interchanging the subscripts in this equation. The term A_{ij} is a function of the molecular weight ratios of the components and can be found by application of Equation 5.30.

$$A_{ij}=m_{ij}M_{ij}^{-1/2}\left(1+\frac{M_{ij}-M_{ij}^{0.45}}{2(1+M_{ij})+\dfrac{(1+M_{ij}^{0.45})m_{ij}^{-1/2}}{1+m_{ij}}}\right) \tag{5.30}$$

The expressions m_{ij} and M_{ij} can be found from Equations 5.31 and 5.32 respectively.

$$m_{ij} = \left(\frac{4}{(1+M_{ij}^{-1})(1+M_{ij})}\right)^{1/4} \tag{5.31}$$

$$M_{ij}=\frac{M_i}{M_j} \tag{5.32}$$

The term S_{ij} is equal to unity for non-polar components. However, because each of the components of MP 39 are polar, the reduced temperature (T^*) and dipole moment parameter (δ) are required, where δ is calculated by;

$$\delta = \frac{\mu^2}{2\varepsilon\sigma^3} \tag{5.33}$$

In order to calculate the reduced temperature and dipole moment parameter of each of the

components of MP 39, the well depth, collision diameter and dipole moment are required, each of which are given in Table 5.5. The well depth and collision diameter of HFC 152a are Stockmayer parameters obtained from Schramm et al.,[3] whereas the well depths and collision diameters of HCFC 22 and HCFC 124 are Corresponding States parameters obtained from Kestin and Wakeham[5] and this work (Table 5.4) respectively. The dipole moment for HFC 152a and HCFC 124 have been obtained from dielectric constant measurements by Meyer and Morrison,[10] whilst the HCFC 22 dipole moment comes from Kestin and Wakeham.[5]

The term S_{ij} can then be calculated by;

$$S_{ij}=S_{ji}=\frac{1+(T_i^*T_j^*)^{1/2}+(\delta_i\delta_j/4)}{[1+T_i^*+(\delta_i^2/4)]^{1/2}\ [1+T_j^*+(\delta_j^2/4)]^{1/2}} \tag{5.34}$$

5.6.4 Comparison of the Methods used to calculate ϕ_{ij}

The viscosities for MP 39 using the Wilke's, Herning and Zipperer and Brokaw approximations were calculated at each of our nominal temperatures on a Supercalc 5.0 spreadsheet and are displayed in Table 5.6 and Figure 5.9. Inspection of Figure 5.9 shows that it is the Wilke's approximation which produces the closest fit to the measured viscosity of MP 39. It produces a maximum deviation of -2.8% (at 308.15 K) compared to -3.3% and +55.5% at 308.15 K for the Herning and Zipperer approximation and Brokaw approximation respectively. The Brokaw approximation cannot be considered as a serious comparison in this study because Corresponding States and Stockmayer potential energy parameters have been used in its formulation, when strictly a consistent set of parameters should be used, ie. either all Corresponding States or all Stockmayer parameters, in order to maintain compatibility. This problem also arises in the calculation of self- diffusion coefficients for MP 39 (Table 5.1) as the well depths for HCFC 22 and HCFC 124 are based on Corresponding States correlations whereas the well depth for HFC 152a is derived from the Stockmayer potential model. This has been used in the

Table 5.5 Parameters used in the calculation of Brokaw's approximation for MP 39.

MP 39 Component	Well Depth /K	Collision Diameter /nm	Dipole Moment /D
HCFC 22	307.3	0.4565	1.42
HFC 152a	177.6	0.4618	2.262
HCFC 124	275.8	0.550	1.469

Table 5.6 Calculated Viscosities for MP 39 using the Wilke's, Herning and Zipperer and Brokaw approximations.

Temperature /K	Wilke's Approximation /μPa s	Herning and Zipperer Approximation /μPa s	Brokaw Approximation /μPa s
308.15	12.607	12.544	20.182
323.15	13.187	13.123	19.600
343.15	13.960	13.893	20.734
363.15	14.730	14.660	21.863
383.15	15.499	15.425	22.988
403.15	16.264	16.186	24.108

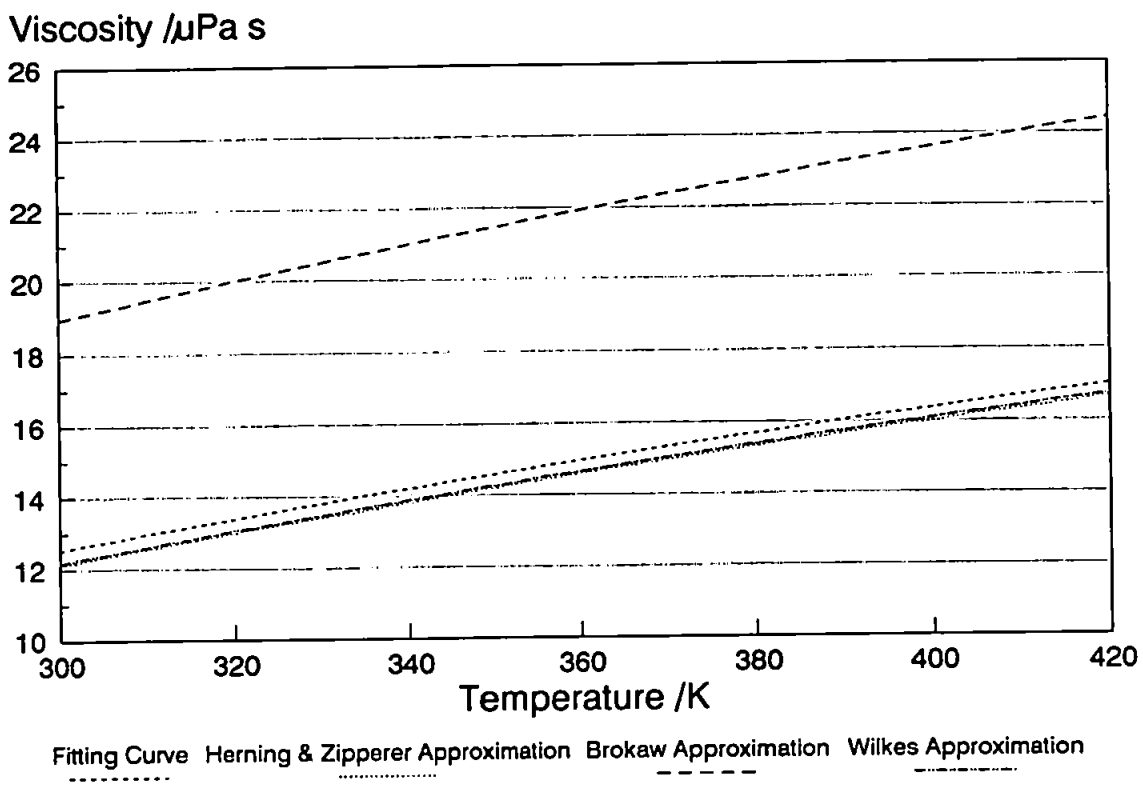

Figure 5.9 Comparison of the measured viscosity of MP 39 with the calculated viscosity based on the Wilke's, Herning and Zipperer and Brokaw approximations for ϕ_{ij}.

absence of a Corresponding States well depth for HFC 152a in the literature.

The Wilke's and Herning and Zipperer approximations have proved successful for non-polar mixtures and produce some good results for polar-polar gas mixtures. Given that MP 39 is a polyatomic mixture, containing non-spherical polar components which fall outside the assumptions imposed by the Chapman Enskog treatment, the calculated viscosities from these two approximations are reasonable.

Chapter 6

The Development of the Chlorine and Bromine Loading Models

6.1 Introduction

Levels of atmospheric chlorine are about 5-6 times higher than natural levels whereas bromine levels are now approximately double what they should be. This long term increase in chlorine and bromine is due to the use and subsequent release of man-made halocarbons, discussed in Chapter 1.

The purpose of the models developed as part of this work is to use globally averaged mass balance equations to predict future levels of atmospheric chlorine and bromine. We also assess the sensitivity of the chlorine and bromine loading to possible forcing factors which may affect both the peak level of chlorine/bromine attained, when that peak occurs, and how quickly levels return to those approaching 'normal'. In this way an insight can be gained as to which factors influence the levels of atmospheric chlorine and bromine, and which are of less significance.

Other workers have modelled future levels of chlorine and bromine.[1-3] However these models have assumed that all halocarbons produced in a year are emitted in that year so no allowance is given for halocarbon retained in equipment for a period of years before emission. This can introduce a phase error into any predictions of future chlorine and bromine loadings.[1] The models presented in this work do take account of how halocarbons are used and introduce an appropriate delay before emission dependent on that use.

6.2 The Evolution of the Models

Initially the models were designed on a Supercalc 5.0 spreadsheet package for the PC, but due to increasing size and complexity, eventually had to be transferred onto an

eXclaim! 0.9 spreadsheet package for a DEC 3100 Workstation. It was decided to base the models on spreadsheets because the nature of the study, ie. sensitivity analyses, lent itself well to their application (as any change in a variable on the spreadsheet will quickly and easily filter through the model and update the final result). Hence use of a spreadsheet based model provides both flexibility and ease of use once it has been set up correctly.

Having decided to use a spreadsheet, a number of steps were taken in bringing the models to their present level of development, and these are discussed in the following sections.

6.2.1 The Choice of Result

The units of the final result can be expressed as chlorine/bromine loadings or ozone depletion potential (ODP) weighted concentrations. The concept of the ODP was introduced in 1981 as a quick reference for estimating the relative effectiveness of a gas at reducing stratospheric ozone. It is defined as the ratio of calculated ozone column change for each mass unit of a gas emitted into the atmosphere relative to the calculated depletion of the reference gas, CFC 11.[4] The ODP provides a useful measure because;

1) It measures cumulative chronic effects on ozone for each unit released into the atmosphere.

2) It yields a single value for each compound rather than a time-dependent multitude of values.

3) It provides an estimate of the calculated effect of a compound compared to the maximum calculated effect of CFC 11 on an equal mass basis.

4) Calculations are easy and inexpensive using models designed to calculate steady state ozone changes.

In order to make the ODP definition consistent, the following criteria were selected;[4,5]

1) Calculations are based on emission rates of each compound required to give a modelled ozone depletion of 1%.

2) Changing concentrations of trace gases affect calculated hydroxyl (OH) concentrations and therefore future depletion. Levels of carbon dioxide, methane, carbon monoxide and nitrous oxide are therefore based on current levels due to uncertainties in future concentrations.

3) The background chlorine level from the long lived CFCs which affect chlorine chemistry throughout the time HCFCs will be used, is assumed to be constant at 3.0 ppbv (parts per billion by volume).

Given these criteria, the ODP is calculated as;

$$ODP = \frac{\left(\frac{\textit{Calculated steady state } O_3 \textit{ depletion (compound X)}}{\textit{Emission rate giving 1\% depletion (compound X)}}\right)}{\left(\frac{\textit{Calculated steady state } O_3 \textit{ depletion(CFC 11)}}{\textit{Emission rate giving 1\% depletion (CFC 11)}}\right)} \qquad (6.1)$$

However there are problems with the ODP concept. Criterion (2) above is important because OH radicals attack 'X' (especially if it is an HCFC) and therefore the hydroxyl concentration in the atmosphere has an influence over the lifetime of 'X'. Methyl chloroform emissions provide an indirect method of assessing global OH levels as its emissions are believed to be known to within 5%. Using observed atmospheric trends and estimated emission data, an averaged lifetime for methyl chloroform can be obtained and therefore an averaged OH concentration. However it is simplistic to assume that the concentration will remain constant in both time and space.

Another problem with ODPs is that they are defined at steady state and therefore are not representative of transient effects. If a CFC and HCFC are both emitted at constant levels, it may take hundreds of years before they reach a steady state concentration ratio, owing to the long lifetime of the CFC. Thus shorter lived compounds

reach a 'steady state' ability to destroy ozone before the longer lived compounds.

The largest problem with the ODP concept is that it does not take into account the heterogeneous chemistry which occurs at the Poles (Chapter 1). These types of reactions depend on the availability of chlorine and bromine at the height of the polar stratospheric clouds (PSCs). As the ODP is based on annually averaged global changes in ozone, and the Poles constitute such a small percentage of the global area, an ODP derived concentration tends to understate the damage due to chlorine and bromine.

Due to the problems associated with ODP weighted concentrations, this method of expressing the results was abandoned in favour of the chlorine and bromine loading. The impact a halocarbon has on ozone depends on the distribution as well as number of chlorine atoms released by the halocarbon. At steady state, the expected chlorine loading (Cl) from a species is given by;[4]

$$Cl \propto F \; x \; L \; x \; N \; / \; MW \qquad (6.2)$$

Here F is the mass of gas emitted per year (the flux), L is the lifetime, N is the number of chlorine atoms in the molecule and MW is the molecular weight or relative molar mass.

This proportionality is valid for species with lifetimes greater than one year, so that they are vertically well mixed in the troposphere. It represents the concentration of chlorine in or above the upper stratosphere, where it is assumed all the chlorine atoms in the molecule are released. Thus we obtain the maximum level of chlorine which is available in the atmosphere to destroy ozone. This measure has been refined using coefficients which represent the amount of chlorine available, particularly in the lower, high latitude stratosphere. The resulting loading is termed free chlorine[1] and is calculated from the total chlorine loading proportional to the relative ODPs of the individual halocarbons. The value of these free chlorine coefficients can be found in Section 7.4.3. For the purposes of this work, results are expressed as a total chlorine loading, ie. the worst case scenario, which represents a more prudent measure.

For interest, chlorine loadings can be related to ODPs by first defining a Chlorine Loading Potential (CLP), which is;

$$CLP(X) = Cl(X) \; / \; Cl(CFC\ 11) \tag{6.3}$$

Equation 6.3 defines a ratio of chlorine available from compound X to that from CFC 11. The CLP can then be related to the ODP by;

$$CLP = ODP \; / \; CEF \tag{6.4}$$

Here CEF is the Chlorine Effectiveness Factor and represents the effect of chlorine distribution on ozone.

6.2.2 The First Models

Prather and Watson[2] give equations for calculating the concentration of halocarbons in the atmosphere and the subsequent chlorine/bromine loading. In a personal communication, Dr MacFarland, based at Du Pont's experimental station in Delaware, USA, confirmed that use of these equations in our models would be perfectly adequate for our intended work. It was decided to reproduce Prather and Watson's model on a Supercalc 5.0 spreadsheet, using both their assumptions and equations, in order to check that the equations were working correctly on the spreadsheet, as results could be agreed to the original paper by Prather and Watson.[2]

A number of terms were used by Prather and Watson, which will be referred to constantly throughout this section of the work. The definition of these terms is given below.

1) Lifetime (L) is in years and is calculated as the global abundance of a gas divided by its annual average loss rate. This decay rate (D) is first order and calculated using Equation 6.5.

$$D = Exp(-1/L) \tag{6.5}$$

2) Flux (F) is in units of kilotonnes per year, ie. 1000 tonnes per year (kt yr^{-1}) and is the amount of gas emitted to the atmosphere in a year from the surface of the Earth.

3) Growth/Decline is the percentage increase or decrease in production of halocarbons.

4) Concentration (C) is in parts per trillion, ie. 10^{12} (ppt) and represents the average tropospheric mixing ratio.

5) Factor (P) is in units of kt ppt^{-1} and represents the amount of gas required to produce a 1 ppt rise in the atmospheric concentration of the gas. It is linked to the molecular weight of the gas, and its derivation can be found in Appendix 5.

Prather and Watson[2] incorporated a number of simplifying assumptions which were included in our first models.

1) The flux is based on estimates of production in 1985.

2) Growth was assumed to be 4% yr^{-1} from 1986 to 1990, and 0% yr^{-1} through to 2000. After 2000, the flux is taken as 0 kt yr^{-1}. All reductions are assumed to occur instantly at the end of the year.

3) The factor assumes a compound is well mixed throughout 95% of the atmosphere.

4) Methyl chloride and methyl bromide concentrations are assumed to be fixed at 600 ppt and 15 ppt respectively.

5) The lifetime of HCFC 22 is 15 years.

6) There is no 'bank' of CFCs.

7) There is no delay between production and emission of the halocarbons to atmosphere.

8) No account is taken of the time it takes for air to travel from the upper troposphere to the middle stratosphere which is about two years.

The models were for twelve halocarbons, namely CFC 11 ($CFCl_3$), CFC 12 (CF_2Cl_2), CFC 113 ($CF_2ClCFCl_2$), CFC 114 (CF_2ClCF_2Cl), CFC 115 (CF_3CF_2Cl), carbon tetrachloride (CCl_4), methyl chloroform (CH_3CCl_3), HCFC 22 (CHF_2Cl), halon 1211 (CF_2ClBr), halon 1301 (CF_3Br), methyl bromide (CH_3Br) and methyl chloride (CH_3Cl).

Data relating to production, lifetimes and atmospheric concentrations were given by Prather and Watson and were current at the time of publication of their paper.

The equation for the atmospheric concentration used by Prather and Watson[2] and subsequently adopted for this work is given below.

$$C(yr+1) = (C(yr) \times D) + (F(yr+1) \times (1-D) \times (L/P)) \quad (6.6)$$

The first half of the equation is concerned with the ongoing atmospheric decay of gas already present in the atmosphere whereas the second part of the equation looks at the flux of gas emitted at the surface and its subsequent impact on the atmospheric concentration according to the ratio of its lifetime and factor.

The concentration is then converted into a chlorine or bromine loading by Equations 6.7 or 6.8 respectively.

$$Cl = C \times N / 1000 \quad (6.7)$$

$$Br = C \times N \quad (6.8)$$

Here N is the number of chlorine or bromine atoms in the molecule whereas Cl and Br are the chlorine loading in parts per billion and the bromine loading in parts per trillion respectively.

As a result of adding these assumptions and equations into the spreadsheet model, the results we obtained for the sensitivity studies employed by Prather and Watson were identical and indicated that everything was working correctly.

6.2.3 Improving and Updating the First Models

A number of shortcomings in the models in Section 6.2.2 were pinpointed, for which improvements could be made and incorporated into the new models, which are discussed further below. It was during this process of developing the later versions of the models that they were transferred from the PC onto the Workstation.

1) The Alternative Fluorocarbon Environmental Acceptability Study (AFEAS) publish production and use data for several of the halocarbons (Section 6.3.2).[6-8] Production data from other literature sources is also utilised (Section 6.3.2),[9-11] and incorporated into the model rather than applying an assumed growth rate based on 1985 production (as used in the Prather and Watson model[2]). It is still an assumption of the models that all production in a year is consumed in some kind of use in that year, ie. none is stored away for use in appliances in later years.

2) Where production data is not available prior to 1985, a growth rate is applied which is based on the historical growth or decline of the gas rather than the 4% used by Prather and Watson for every gas. It is appreciated that the historical growth rate is not necessarily an accurate indication of trends but is taken as a reasonable approximation where there is a scarcity of reliable data. Between 1985 and the onset of the Montreal Protocol 3 restrictions, growth factors given in WMO 1991[1], are applied for those years where no production data is available.

3) Recent data for atmospheric concentrations and lifetimes of the halocarbons[1] supersedes data used by Prather and Watson, where applicable.

4) Unlike other models[1-3] the application of the halocarbons is included in the model under eight general headings which are aerosol propellants, solvents/cleaning agents, blowing agents in open and closed cell foams, refrigerants in hermetic and non-hermetic systems, fire retardants and a residual miscellaneous category. Data for the division of the halocarbons into each of these categories is based on published work[6-10] and comes from a variety of sources which are discussed in more detail in Section 6.3.2. The division into these usage categories is not always clear, especially for the foams. For instance, closed cell foams are generally taken as being rigid polyurethane and isocyanurate foams and non-urethane foams, polystyrene and some extruded polyolefins.[12]

Each use category has an associated delay between production and emission (the

Table 6.1 Delay parameters according to use (except as fire retardants).

Use	Emission Delay (years from production)	Period of Emission (years from production)	Delay Coefficient (%)
Aerosols	-	0	100
Cleaning Agents	-	0	100
Open Cell Foams	-	0	100
Closed Cell Foams	0-9	10-20	9.09
Non-Hermetic Refrigeration	0-1	2-5	25
Hermetic Refrigeration	0-14	15-20	16.67
Other	-	0	100

emission delay) and an associated period over which emission is likely to occur (the period of emission), shown in Table 6.1. We assume that emission of halocarbon retained in appliances over this period is averaged over the period of emission as a whole. A representation of this would be a refrigerator for which the period of emission of the CFC contained in its foam takes place between 10 and 20 years after the CFC's production. We are assuming that the refrigerator will lose 1/11th of its CFC content in the foams over years 10 to 20 inclusive. Realistically the refrigerator will either lose all its CFC content rapidly (maybe through crushing after disposal) or slowly through influx of moisture while the refrigerator sits in a landfill. For an individual refrigerator, these processes will not approximate the period of emission utilised in the model. However for a large number of refrigerators, the actual time of emission for each refrigerator will vary, but taken as a whole, will more closely approximate the emission characteristics of the model. These characteristic emission delays and periods of emission are taken from Du Pont[13] who based their work on a study by Gamlen et al.[12] The delay coefficient (expressed as a percentage in Table 6.1) represents the proportion of the original production in year 0 which is emitted yearly over the period of emission. In the example above, this is 1/11th which is 9.09% (Table 6.1). It is an assumption of the model that all halocarbons in the 'other' category are released in the year of production.

The delay period and delay coefficients for the halons are calculated differently, based on work by McCulloch[14] and McCulloch (*personal communication*). A proportion of the production in year 0 is emitted in that year, the amount depending on the halon and the year (Table 6.2).[14] Therefore each has a characteristic period of emission after year 0 shown in Table 6.2.

5) In addition to the chlorocarbons modelled by Prather and Watson, an additional four gases are included bringing the total to fourteen. The four gases are the replacement hydrochlorofluorocarbons HCFC 123, HCFC 124, HCFC 141b and HCFC 142b.

Table 6.2 Delay parameters adopted for fire retardants.

Fire Retardant	Years	Emission as a percentage of production in year 0 (%)	Period of remaining emission (years)	Delay Coefficient (%)
Halon 1211	1969-1980	66	13	7.69
	1981-1985	69	13	7.69
	1986-1992	58	13	7.69
Halon 1301	1969-1980	36	8	12.5
	1981-1985	52	8	12.5
	1986-1992	33	8	12.5

6) When the models were installed on the workstation computer, Montreal Protocol 2 was the current legislation governing the level of use of the halocarbons. Subsequent to this, Montreal Protocol 3 was signed in November 1992, and as a result, the models were updated for its stipulations. The requirements of the Montreal Protocols are modelled as a stepped phase out in which we assume full compliance by signatory countries and no delayed use by developing countries (Section 1.4), unless otherwise stated. The sensitivity analyses presented in Chapter 7 are based on Montreal Protocol 3, but some work still uses Montreal Protocol 2 as a reference level. This is indicated where applicable in Chapter 7 and any differences from the Montreal Protocol 3 model assumptions are discussed under the relevant sensitivity study.

6.3 The Layout and Workings of the Chlorine and Bromine Loading Models

There are three chorine loading models and a bromine loading model (which represent the final versions of these models), all of which are saved as separate spreadsheet files. Each of the chlorine loading models use the same data, but are designed with modifications to model a particular area of work, eg. use by developing countries. A list of the spreadsheet file names and their function is given in Appendix 6.

The models consist of a number of tables which contain data and equations, the results of which filter into and are used in other tables. How these tables relate to each other is shown in Figure 6.1, and an explanation of the function of each is given below.

6.3.1 Introduction Screen

On loading eXclaim! and selecting the appropriate spreadsheet file (Appendix 6), the user is faced with an Introduction Screen which lists where all the other tables can be found on the grid of the spreadsheet. The position of the other tables is given by the top left hand cell address of each table. The Introduction Screen is shown in Figure 6.2.

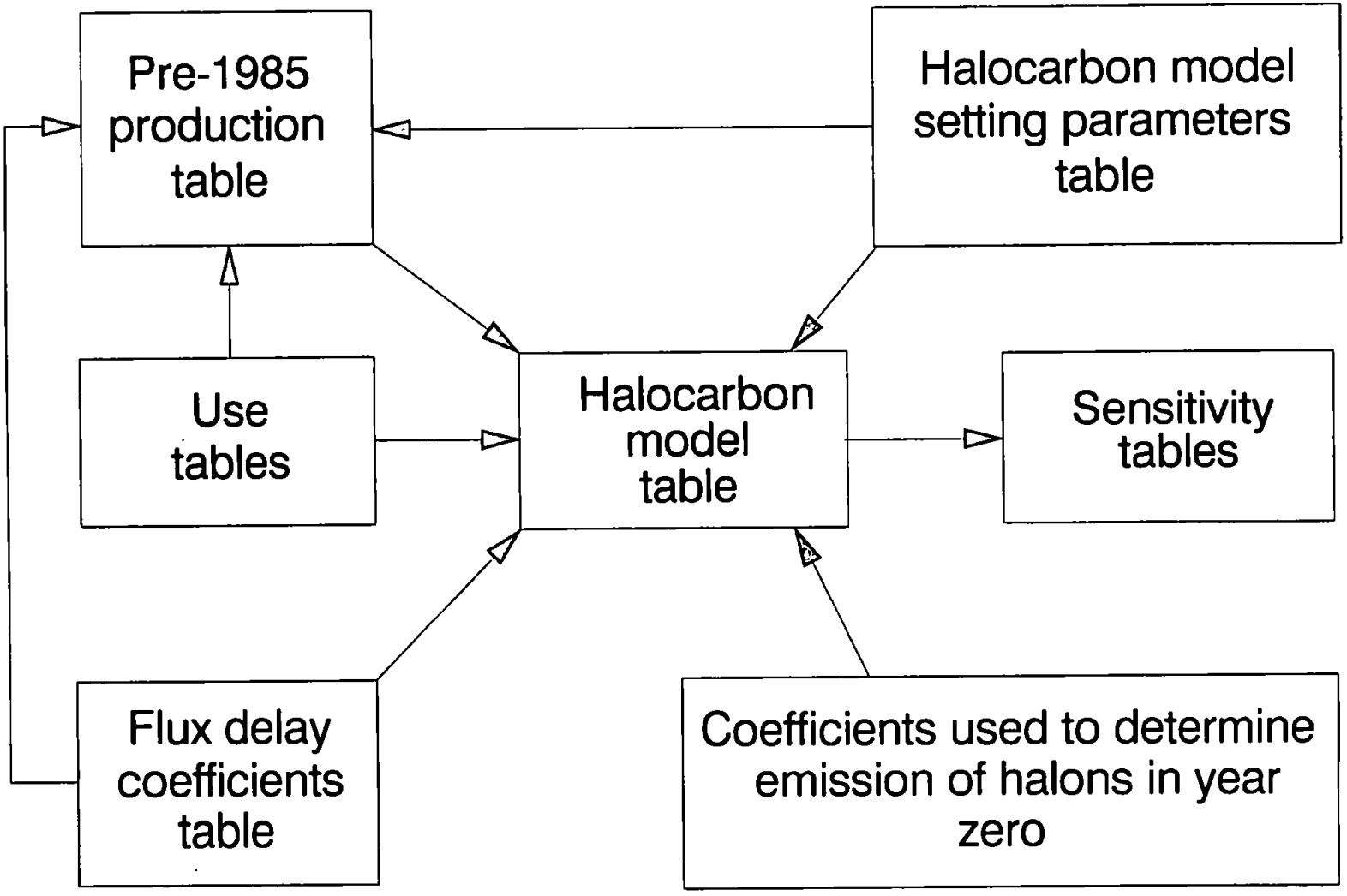

Figure 6.1 Schematic diagram of the chlorine and bromine loading models.

MOD9 MODEL OF CHLORINE LOADING IN ATMOSPHERE 1985–2100

TO FIND	GO TO
THE HALOCARBON MODEL TABLE	I24
THE HALOCARBON MODEL SETTING PARAMETERS TABLE	GV162
THE PRE–1985 PRODUCTION TABLE	A206
USE TABLE 1 PRE 1985	HD166
USE TABLE 2 PRE 1985–1996	HD183
USE TABLE 3 PRE 1997–2015	HD208
USE TABLE 4 PRE 2016–2030	HD230
FLUX DELAY COEFFICIENTS TABLE	GL149
COEFFICIENTS USED TO DETERMINE EMISSIONS OF HALONS IN YEAR ZERO	EQ2
SENSITIVITY TABLES	FS25

Figure 6.2 The Introduction Screen on the chlorine loading model.

6.3.2 The Halocarbon Model Table

This table features the main workings of the model and draws upon other tables within the spreadsheet for data. It contains the fourteen chlorocarbons (CFCs 11, 12, 113, 114 and 115, HCFCs 22, 123, 124, 141b and 142b, halon 1211, carbon tetrachloride, methyl chloroform and methyl chloride) in the chlorine loading model and the three bromocarbons (halons 1211 and 1301 plus methyl bromide) in the bromine loading model. An example from the chlorine and bromine loading models is shown for CFC 11 and halon 1301 in Tables 6.3 and 6.4 respectively.

Both models run from 1985 to beyond 2100, although results are graphically presented to 2100. Production data for each gas in included where available and where not, a historical or literature growth rate is applied until the conditions of Montreal Protocol 3 begin (Table 1.1). The relative growth/decline column expresses the increase or decrease in production of the halocarbons relative to 1986, and is useful when modelling the Montreal Protocol restrictions, as the percentage reductions are relative to production in 1986. The total production column is then divided into the relevant use categories, the proportion of production allocated to each usage category being dictated by the Use Tables (Section 6.3.5). Each usage type has an associated delay (Tables 6.1 and 6.2) which is incorporated into the flux equation. In the chlorine loading model the flux equation takes the form below.

$$F(yr) = (U_A \, x \, E_A) + (U_C \, x \, E_C) + (U_{OCF} \, x \, E_{OCF}) + (U_O \, x \, E_O)$$

$$+ \sum_{yr-X}^{yr-Y} (U_{CCF} \; x \; E_{CCF}) + \sum_{yr-X}^{yr-Y} (U_{HR} \; x \; E_{HR}) + \sum_{yr-X}^{yr-Y} (U_{NHR} \; x \; E_{NHR}) \qquad (6.9)$$

Here U is the amount of gas (in kt) consumed in a particular usage category and E is the delay coefficient (Table 6.1) which is applied for the period of production marked by the boundary years *yr-X* and *yr-Y* inclusive, for emission in year *yr* (for those use categories that incorporate a delay). The subscripts *A*, *C*, *OCF*, *CCF*, *HR*, *NHR* and *O* refer to

Table 6.3 CFC 11 as an example of the format used for the halocarbons in the chlorine loading model. Note that the table is shown to the year 2000, but in the model this extends to beyond 2100.

CFC 11 (CFCl3)

YEAR	RELATIVE GROWTH/ DECLINE	RELATIVE GROWTH/ DECLINE 1986	TOTAL PRODUCTION SALES (kt/yr)	USE Hermetic Refrigeration (kt/yr)	Non-Hermetic Refrigeration (kt/yr)	Open Cell Foams (kt/yr)	Closed Cell Foam (kt/yr)	Cleaning Agent (kt/yr)	Aerosol Propellant (kt/yr)	Fire Retardant (kt/yr)	Other (kt/yr)	FLUX (kt/yr)	CONCENTRATION (ppt)	Cl LOADING (ppb)
1985		0.93	326.81	0.00	27.48	59.51	116.14	0.00	104.17	0.00	19.52	242.98	238.51	0.72
1986		1.00	350.15	0.00	29.44	63.75	124.43	0.00	111.61	0.00	20.92	258.50	245.24	0.74
1987		1.09	382.05	0.00	32.12	69.56	135.77	0.00	121.77	0.00	22.82	281.04	252.81	0.76
1988		1.07	375.99	0.00	32.32	69.03	195.81	0.00	57.43	0.00	21.40	220.50	257.67	0.77
1989		0.86	302.49	0.00	26.00	55.54	157.53	0.00	46.21	0.00	17.21	198.67	261.50	0.78
1990		0.67	232.92	0.00	20.02	42.76	121.30	0.00	35.58	0.00	13.26	178.75	264.42	0.79
1991	1.00	0.67	232.92	0.00	20.02	42.76	121.30	0.00	35.58	0.00	13.26	184.39	267.53	0.80
1992	1.00	0.67	232.92	0.00	20.02	42.76	121.30	0.00	35.58	0.00	13.26	187.56	270.71	0.81
1993	0.80	0.53	186.33	0.00	16.02	34.21	97.04	0.00	28.46	0.00	10.60	171.26	273.14	0.82
1994		0.25	87.54	0.00	7.52	16.07	45.59	0.00	13.37	0.00	4.98	134.69	273.97	0.82
1995	1.00	0.25	87.54	0.00	7.52	16.07	45.59	0.00	13.37	0.00	4.98	137.12	274.89	0.82
1996	0.00	0.00	0.00	0.00	0.00	0.00	0.00	0.00	0.00	0.00	0.00	105.84	274.46	0.82
1997	0.00	0.00	0.00	0.00	0.00	0.00	0.00	0.00	0.00	0.00	0.00	110.32	274.23	0.82
1998	0.00	0.00	0.00	0.00	0.00	0.00	0.00	0.00	0.00	0.00	0.00	117.19	274.29	0.82
1999	0.00	0.00	0.00	0.00	0.00	0.00	0.00	0.00	0.00	0.00	0.00	121.50	274.54	0.82
2000	0.00	0.00	0.00	0.00	0.00	0.00	0.00	0.00	0.00	0.00	0.00	123.36	274.86	0.82

Table 6.4 Halon 1301 as an example of the format used in the bromine loading model. Note that the table is shown to the year 2000, but in the model this extends to beyond 2100.

HALON 1301 (CF3Br)

YEAR	RELATIVE GROWTH/	RELATIVE GROWTH/ DECLINE 1986	TOTAL PRODUCTION SALES (kt/yr)	HALON NOT EMITTED IN YEAR ZERO (kt/yr)	FLUX (kt/yr)	CONCENTRATION (ppt)	Br LOADING (ppt)
1971			0.55	0.35			
1972			0.84	0.54			
1973			1.29	0.83			
1974			1.46	0.94			
1975			2.02	1.29			
1976			3.17	2.03			
1977			3.55	2.27			
1978			4.02	2.57			
1979			4.72	3.02			
1980			4.88	3.12			
1981			5.69	2.73			
1982			7.57	3.63			
1983			7.39	3.55			
1984			8.69	4.17			
1985		0.88	9.78	4.69	8.22	1.70	1.70
1986		1.00	11.08	7.42	7.09	1.95	1.95
1987		1.05	11.60	7.77	7.87	2.23	2.23
1988		1.13	12.55	8.41	8.78	2.55	2.55
1989		1.01	11.15	7.47	8.98	2.86	2.86
1990		0.82	9.12	6.11	8.90	3.17	3.17
1991	1.00	0.82	9.12	6.11	9.21	3.49	3.49
1992	1.00	0.82	9.12	6.11	9.53	3.81	3.81
1993	1.00	0.82	9.12	6.11	9.77	4.14	4.14
1994	0.00	0.00	0.00	0.00	6.94	4.35	4.35
1995	0.00	0.00	0.00	0.00	6.01	4.52	4.52
1996	0.00	0.00	0.00	0.00	5.04	4.65	4.65
1997	0.00	0.00	0.00	0.00	3.99	4.73	4.73
1998	0.00	0.00	0.00	0.00	3.05	4.78	4.78
1999	0.00	0.00	0.00	0.00	2.29	4.80	4.80
2000	0.00	0.00	0.00	0.00	1.53	4.79	4.79

aerosols, cleaning agents, open cell foams, closed cell foams, hermetic refrigeration, non-hermetic refrigeration and 'other' respectively.

Halon 1211 in the chlorine loading model is treated in the same way as the halons in the bromine loading model, for which the flux is calculated using Equation 6.10.

$$F(yr) = (P \times M) + \left[\sum_{yr-1}^{yr-Y} (P \times (100 - M) \times E\right] \qquad (6.10)$$

Here P is the total production in a year (all of which is assumed to be used in fire retardants), M is the proportion of the production of halon in a year which is emitted in that year (Table 6.2), and yr-Y is the maximum delay year for the period of production for emission in year yr ie. year 13 for halon 1211 and year 8 for halon 1301 (Table 6.2).

As the maximum delay before emission featured in the chlorine loading model is 20 years, and 13 years in the bromine loading model, it is necessary to calculate after 1985 the flux due to use before 1985 in delayed emission categories. In the chlorine loading model, this is performed in the Pre-1985 Production Table (Section 6.3.4) whereas in the bromine loading model, the pre-1985 production is incorporated into the Halocarbon Model Table (Table 6.4).

Once the flux is known, the atmospheric concentration can be calculated using Equation 6.6. The initial concentration in 1985 is taken from the Halocarbon Model Setting Parameters Table (Section 6.3.3), which also contains the decay rate, lifetime and factors for each of the halocarbons, also required for the calculation of atmospheric concentration. Finally the chlorine or bromine loading for each gas is produced (Equations 6.7 and 6.8) using the calculated concentrations and the number of chlorine (or bromine) atoms in the molecule, which are also taken from the Halocarbon Model Setting Parameters Table (Section 6.3.3).

The individual chlorine (or bromine) loadings for each gas are totalled to produce a total chlorine (or bromine) loading.

Each of the gases contained in the Halocarbon Model Table for both the chlorine

and bromine loading models are now briefly described.

1) CFC 11 ($CFCl_3$) - Production and use data has come from AFEAS,[6] whereas lifetime, atmospheric concentration and growth rates have all come from the World Meteorological Organization (WMO).[1] From a modest start in 1934, production has increased to a maximum in 1987 of over 380 kt. It is primarily used as a refrigerant in non-hermetic systems, a blowing agent in both open and closed cell foams, a propellant in aerosols plus minor applications in other uses.[6] It is considered one of the more ozone depleting CFCs, and forms the reference against which the ODP of other halocarbons is measured. Its ODP is therefore 1.0. As with the other CFCs, the 1994 consumption of CFC 11 is reduced to 25% of the 1986 level, with a complete removal by 1996, according to Montreal Protocol 3 (Table 1.1).

2) CFC 12 (CF_2Cl_2) - Production, use, growth, lifetime and atmospheric concentration data have all come from the same sources as for CFC 11.[1,6] Recorded production began in the early 1930s and reached a maximum in 1974 of over 442 kt. CFC 12 is a refrigerant in both hermetic and non-hermetic refrigeration systems, a blowing agent in open and closed cell foams and an aerosol propellant, as well as having minor applications in other uses.[6] It is another important ozone depleting gas and has an ODP of 0.87 - 1.00.[5]

3) CFC 113 ($C_2F_3Cl_3$) - Production and use data has been obtained from AFEAS[7] and Fisher and Midgley.[9] Lifetime, concentration and growth data all come from WMO.[1] Between 1986 and 1990, more than 99% of all CFC 113 produced was used in applications leading to immediate release, this being primarily as a cleaning agent.[7] Maximum production was attained in 1989 with over 251 kt. The ODP is calculated as 0.91.[15]

4) CFC 114 ($C_2F_4Cl_2$) - Production, use, lifetime and concentration data all come from the same sources as for CFC 113.[1,7,9] Prior to 1980, a growth rate is applied based on production data for 1980-1986, giving a growth rate of 2.9% yr^{-1}, allowing an estimate of

production to be estimated back to 1965. Maximum production reached over 19 kt in 1986. The two major uses for CFC 114 are as a blowing agent in open cell foams (it is used in polyolefin foams which, although of the closed cell type, are very permeable and tend to lead to rapid emission), and as a refrigerant in centrifugal chillers (which are hermetically sealed).[9] It has an ODP of 0.56 - 0.82.[5]

5) CFC 115 (C_2F_5Cl) - Production, use, lifetime and concentration data are again from the same sources as for CFCs 113 and 114.[1,7,9] Maximum production was about 14 kt in 1989. CFC 115 is primarily used in non-hermetic refrigeration systems such as low temperature food cases, chill cabinets and in transportation, ie. industrial applications.[9] In these applications it forms 51.2% of a binary azeotropic mixture called CFC 502, the other part being 48.8% HCFC 22. Its ODP is around 0.27 - 0.45.[5]

6) HCFC 22 (CHF_2Cl) - Production data has been obtained from AFEAS[8] whereas lifetime, concentration and growth (after 1990) have come from WMO.[1] A growth rate (6.4% yr^{-1}) before 1970 has been calculated from production data from 1970-1975,[8] so that an estimation of production is obtained back to 1965. HCFC 22 is a hydrochlorofluorocarbon which has had a large established market and up until recently, was the only mass produced HCFC. Its primary uses are in commercial non-hermetic refrigeration, and hermetic refrigeration, as well as a blowing agent in open and closed cell foams.[8] Being an HCFC it has a low ODP of 0.058 - 0.099.[15]

7) HCFC 123 ($CHCl_2CF_3$) - This gas, together with HCFC 124, HCFC 141b and HCFC 142b form some of the most promising replacement HCFCs for commercial use. The problem with introducing each of these into the model, is that they are at various stages of production readiness. According to Hoffman,[16] HCFCs 123 and 124 were in testing and pilot production in 1990, whereas HCFCs 141b and 142b were in production. For simplicity, it is assumed that 7.2 kt each of HCFCs 123, 124, 141b and 142b are produced in 1990, rising to 146.6 kt each in 1996. HCFC 22 production is assumed to remain

constant at 213.7 kt between 1990 and 1996. Thus, total hydrochlorofluorocarbon availability is 800 kt which is the limit set under Montreal Protocol 3. After this, the phase out conditions of Montreal Protocol 3 are modelled leading to their complete removal by 2030 (Table 1.1).

Originally, it was intended for HCFC 123 to be a replacement for CFC 11 in all applications. However, after the discovery of benign tumours in the pancreas and testes of laboratory rats as part of the Programme for Alternative Fluorocarbon Toxicity Testing (PAFT),[17] its applications are likely to be limited to refrigeration applications where there is less human contact. Lifetime data comes from WMO.[1] HCFC 123 has an ODP of 0.013 - 0.027.[5]

8) HCFC 124 ($CClFHCF_3$) - Production is as explained for HCFC 123 and lifetime data comes from WMO.[1] It is intended as a replacement for CFC 114 in hermetic refrigeration appliances such as chillers and is also intended for use in open and closed cell foams.[18,19] As with HCFC 141b and 142b, where the intended use is divided amongst more than one usage category, then the split is assumed to be equal. HCFC 124 is also one of the constituents of ternary blends such as MP 33, MP 39 and MP 66. The ODP of HCFC 124 is 0.013 - 0.030.[5]

9) HCFC 141b (CCl_2FCH_3) - Production is as explained for HCFC 123, and lifetime data comes from WMO.[1] It is intended as a possible replacement for CFC 11 in open and closed cell foams, as well as being a component of a cleaning agent blend.[18,19] Its ODP is about 0.140 - 0.145.[15]

10) HCFC 142b ($CClF_2CH_3$) - Production is as explained for HCFC 123, and lifetime data comes from WMO.[1] It is intended as a propellant and for use in open and closed cell foams.[18,19] Its ODP is 0.074 - 0.100.[15]

11) Methyl Chloroform (CH_3CCl_3) - Production data comes from Midgley[10] whereas lifetime, concentration and growth data have been obtained from WMO.[1] It is used

primarily as a solvent and degreaser as well as a solvent in paints, adhesives and varnishes. Under the terms of Montreal Protocol 3, its consumption level in 1994 will be 50% of its level in 1989, with a complete phase out by 1996. It has an ODP of 0.128 - 0.131.[15]

12) Carbon Tetrachloride (CCl_4) - Levels of its production have been taken from den Elzen et al.[19] whereas lifetime, concentration and growth rates have come from WMO.[1] Much of carbon tetrachloride use is as an intermediate from which emission to atmosphere is considered to be small. Its main uses leading to emissions are as a solvent, with declining use as a grain fumigant owing to worries about its toxicity. Under Montreal Protocol 3, its consumption will be cut by 85% in 1995, relative to 1986, and all consumption is set to stop by 1996. It has an ODP of 1.074.[15]

13) Halon 1211 (CF_2BrCl) - Found in both the chlorine loading and bromine loading models, production data for halon 1211 is based on work by McCulloch,[14] its lifetime comes from Butler et al.,[20] whereas its concentration and growth rate are taken from WMO.[1] It is used mainly in portable fire extinguishers and reached an estimated global production of over 20 kt in 1988.[14] As with halon 1301, it is due for complete removal by 1994, under the terms of Montreal Protocol 3. It has an ODP of 2.2 - 3.0.[21]

14) Halon 1301 (CF_3Br) - Used exclusively in the bromine loading model, data for halon 1301 production, lifetime, concentration and growth come from the same sources as for halon 1211.[1,14,20] Estimated world maximum production peaked at over 12 kt in 1988.[14] It is generally used in fixed fire extinguishing systems such as in libraries and computer rooms. It has an ODP of 7.8 - 13.2.[21]

15) Methyl Chloride (CH_3Cl) - With a constant concentration of 600 ppt,[22] the model assumes a global production of methyl chloride of 4500 kt which is within the range of uncertainty in the literature.[22] Of this 4500 kt, 500 kt is man-made.[22] Khalil et al.[23] estimated the lifetime of methyl chloride to be 1-2 years. In order to maintain a steady

state between a flux of 4500 kt and an atmospheric concentration of 600 ppt in the model, we use a lifetime of 1.12 years which is within this range of uncertainty. The calculation of the chlorine loading from methyl chloride is started before 1985, so that it has already reached a steady state at the onset of the model in 1985.

The primary natural sources of methyl chloride (which is the main source for the Earth's natural chlorine loading of about 0.6 ppb) are from the ocean, forests and combustion of vegetation. Singh et al.[24] estimated a flux of about 3000 kt from the oceans. A possible source for this was postulated by Zafiriou[25] in which methyl iodide manufactured by photosynthetic marine organisms reacts with chlorine ions in seawater to yield methyl chloride, which escapes to atmosphere. However, Manley and Dastoor[26] found higher concentrations of methyl chloride, bromide and iodide around macroalgae such as kelp and also that there was a greater production of methyl chloride than methyl iodide by these species, which seemed to contradict Zafiriou's findings. However they could not determine whether the source of methyl chloride was from the kelp itself or microbes on the surface of the kelp. When they calculated an estimated global production of methyl chloride from their measurements, it came to only 2 kt yr^{-1}, being less than 0.1% of total methyl chloride production. This implied that either the oceans were not a major source as once thought, or other macroalgae and phytoplankton produced methyl chloride to make up the deficit.

Methyl chloride is also produced by species of white rot fungi of the genus *Hymenochaetaceae*. It is strongly expressed in wood rotting fungi such as *Phellinus* and represents a potentially large source as these species are common throughout both temperate and tropical forests.[27]

Combustion of vegetation can be both natural and man-made. Methyl chloride arises from the production of methane during combustion, which is converted to methyl chloride by chlorine available in the wood, such as from cellulose.[28] Natural and man

made 'slash and burn' techniques provide an estimated flux of 400-1000 kt yr^{-1}.[29,30]

Industrial uses for methyl chloride include blowing of polystyrene foams, as well as use in silicones, butyl rubber and some herbicides. Production levels are not expected to increases significantly[31] and therefore, for simplicity, remain constant in the model. All emissions (both natural and man-made) arise in the year of production. There are no requirements under Montreal Protocol 3 for man-made use of methyl chloride to be reduced or stopped. Methyl chloride has an ODP of 0.023-0.024.[15]

16) Methyl Bromide (CH_3Br) - The level of man-made methyl bromide production is based on a report by Albritton and Watson.[11] Natural methyl bromide production is assumed to be constant at 131.2 kt, being the average total atmospheric burden less the average man-made contribution for the period 1984-1990,[11] which produces a steady state natural concentration of 11.39 ppt. Together with man-made methyl bromide, the total bromine concentration is initially 12.43 ppt which is within measured atmospheric concentrations.[3,4,11] The atmospheric lifetime is taken from a report by the UK Stratospheric Ozone Review Group (SORG).[3]

Man-made sources of methyl bromide arise from its use as a re-planting, post harvesting and structural fumigant.[11]

The major natural source is thought to be the oceans. Quantifying the source on a global scale has proved difficult, but oceanic concentrations of methyl bromide and chloride are significantly correlated, suggesting a common source.

No firm decision has been made as part of Montreal Protocol 3 on a timetable for the removal of man-made methyl bromide. All that has been decided to date is that there should be a freeze in its consumption by 1995, at the 1991 level (Table 1.1). Therefore we assume that man-made methyl bromide production is constant from 1990 and subsequently phased out over a twenty year period from 2000. The schedule we use is shown in Table 6.5. The ODP of methyl bromide is about 0.7.[11]

Table 6.5 Assumed phase out schedule for man-made methyl bromide.

Years	Production relative to 1990 production (%)
1991-1999	100
2000-2009	75
2010-2014	50
2015-2019	25
2020+	0

17) All other halocarbons - Other gases such as methylene chloride and halon 2402 have the capability to affect ozone levels, but their combined flux into the stratosphere is assumed to be small, and hence their affect on ozone is assumed to be negligible in comparison to the sixteen gases considered in the chlorine and bromine loading models.

6.3.3 The Halocarbon Model Setting Parameters Table

This table contains reference material for the equations in the Halocarbon Model Table (Section 6.3.2). For each of the gases in both the chlorine and bromine loading models, it contains data on atmospheric lifetime, atmospheric concentration in 1985, factor, the number of chlorine (and bromine) atoms in the molecule and the decay rate. Tables 6.6 and 6.7 show the table for the chlorine and bromine loading models respectively.

6.3.4 The Pre-1985 Production Table

For those gases being produced in 1985 which are used in applications leading to a delay in emission, ie. CFCs 11, 12, 114 and 115 and HCFC 22, a contribution to their flux after 1985 will be from production up to 20 years before. Therefore their production, and the use to which they have been put (from the Use Tables, Section 6.3.5), are contained within the Pre-1985 Production Table, which calculates a contribution to the flux after 1985 from these sources. This contribution is added to the flux equations in the Halocarbon Model (Section 6.3.2). Data used in the Pre-1985 Production Table (Table 6.8) comes from AFEAS,[6-8] as discussed in Section 6.3.2.

The bromine loading model does not feature a separate table for pre-1985 production, but incorporates it into the main halocarbon model. Halon 1211 in the chlorine loading model is also set up in this way.

Table 6.6 The Halocarbon Model Setting Parameters Table for the chlorine loading model.

HALOCARBON	LIFETIME (yr)	CONCENTRATION (ppt)	FACTOR (kt/ppt)	NO Cl ATOMS	NO Br ATOMS	DECAY RATE
CFC 11	55	238.51	23.2	3	0	0.9820
CFC 12	116	404.37	20.4	2	0	0.9914
CFC 113	110	36.71	31.6	3	0	0.9910
CFC 114	220	15.7	28.9	2	0	0.9955
CFC 115	550	3.34	26.1	1	0	0.9982
HCFC 22	15.8	92.25	14.6	1	0	0.9388
HCFC 123	1.71	0	25.4	2	0	0.5579
HCFC 124	6.9	0	22.7	1	0	0.8653
HCFC 141b	10.8	0	19.4	2	0	0.9117
HCFC 142b	22.4	0	16.7	1	0	0.9564
HALON 1211	13	1.5	27.9	1	1	0.9261
CARBON TETRACHLORIDE	47	99.93	25.9	4	0	0.9790
METHYL CHLOROFORM	6.1	93.2	22.4	3	0	0.8491
METHYL CHLORIDE	1.12	600	8.4	1	0	0.4102

Table 6.7 The Halocarbon Model Setting Parameters Table for the bromine loading model.

Halocarbon	Lifetime (yr)	Concentration (ppt)	Factor (kt/ppt)	No. of Cl atoms	No. of Br atoms	Decay Rate
CH3 Br	1.5	11.39	15.8	0	1	0.5141
CF3 Br(H1301)	65	1.7	25.1	0	1	0.9848
CF2 BrCl(H1211)	13	1.5	27.9	1	1	0.9261

Table 6.8 The Pre-1985 Production Table for the chlorine loading model (CFC 115 and HCFC 22 are not shown for clarity).

	CFC 11		NUMBERS				CFC 12		NUMBERS				CFC 114		FORMULAE			
YEAR	RELATIVE GROWTH	PRODUCTION (kt/yr)	Hermetic Refrigerant (kt/yr)	Non Hermetic Refrigerant (kt/yr)	Closed Cell Foams (kt/yr)	FLUX (kt/yr)	RELATIVE GROWTH	PRODUCTION (kt/yr)	Hermetic Refrigerant (kt/yr)	Non Hermetic Refrigerant (kt/yr)	Closed Cell Foams (kt/yr)	FLUX (kt/yr)	RELATIVE GROWTH	PRODUCTION (kt/yr)	Hermetic Refrigerant (kt/yr)	Non Hermetic Refrigerant (kt/yr)	Closed Cell Foams (kt/yr)	FLUX (kt/yr)
1945		122.83	0.00		11.20			190.06	1.60		2.30		0.97	9.70	0.92		0.00	
1946		141.01	0.00		13.40			216.15	1.90		2.70		0.97	9.99	0.94		0.00	
1947		159.76	0.00		16.80			243.76	2.20		2.80		0.97	10.25	0.97		0.00	
1948		183.12	0.00		19.80			267.48	2.60		3.40		0.97	10.55	1.00		0.00	
1949		217.27	0.00		25.40			297.29	2.80		4.70		0.97	10.89	1.03		0.00	
1950		238.14	0.00		31.60			321.10	3.00		5.00		0.97	11.22	1.06		0.00	
1951		263.18	0.00		36.20			341.56	3.40		5.40		0.97	11.55	1.09		0.00	
1952		304.86	0.00		42.50			379.83	3.70		7.20		0.97	11.89	1.12		0.00	
1953		349.09	0.00		51.70			423.34	3.90		8.80		0.97	12.24	1.16		0.00	
1954		369.72	0.00		61.90			442.88	3.60		9.80		0.97	12.60	1.19		0.00	
1955		314.07	0.00		55.50			350.97	4.50		9.50		0.97	12.97	1.23		0.00	
1956		339.83	0.00		52.07			410.73	4.50		6.40		0.97	13.35	1.26		0.00	
1957		320.46	0.00		65.23			382.83	5.50		10.20		0.97	13.74	1.30		0.00	
1958		303.85	0.00		66.09			372.08	5.60		10.10		0.97	14.15	1.34		0.00	
1959		239.48	0.00		58.11			357.16	5.70		10.10		0.97	14.56	1.38		0.00	
1960		259.62	0.00	29.03	84.05			350.22	5.70	156.60	23.90			14.99	1.43	0.00	0.00	
1961		286.94	0.00	27.67	97.70			351.31	5.80	161.20	21.30			14.01	1.32	0.00	0.00	
1962		271.44	0.00	24.33	94.94			328.04	5.50	150.30	22.70			13.58	1.28	0.00	0.00	
1963		291.73	0.00	25.73	97.99			355.33	6.20	169.90	26.20			14.77	1.40	0.00	0.00	
1964		312.36	0.00	23.92	110.64			382.11	6.50	180.90	30.70			15.57	1.47	0.00	0.00	
1985						59.78						167.45						0.99
1986						62.22						174.20						1.02
1987						60.01						134.88						1.05
1988						53.41						91.98						1.08
1989						57.46						53.01						1.11
1990						56.81						14.81						1.14
1991						62.82						16.54						1.17
1992						68.36						18.47						1.21
1993						73.39						20.51						1.24
1994						78.75						22.89						1.28
1995						73.12						22.26						1.32
1996						68.97						21.61						1.34
1997						63.36						21.20						1.34
1998						57.41						20.39						1.36
1999						51.40						18.89						1.38
2000						44.12						16.30						1.15
2001						36.43						13.17						0.91
2002						27.60						10.27						0.69
2003						18.97						7.29						0.43
2004						10.06						3.87						0.25

6.3.5 The Use Tables

There are four Use Tables covering the periods pre-1985 (which is used by the Pre-1985 Production Table (Section 6.3.4)), 1985 to 1996, 1997 to 2015 and 2016 to 2030 (which are used by the Halocarbon Model Table (Section 6.3.2)). Each expresses the proportion (as a percentage) of each halocarbon used in each of eight possible applications, discussed in Section 6.2.3. The Use Table for pre-1985 only contains data on those halocarbons with delayed emission uses, which is based on averaged literature values (Section 6.3.2). The Use Table for 1985 to 1996 is based on average use after 1988, taken from the published sources in Section 6.3.2. In this way, an allowance is made for changing usage patterns, eg. the rapid decline in the use of propellants. For simplicity, in the absence of predictions of future usage patterns, the 1997 to 2015 and 2016 to 2030 Use Tables are copies of the 1985 to 1996 Use Table. The Use Tables are shown in Table 6.9.

6.3.6 Flux Delay Coefficients Table

This table holds the delay coefficients shown in Table 6.1 for the chlorine loading model and Table 6.2 for the bromine loading model and is utilised by the flux equations in the Halocarbon Model (Section 6.3.2).

6.3.7 Coefficients used to determine Emissions of Halons in Year Zero

This contains the values of the percentage of the production of the halons which are emitted in the year of production, as given by McCulloch[14] and shown in Table 6.2.

6.3.8 Sensitivity Tables

The chlorine and bromine loadings under Montreal Protocol 3 form the reference levels for most of the results in this work (as mentioned in Section 6.2.3, some results for

Table 6.9 The Use Tables - Pre-1985, 1985-1996 and 1997-2015 - for the chlorine loading model. The Use Table 2016-2030 is a copy of the 1997-2015 Use Table and is therefore not shown.

USE TABLE 1 PRE 1985

PERCENTAGE USED IN EACH CATEGORY

HALOCARBON	Refrigerant		Foams		Cleaning	Aerosol	Other
	Hermetic	Non Hermetic	Open Cell	Closed Cell	Agent	Propellant	
CFC 11		8.41	18.21	35.54		31.87	5.97
CFC 12	1.73	47.18	4.29	8.53		32.79	5.49
CFC 114	9.45		90.55				
HCFC 22	0.05	94.87	5.04	0.05			

USE TABLE 2 1985-1996

PERCENTAGE USED IN EACH CATEGORY

HALOCARBON	Refrigerant		Foams		Cleaning	Aerosol	Fire	Other
	Hermetic	Non Hermetic	Open Cell	Closed Cell	Agent	Propellant	Retardant	
CFC 11		8.60	18.36	52.08		15.28		5.69
CFC 12	2.18	60.18	1.84	12.31		17.79		5.70
CFC 113					100.00			
CFC 114	24.19		75.81					
CFC 115		100.00						
HCFC 22	0.19	88.30	11.33	0.19				
HCFC 123		100.00						
HCFC 124	33.33		33.33	33.33				
HCFC 141b			33.33	33.33	33.33			
HCFC 142b			33.33	33.33		33.33		
HALON 1211							100.00	
CARBON TETRACHLORIDE					100.00			
METHYL CHLOROFORM					100.00			

USE TABLE 3 1997-2015

PERCENTAGE USED IN EACH CATEGORY

HALOCARBON	Refrigerant		Foams		Cleaning	Aerosol	Fire	Other
	Hermetic	Non Hermetic	Open Cell	Closed Cell	Agent	Propellant	Retardant	
CFC 11		8.60	18.36	52.08		15.28		5.69
CFC 12	2.18	60.18	1.84	12.31		17.79		5.70
CFC 113					100.00			
CFC 114	24.19		75.81					
CFC 115		100.00						
HCFC 22	0.19	88.30	11.33	0.19				
HCFC 123		100.00						
HCFC 124	33.33		33.33	33.33				
HCFC 141b			33.33	33.33	33.33			
HCFC 142b			33.33	33.33		33.33		
HALON 1211							100.00	
CARBON TETRACHLORIDE					100.00			
METHYL CHLOROFORM					100.00			

the chlorine loading model still have Montreal Protocol 2 as a reference level). In order to perform a sensitivity analysis, one or several of the variables in the models are altered, and a new chlorine (or bromine) loading is obtained. These new values can be compared to the reference level to form a table of results which is displayed graphically. The results of such analyses are given in Chapter 7 for the chlorine loading model and Chapter 8 for the bromine loading model.

Chapter 7

Results and Discussion of the Chlorine Loading Model

7.1 Introduction

There are three features of the chlorine loading model results which are of interest. These are;

1) the magnitude of the peak chlorine loading which is attained as a result of the maximum impact of the halocarbons that have been emitted to atmosphere.

2) the timing of that peak chlorine loading.

3) as chlorine levels fall due to the Montreal Protocol 3 stipulations, the date at which chlorine levels return to 2 ppb, which represents the approximate atmospheric chlorine loading when the Antarctic ozone hole was first discovered[1] by Joe Farman and his co-workers,[2] but which is still some three times higher than natural levels of chlorine of 0.6-0.7 ppb.

7.2 The Montreal Protocol 3 Reference Level

This is the level used as a comparison for most of the sensitivity studies performed in this work. It represents the most up to date international agreement at the time of writing.

7.2.1 Montreal Protocol 3 in terms of Chlorine Loading

Figure 7.1 illustrates the chlorine loading under Montreal Protocol 3, assuming full compliance by signatory countries and no delay in compliance by developing countries (which in reality is allowed, and is discussed in Section 1.4). The chlorine loading rises from an initial level of 3.04 ppb in 1985 to a peak of 3.80 ppb in 1994. This peak then decays to 2 ppb in 2053 and 1.38 ppb by the end of next century.

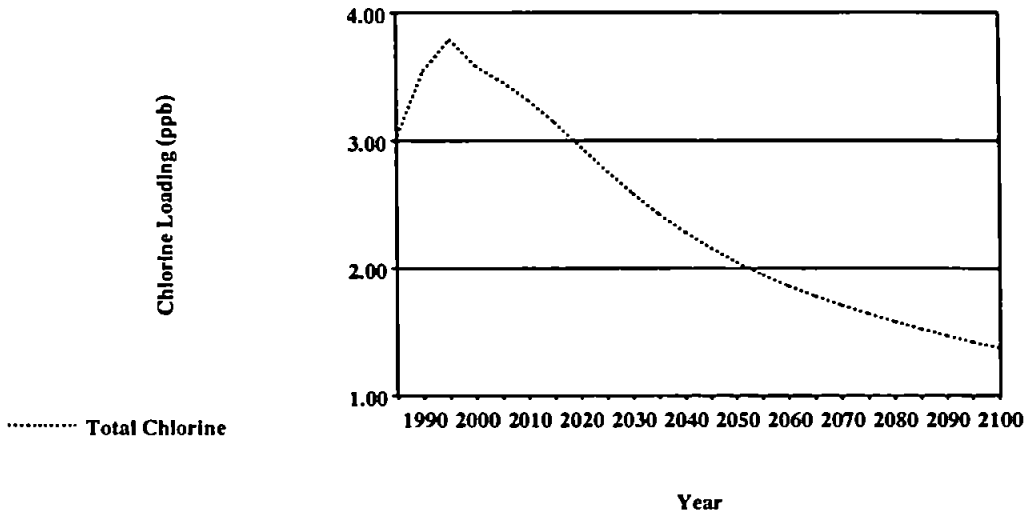

Figure 7.1 The total chlorine loading under Montreal Protocol 3.

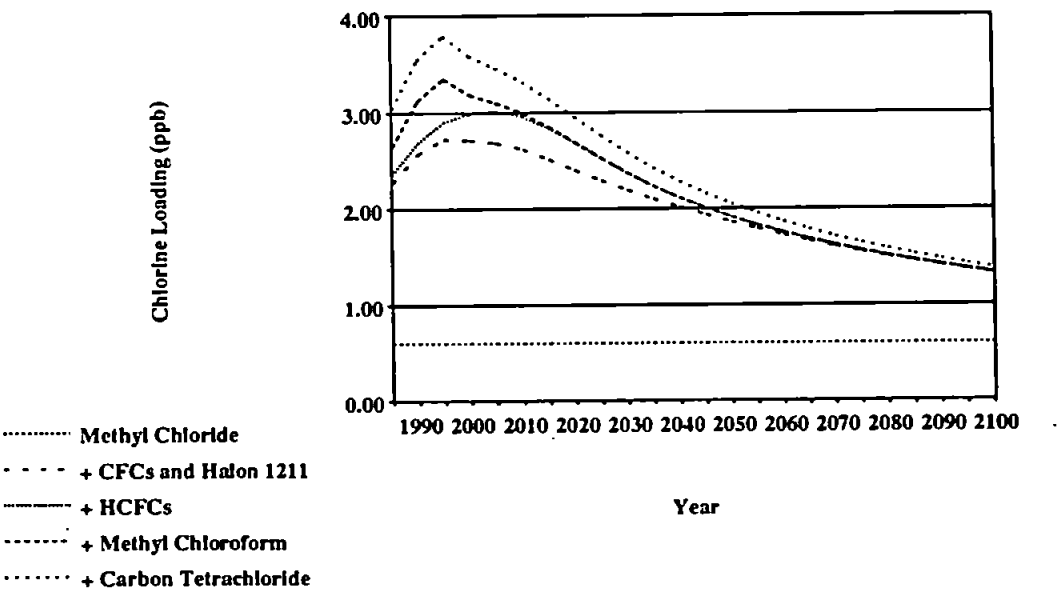

Figure 7.2 The cumulative contribution of the halocarbon groups which generate the total chlorine loading under Montreal Protocol 3.

The total chlorine loading under Montreal Protocol 3 (Figure 7.1), can be sub-divided into the cumulative contribution of the halocarbon groups which generate it (Figure 7.2). The contribution these halocarbon groups make to the total chlorine loading is also illustrated as a percentage contribution in Figure 7.3. For the purposes of these graphs, the divisions are methyl chloride, CFCs and halon 1211, HCFCs, methyl chloroform and carbon tetrachloride. Observation of Figure 7.2 shows that the dotted straight line is the contribution of methyl chloride, which is constant at 0.6 ppb. The lowest curve shows the extent to which the CFCs add to the chlorine loading, contributing 56% (66% of man-made chlorine) in 1995 and 53% (94% of man-made chlorine) in 2100. The HCFCs contribute about 5% to the total chlorine loading in 1995 rising to around 10% by 2015 (13% of man-made) and is negligible by 2070. Methyl chloroform adds 12% to total chlorine (14% of man-made) in 1995, but due to its short lifetime of 6.1 years has a negligible effect by 2020. Carbon tetrachloride, which is relatively long lived (47 years) adds 0.44 ppb (12% and 14% of total and man-made chlorine respectively) to the chlorine loading in 1995 and 4% and 6% to total and man-made chlorine respectively in 2100.

Figures 7.4 to 7.6 show the contribution of the individual halocarbons to the total chlorine loading. These figures illustrate which of the halocarbons contribute most to atmospheric chlorine. The dominance of CFC 12 is caused in part by the large level of production (up to 424.7 kt in 1987) and its long atmospheric lifetime (Table 6.6). The combination of these factors means that it continues to increase its contribution to the chlorine loading until 2065 (when it contributes 33.4%) before decreasing back to 32.0% by 2100. CFC 11 is similarly at high levels of production, reaching 382.05 kt in 1987, but owing to its shorter lifetime (Table 6.6) its contribution to the chlorine loading peaks at 24.3% in 2010 and decreases back to 11.6% by 2100. The long lifetime of CFC 113 (Table 6.6) means that once it has been phased out, its contribution to atmospheric

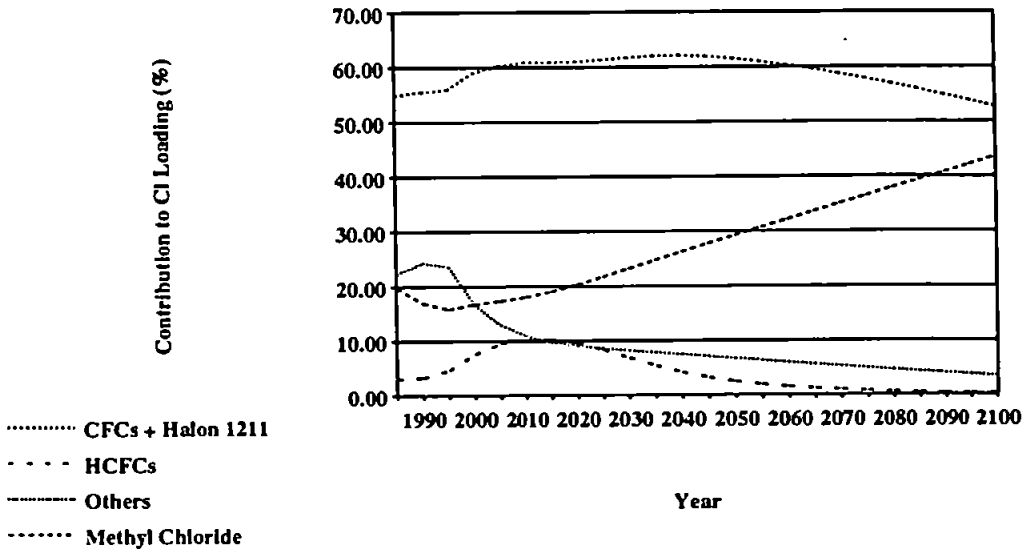

Figure 7.3 The contribution to the total chlorine loading of each of the halocarbon groups.

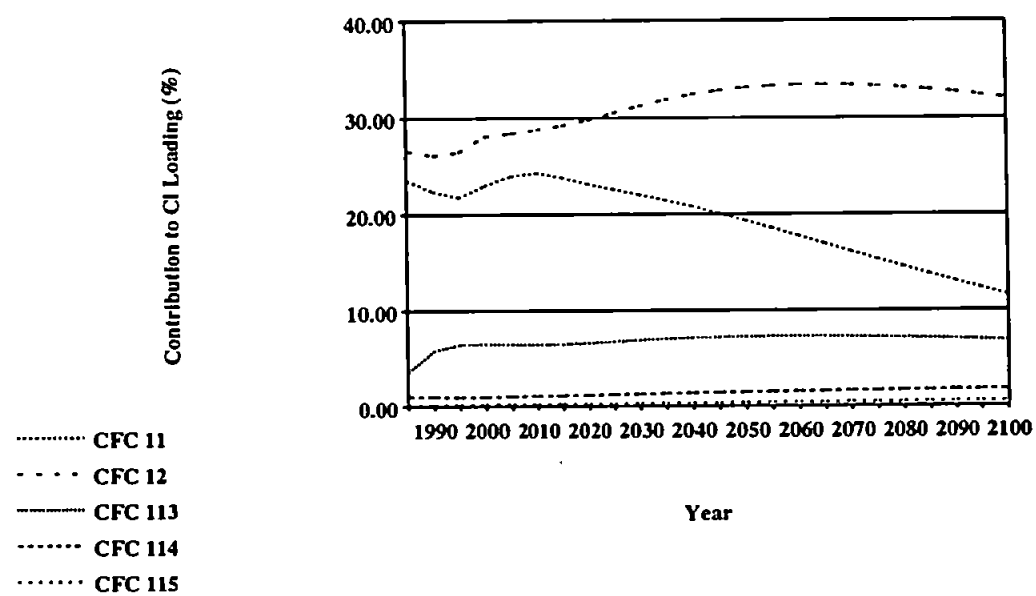

Figure 7.4 The contribution to the total chlorine loading of the CFCs.

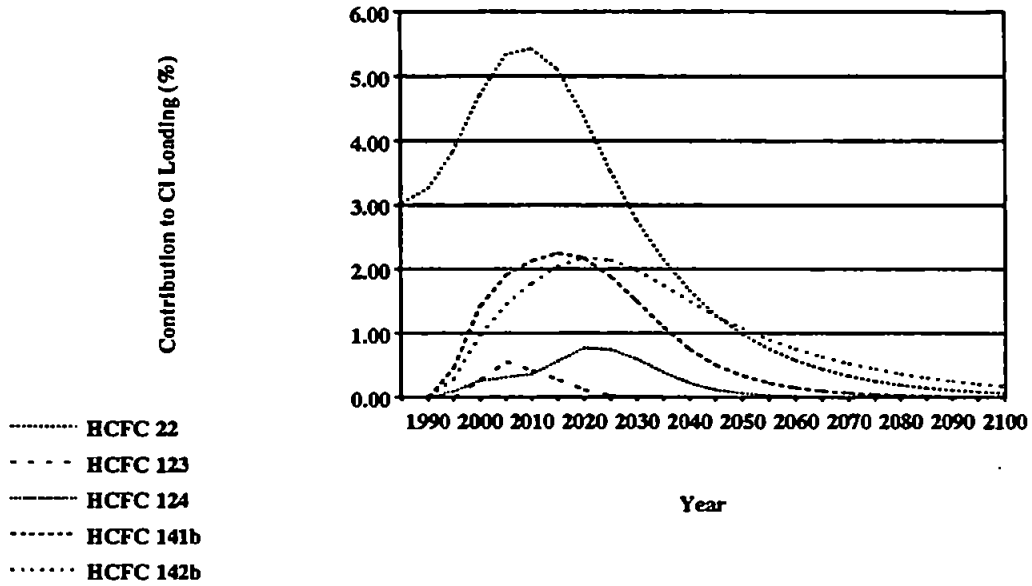

Figure 7.5 The contribution to the total chlorine loading of the HCFCs.

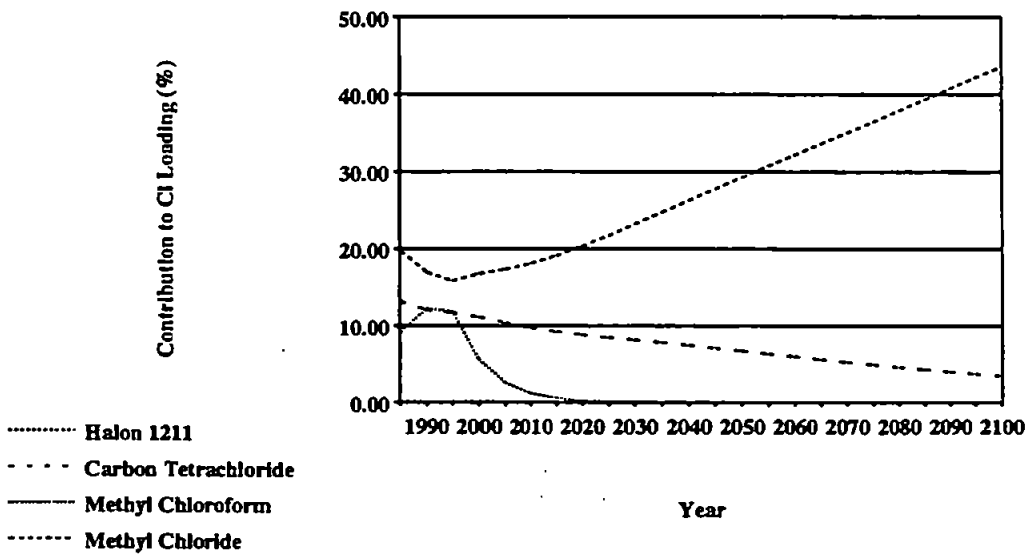

Figure 7.6 The contribution to the total chlorine loading of the other halocarbons.

chlorine remains relatively stable between 6.5% and 7.3% for much of the next century. CFCs 114 and 115 contribute a small amount to atmospheric chlorine, due to low levels of production (maximum 19.1 kt and 14.2 kt respectively). However, owing to their very long lifetimes (Table 6.6), both exhibit an increase in their respective contributions throughout next century.

Figure 7.5 shows that HCFC 22 is the dominant contributor to the chlorine loading amongst the HCFCs, reaching a maximum of 5.4% by 2010. This makes it comparable with CFC 113 at its peak and therefore, although an HCFC, is a significant contributor of chlorine. Of the other replacement HCFCs, HCFCs 141b and 142b contribute most (2.3% in 2015 and 2.2% in 2020 respectively). Such is the longevity of HCFC 142b that it contributes more to the chlorine loading after 2050 than HCFC 22. HCFCs 123 and 124 exhibit only minor affects.

The contribution from the chlorine in halon 1211 (Figure 7.6) is so small that its line on the graph is obscured by the bottom axis. Carbon tetrachloride exhibits a slow decay from 13.0% to 3.5% owing to its 47 year lifetime (Table 6.6). The contribution from methyl chloroform is large at present due to its levels of production (793.8 kt in 1992-93), but declines to nothing by 2050 because of its short lifetime (Table 6.6). The gradual rise in the contribution of methyl chloride to the chlorine loading throughout next century is solely due to the decrease in contribution of the man-made halocarbons (as methyl chloride levels remain constant throughout the model). Obviously if there were no influence from these anthropogenic sources, methyl chloride would make up 100% of the contribution to the chlorine loading, which would correspond to a return to natural total chlorine levels of 0.6-0.7 ppb. The fact that the contribution of methyl chloride is still only 43.6% in the year 2100 is due to the longevity and levels of production of many of the man-made halocarbons, phased out over a century before this date.

The proportion of halocarbons in each of the use categories (Section 6.2.3) is

illustrated in Figure 7.7 for 1988, 2000 and 2020. Owing to lack of estimates and in the absence of better information, usage patterns in 2020 are assumed to be the same as in 2000. The predominant use as cleaning agents in the late 1980s is due to the large production of methyl chloroform. However as the CFCs, methyl chloroform and carbon tetrachloride are removed under Montreal Protocol 3, it is the cleaning agents which are more likely to be replaced by ozone benign technologies. However, use in refrigeration and foam blowing provides technical difficulties for which replacement HCFCs are likely to be primarily used, reflecting the increase in these applications at the expense of the cleaning agents.

7.2.2 Montreal Protocol 3 in terms of Production

Figure 7.8 shows the production of the halocarbons by halocarbon group, while Figures 7.9 to 7.11 show this broken down further to show the proportion of production which is due to the individual CFCs, HCFCs and other halocarbons. Figure 7.8 illustrates the rapid decline in the use of the CFCs and 'other' (halon 1211, methyl chloroform and carbon tetrachloride) halocarbons as a result of the Montreal Protocol 3 measures. The prolonged use of the HCFCs in the model is at the levels shown in Figure 7.8. Figure 7.9 shows that it is CFCs 11 and 12 which contribute most to the CFC peak in Figure 7.8. CFCs 114 and 115 maintain a relatively stable but small proportion of the total CFC market share until their phase out by 1996. Figure 7.10 shows how the assumed rise in HCFC use in the model, increases the market share of HCFC 22 and the other hydrochlorofluorocarbons, at the expense of the halocarbons phased out under Montreal Protocol 3. After 1996, they therefore total 100% of halocarbon production. The increase in the halocarbon market share shown by carbon tetrachloride and methyl chloroform in Figure 7.11, is as a result of more severe cutbacks placed on the CFCs by 1994 (Table 1.1).

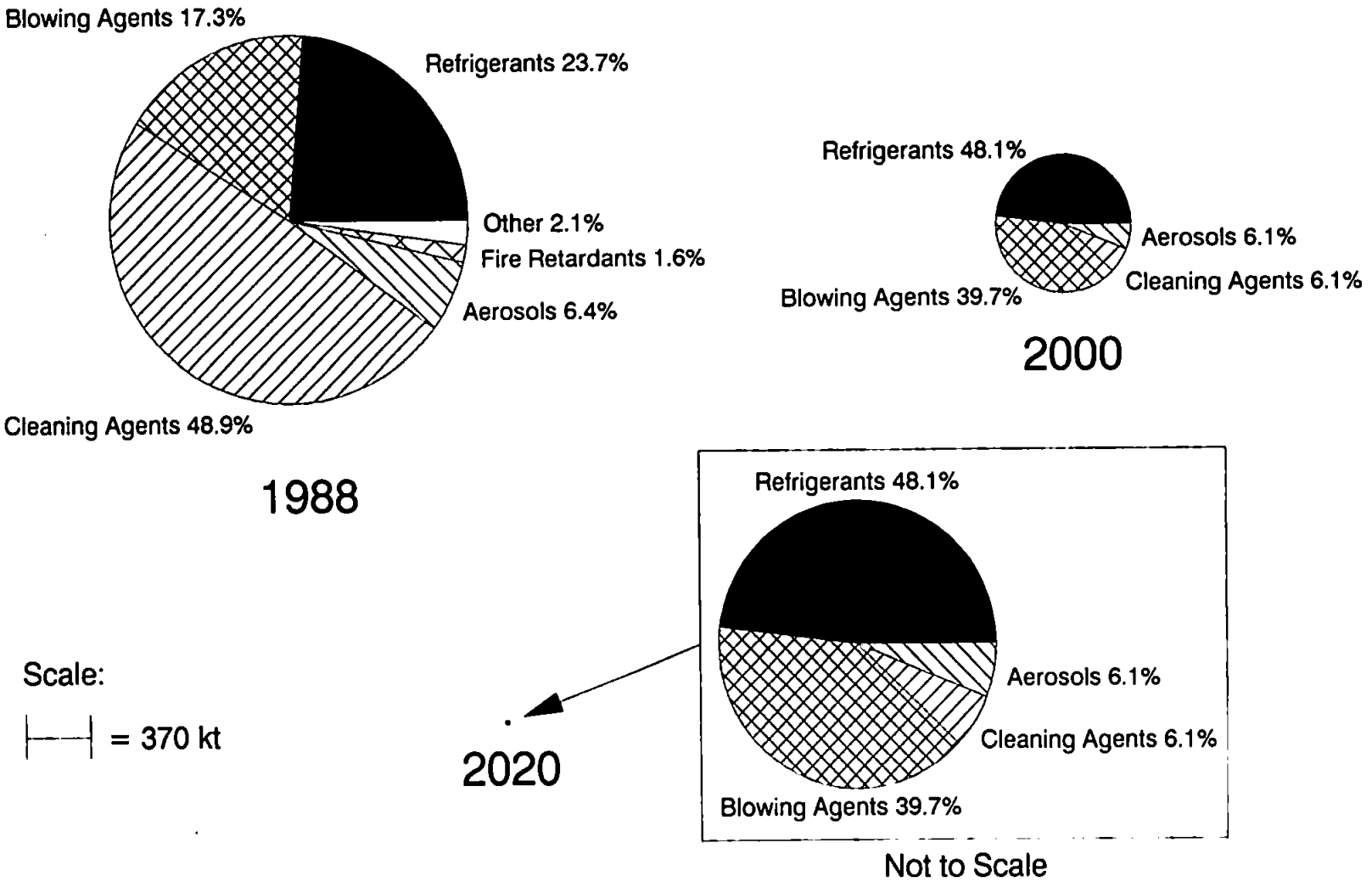

Figure 7.7 Diagram illustrating how the man-made halocarbons are used in the model. The size of the pie charts reflects the level of consumption. Methyl chloride and methyl bromide are omitted.

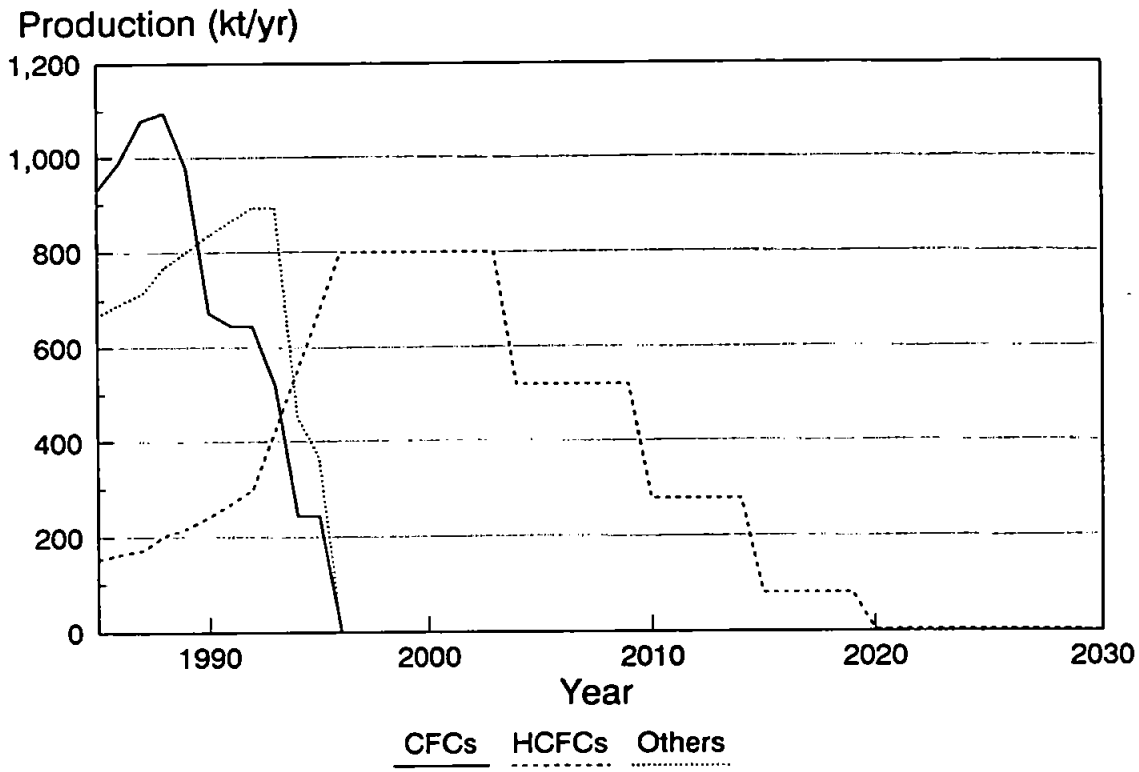

Figure 7.8 Diagram of the total production of the halocarbons by group.

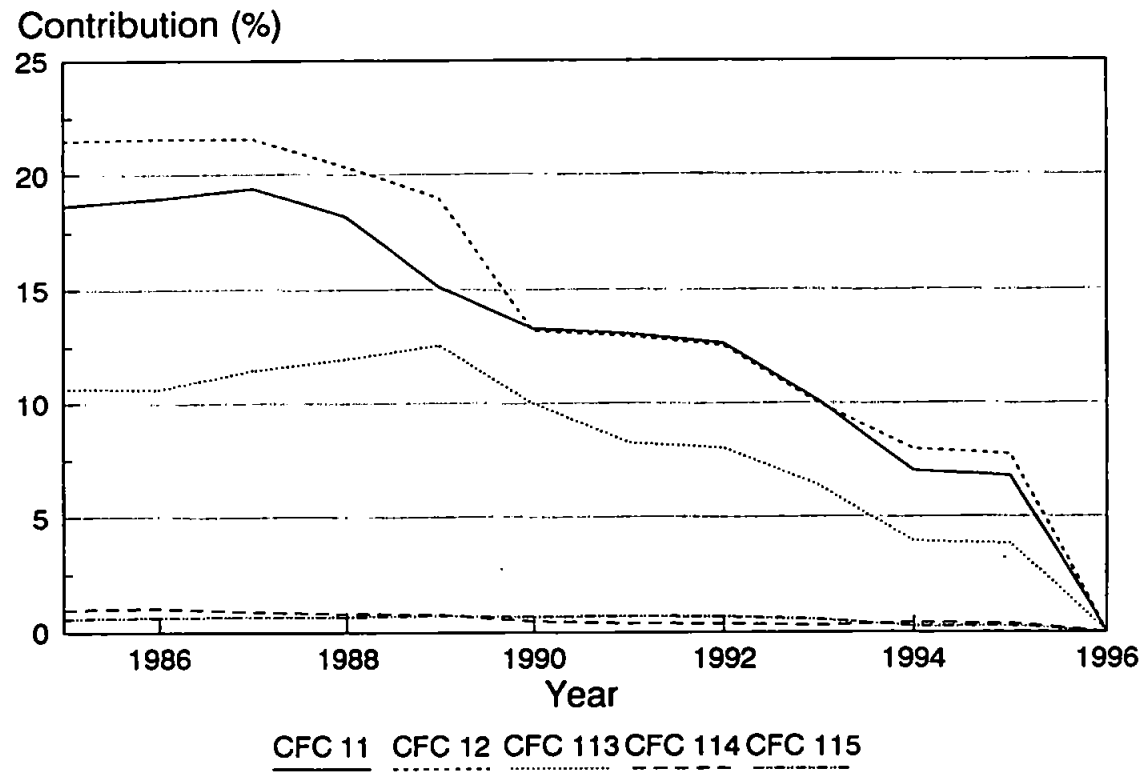

Figure 7.9 The contribution to total production of the CFCs.

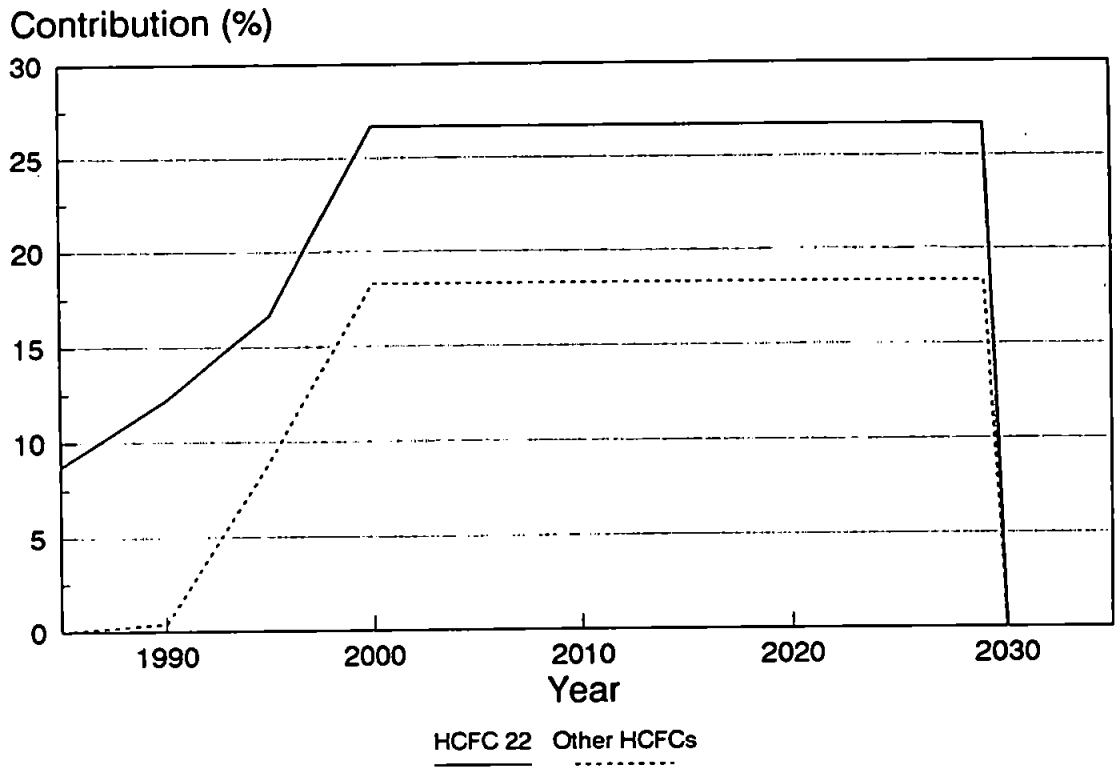

Figure 7.10 The contribution to total production of the HCFCs.

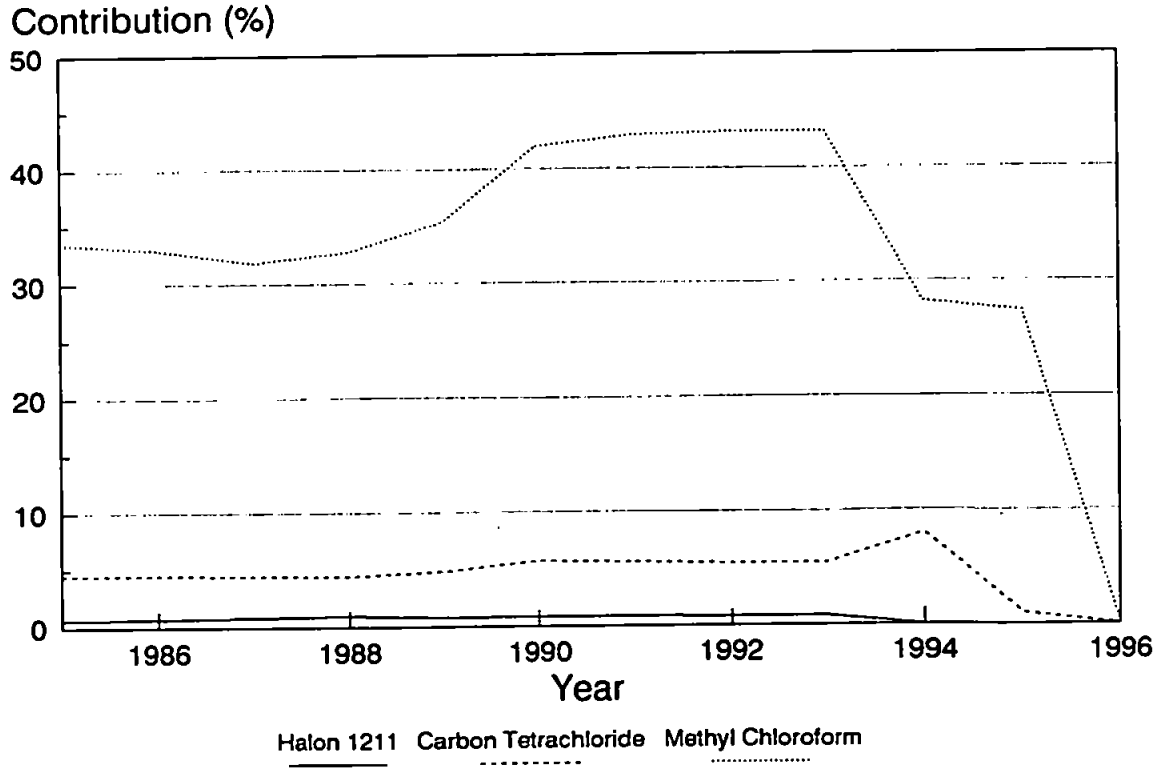

Figure 7.11 The contribution to total production of the other halocarbons.

Figure 7.12 is included for interest as it shows the cumulative contribution of CFCs used in each of the usage categories relative to the Montreal Protocol 3 reference year, 1986 (when the total cumulative contribution was 100%). It shows that, for the CFCs, application in refrigeration, foam blowing and cleaning form the dominant market share, taking up over 80% of all CFCs produced in 1988. It also reflects the rapid decline in the use of CFCs as aerosol propellants from 25% of the market in 1985 to 13% by 1994, due to the use of easily available alternatives. Total production reaches a maximum of only 10% above the 1986 reference level, by 1988, before its eventual decline to nothing by 1996.

7.3 Comparison of Modelled Results with Measured Data

If a computer model is to be of use, it must produce predicted results in line with measured trends. In such a way, the model will inspire confidence for predictions which cannot be confirmed by measurement. Therefore the results of the reference scenario for the early years of the chlorine loading model have been compared to published measurements. Some comparisons are given below;

1) The published rise in atmospheric chlorine for the late 1980's is approximately 0.1 ppb yr^{-1}.[3] Between 1985 and 1990, the model predicts an average rise in atmospheric chlorine which matches this.

2) The published atmospheric concentration of chlorine in 1985 is 3.00 ppb.[3] The model value is 3.04 ppb, only 1.3% above the measured level.

3) The uses to which CFCs and HCFCs are employed in the model have been checked to several sources[4-10] where we find good agreement.

4) The proportion of CFCs used in the late 1980s in each of the usage categories can be compared to estimates by Du Pont[11] and den Elzen et al.[12] (Figure 7.13). The major difference arising between these results is in the allocation of the market share for

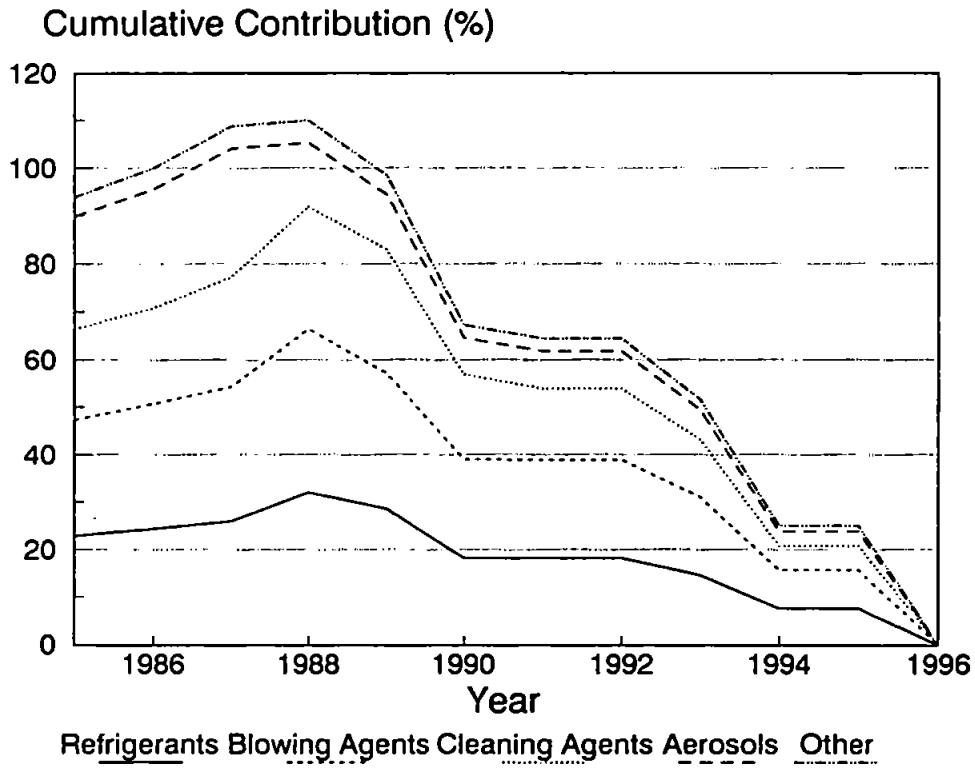

Figure 7.12 The cumulative use of CFCs relative to 1986 production.

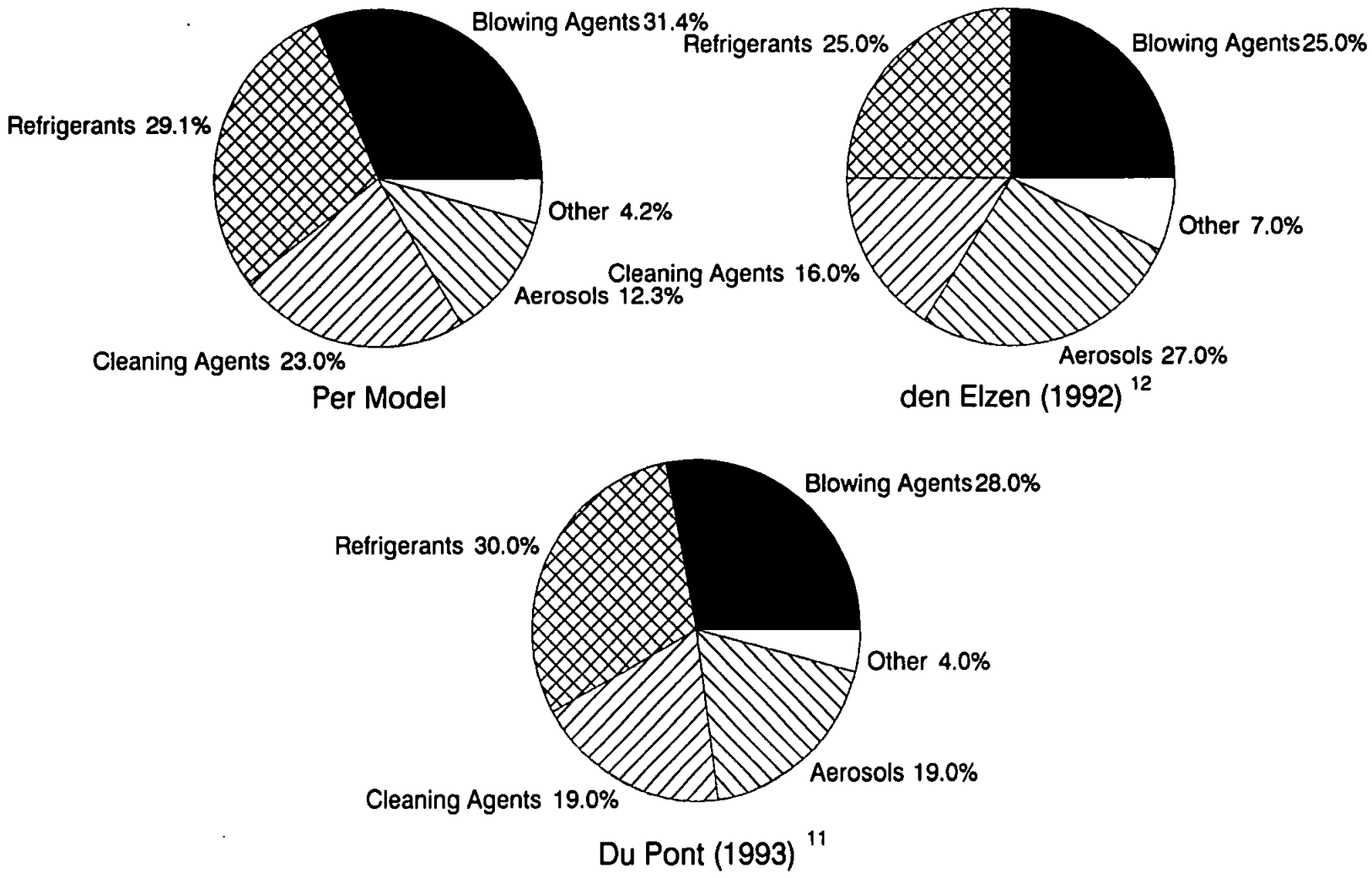

Figure 7.13 Comparison of CFC usage patterns in the chlorine loading model with published usage patterns.

aerosols. We believe our study more accurately reflects the rapid decline in use of CFCs in this application and the corresponding rise in the blowing agent and refrigerant markets. Overall, the similarities between the studies (especially our own and Du Pont's) are encouraging.

7.4 Results and Discussion of the Sensitivity Analyses

This section details the findings of a number of sensitivity studies used in the chlorine loading model. A sensitivity study is designed to show to what degree the atmospheric chlorine loading is influenced by actual or possible forcing factors.

7.4.1 Sensitivity to Uncertainty in the Data used in the Model

Before modelling possible future scenarios, it is useful to assess the sensitivity of the atmospheric chlorine loading to basic uncertainties in the published data used in the model.

Lifetime - the lifetimes used in the model[3,13] for the CFCs and other halocarbons have an associated large level of uncertainty (Table 7.1). A published estimate of the uncertainty in the atmospheric lifetimes of the HCFCs has not been found, so we have adopted an estimated ±30% change on the lifetime of the HCFCs 22, 123, 124, 141b and 142b in order to account for the greater sensitivity of the HCFCs to hydroxyl (OH) concentrations in the atmosphere. Hydroxyl radicals form one of the main removal processes for the HCFCs and therefore their concentration, which is not accurately known and is likely to change with time, is an important consideration. Before looking at the overall effect of uncertainties in atmospheric lifetimes we should assess the effect of our assumed uncertainty in HCFC lifetime of ±30% (Table 7.2, Figure 7.14).

Figure 7.14 shows that even a large uncertainty of ±30% in HCFC lifetime has a minimal effect on the peak chlorine loading (Table 7.2) of 0.5% or less. There is more

Table 7.1 Uncertainty in published atmospheric lifetimes.[3]

Halocarbon	Lifetime /years	Range /years	Uncertainty /% less than Lifetime	Uncertainty /% more than Lifetime
CFC 11	55	42-66	23.6	20.0
CFC 12	116	95-130	18.1	12.1
CFC 113	110	75-144	31.8	30.9
CFC 114	220	197-264	10.5	20.0
CFC 115	550	400-800	27.3	45.5
Halon 1211	13	11-16	15.4	23.1
Carbon Tetrachloride	47	30-58	36.2	23.4
Methyl Chloroform	6.1	5.1-6.4	16.4	4.9

Table 7.2 Sensitivity to uncertainty in the data used in the chlorine loading model.

Data Category	Limit	Change on Peak Chlorine in Reference Scenario (%)	Year of Peak Chlorine (years)	Change in 2 ppb Date (years)
HCFC Lifetime	+30%	+0.3	-	+5
	-30%	-0.5	-	-2
Lifetime	Upper	+2.1	+1	+12
	Lower	-4.5	-1	-15
Concentration	Upper	+2.1	-	+1
	Lower	-2.4	-	-2
Production	Upper	+0.3	-	-
	Lower	-0.3	-	-
Growth CCl_4	0%	-0.3	-	-1
Growth	Long Term	+0.3	-	-
	Short Term	-0.3	-	-1
Use	±50%	-0.5	-	-
	±100%	-1.3	-	-
Gradual Phase Out	-	-1.8	-	-3

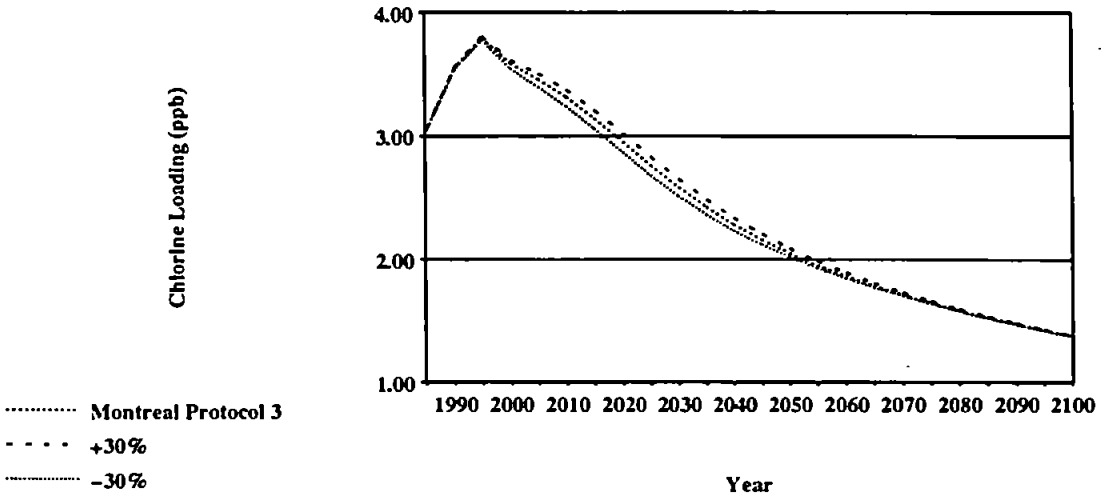

Figure 7.14 The sensitivity of the total chlorine loading to an error in HCFC lifetime.

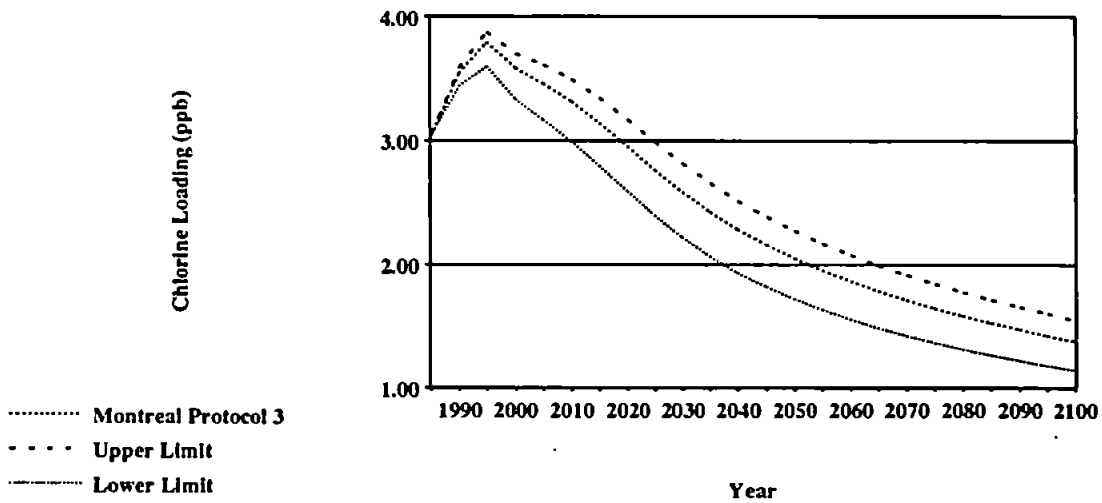

Figure 7.15 The sensitivity of the total chlorine loading to uncertainty in halocarbon lifetime.

of an affect on the 2 ppb date (Table 7.2) because HCFCs contribute around 3% of man-made chlorine at this time.

Now using the published upper and lower limits for lifetimes (Table 7.1)[3] and the ±30% limits for the HCFCs, the overall sensitivity of the atmospheric chlorine loading to lifetime of the halocarbons can be assessed (assuming methyl chloride to be held constant), and is shown in Figure 7.15 and Table 7.2. It should be noted that this result assumes that the uncertainties in lifetime for each gas operate systematically, which in reality is unlikely to be the case. Figure 7.15 and Table 7.2 therefore represent an absolute maximum in uncertainty of the chlorine loading to halocarbon lifetime. Within this, the assumed uncertainty in HCFC lifetime accounts for +14%/-11% in peak chlorine and +42%/-13% in the 2 ppb date.

These results show that atmospheric lifetime remains a major uncertainty. Other sensitivity studies should be viewed in the context of this large uncertainty, which arises due to the difficulty in modelling the complicated reaction sequences which remove these compounds from the atmosphere, a discussion of which is beyond the scope of this work.

1985 Concentration - the atmospheric concentrations initially used in the model are subject to a calibration uncertainty which is shown in Table 7.3.[3] HCFCs 123, 124, 141b and 142b are not included as they are not present in 1985, and methyl chloride remains constant. No calibration uncertainty is given for CFCs 114 and 115 in published sources so these are assumed to have a maximum uncertainty of ±10%. Assessing the affect of this assumed uncertainty, revealed a negligible difference to both peak chlorine loading and the timing of the 2 ppb date. When applying the upper and lower limits of the calibration uncertainty to the model, the results in Figure 7.16 and Table 7.2 are produced. The interpretation is subject to the same limitations expressed for the lifetime uncertainties above, concerning the assumption of systematic error. Uncertainty in calibration of methyl chloroform and carbon tetrachloride contribute 31% each to the overall uncertainty,

Table 7.3 Uncertainty in published atmospheric concentrations due to calibration error.[3]

Halocarbon	Calibration Uncertainty /±%	1985 Concentration /pptv	Upper Limit /pptv	Lower Limit /pptv
CFC 11	1	238.51	240.90	236.12
CFC 12	2	404.37	412.46	396.28
CFC 113	10	36.71	40.38	33.04
HCFC 22	10	92.25	101.48	83.03
Halon 1211	15	1.50	1.73	1.28
Carbon Tetrachloride	10	99.93	109.92	89.94
Methyl Chloroform	15	93.20	107.18	79.22

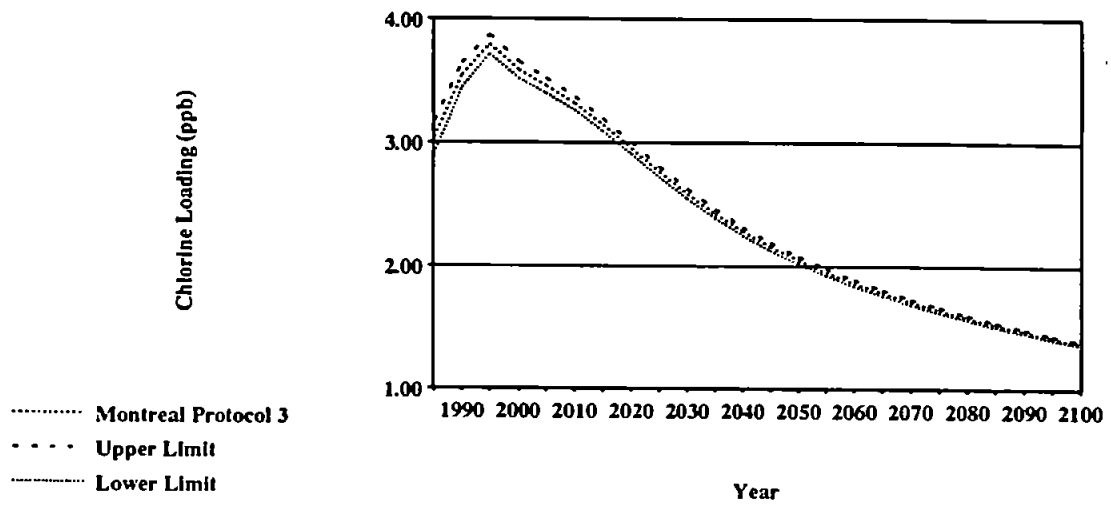

Figure 7.16 The sensitivity of the total chlorine loading to calibration error in determination of halocarbon concentrations in the atmosphere.

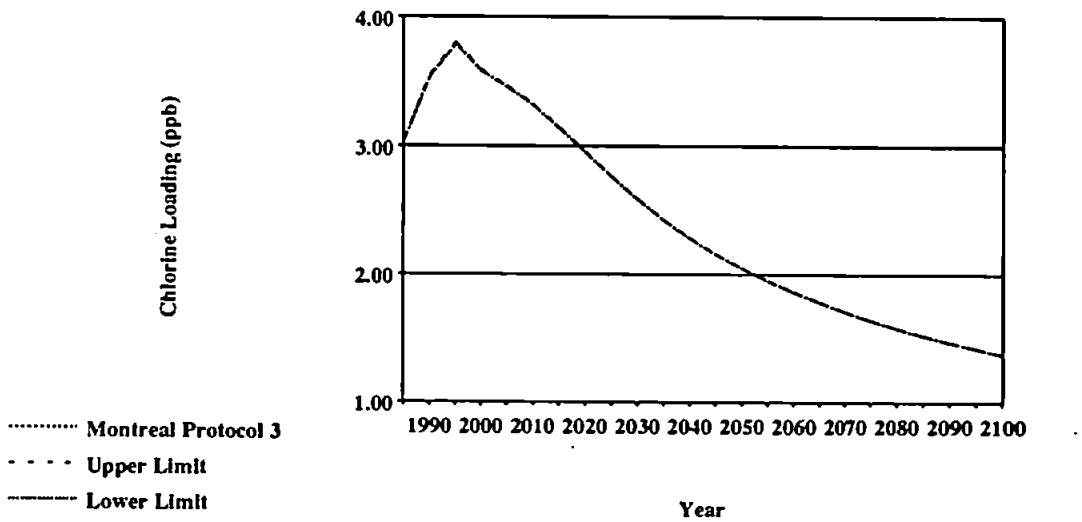

Figure 7.17 The sensitivity of the total chlorine loading to errors in production data used in the model.

compared with 23% for CFC 11 and 12. These four halocarbons are the major contributors.

Production - as with lifetime and concentration, data used in the model for production has an associated uncertainty, the limits of which are given in the relevant published sources (Section 6.3.2).[14-19]

It is assumed that the accuracy of production data for the replacement HCFCs 123, 124, 141b and 142b will be at least as good as that for the CFCs and HCFC 22, because of increased awareness of the level of halocarbons being used. Therefore we take the estimated uncertainty in production of the HCFCs as being the average uncertainty for the CFCs and HCFC 22, which amounts to ±0.4%. This estimate is also applied to carbon tetrachloride production data, as no error limits could be found from published sources. All pre-1985 production and methyl chloride production remain unaffected. Figure 7.17 and Table 7.2 show the results of the sensitivity analysis.

The effects on peak chlorine are negligible, increasing and decreasing it by only 0.01 ppb only. The timing of the peak and the 2 ppb date are unaffected. The model is therefore not sensitive to errors in production data as these errors are small.

Growth/Decline - The aim of this study is to ascertain whether the atmospheric chlorine loading is sensitive to the use of the growth factors given in WMO 1991,[3] and subsequently used in the model. Instead of the WMO growth factors,[3] a long term and short term growth/decline has been calculated (Table 7.4) from historical production data for the CFCs,[14,15,17] halon 1211[18] and methyl chloroform.[19] The replacement HCFCs and methyl chloride are assumed to remain constant, as growth factors given in WMO 1991[3] are not given for them.

In the absence of historical data for carbon tetrachloride, a sensitivity study on its estimated growth rate must be performed, before the effect of overall growth/decline of the halocarbons can be found. We use the estimate given in WMO 1985[20] that carbon

Table 7.4 Uncertainty in the growth rates of the halocarbons.

Halocarbon	Long Term		Short Term	
	Years	Growth /%	Years	Growth /%
CFC 11	1980-90	-1.36	1988-90	-14.71
CFC 12	1980-90	-2.84	1988-90	-16.62
CFC 113	1981-91	4.51	1989-91	-14.81
CFC 114	1981-91	-5.55	1989-91	-24.34
CFC 115	1981-91	3.08	1989-91	-2.26
Halon 1211	1980-90	9.05	1988-90	-3.24
Methyl Chloroform	1980-88	2.76	1986-88	+4.94

tetrachloride production is roughly stable, and therefore assume 0% growth from 1985 onwards. Such a change reduces the peak chlorine loading to 3.78 ppb and brings the 2 ppb date forward one year (Table 7.2).

Now applying the historical growth/decline figures in Table 7.4, and the 0% growth assumption for carbon tetrachloride, the results shown in Figure 7.18 and Table 7.2 are found.

This sensitivity study shows that the atmospheric chlorine loading is not sensitive to the use of the production growth factors given in WMO 1991[3] for the halocarbons, as peak chlorine rises to 3.81 ppb for the long term average and decreases to 3.79 ppb for the short term average. This lack of sensitivity is most probably due to the limited number of years over which they are applied (a minimum of 2 years for CFCs 113, 114 and 115 and a maximum of 9 years for carbon tetrachloride). Comparison with the assumed growth/decline for carbon tetrachloride shows that this has the dominant effect, in part due to the use of carbon tetrachloride growth factors over a greater number of years than for the other halocarbons.

Use - The aim of this study is to assess the affect of changes in the averaged usage patterns for the period 1985 to 1996. Usage patterns prior to 1985 are based on historical data[14-19] and therefore remain unchanged. The usage patterns after 1985 are based on the average percentage use for each gas in each application (Section 6.3.5). Comparison with pre-1985 use reveals changing trends in usage patterns for each of the halocarbons. CFCs 11, 12 and 114 all reveal an increasing trend towards use in categories leading to a delay in emission at the expense of immediate release categories. Only HCFC 22 shows a reversal of this trend with increased use in non-hermetic refrigeration at the expense of open cell foams.[16] CFCs 113 and 115, halon 1211, carbon tetrachloride and methyl chloroform are excluded from this analysis as they are associated with one usage type only. Future use of the HCFCs 123, 124, 141b and 142b is unknown and will be the

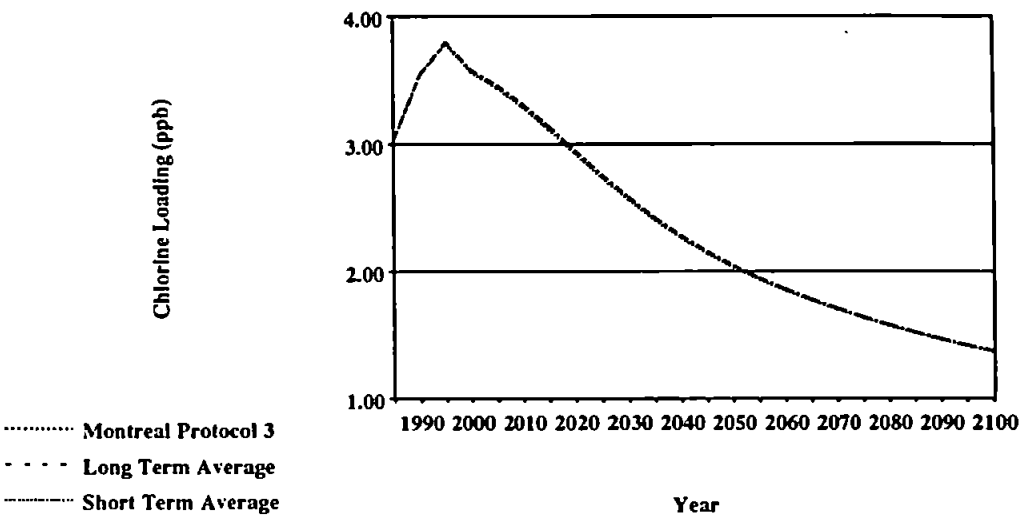

Figure 7.18 The sensitivity of the total chlorine loading to use of growth factors from WMO 1991.[3]

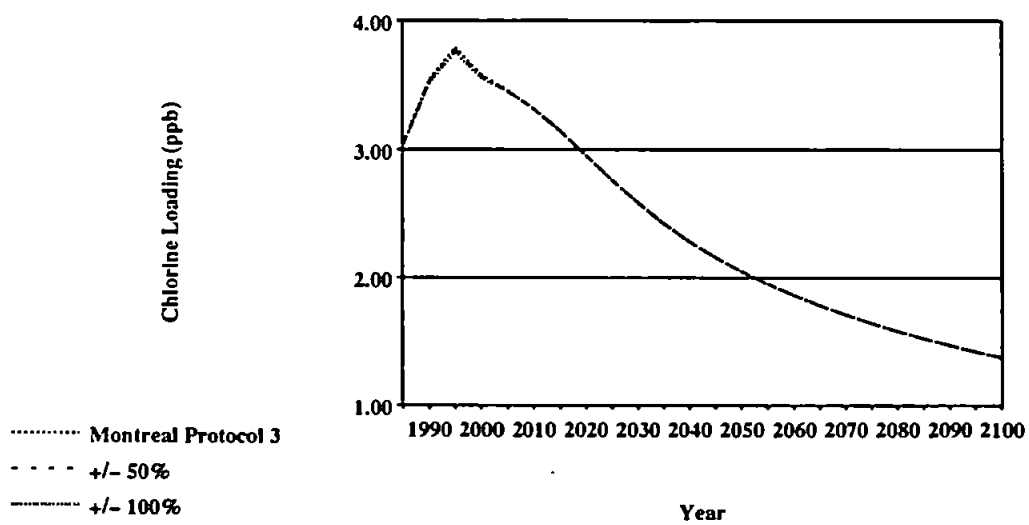

Figure 7.19 The sensitivity of the total chlorine loading to patterns of changing use.

subject of a separate sensitivity study (Section 7.4.9). Methyl chloride remains unchanged.

The effect of a change in usage patterns is illustrated by decreasing/increasing the smaller usage category by 50% and compensating the larger usage category to maintain 100% total usage. In a further calculation, the smaller usage category is reduced to zero and the contribution from the larger category compensated accordingly. Only the 1985 to 1996 usage table is altered for CFCs 11, 12 and 114 as they are phased out by 1996. The 1997 to 2015 and 2016 to 2030 tables are also altered for HCFC 22 owing to its continued production until 2030.

The effect of changes in the proportion of use allocated to short term release and long term release categories is illustrated in Figure 7.19 and Table 7.2. The effects of changes in CFC 114 and HCFC 22 use are negligible.

The chlorine loading under the ±50% and ±100% change in usage categories reduces from 3.80 ppb to 3.78 ppb and 3.75 ppb respectively. The reduction is an obvious consequence of reducing immediate use categories and increasing delayed release categories, thus causing more halocarbon to be retained in apparatus rather than being released into the atmosphere. Further analysis of these results reveals that it is the change in use of CFC 11 from aerosols to closed cell foams (75%) and CFC 12 from aerosols and open cell foams to non-hermetic refrigeration and closed cell foams (25%) which are the predominant causes of the trends shown in Figure 7.19. Usage in categories which give rise to immediate emission is generally declining. The market share of CFCs consumed by the aerosol industry has decreased by 50% between 1974 and 1988 due to replacement by ozone benign technology such as butane, propane and dimethylether (DME).[21] Of the existing CFC market, the area most likely to continue relying on halocarbon technology is the refrigeration industry, which is a delayed release category. These changes in usage patterns will serve to lower the peak chlorine loading. However they are also likely to extend the period before the 2 ppb date is reached.

Stepped vs Gradual Phase Out - the model assumes a simple stepped function, ie. production is maintained at a level until the next phase down requirements per Montreal Protocol 3 (Figure 7.8). In reality we might expect that instead of maintaining a plateau level, halocarbon production will gradually decrease into the next phase down objective of Montreal Protocol 3.

For this study, all the halocarbons (except methyl chloride which remains constant) are decreased linearly between Montreal Protocol 3 phase out requirements. The results are shown in Figure 7.20 and Table 7.2.

The difference between the reference case (stepped) and the sensitivity case (gradual) is solely due to the decreased production allocated to each halocarbon in the gradual phase out scenario. Further analysis reveals that a gradual phase out of methyl chloroform and carbon tetrachloride produces the dominant effect on the peak chlorine loading. CFCs 11, 12 and 114, plus carbon tetrachloride, exert the greatest influence on the 2 ppb date.

7.4.2 Sensitivity of the Chlorine Loading to use of Delay Coefficients.

The delay coefficients used in this work (Tables 6.1 and 6.2) are based on work by Gamlen, Lane and Midgley,[22] as are delay parameters used by AFEAS,[14-16] Brühl and Crutzen,[23] McCarthy et al.[24] and den Elzen et al.[12] It is of interest to compare the effect of using a delay coefficient against an assumption of no delay between production and flux, as used by Prather and Watson[1] and SORG 1990.[25] The purpose of this study is to provide a comparison between the simpler, no delay assumption and our own model, which incorporates an emission delay due to type of use.

Figure 7.21 and Table 7.5 show results of Montreal Protocol 3 for both the immediate and delayed emission scenarios. An immediate release assumption leads to a rise in peak chlorine of 0.09 ppb, which occurs in the same year as our reference scenario

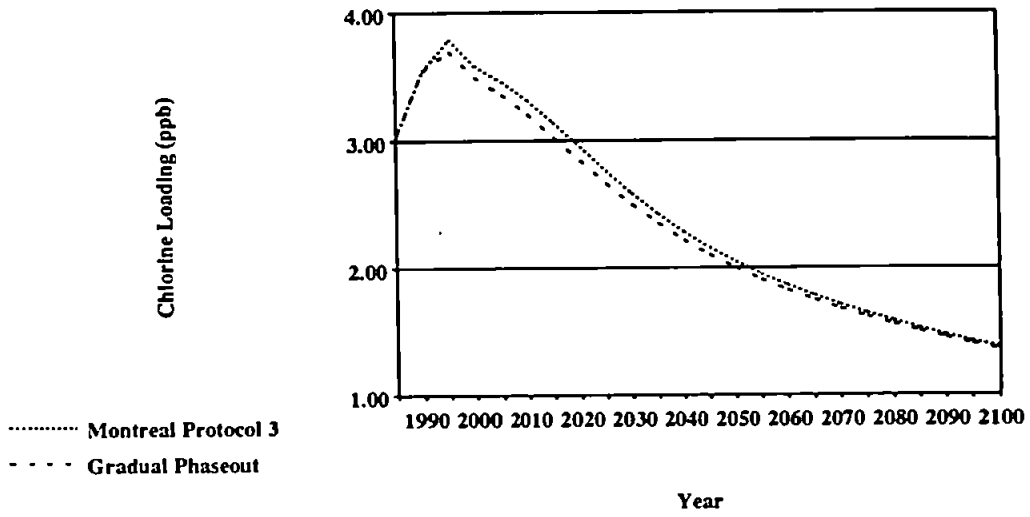

Figure 7.20 The sensitivity of the total chlorine loading to the stepped phase out assumption.

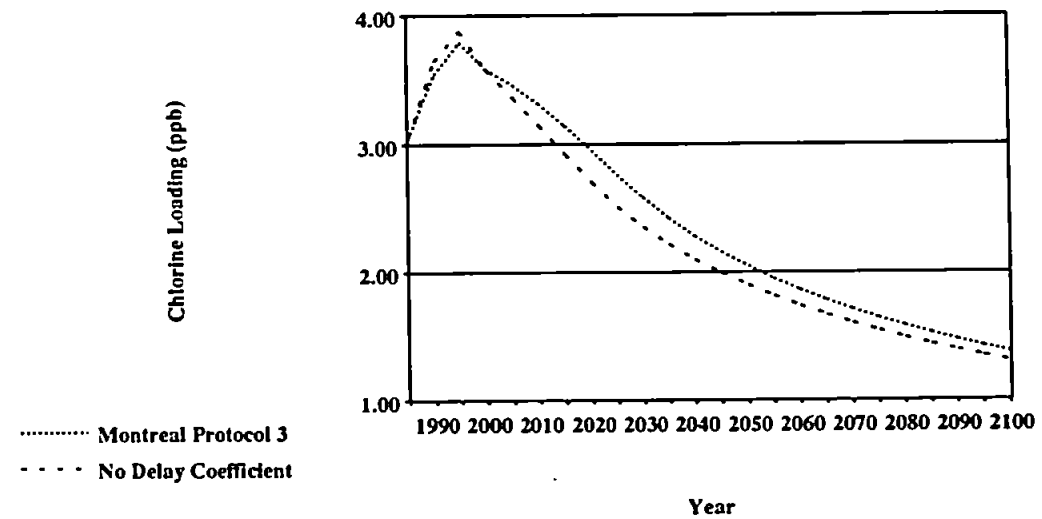

Figure 7.21 The sensitivity of the total chlorine loading to use of delay coefficients.

Table 7.5 Results of modelled sensitivity studies in the chlorine loading model.

Study Section	Variable	Forcing Factor	Change on Peak Chlorine in Reference Scenario (%)	Year of Peak Chlorine (years)	Change in 2 ppb Date (years)
7.4.2	Use of Delay Coefficients	No Delay	+2.4	-	-8
7.4.3	Free Chlorine	-	-21.1	-	-24
7.4.4	Montreal Protocols	One	-	-	-
		Two	+9.7	+5	+7
7.4.5	Tightening/ Loosening MP3	HCFC 2010	-2.1	-	+3
		HCFC 2020	-2.1	-	+2
		Loosened	-	-	-
7.4.6	Unknown Production	Maximum	+3.4	-	+5
		50% of Maximum	+1.6	-	+2
7.4.7	Fugitive Emissions	-	+0.3	-	-
7.4.8	HCFC Characteristics	More Cl	-	-	-
		Less Cl	-0.3	-	-2
7.4.9	HCFC Use	HCFC 124 (HR)	-0.3	-	-
		HCFC 124 (OCF)	-	-	-
		HCFC 124 (CCF)	-0.3	-	-
		HCFC 141b (OCF+CA)	-	-	-
		HCFC 141b (CCF)	-0.3	-	-
		HCFC 142b (OCF+AP)	-	-	-
		HCFC 142b (CCF)	-0.3	-	-

(1994). The date at which the chlorine loading falls to 2 ppb is brought forward to 2045.

This study shows that the use of delay coefficients influences the chlorine loading to a degree and provides an indication of the magnitude of the phase error introduced into any model which does not take into account delays in emission of halocarbons as a result of their use. Section 7.4.1 showed that the atmosphere is relatively insensitive to changes between usage categories of differing emission rates over time. However this study indicates that an allowance for delayed release categories can improve the accuracy of the model by approximately 2% in peak chlorine loading and 8 years in the timing of the 2 ppb date. However, it can be argued that these improvements are small given basic uncertainties in the data in the model (Section 7.4.1).

7.4.3 Comparison of Total Chlorine Loading and Free Chlorine Loading.

As highlighted in Section 6.2.1, the free chlorine coefficients are designed to reflect the amount of chlorine available for ozone depletion in the higher latitude, lower altitude stratosphere.[3] The value of these coefficients for each of the halocarbons is as follows; CFC 11, 2.7; CFC 12, 1.08; CFC 113, 1.8; CFC 114, 1.16; CFC 115, 0.12; HCFC 22, 0.32; HCFCs 123, 124, 141b and 142b, 0.99; carbon tetrachloride, 3.8; methyl chloroform, 2.94 and methyl chloride, 0.99. A free chlorine coefficient for halon 1211 of 1.00 is assumed in the absence of a published figure. Given that the chlorine in halon 1211 has a negligible effect on the chlorine loading, this assumption is not thought to produce any material error.

The result is shown in Figure 7.22 and Table 7.5. Figure 7.22 illustrates the large difference arising from the use of coefficients for total and free chlorine loading. The free chlorine loading generates a peak of 3.00 ppb, which is 21% less than the total chlorine loading peak, and brings the 2 ppb date forward 24 years. However the free chlorine coefficient only takes account of chlorine within a limited (but important) section of the

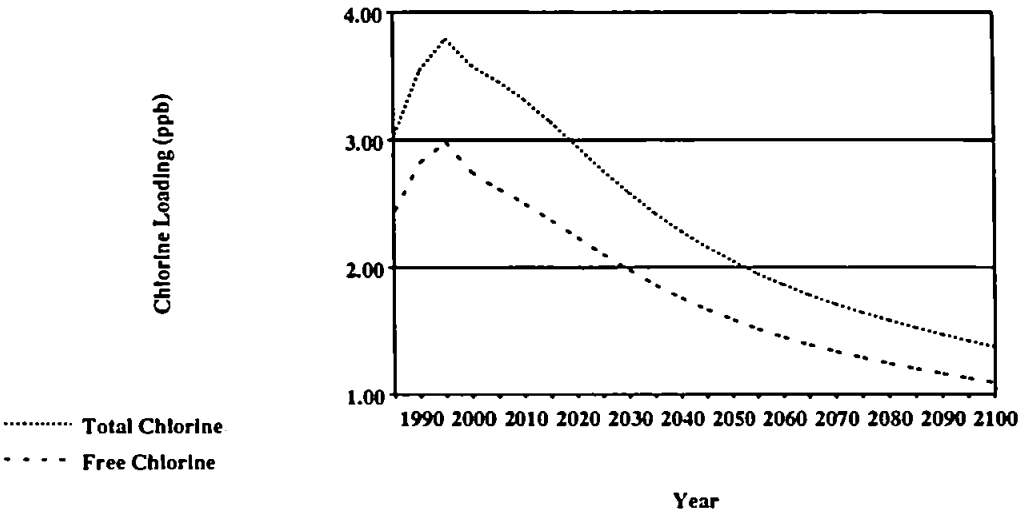

Figure 7.22 Comparison of total and free chlorine.

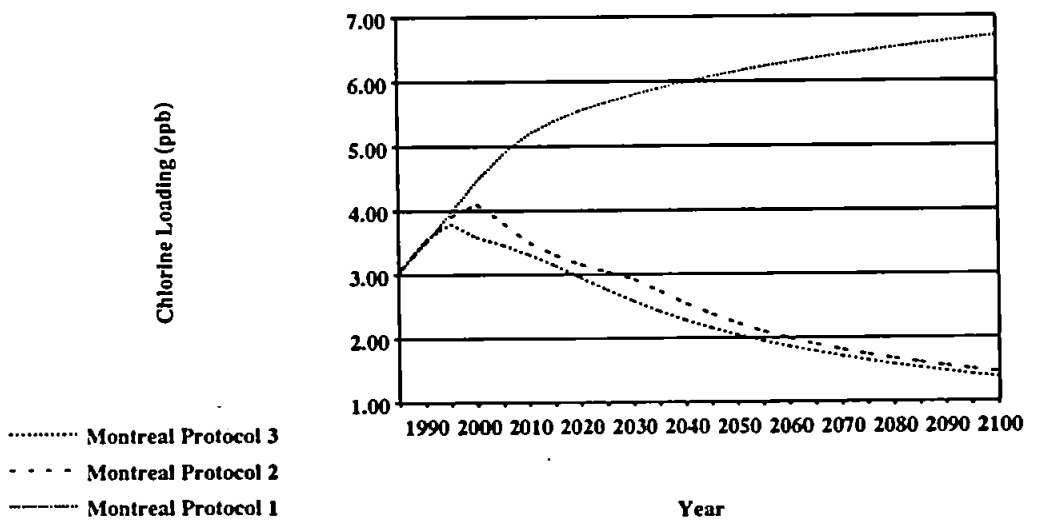

Figure 7.23 Comparison of the total chlorine loading under Montreal Protocols 1, 2 and 3.

atmosphere. We adopt the total chlorine loading measure which assumes that all the chlorine in a halocarbon molecule is available for ozone depletion, and therefore represents a 'worst case' scenario.

7.4.4 Comparison of Montreal Protocols 1, 2 and 3.

This study shows the relative effectiveness of previous and current international agreement relating to the production and use of halocarbons. The requirements of each of the Protocols has been shown in Table 1.1.

For the purposes of modelling Montreal Protocol 2, the assumptions for growth and production used for Montreal Protocol 3 remain the same, except that production is maintained at the last published level for each halocarbon, until the first Montreal Protocol 2 requirements in 1995. HCFC 22 production levels remain at the 1990 level (213.7 kt) until 2030, whereas the other replacement HCFCs remain constant at the 1996 level of 146.6 kt until 2030. These HCFC production levels were assumed because no phase out schedule was decided for the HCFCs under Montreal Protocol 2 (Table 1.1).

For Montreal Protocol 1, we assume that CFC consumption remains constant at the 1998 level (which is 50% of 1986 consumption) for the duration of the model. Halon 1211 is assumed to remain at the 1992 level for the rest of the model, whereas methyl chloroform and carbon tetrachloride (which are not included in Montreal Protocol 1) remain at their 1992 levels of 793.8 kt and 100.0 kt respectively. Use of the HCFCs is assumed to remain at their respective 2029 levels for the rest of the model.

The comparison is illustrated in Figure 7.23 and Table 7.5. The inadequacy of Montreal Protocol 1 is clearly illustrated as the chlorine loading continues to climb indefinitely. Montreal Protocol 2 produces a reversal in the rising chlorine loading trend. The peak chlorine loading arises in 1999 at 4.17 ppb and the 2 ppb date becomes 2060. It is the earlier phase down and removal of the CFCs under Montreal Protocol 3, which

is primarily responsible for the 2 ppb date which is seven years earlier, whereas earlier removal of methyl chloroform in important in reducing the peak chlorine loading by 9.7%.

7.4.5 Sensitivity of the Chlorine Loading to a Tightening/Loosening of the Montreal Protocol 3 Restrictions.

With the likelihood of further restrictions as part of Montreal Protocol 4 within the next two years, we examine the effects of an even tighter phase out schedule. Given that the complete removal of CFCs is imminent, it is unlikely there will be any further cuts except on a voluntary basis. Therefore we assume a one year advance on the Montreal Protocol 3 restrictions so that CFCs are totally removed by 1995. We also assume a one year advance for the total removal of carbon tetrachloride and methyl chloroform, so they are removed by 1995 also. Halons are assumed unchanged as they are already due to be phased out by the end of 1993. The HCFCs provide the largest scope for cutbacks. In two separate studies, we assume a complete phase out by 2010 and 2020, following a phase down as shown in Table 7.6, the HCFCs being prematurely replaced by hydrofluorocarbons (HFCs) or other ozone benign technology. Finally, for comparison, we also consider a slight relaxation of the Montreal Protocol 3 terms, where we assume that 5% of the 1985 production of each of the halocarbons is used for essential purposes such as for medical reasons, until 2000.

Results are shown in Figure 7.24 and Table 7.5 and show that a complete removal of CFCs, carbon tetrachloride and methyl chloroform one year in advance of the complete phase out date stipulated by Montreal Protocol 3 reduces the peak chlorine loading by 2.1% when compared to the reference level. This is as a result of saving 609.4 kt of halocarbon reaching the atmosphere. Removing methyl chloroform, which is predominately used as a cleaning agent and therefore involves an immediate flux to atmosphere, contributes over 80% to the reduction in peak chlorine.

Table 7.6 HCFC phase out conditions assumed for Section 7.4.5.

Phase out by:	Reduction
2010	35% cut 2000
	65% cut 2004
	100% cut 2010
2020	35% cut 2004
	65% cut 2010
	90% cut 2015
	100% cut 2020

If HCFCs are completely phased out by 2010, the total chlorine loading is reduced by approximately 5.1% around 2015-2020, of which over 60% is due to the HCFC removal. The phase down and removal of the CFCs by 1995 contributes 25% to the reduction in chlorine under the HCFC phase out in 2010 scenario, and 80% under the HCFC phase out in 2020 scenario, between 2015 and 2020. The large influence of the CFCs is due to some delay in emission through their use in refrigeration and closed cell foams and due to their long lifetimes. The effect on the 2 ppb date is small under either of the HCFC phase out scenarios, being 2 and 3 years earlier than the Montreal Protocol 3 scenario for the HCFC phase out by 2020 and 2010 respectively. The removal of HCFCs by 2020 has minimal effect on the total chlorine loading because the only saving in emission of the HCFCs is the residual amount allowed under Montreal Protocol 3 between 2020 and 2030 (Table 1.1).

It is also of interest to note that an allowance for a small continued release of 87.6 kt of halocarbons until the year 2000 has a less than 1% effect on the chlorine loading of the atmosphere throughout the next century. This indicates that a controlled residual use of halocarbons for essential needs would not materially affect the chlorine loading.

7.4.6 Sensitivity of the Chlorine Loading to Unpublished Production Data.

Published production data[14-19] represents that which has been reported, but in most cases, these data are not believed to represent 100% of world production (the remainder being production by halocarbon producers who are non-reporters to AFEAS).[14-16] According to sources, data for CFC 11 and 12 accounts for at least 70% of worldwide production,[14] whereas data for CFCs 113, 114 and 115 make up over 85% of global production.[15,17] HCFC 22 production data is believed to represent at least 90% of world figures.[16] Estimates of global production for halon 1211[18] and carbon tetrachloride[12] are already employed in the model, hence these figures are not altered for the purposes of this

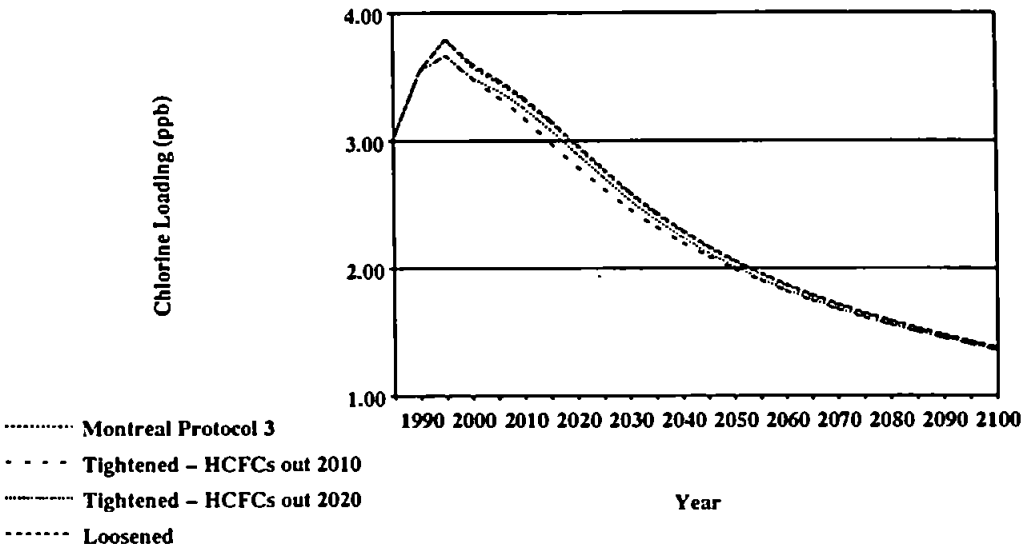

Figure 7.24 The sensitivity of the total chlorine loading to a tightening and loosening of the Montreal Protocol 3 requirements.

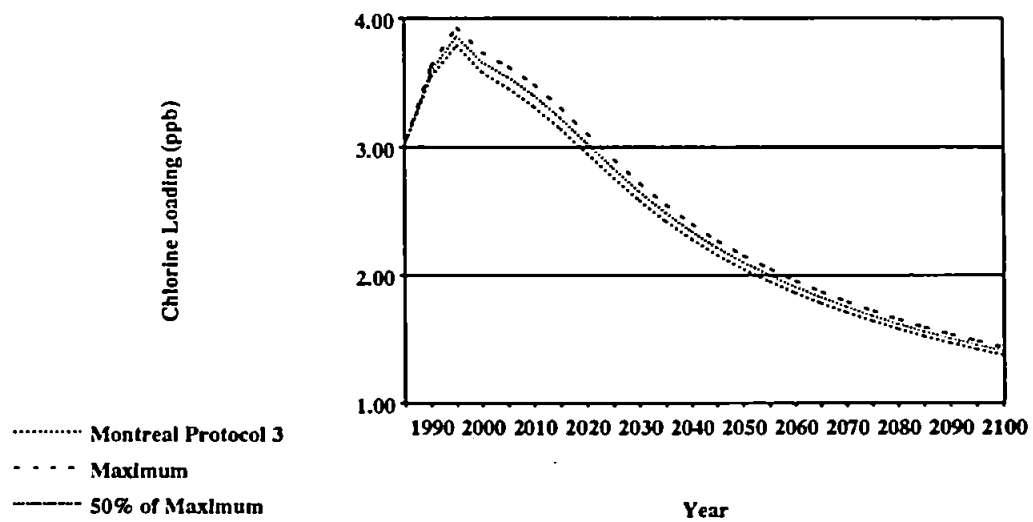

Figure 7.25 The sensitivity of the total chlorine loading to possible production of halocarbons by non-reporting companies.

study. It is generally believed that reporting companies for methyl chloroform account for approximately 100% of world production,[19] so no alteration for methyl chloroform is necessary. We assume that production of the new replacement HCFCs will be closely monitored (given that the new patented processes involved in their manufacture mean fewer companies will be producing them and increased awareness of halocarbons will necessitate greater accountability) and hence the production estimates used in the model represent 100% of production. Methyl chloride production is assumed to be 100% of global production.

The increased production is initiated in 1985 at both the full level of possible unreported production shown above and half this amount, eg. an increase in production of 30% and 15% for CFC 11 and 12. It is assumed that this unknown production is by countries who are signatory to the Protocol (such as the Eastern bloc) and therefore follow its requirements. The results are illustrated in Figure 7.25 and Table 7.5.

This study highlights the sensitivity of the atmospheric chlorine loading to production of CFCs (and HCFC 22) as all other variables remain unaffected. The major uncertainty is production of CFCs 11 and 12 for which up to 30% extra production is possible above reported amounts, and causes 79% of the increase in peak chlorine. The actual breakdown by halocarbon is 36% CFC 11, 43% CFC 12, 14% CFC 113 and 7% HCFC 22. CFCs 114 and 115 have a negligible affect. The increase in the 2 ppb date is due to CFC 11 (40%), CFC 12 (50%) and CFC 113 (10%).

7.4.7 Sensitivity of the Chlorine Loading to the Release of Fugitive Emissions.

Fugitive emissions are those which escape during production and transport of the halocarbons. They are therefore not accounted for in production/sales figures and are assumed to be immediate. Estimates of the proportion of production which escapes as fugitive emissions varies. Estimates for CFC 11 and CFC 12 are 2.0% and 3.3%

respectively,[22] whereas an overall figure of 1.3% is given for each of CFC 113, 114 and 115.[17] Midgley estimates fugitive emissions of methyl chloroform are 0.2-0.3% of production (we adopt 0.25%).[19] Estimates for carbon tetrachloride and halon 1211 could not be found, so are assumed to be 2.0%. This figure is also adopted for the replacement HCFCs. HCFC 22 production data used in the model includes an estimate for fugitive emissions and therefore is unaltered.[16] Fugitive emissions of industrial methyl chloride are around 3-5% of production (Figure 7.26, Table 7.5).[26]

Fugitive emissions make up a small proportion of total production and hence their effect is negligible upon both the peak chlorine loading and 2 ppb date.

7.4.8 Sensitivity of the Chlorine Loading to Chlorine Contribution by HCFCs.

The aim of this study is to assess the possible effect of the HCFCs according to the level of chlorine which they impart to the atmosphere. This has been achieved by selecting two HCFCs, one of which contributes more chlorine and one which contributes less. HCFC 22 production is maintained until 1996 before its production is transferred to the allotted HCFC in 1997. All replacement HCFC production is transferred to the allotted HCFC.

HCFC 141b has been selected to represent a larger chlorine contributor. It has a relatively long lifetime (for HCFCs) of 10.8 years and contains two chlorine atoms in its molecule. HCFC 123 was selected to represent a smaller chlorine contributor. The ratio of uses amongst all the HCFCs is transferred to the allocated gas, so that the effect of differing use is removed. The results are shown in Figure 7.27 and Table 7.5.

The influence of the HCFCs is understated by the conventional parameters in Table 7.5, because maximum HCFC production is not reached until after the peak chlorine loading of the model, and because by the 2 ppb date the influence of the HCFCs is minor owing to their relatively short lifetimes when compared to other halocarbons. However

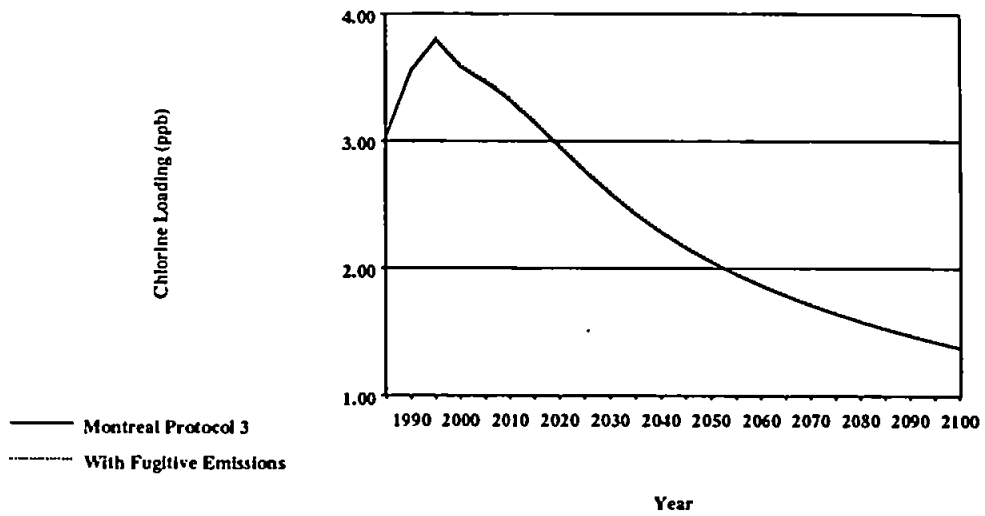

Figure 7.26 The sensitivity of the total chlorine loading to release of fugitive emissions of halocarbon.

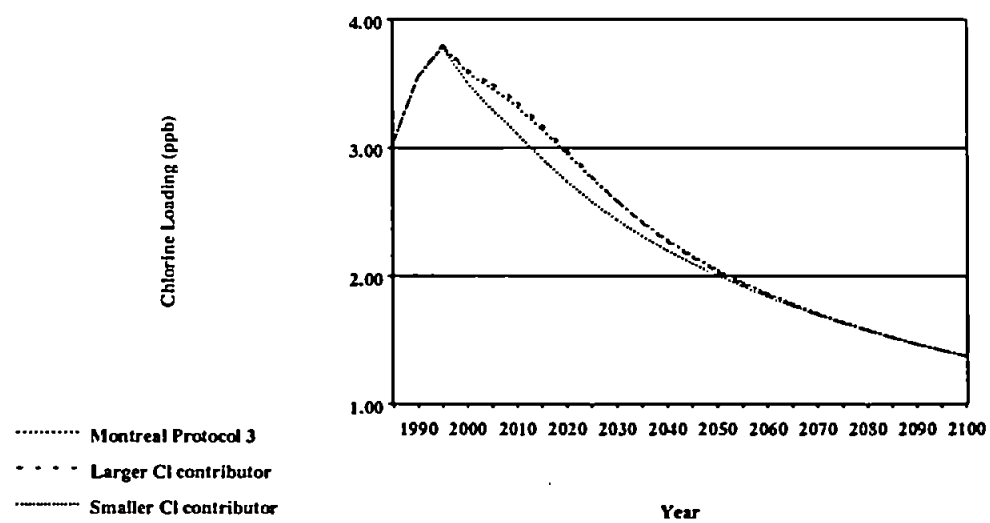

Figure 7.27 The sensitivity of the total chlorine loading to level of chlorine imparted to the atmosphere by HCFCs.

during the period 2000 to 2040, HCFCs can have an important effect on how quickly chlorine levels decline. Figure 7.27 shows that the chlorine loading for the Montreal Protocol 3 reference scenario is very nearly as high as that for the 'larger Cl contributor' curve. This is due to the predominance of HCFC 22 use, which is a large contributor of chlorine (by chemical characteristics only) amongst the HCFCs. It also commands a large portion of the replacement HCFC market (about 27% in 1996) owing to its long established use as a refrigerant.

Even if only the largest chlorine contributing HCFC was used, the chlorine loading would increase by merely a further 1.3% in 2015. However if HCFCs were employed which contribute less chlorine, then the chlorine loading around 2015 to 2020 could be over 7% less, representing a considerable saving. Thus choice of HCFCs employed as replacements for CFCs will have an important bearing on chlorine levels during the early part of next century. Reducing the large reliance on HCFC 22 as a replacement for the CFCs in favour of less chlorine contributing HCFCs (such as HCFC 124) would be an important first step.

7.4.9 Sensitivity of the Chlorine Loading to Uncertainty in HCFC Use.

With the exception of HCFC 123 (which is used solely in non-hermetic refrigeration applications (Section 6.3.2)), we assume that the other new replacement HCFCs are allocated equally between their respective possible markets.

We assume that HCFC 22 use remains as in the reference scenario as this is based on published data. (The effect of its changing use was investigated as a part of Section 7.4.1). HCFC 123 remains as in the reference scenario because it only has one assumed use. The remaining replacement HCFCs, namely HCFCs 124, 141b and 142b, are then tested separately by increasing each of their respective uses to 100% in order to assess the maximum effect of each on the chlorine loading as shown in Figures 7.28 to 7.30

respectively and Table 7.5.

Figures 7.28 to 7.30 show that the atmospheric chlorine loading is not sensitive to the use of replacement HCFCs. It is most sensitive to the use of HCFC 141b in immediate release categories (cleaning agents and open cell foams) and the delayed release category 'closed cell foams'. This sensitivity is not revealed by the parameters in Table 7.5, but by the fact that the maximum deviation from the reference scenario is +0.9% for 100% use in open cell foams in 2005, compared to -2.0% in the same year for 100% use in closed cell foams. However, 100% use of each of these gases in any of their applications is an extreme case, so those sensitivities represent an absolute maximum which is unlikely to occur in reality.

7.4.10 Sensitivity of the Chlorine Loading to Total HCFC Production.

HCFC consumption allowed under Montreal Protocol 3 is 800 kt in 1996. This study examines the effect of not reaching this maximum. Minimum consumption is taken as 40% of this maximum, as well as 60% and 80% of the 800 kt. The reductions are applied equally to each of the HCFCs. HCFC 22 is allowed to reach a maximum of 213.7 kt in 1990, before declining to the new figure after 1996. The results are shown in Figure 7.31 and Table 7.7.

This study reveals that a 60% reduction in HCFC use leads to a maximum decrease of 5.1% in the chlorine loading around 2010-2015. As with the other HCFC studies, the effects on peak chlorine loading and the 2 ppb date are small producing a change of only 0.01 ppb in peak chlorine and no change to the 2 ppb date.

7.4.11 Sensitivity of the Chlorine Loading to Natural Methyl Chloride Emissions.

The total methyl chloride concentration is set at 600 ppt in line with measurements of its atmospheric concentration.[3] However, measurements are few and with our increasing

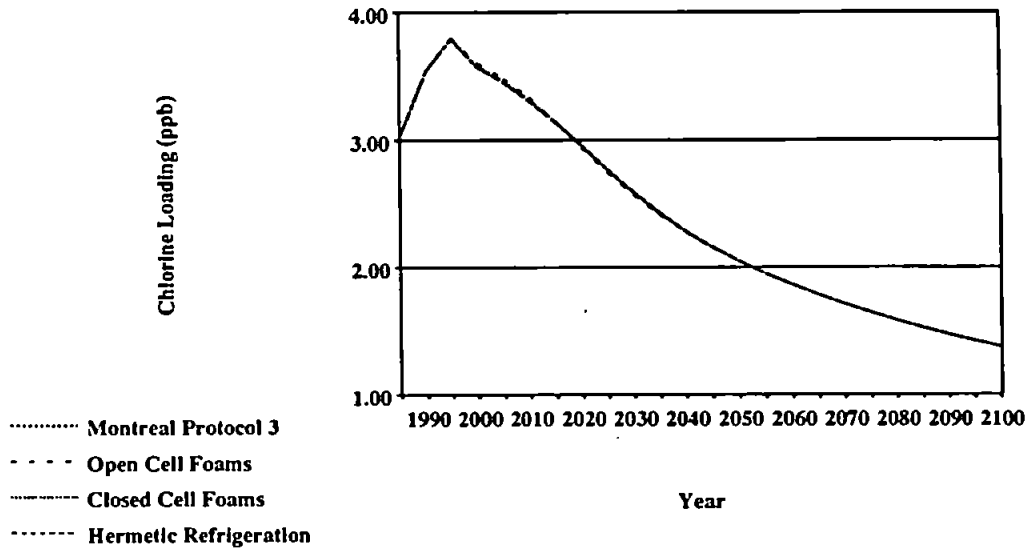

Figure 7.28 The sensitivity of the total chlorine loading to future use of HCFC 124.

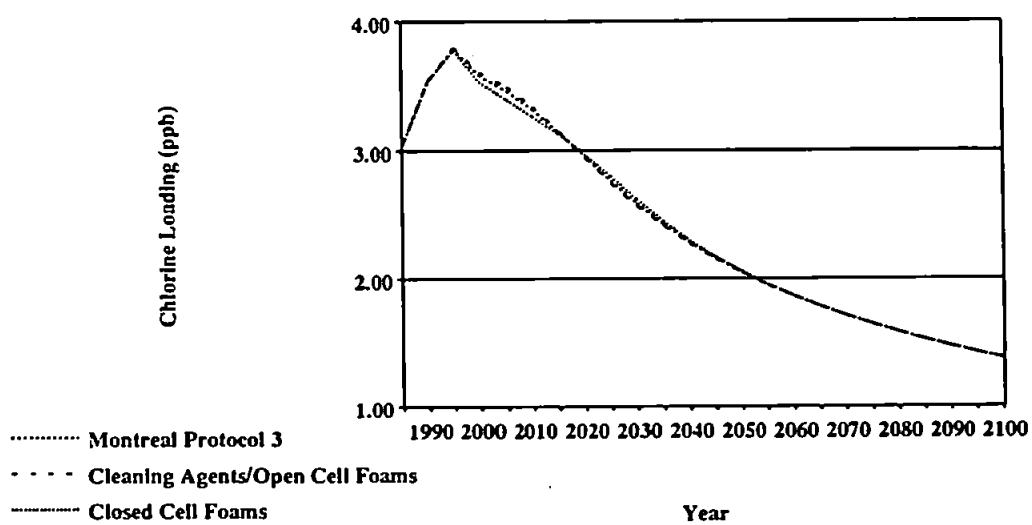

Figure 7.29 The sensitivity of the total chlorine loading to future use of HCFC 141b.

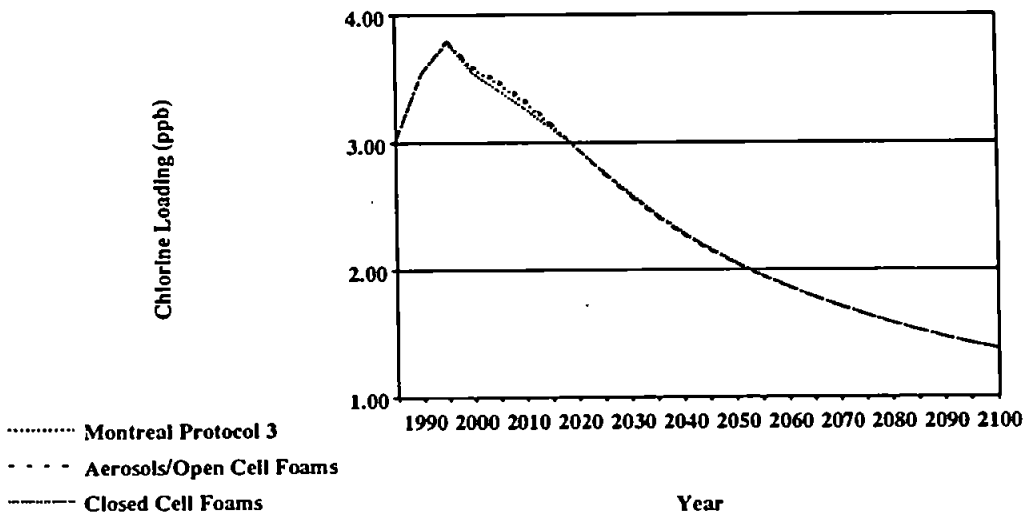

Figure 7.30 The sensitivity of the total chlorine loading to future use of HCFC 142b.

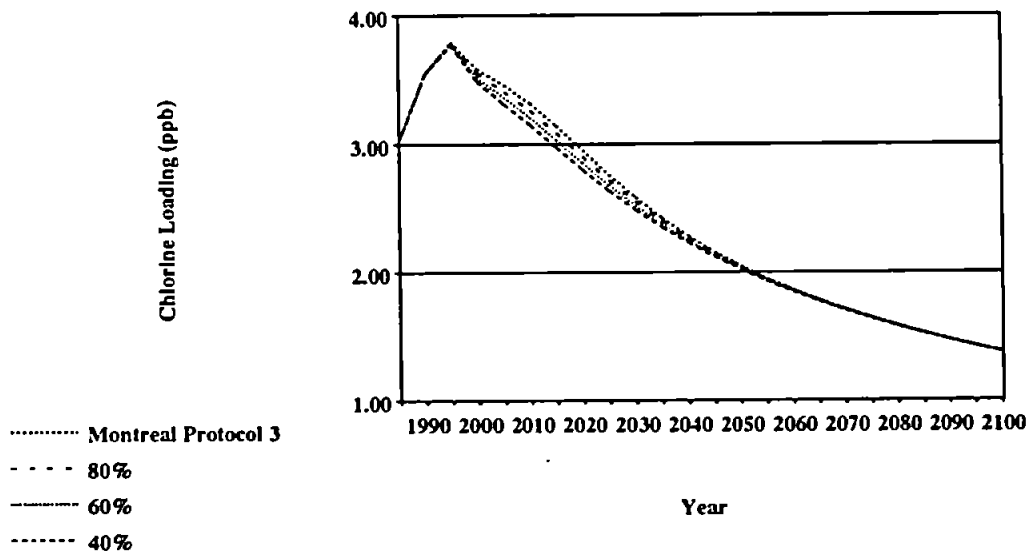

Figure 7.31 The sensitivity of the total chlorine loading to total HCFC production.

Table 7.7 Results of modelled sensitivity studies in the chlorine loading model II.

Study Section	Variable	Forcing Factor	Change on Peak Chlorine in Reference Scenario (%)	Year of Peak Chlorine (years)	Change in 2 ppb Date (years)
7.4.10	HCFC Production	80%	-0.3	-	-1
		60%	-0.3	-	-1
		40%	-0.3	-1	-2
7.4.11	Methyl Chloride Emissions	+10%	+1.3	-	+3
		-10%	-1.6	-	-3
7.4.12	Total Recycling	A	-1.1	-	-2
		B	-2.6	-	-3
		C	-4.2	-1	-5
		D	-5.8	-1	-6
7.4.13	Recycling by Halocarbon Group	CFCs	-1.6	-	-4
		HCFCs	-0.5	-	-1
		Others	-2.1	-	-

ability to change the atmosphere and climate on a global scale through activities such as tropical rain forest destruction, we assess the effect of a change in the level of natural methyl chloride emissions. The sensitivity of the steady state atmosphere to an increase and decrease in natural methyl chloride emissions of ±10% is ascertained. All other halocarbons remain constant. The result is shown in Figure 7.32 and Table 7.7.

We find that a 10% variation in natural methyl chloride emissions leads to a +1.3%/-1.6% change in the peak chlorine loading and a 3 year difference in the 2 ppb date. It is difficult to assess how man's activities will influence the natural methyl chloride balance in the atmosphere, and to what extent. A major source of methyl chloride appears to be from the activities of species of wood rotting fungi (Section 6.3.2).[27] It is hard to predict whether this activity would be reduced (through loss of habitat) or enhanced (through an increase in degradable material) because of logging activities in tropical forest destruction.

7.4.12 Sensitivity of the Chlorine Loading to Recycling of Halocarbons.

For the purposes of the model, recycling is interpreted as a reduction in the flux of the halocarbons to atmosphere, ie. instead of being emitted to atmosphere a proportion of the flux is recycled or destroyed and therefore makes no contribution to the flux.

For simplicity the periods over which recycling can take place have been divided into five arbitrary blocks, these being 1985-89, 1990-99, 2000-09, 2010-19 and 2020+. Four recycling scenarios labelled A to D have been devised, with varying recycling rates, shown in Table 7.8 as the proportion of the flux not emitted to atmosphere. Methyl chloride is assumed to remain constant. Table 7.7 and Figure 7.33 show the results of this study.

Recycling scenarios A and B represent more modest rates of recycling, and have the affect of lowering peak chlorine by 1.1% to 3.76 ppb and 2.6% to 3.70 ppb

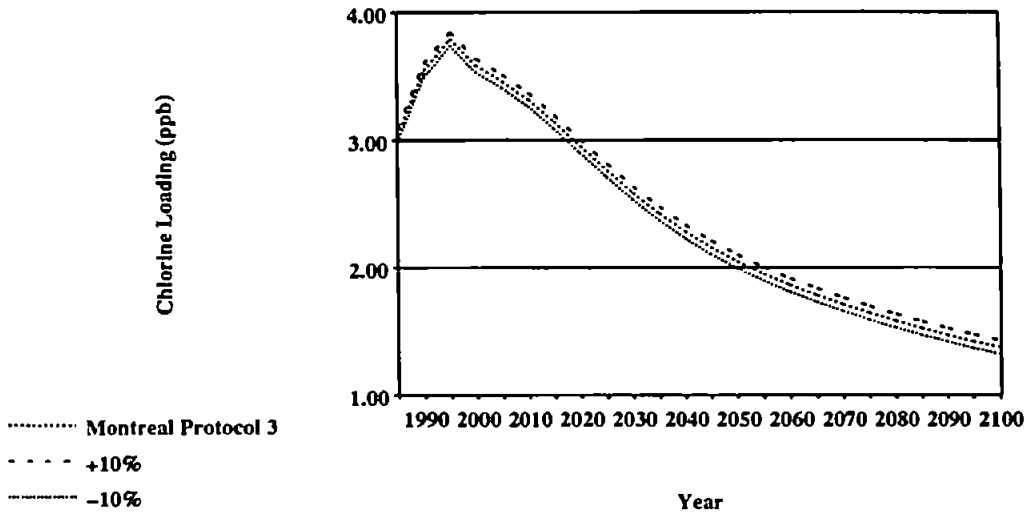

Figure 7.32 The sensitivity of the total chlorine loading to changes in emission of natural methyl chloride.

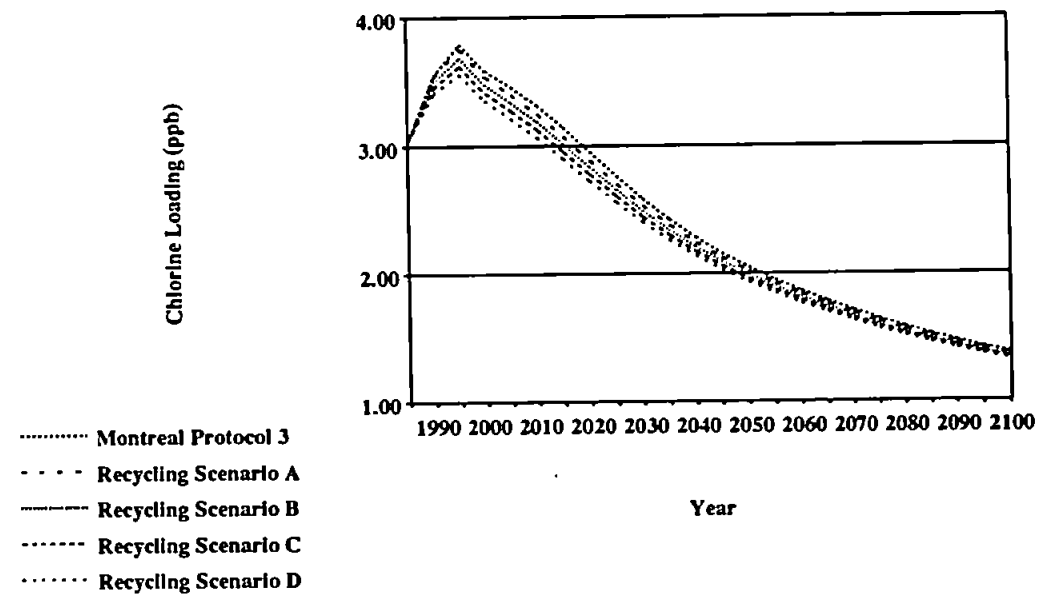

Figure 7.33 The sensitivity of the total chlorine loading to recycling of halocarbons.

Table 7.8 Recycling scenarios for Section 7.4.12.

Years	Reduction on Flux /%			
	A	B	C	D
1985-1989	0	5	10	15
1990-1999	5	10	15	20
2000-2009	10	15	20	25
2010-2019	15	20	25	30
2020+	20	25	30	35

respectively. Historically, global levels of halocarbon recycling have been, and continue to be, small. Recycling scenarios C and D show how levels of recycling from an earlier date would have brought the peak chlorine loading forward by a year, and reduce it by 4.2% to 3.64 ppb and 5.8% to 3.58 ppb respectively, which represents better savings. This is due to a greater proportion of the CFCs, carbon tetrachloride and methyl chloroform being prevented from reaching the atmosphere. The 2 ppb date under scenarios A, B, C and D is brought forward 2, 3, 5 and 6 years respectively, predominantly due to the enhanced removal of the CFCs. Only recycling now at large rates would have any impact on the peak chlorine loading and even then, its effects are only likely to be small as most of the CFC which has been produced is already in the environment.

7.4.13 Sensitivity of the Chlorine Loading to Enhanced Recycling of Individual Halocarbon Groups.

This study aims to provide a comparison of the effectiveness achieved by recycling each of the halocarbon groups, these being divided into the CFCs (CFCs 11, 12, 113, 114 and 115), the HCFCs (HCFCs 22, 123, 124, 141b and 142b) and others (halon 1211, carbon tetrachloride and methyl chloroform). We assume that 20% of each of these groups is recycled from 1990 onwards (this date being closest to present day according to the groupings in Table 7.7). The results are shown in Figure 7.34 and Table 7.7.

This study reflects the characteristics of these three groups of halocarbons. Recycling of heavily used, long lived CFCs reduces the peak chlorine loading to 3.74 ppb and brings the 2 ppb date forward to 2049. Recycling of halon 1211, carbon tetrachloride and methyl chloroform reduces peak chlorine to 3.72 ppb but has no effect on the 2 ppb date. This is due to the dominance of short lived methyl chloroform. Of the three groups, the HCFCs have the least overall affect which is to be expected as they contribute less chlorine to the atmosphere and do not reach maximum production until after the peak

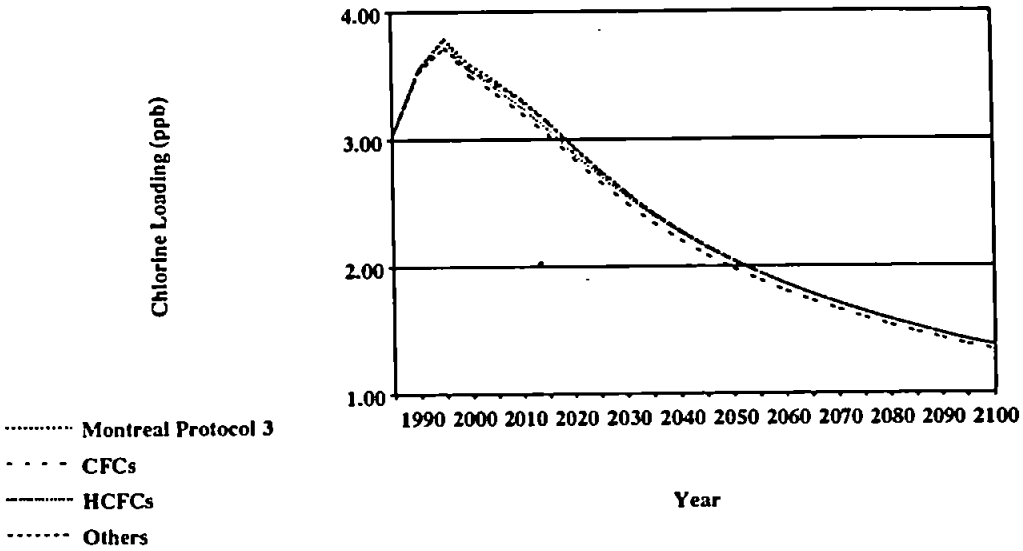

Figure 7.34 Comparison of the effectiveness of recycling of CFCs, HCFCs and other halocarbons.

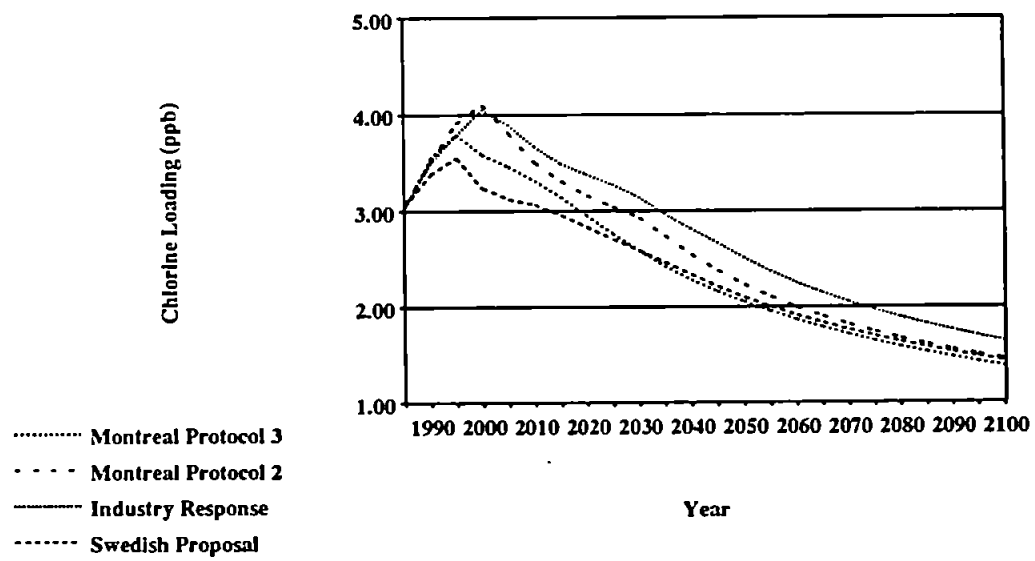

Figure 7.35 Comparison of published proposals for removing halocarbons, with the Montreal Protocol 2 and 3 stipulations.

chlorine loading in 1994. As this group of gases is also short lived, they also have little affect on the 2 ppb date, only bringing it forward by one year.

7.4.14 Comparison of Early Proposals with Current Agreement.

During the early stages of the development of this computer model, when Montreal Protocol 2 was the most recent agreement, a number of proposals were published on how the removal of halocarbons could be hastened. One of these, which we term 'Industry Response', is based on a paper by Moore[28] which detailed the viewpoint of the various industries which use CFCs, and gave estimates of how quickly they thought they could reduce and eventually stop using these compounds. The general consensus in this paper was that those industries using CFCs as aerosol propellants, cleaning agents and closed cell blowing agents could probably stop using them by the early 1990s. However those industries using CFCs for refrigeration and open cell foam blowing thought it would be difficult to stop their reliance on CFCs until after 2000.

The second paper we term 'Swedish Proposal' and represents a phase out program adopted by the Swedish Parliament in May 1988, in lieu of the Montreal Protocol 1 agreement.[29] In this proposal, all use (except for essential purposes) is set to cease by 1995 with use in some applications being stopped in the late 1980s and early 1990s. Thus it represents a radical series of measures for removing CFCs. These phase out requirements are easier for Sweden to apply as it does not have a heavy reliance on use of halocarbons when compared to other industrialised countries. For this study, we assume that the world adopts this phase out schedule. For comparison we also show Montreal Protocol 2 (which forms the reference level for the remaining chlorine loading sensitivity studies) and Montreal Protocol 3. The results are shown in Figure 7.35 and Table 7.9.

The results of Montreal Protocol 2 have been discussed in an earlier study (Section 7.4.4), so no further analysis is necessary here.

Table 7.9 Results of modelled sensitivity studies in the chlorine loading model III.

Study Section	Variable	Forcing Factor	Change on Peak Chlorine in Reference Scenario (%)	Year of Peak Chlorine (years)	Change in 2 ppb Date (years)
7.4.14	Early Proposals	Industry Response	-1.7	-	+13
		Swedish Proposal	-13.7	-5	-5
		Montreal Protocol 3	-9.7	-5	-7
7.4.15	Delay by Developing Countries	10 Years	+1.6	-	+21
		5 Years	+1.6	-	+16
7.4.16	Population Size	+20%	+4.8	+5	+26
7.4.17	Proportion of Non-Signatory Developing Countries	85/5/10	-	-	-
		85/10/5	+4.8	+14	-
		85/12/3	+2.3	+10	-
		85/13.5/1.5	+1.8	+6	-
7.4.18	Level of Consumption by Developing Countries	1.2 kg per capita	+4.6	+10	-
		0.8 kg per capita	+2.3	+10	-
		0.4 kg per capita	+1.7	-	-

The Industry Response measures produce a similar peak chlorine loading to the Montreal Protocol 2 restrictions, decreasing it by only 1.7% (which represents an 8.0% increase on Montreal Protocol 3) and increasing the 2 ppb date by 13 years (20 years relative to Montreal Protocol 3). The long period before reaching the 2 ppb date is as a result of sustained use of CFCs, over and above the requirements of Montreal Protocol 2. This highlights the drastic effect prolonged use of CFCs can have on the 2 ppb date, despite being phased out over 70 years earlier.

The Swedish Proposal line shows how early drastic cuts in halocarbon production could have reduced the peak chlorine loading (by 13.7% on Montreal Protocol 2 and 5.3% on Montreal Protocol 3), but it is of interest to note that the Montreal Protocol 3 conditions actually bring the 2 ppb date further forward (by 2 years), probably due to residual use of CFCs allowed in the Swedish Proposal.

7.4.15 Sensitivity of the Chlorine Loading to length of delay adopted by Developing Countries signatory to the Montreal Protocol.

Under the conditions of Montreal Protocol, developing countries are allowed to delay the conditions of the Protocol by 10 years, provided that their per capita consumption is less than 0.3 kg.

The proportion of production allotted to developing countries at the start of the model is 15%.[30] We examine the effect of the developing countries utilising the full ten years afforded to them or just five years. We assume full compliance by developing countries. For the purposes of this and following studies, use by developing countries is assumed to grow at such a rate that a maximum per capita consumption of 0.3 kg is achieved (per Montreal Protocol 2). In order to calculate the rise in production from an initial level of 15% of world production to the maximum level of 0.3 kg per capita reached in 2004 (the last year before the phase out requirements of Montreal Protocol 2

affect the developing countries) we need an estimate of the population size of developing countries. Therefore, we assume a 1990 world population of 4.7 billion people[31] of which three-quarters live in developing countries.[30] This allows a maximum halocarbon usage by developing countries of 1058 kt. Use of replacement HCFCs is delayed by five or ten years accordingly. The overall growth rate applied to the halocarbons from 1985 to 2004 in order to reach this maximum is calculated as an annual compounded rate so that the sum total of halocarbon production in 2004 is equal to the maximum production required. It is an inherent assumption that the allocation of usage categories in developing countries is the same as in developed countries. Generally developing countries use CFCs predominately in refrigeration applications. For example, 74% of India's CFCs are used in refrigeration[32] and this is considered low in comparison with other developing countries due to India's expanding industry base. However, much of the equipment used in developing countries is second hand and thus CFCs may leak out more readily; this is certainly the case for China.[33] Therefore it may be less valid to assume the same delay coefficients for developing countries. However, using the same usage categories as for developed countries puts more halocarbon in immediate release categories than is truly the case, and this then gives some allowance for more rapid release of halocarbons in refrigeration and other delayed release categories in developing countries. We maintain the assumption regarding usage by developing countries for simplicity.

Figure 7.36 and Table 7.9 show the deviation of these scenarios from the basic Montreal Protocol 2 scenario. The figure is displayed as a '% change' relative to Montreal Protocol 2, so that the change through time can be more easily applied to Montreal Protocol 3. However these results should be viewed with more caution for two reasons. Firstly they are dependent on the population figure for developing countries assumed in the model. The effect of such an error is investigated in Section 7.4.16. Secondly, these results will tend to overstate changes when applied to Montreal Protocol 3 because they

are based on the percentage reductions of Montreal Protocol 2. As these restrictions are less severe than for Montreal Protocol 3, the amount of halocarbon used in developing countries will be larger than if the use of halocarbons in these countries was modelled under a Montreal Protocol 3 scenario. The percentage reductions and phase out dates of Montreal Protocol 3 would cause the chlorine contribution from developing countries to decline more quickly than is shown in these results. This work could not be updated in the time available for the completion of this project. Although of less accuracy in percentage terms, they do show the order of magnitude of the effect of use by developing countries, and in this context, remain of use. The results shown in Figure 7.36 and Table 7.9 show that a 5 or 10 year delay utilized by developing countries has little affect on the peak chlorine loading of 4.17 ppb, increasing it by 1.6% in both cases. There is no change to the time of this peak (1999). The most dramatic effect is in the timing of the 2 ppb date which is increased by 21 and 16 years for a 10 and 5 year delay. This is primarily due to the prolonged use of the CFCs. Clearly it would be advantageous to encourage signatory developing countries to stop using CFCs in advance of the 10 year delay afforded to them. One way of doing this is for developed countries to 'adopt' a developing country, and provide technical and financial assistance in removing CFCs and replacing them with HFAs, such as has been occurring between the USA and Brazil. As a result of such a scheme, Brazil should remove its reliance on CFC technology well in advance of the 10 year delay it is allowed to utilize under the terms of Montreal Protocol.

7.4.16 Sensitivity to the Effect of an Error in Estimated Population Size in Developing Countries.

For this study we assume an error in the estimated population size of the signatory developing countries of +20% and assume that the 10 year delay is fully utilised. This leads to a maximum use in 2004 of 1269 kt. The overall total increase in growth required

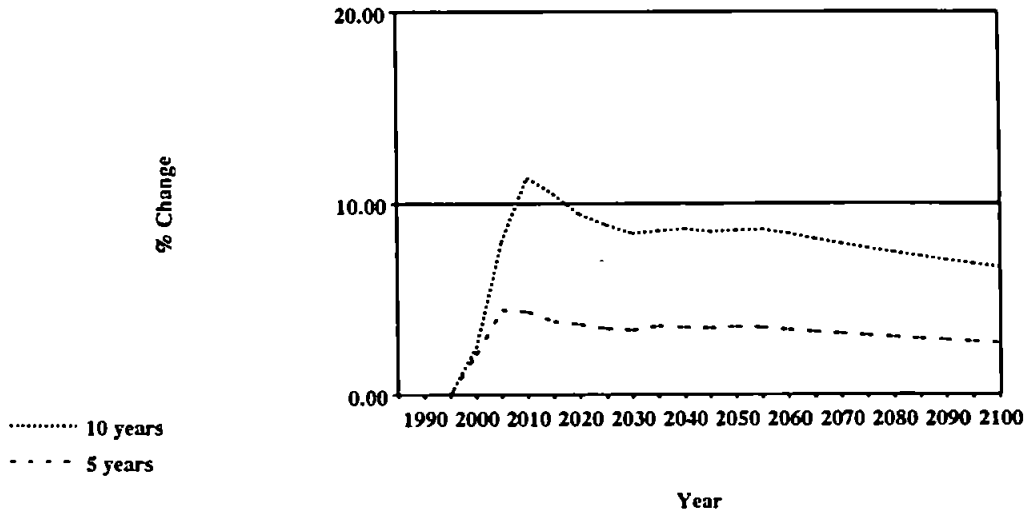

Figure 7.36 Change on the Montreal Protocol 2 reference level as a result of signatory developing countries utilising the delay period allowed to them under the terms of Montreal Protocol.

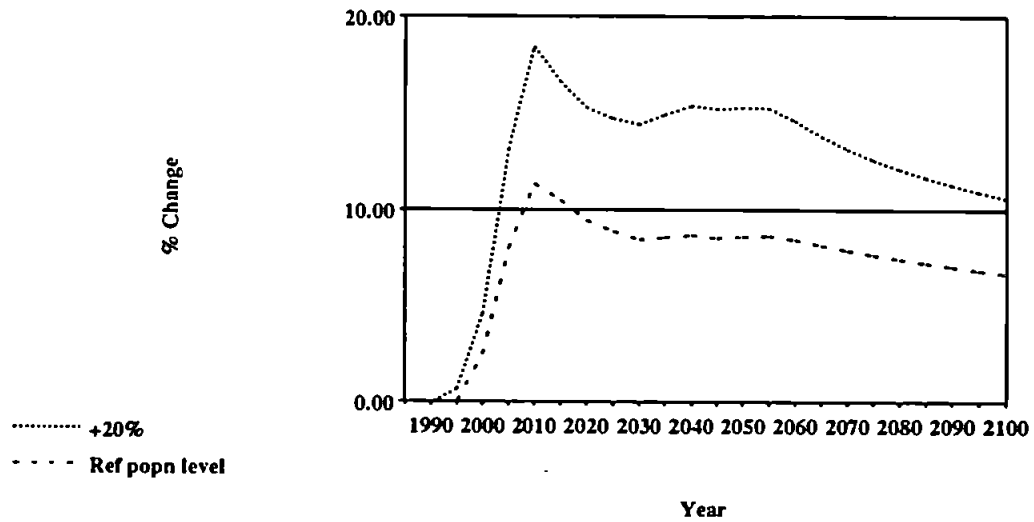

Figure 7.37 Change on the Montreal Protocol 2 reference level as a result of an error in the estimation of the population size of developing countries for the calculation of per capita consumption.

to obtain the maximum production level is calculated as an annual compounded rate applied to each of the halocarbons between 1985 and 2004. The result is shown in Figure 7.37 and Table 7.9.

This shows that the largest difference between the sensitivity case and the Montreal Protocol reference case is approximately 18% around the year 2010. The difference is, in fact, due to the peak of the +20% population scenario occurring in 2004, when the chlorine loading in the Montreal Protocol 2 case is tailing off. The peak chlorine loading is pushed back to 2004 from 1999 and is 4.8% above the Montreal Protocol 2 reference (and 3.2% above the reference developing country population level, shown as a dashed line in Figure 7.37). The 2 ppb date is also pushed back a further 5 years on this level.

This study clearly shows that the size of the developing country population is an important criterion as an error of 20% can lead to fundamental changes in both the size and timing of the peak chlorine loading, as well as the timing of the 2 ppb date.

7.4.17 Sensitivity of the Chlorine Loading to the Proportion of Developing Countries who are Non-Signatory to the Protocol.

In this study, we look at a further assumption that a proportion of developing countries are not signatory to the Protocol, and can therefore continue their growth in production of CFCs and other halocarbons. At the time this work was undertaken, it was estimated that unsigned developing countries made up two-thirds of all production by developing countries.[34] Firstly, we assume that those developing countries who are unsigned build up their use of halocarbons to a level equivalent to 0.8 kg per capita (which is two-thirds the current consumption level in the USA). Secondly, we assume that they reach this maximum by 2010 at which point their production remains constant at the 2010 level. Thirdly, we assume that they do not use replacement HCFCs as they do not

need too, given their continued reliance on CFCs. These results were obtained by calculating the maximum production of developing non-signatories (by taking the fraction of the world population living in developing countries, finding the fraction of this population living in non-signatory countries and multiplying by the per capita consumption). The total growth required to achieve the maximum production by 2010 is calculated for each halocarbon as an annual compounded rate, in addition to the compounded growth rate for the developing countries signatory to the Protocol and the production of the developed countries. The results are shown in Figure 7.38 and Table 7.9.

In the figure, we adopt the notation X/Y/Z where X represents the proportion of 1985 world production allocated to the developed countries, Y represents the allocation to signatory developing countries and Z represents the non-signatory developing countries. Thus 85/5/10 looks at the change in the chlorine loading of two-thirds of production by developing countries being in the non-signatory category.

Under the 85/5/10 scenario, the drastic change in the chlorine loading is very evident in Figure 7.38, rising to over 300% above the Montreal Protocol 2 reference level by the end of next century. If unsigned developing signatory countries account for a third of total use by developing countries, ie. 85/10/5, a peak of 4.37 ppb is attained some 14 years after the reference year of 1999. Levels then decline until around 2025 when they begin to rise again reaching 4.31 ppb, by the end of the century.

With only a fifth and tenth of total developing country production initially allotted to non-signatories, peak chlorine rises by 2.3% (4.27 ppb) and 1.8% (4.25 ppb) before declining to 3.24 ppb and 2.43 ppb by 2100 respectively. Figure 7.38 shows the alarming increase in chlorine under each of the aforementioned scenarios, even with only a tenth of developing countries non-signatory (which itself produces a rise on the Montreal Protocol 2 conditions of almost 50% by 2100). This clearly illustrates the dangers of prolonged use of CFCs and other halocarbons and indicates that only by total global

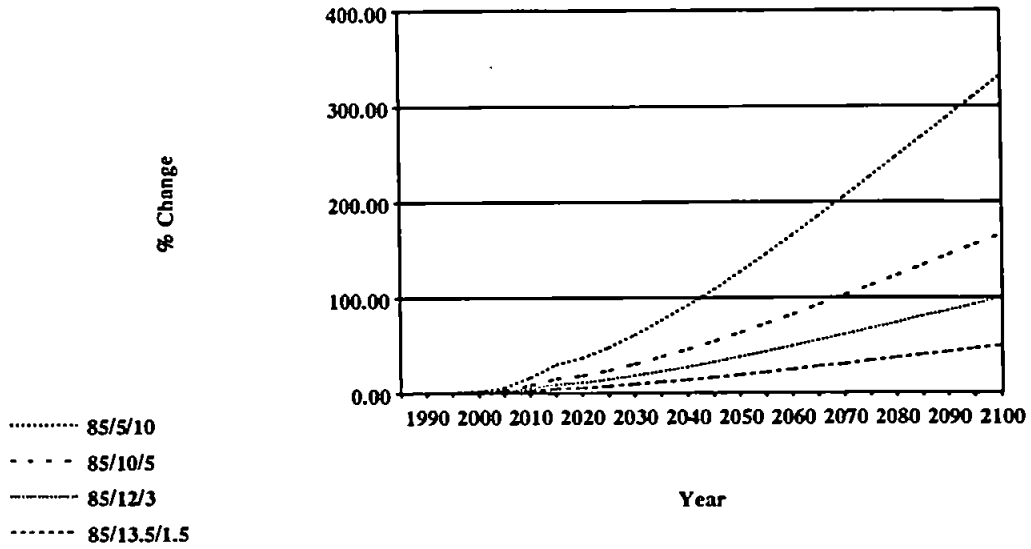

Figure 7.38 Change on the Montreal Protocol 2 reference level as a result of the proportion of sustained production by developing countries who are non-signatory to the Protocol.

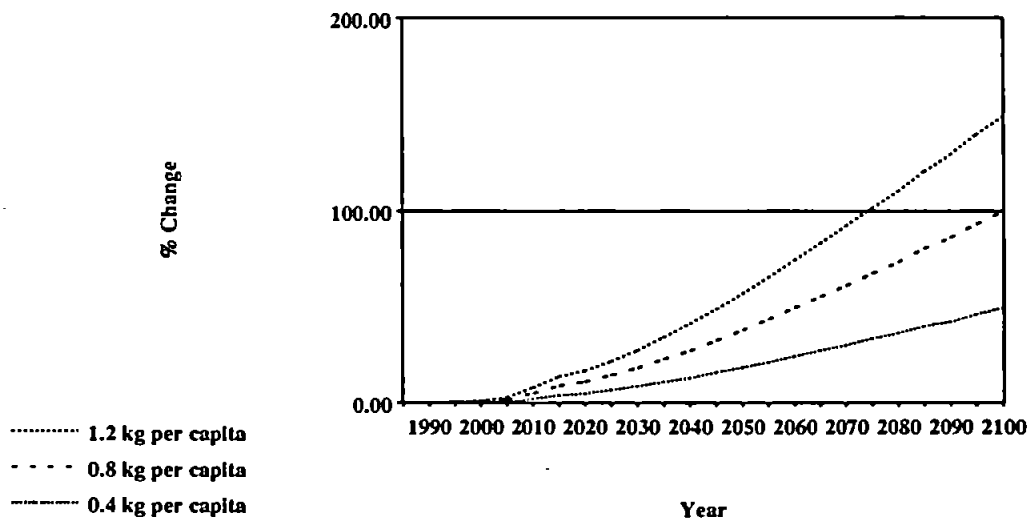

Figure 7.39 Change on the Montreal Protocol 2 reference level as a result of the per capita consumption of halocarbons by non-signatory developing countries.

accord and action, will it be possible to get atmospheric chlorine levels down to reasonable levels.

Although no diagram is shown, we have performed the same study assuming a per capita consumption in non-signatory countries of 0.4 kg (ie. half the amount in the study above and 0.1 kg above the limit set by Montreal Protocol). We find that if non-signatories account for two-thirds of use by developing countries, then the peak chlorine loading rises by 2.7% to 4.28 ppb, which occurs 14 years after the reference peak. The chlorine loading then drops, only to rise gradually through next century to 4.30 ppb by 2100. Under the 85/10/5, 85/12/3 and 85/13.5/1.5 scenarios the peaks are 4.24 ppb, 4.24 ppb and 4.23 ppb all in 1999, with 2100 chlorine loadings of 2.97 ppb, 2.43 ppb and 2.03 ppb respectively. This still represents a significant source of chlorine. Clearly getting developing countries to sign the Protocol must be a prerogative, even if this requires further concessions by developed nations. If this is not achieved, no amount of cutbacks by signatories will prevent a rise in atmospheric chlorine.

7.4.18 Sensitivity of the Chlorine Loading to Per Capita Consumption by Non-Signatory Developing Countries.

This study assumes that a fifth of developing countries are non-signatory and reach maximum use by 2010. We look at a peak consumption of 0.4 kg, 0.8 kg (both of which featured in Section 7.4.17) and 1.2 kg (which is the approximate amount used in the USA). The results are shown in Figure 7.39 and Table 7.9.

This study acts as a corollary to Section 7.4.17 and reinforces its conclusions. The level of consumption achieved by non-signatory countries can have a large affect on both the 2 ppb date, its timing and ultimately the chlorine loading achieved by the end of next century, as chlorine loadings increase to approximately 50%, 100% and 150% of reference 2100 values for a per capita consumption of 0.4 kg, 0.8 kg and 1.2 kg respectively.

7.5 General Conclusions

It is evident from the studies illustrated above that the atmospheric chlorine loading is sensitive to prolonged or enhanced production of halocarbons (Sections 7.4.4, 7.4.6, 7.4.14-7.4.18). In the event of increased use, it is the CFCs which have a major influence on both the peak chlorine loading and the timing of the 2 ppb date (Section 7.2.1). The other halocarbons, particularly methyl chloroform, make a significant contribution to the peak chlorine loading (Section 7.2.1). Although measures for reducing and ultimately removing reliance on CFCs and other halocarbons have been successful in stopping the rising chlorine loading trend (Section 7.4.4), other measures such as recycling will prove less effective as most of the harmful CFC is already in the environment (Section 7.4.13). A residual consumption of CFCs (for essential uses only) would be acceptable, provided it can be strictly controlled, as the atmospheric chlorine loading is not sensitive to a small sustained use of halocarbons (Sections 7.4.5 and 7.4.7). Although they have little effect on both the peak chlorine loading and 2 ppb date, the HCFCs do have significant effects on the chlorine loading throughout the first half of next century, and therefore the choice of HCFC, level of production and date of phase out, are important considerations (Sections 7.4.8 and 7.4.10).

Only globally accepted policy for halocarbon removal will be effective in reducing levels of man-made chlorine in the atmosphere. If this is not achieved, chlorine levels may maintain elevated levels at the very least, and at the most, will rise to unprecedented levels during next century (Sections 7.4.15-7.4.18). Mankind now has the ability to alter the planet on a global scale (Section 7.4.11), and it is only through combined action that we will be able to tackle and solve the problem of atmospheric chlorine and ozone depletion. If we cannot remedy the problem of halocarbon emissions, then what hope do we have in solving other possible global environmental problems, such as the Greenhouse Effect?

The model presented in this work features coefficients which allow for the release characteristics of halocarbons used in different applications (Section 7.4.2). The result of this and the other sensitivity studies (Sections 7.4.3-7.4.18), must be viewed in the context of inherent uncertainty in the data used in the model (Section 7.4.1). However, the magnitude of the sensitivity of the chlorine loading to these errors in data have been treated as systematic, which in reality, is unlikely to be the case.

Chapter 8

Results and Discussion of the Bromine Loading Model

8.1 Introduction

The bromine loading model features three bromocarbons, these being halon 1211, halon 1301 and methyl bromide. The combined contribution of other bromocarbons, such as halon 2402, is considered to be negligible. We are interested in looking at three features within the model, these being the value and timing of the peak bromine loading and the date at which the bromine loading reaches 11.39 ppt. This value is adopted as the natural level of bromine (Section 6.3.2), but is subject to a degree of uncertainty, which is discussed further in Section 8.4.1.

8.2 The Montreal Protocol 3 Reference Level

This is the level used for comparison in all the sensitivity studies in this chapter. Its requirements regarding halons, can be found in Table 1.1, and our assumed phase out schedule for man-made methyl bromide can be found in Table 6.5 as no decision has yet been made on a timetable for its removal.

Figure 8.1 illustrates the bromine loading under Montreal Protocol 3. Initially the bromine loading in 1985 rises from 15.60 ppt to a peak in 1994 of 22.18 ppt. The adopted natural level is shown as a horizontal line. This level is not reached by the end of next century under Montreal Protocol 3 requirements, as the bromine loading only falls as far as 12.43 ppt by 2100 (although natural levels range between 9-15 ppt, Section 8.4.1).

If Figure 8.1 is subdivided into the cumulative contribution of the individual bromocarbons which produce it, we get Figure 8.2. This figure shows that man-made methyl bromide adds 2.79 ppt in 1990 to natural levels which is 32% of man-made bromine, but reduces to a negligible amount by 2020. Halon 1211 reaches its peak around

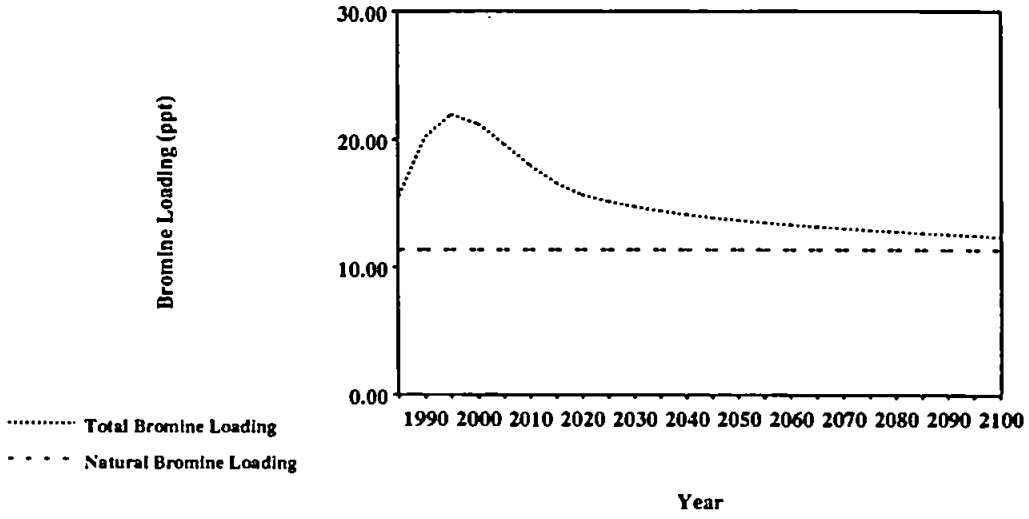

Figure 8.1 The bromine loading under Montreal Protocol 3.

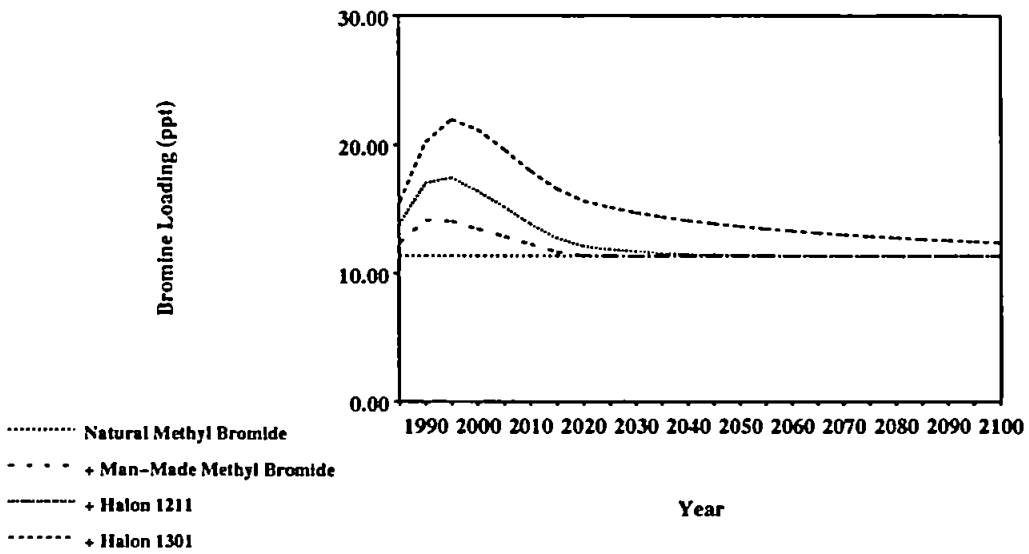

Figure 8.2 The cumulative contribution of each of the bromocarbons to the Montreal Protocol 3 reference bromine loading.

1995, contributing a further 32% of the man-made loading. Halon 1301 contributes a further 43% in 1995 and after 2045, contributes all man-made bromine due to its long lifetime of 65 years.[1]

The use of halons has increased dramatically (Figure 8.3) owing to their ideal fire extinguishing properties (electrically non-conductive, highly volatile, leave no residue on evaporation and have relatively low toxicity). It is only due to impending restrictions under Montreal Protocol 3, that recent production has decreased, and is set to cease by the end of 1993. Figure 8.3 also shows the rise in use of man-made methyl bromide up to 1990 due to growing demands in the international trade in fruit and vegetables.

8.3 Comparison of Modelled Results with Measured Data

As with the chlorine loading model, we present some comparisons of the bromine loading model with measured trends.

1) The modelled concentration of methyl bromide in 1985 is 12.43 ppt, rising to 13.99 ppt in 1989. This is within the quoted concentration of 10-15 ppt,[2-4] but extends slightly above that quoted by Albritton and Watson of 9-13 ppt.[5]

2) Two estimates are given in WMO 1991[2] for halon growth in the late 1980's. For halon 1211 this is 12% and 15% and for halon 1301, it is 15% and 20%. The model shows a rise in the atmospheric concentration of halons 1211 and 1301 of approximately 15% and 14% respectively.

3) Peak bromine is predicted to be approximately 25 ppt in the late 1990's in WMO 1991,[2] compared to our value of 22.18 ppt in 1994. However this discrepancy is due to the WMO prediction being based on Montreal Protocol 2 requirements. Comparison with our predicted bromine loading under Montreal Protocol 2 is closer, and can be found in Section 8.4.3.

4) Total bromine abundance is given as 15-20 ppt for the mid-1980's to early 1990's,[5]

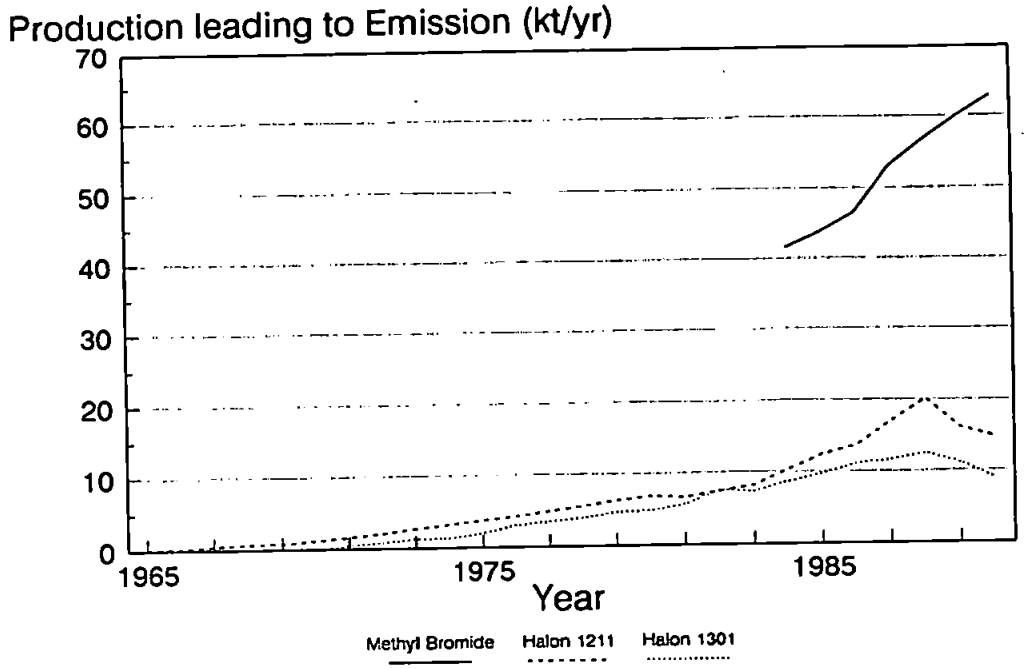

Figure 8.3 Diagram of the total production leading to emission of each of the bromocarbons.

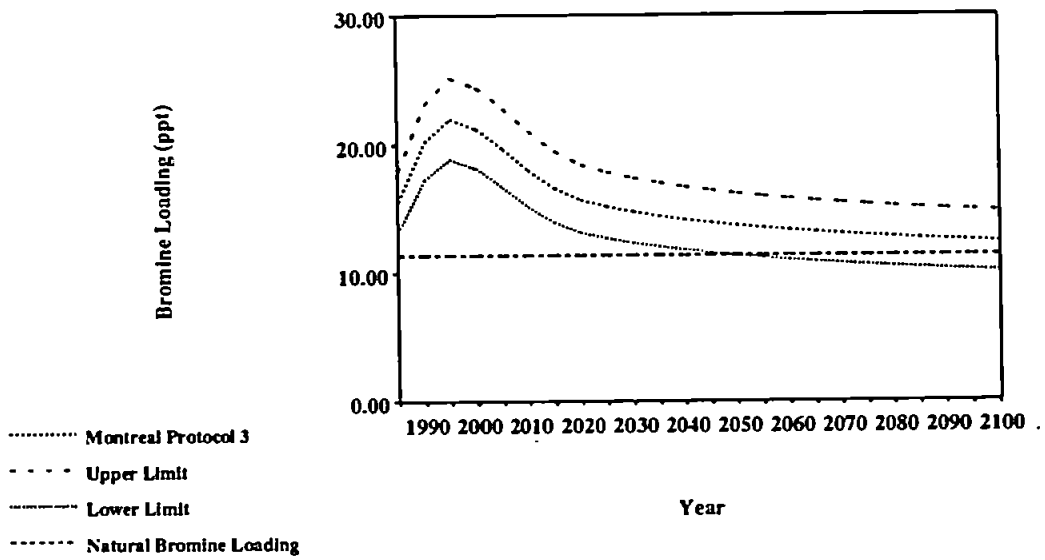

Figure 8.4 The sensitivity of the bromine loading to uncertainty in bromocarbon lifetime.

compared to 15.6-22.18 ppt in the bromine loading model.

5) The 1989 concentration of halon 1301 has been measured as between 1.8-3.5 ppt,[2] compared to a value in the model of 2.86 ppt. Comparison with halon 1211 is not so good however, as measured values are given as 1.6-2.5 ppt,[2] and the model result is 2.65 ppt. This value has been obtained from published production and emission estimates,[6] and is still within the ±15% calibration error associated with the halon 1211 measurements.[2]

8.4 Results and Discussion of the Sensitivity Analyses

We begin this section by looking at the sensitivity of the bromine loading model to inherent uncertainty in the data comprising it.

8.4.1 Sensitivity to Uncertainty in the Data used in the Model.

The same methods are used in this section as were used in Section 7.4.1 for the chlorine loading model.

Lifetime - the published upper and lower limits for lifetimes of each of the bromocarbons were substituted into the model, in order to assess the effect on the bromine loading of an uncertainty in atmospheric lifetime. The limits used for halons 1301, 1211 and methyl bromide were 65-68.6 years,[2,7] 11-16 years[7] and 1.2-1.8 years[2] respectively. Results of this analysis are shown in Figure 8.4 and Table 8.1.

This analysis shows that lifetime of the bromocarbons represents a major uncertainty to which the atmosphere is very sensitive, as peak levels are raised and lowered to 25.33 ppt and 19.07 ppt respectively. At the peak bromine loading it is the atmosphere's sensitivity to the lifetime of methyl bromide which is of prime importance, contributing 89.6% to the change in the bromine loading, compared to only 0.9% for halon 1301 and 9.5% for halon 1211. By 2100, the level of uncertainty caused by methyl bromide rises to 95.8%, with halon 1301 making up the balance. This study shows that

Table 8.1 Sensitivity to uncertainty in the data used in the bromine loading model.

Data Category	Limit	Change on Peak Bromine in Reference Scenario (%)	Year of Peak Bromine (years)	Change in 2100 Bromine Level (%)
Lifetime	Upper	+14.2	-	+19.1
	Lower	-14.0	-	-18.3
Concentration	Upper	+3.2	-	+1.0
	Lower	-3.2	-	-0.9
Production	Upper	+1.4	-	-
	Lower	-1.9	-	-
Growth	Short Term	+3.7	-	-
	Long Term	+2.6	-	-
	Gradual Phase Out	-3.1	-	-0.9

whereas halon 1211 has more importance for the peak bromine loading and halon 1301 for the level in 2100, it is uncertainty in the determination of atmospheric lifetime for methyl bromide which has major implications for the future bromine loading. If the atmospheric residence time for methyl bromide is towards 1.2 years,[2] then the bromine loading is lowered to such an extent that we attain the assumed natural level of 11.39 ppt by 2052. More accurate determinations of the lifetime for methyl bromide would dramatically reduce the inherent uncertainties in the data used in this model.

1985 Concentration - the initial concentrations used in the model are subject to an absolute calibration uncertainty (between instruments measuring the atmospheric concentration) of ±15% for halon 1211 and ±40% for halon 1301, based on the data of three independent laboratories (the Oregon Graduate Institute for Science and Technology, the National Oceanic and Atmospheric Administration - Climate Monitoring and Diagnostics Laboratory and the Max Planck Institute for Aeronomy).[2] Results are shown in Figure 8.5 and Table 8.1 and show that this calibration uncertainty raises and lowers peak bromine by ±3.2% to 22.89 ppt and 21.47 ppt respectively. This trend is predominately (85%) due to the uncertainty in halon 1301. The bromine loading in 2100 is altered by ±0.12 ppt on the reference level.

The published uncertainty in concentration for methyl bromide is 9-15 ppt.[2-5] Assuming that this is primarily due to natural production (which represents the major source of methyl bromide), this uncertainty would simply have the effect of uniformly raising and lowering the natural bromine loading line in Figure 8.5 by +3.61 ppt and -2.39 ppt, as more or less atmospheric bromine would be attributed to natural sources. This would have far reaching effects on the date at which we would define the bromine loading to become 'natural'. For example, under a natural bromine loading of 15 ppt, the reference bromine loading for Montreal Protocol 3 would become 'natural' in 2027, representing a radical decrease on our adopted level of 11.39 ppt, for which natural levels are not

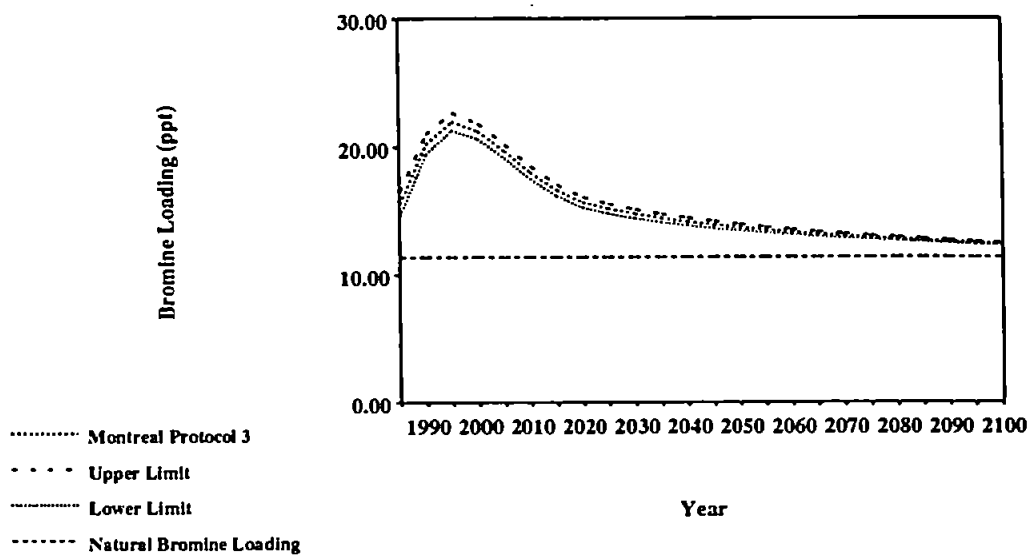

Figure 8.5 The sensitivity of the bromine loading to a calibration error in determination of halon concentrations in the atmosphere.

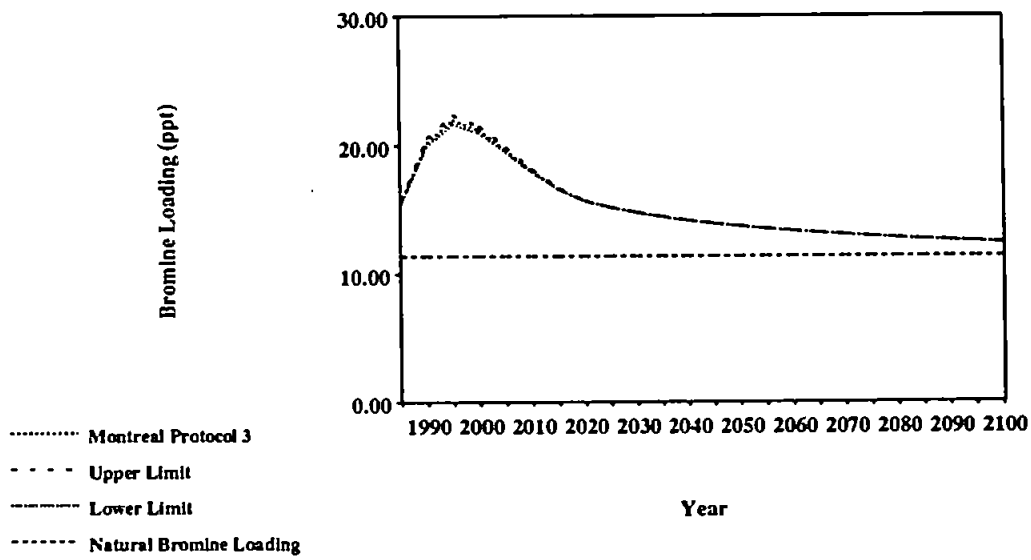

Figure 8.6 The sensitivity of the bromine loading to errors in production data used in the model.

obtained before the end of next century.

Production - McCulloch[6] gives a range of error in his estimates for world production of halons 1211 and 1301, which are substituted into the model for this study. In the model, production of man-made methyl bromide is equal to emission (due to our assumption of immediate release) and therefore we adopt the published estimate of ±10% for errors in emission data[5,8] as our estimate for error in production. Natural methyl bromide production remains constant.

The results are shown in Figure 8.6 and Table 8.1, and show that errors in production data have a minor affect on peak bromine (+0.32 ppt / -0.43 ppt) and no affect on the 2100 level. This is because the limits for error in the halon data are small and although the range of error for man-made methyl bromide is larger, it only contributes around 25% to total methyl bromide production and therefore does not represent the major source of the gas.

Growth/Decline - here we assess the effect of utilising the growth factors of 1.00 between 1990-1993 for the halons in WMO 1991,[2] by replacing them with a long term (1980-1990) and short term (1988-1990) historical mean growth rate, derived from published production data.[6] We also relax the assumption of production at a constant rate between 1991 and 1994 inclusive of methyl bromide, by similarly calculating a historical growth rate from published data.[5] For halons 1211, 1301 and methyl bromide the calculated long term yearly rates are +9.05%, +7.05% and +6.48% (the methyl bromide rate is calculated from the years 1984-1990) respectively and the short term rates are -3.24%, -7.09% and +6.09% respectively.

The growth factors represent a stepped phase out for the halons as production is maintained at the 1990 level until 1993. Therefore, we also look at the effect of a linear decline (a gradual phase out scenario) over this period. Methyl bromide is assumed to remain constant. Results are shown in Figure 8.7 and Table 8.1.

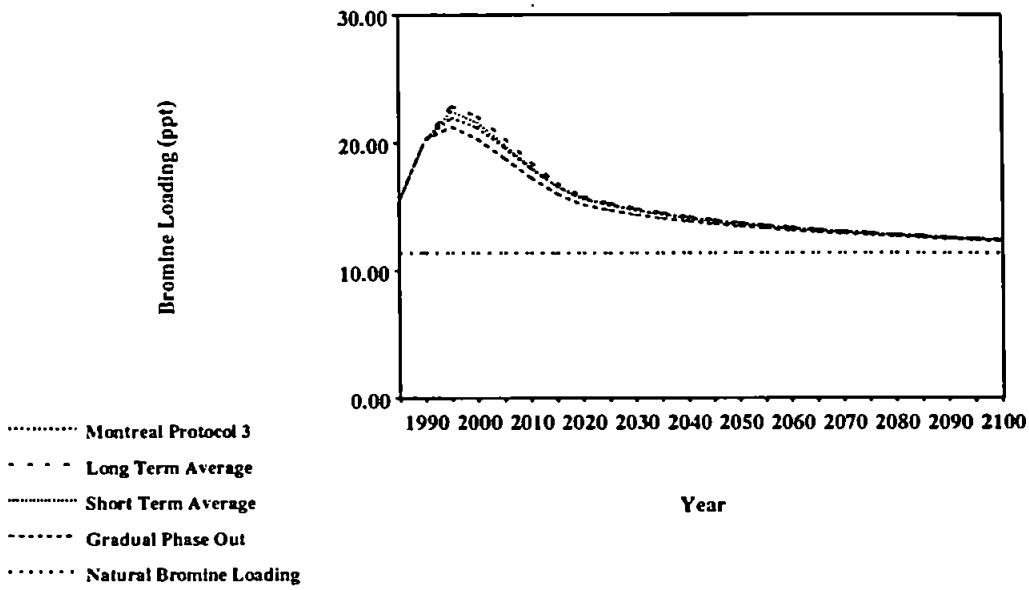

Figure 8.7 The sensitivity of the bromine loading to the use of growth factors from WMO 1991.[2]

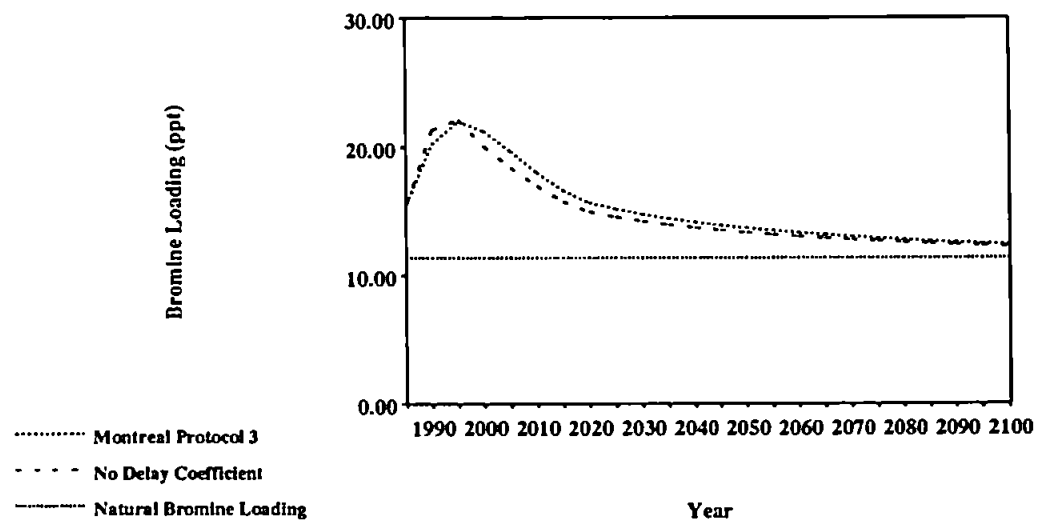

Figure 8.8 The sensitivity of the bromine loading to the use of delay coefficients.

Under the growth scenarios the peak bromine loading was raised owing mainly to the historical increase in man-made methyl bromide production. The maximum increase was under the long term growth rate scenario, which raised bromine levels by 3.7% (an increase of 0.82 ppt). The 2100 level is unchanged.

For the gradual phase out schedule, peak bromine loading reduces to 21.50 ppt in 1994 with a negligible affect on the 2100 level. This reduction in peak bromine is caused by a saving in halon 1301 production of 13.68 kt and halon 1211 of 22.28 kt over a three year period representing a saving of 50% in halon production over this period.

Clearly any increase or decrease in halon production can influence peak bromine levels in the short term. However that influence is small as most halon has already been used and in this study we are only influencing the last 3 years of over 25 years of production.

8.4.2 Sensitivity of the Bromine Loading to use of Delay Coefficients.

This study highlights the phase error associated with an assumption of immediate release on production, as used by other workers,[9] compared to our use of delay coefficients based on work by McCulloch[6] and McCulloch (*personal communication*). The results are shown in Figure 8.8 and Table 8.2.

The results of this analysis reveal that an immediate release assumption increases peak bromine to 23.11 ppt and brings it forward to 1993, whereas the 2100 bromine loading reduces to 12.28 ppt. These trends are an obvious result of premature emission of the halons, when compared to the reference delayed emission scenario.

8.4.3 Comparison of Montreal Protocols 1, 2 and 3.

This study shows the effectiveness of international legislation in reducing atmospheric bromine levels.

Table 8.2 Results of modelled sensitivity studies in the bromine loading model.

Study Section	Variable	Forcing Factor	Change on Peak Bromine in Reference Scenario (%)	Year of Peak Bromine (years)	Change in 2100 Bromine Level (%)
8.4.2	Use of Delay Coefficients	No Delay	+4.2	-1	-1.2
8.4.3	Montreal Protocols	One	-	-	+202.8
		Two	+7.9	+5	+2.5
8.4.4	Removal of Methyl Bromide	By 1995	-2.8	-1	-
		By 2000	-	-	-
		By 2005	-	-	-
		By 2010	-	-	-
8.4.5	Proportion of Halons emitted in Year 0	±5%	±0.1	-	±0.1
		±10%	±0.3	-	±0.2
8.4.6	Length of Delayed Emission Period	Long	-2.0	-	+0.5
		Short	+2.1	-	-0.5
8.4.7	Recycling of Halons	A	-0.8	-	-0.2
		B	-2.0	-	-0.5
		C	-3.3	-	-0.8
		D	-4.6	-	-1.1
8.4.8	Extended Use of Halons	-	+4.0	+5	+1.9

Under Montreal Protocol 1 (Table 1.1), halon production in 1992 and for the rest of the model, is maintained at the 1986 level. Man-made methyl bromide is assumed to remain constant at the 1990 level. For Montreal Protocol 2 (Table 1.1), the halons are phased out by 2000, with a stepped phase down from 1995. Methyl bromide is assumed to be phased down and removed between 2000 and 2030.

The comparison is illustrated in Figure 8.9 and Table 8.2. Throughout the model the bromine loading under Montreal Protocol 1 continues to rise indefinitely and as a result, reaches 37.64 ppt by 2100. Under Montreal Protocol 2, a peak of 23.94 ppt is achieved in 1999, which then dissipates to 12.74 ppt by 2100. Montreal Protocol 3 is shown to be more effective in reducing the peak bromine loading than the long term bromine loading, which is due to the longevity of halon 1301 already in the environment.

8.4.4 Sensitivity of the Bromine Loading to the Premature Removal of Man-Made Methyl Bromide.

In this study, the effect of a premature removal of methyl bromide before our reference phase out schedule (Table 6.5) is examined. Four different complete phase out dates are assumed in 1995, 2000, 2005 and 2010, with assumed phase downs as shown in Table 8.3. The percentage reductions in Table 8.3 are relative to production in 1992. The results are shown in Table 8.2 and Figure 8.10.

A complete phase out of methyl bromide by the year 2000 is the goal set in the USA as part of its Environmental Protection Act. Assuming that the rest of the world were to follow this target, there would be no difference in peak bromine from our reference level. The benefits of such a cut would come after 1994 with an accelerated rate of removal of bromine. Complete removal of man-made methyl bromide by 1995 reduces the peak bromine loading by 2.8%, a magnitude of effect which should be considered in the context of the uncertainties listed in Table 8.1. As methyl bromide is

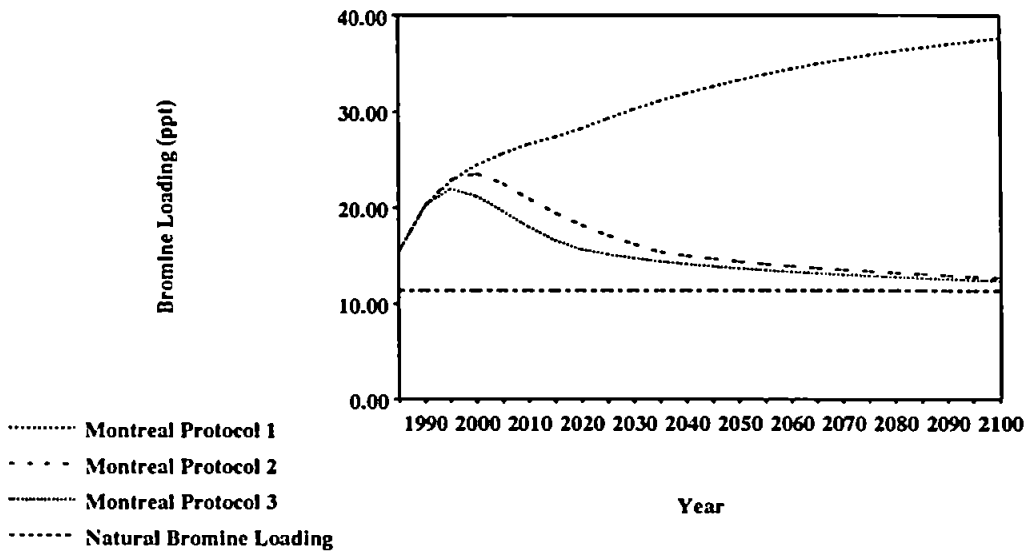

Figure 8.9 Comparison of the bromine loading under Montreal Protocol's 1,2 and 3.

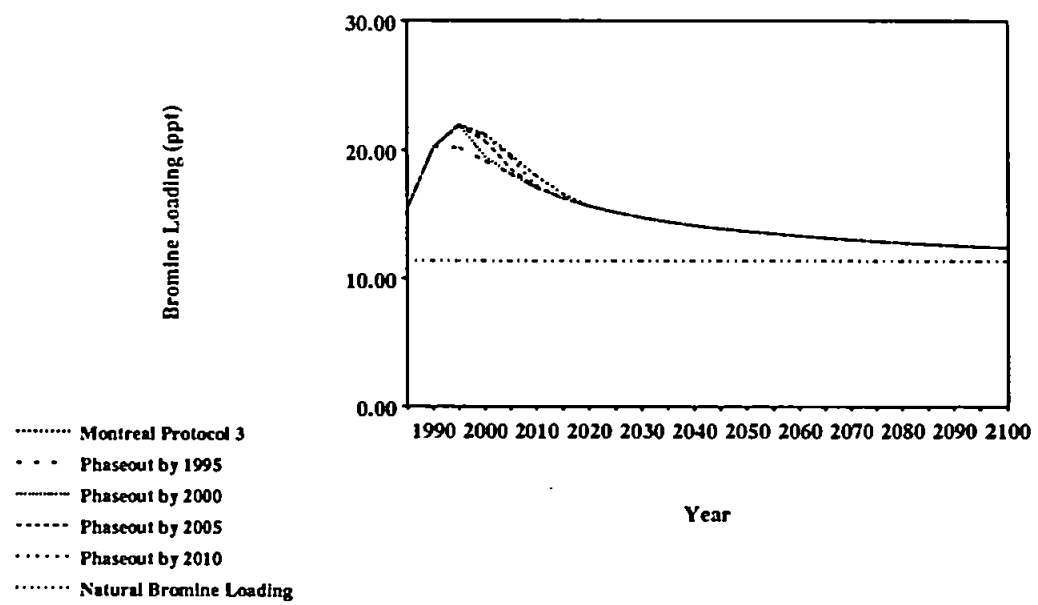

Figure 8.10 The sensitivity of the bromine loading to an accelerated phase out schedule for man-made methyl bromide production.

Table 8.3 Assumed man-made methyl bromide phase out for Section 8.4.4.

Phase out by:	Reduction
1995	50% cut by 1993
	75% cut by 1994
2000	20% cut by 1995
	40% cut by 1996
	60% cut by 1997
	80% cut by 1998
	90% cut by 1999
2005	20% cut by 1997
	40% cut by 1999
	60% cut by 2001
	80% cut by 2003
2010	20% cut by 1995
	40% cut by 1999
	60% cut by 2003
	80% cut by 2007

a short lived gas of 1.2 to 1.8 years, the effect of its accelerated removal is negligible by 2015. Beyond this, the bromine loading is the same as for the reference scenario.

Obviously, the sooner the complete phase out of methyl bromide, the more effective the reduction in bromine loading. However, if it is not agreed to remove methyl bromide within the next few years as part of Montreal Protocol 4, only a considerable phasing down by the end of this century will have any effect on lowering the predicted bromine loading.

8.4.5 Sensitivity of the Bromine Loading to the Proportion of the Halons emitted in the Year of Production.

Due to their use as fire retardants, it is reasonable to assume that a proportion of the production of halons 1211 and 1301 is emitted in the year of production. The amount for each which is assumed to be emitted in this year is shown in Table 6.2.[6] For this study the proportion emitted was altered by ±5% and ±10% in order to assess the effect of an error in these estimates (which are based on the results of questionnaires). The results can be seen in Figure 8.11 and Table 8.2.

These results show that the atmosphere is not sensitive to an alteration in the amount of halons emitted in the year of production, thus any error in the questionnaire results collected by McCulloch,[6] will not materially affect the reference bromine loading under Montreal Protocol 3.

8.4.6 Sensitivity of the Bromine Loading to the Period of Emission of the Halons after the Year of Production.

Following on from Section 8.4.5, the period of time over which the halons are emitted after production (Table 6.2) has been altered in this study. This is to assess the affect of an error in the delay coefficients applied in the model, as a result of uncertainties

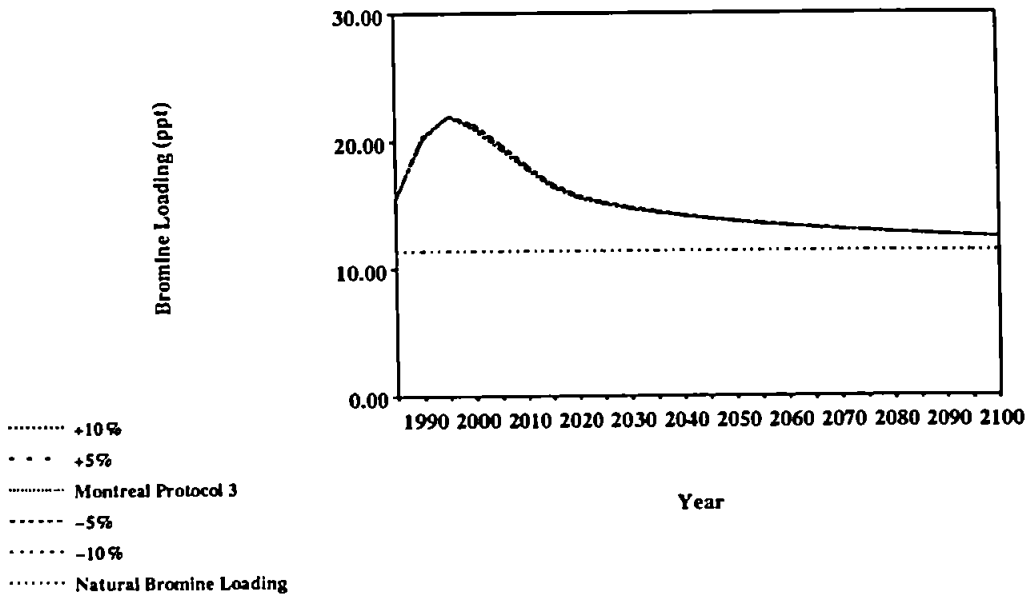

Figure 8.11 The sensitivity of the bromine loading to the proportion of the total production of halons emitted in the year of production.

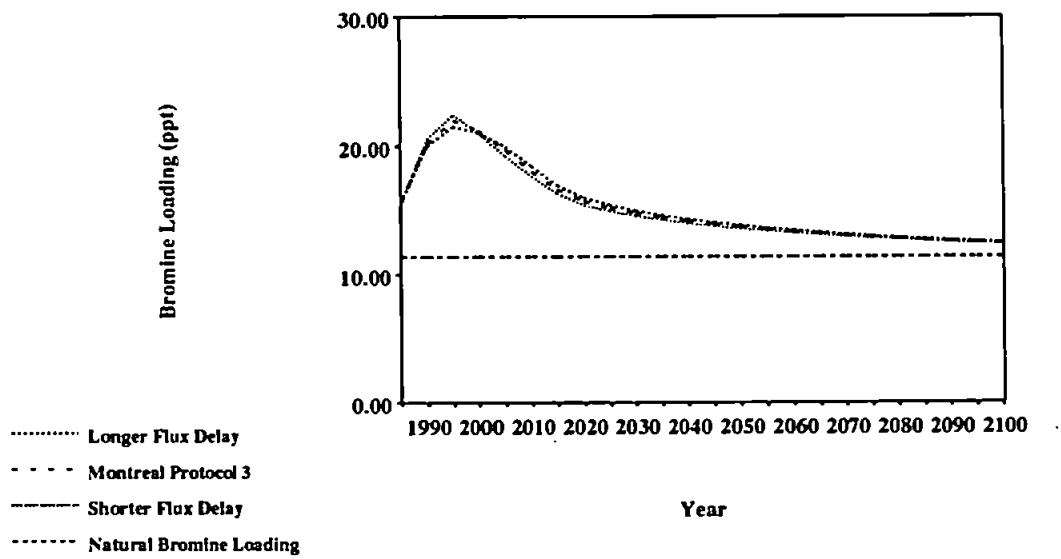

Figure 8.12 The sensitivity of the bromine loading to the period of emission after the year of production.

in the results of the questionnaires given by McCulloch.[6] Instead, halon 1301 has been modelled assuming flux delays of 4 and 12 years and halon 1211 with flux delays of 9 and 17 years. Methyl bromide remains unchanged. The results are displayed in Figure 8.12 and Table 8.2.

This study shows that the atmospheric bromine loading is more sensitive to the length of time over which the halons are emitted. With the longer period of emission, the peak bromine loading is lowered to 21.74 ppt, although the date of occurrence is unaffected. However, due to the longer period of time over which the halons are emitted, the bromine loading by 2100 rises to 12.49 ppt. The shorter period of emission reveals an expected reversal of these trends. Comparing the results of Section 8.4.5 and this section, the bromine loading appears to be more sensitive to the period of time over which halons are emitted than the proportion of production emitted in the year of production.

8.4.7 Sensitivity of the Bromine Loading to Recycling of Halons.

This study uses the same recycling scenarios (Table 7.8) as used in Section 7.4.12 for the chlorine loading model. Man-made methyl bromide remains the same. The results are shown in Figure 8.13 and Table 8.2.

The conclusions of this study produce comparable conclusions to those for the chlorine loading model. Recycling at modest rates at present (such as in scenario A) only has a minor affect on the peak bromine loading, by lowering it to 22.01 ppt, and a minimal affect on the 2100 level. Had a better developed recycling program been implemented and operating for a number of years, then material differences could have been made to the peak bromine loading and the 2100 level (as peak bromine reduces by 1.01 ppt and the 2100 level by 0.14 ppt under scenario D). Only a large level of recycling will have any major affect on the atmospheric bromine loading because so much halon is already in the environment.

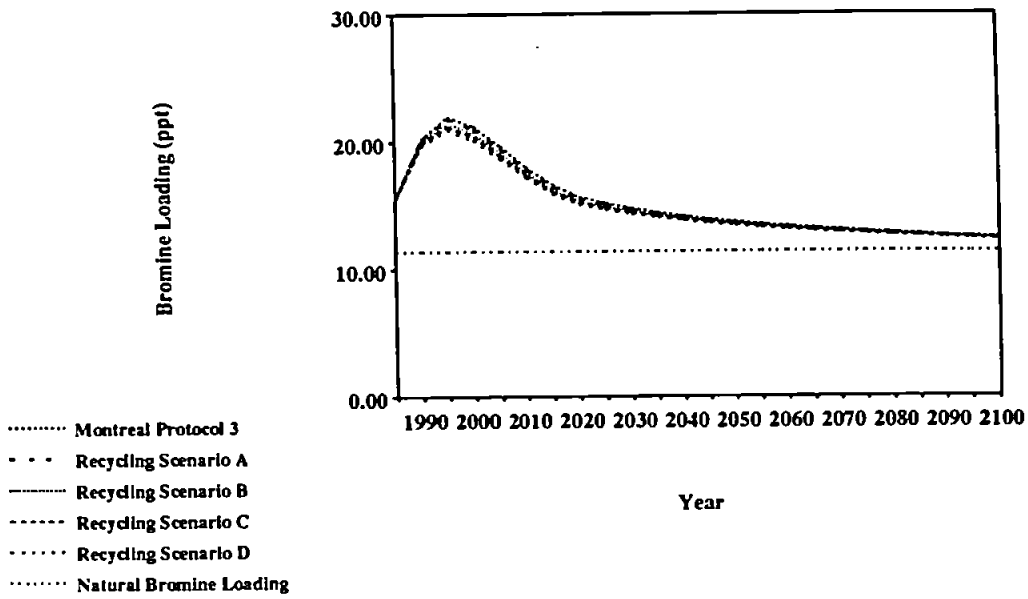

Figure 8.13 The sensitivity of the bromine loading to recycling of halons.

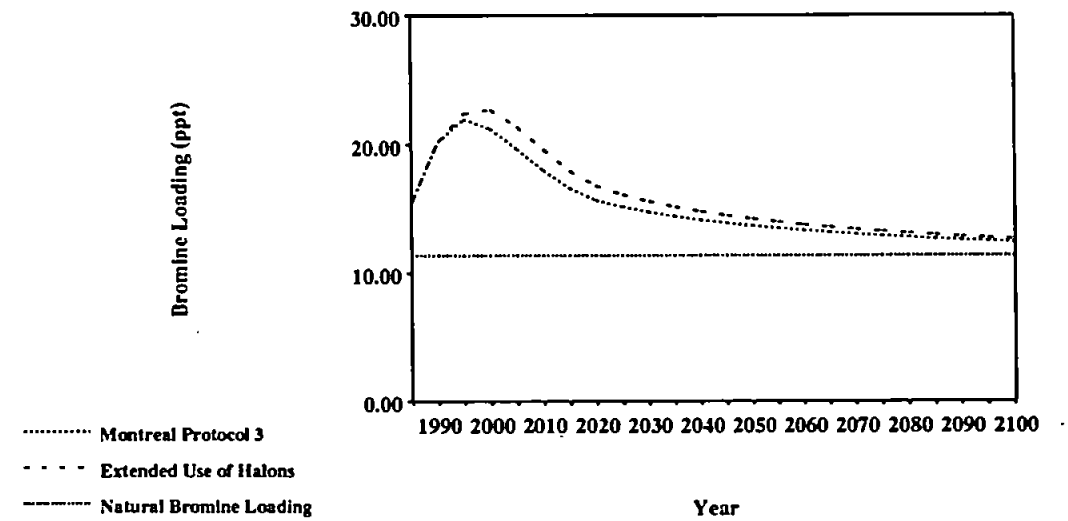

Figure 8.14 The sensitivity of the bromine loading to extended use of halons.

8.4.8 Sensitivity of the Bromine Loading to Extended Use of Halons.

For this study, we assume that some halon production is maintained after the Montreal Protocol 3 requirement of zero production by 1994 through use by non-signatories to the Protocol or those countries disregarding their responsibilities as signatories to the Protocol. We assume that the level of production is 50% of the 1993 level and is maintained until 1999 (so that production ceases by 2000). This has the affect of introducing an extra 27.36 kt of halon 1301 into the environment and 44.55 kt of halon 1211.

Figure 8.14 and Table 8.2 show that this extended use of halons increases the peak bromine loading by 0.88 ppt and brings it back to 1999. This rise in the bromine loading is about 65% due to halon 1301 and the balance due to halon 1211. The 2100 bromine level is also raised to 12.66 ppt, representing a rise of 1.9%. This study shows that the timing of the peak bromine loading is particularly sensitive to the continued production and emission of halons.

8.4.9 Effect of a Combined Chlorine and Bromine Loading.

Bromine present in the atmosphere has a greater potential to destroy ozone than chlorine on a per atom or molecule basis, because approximately 50% of the available bromine is present in a reactive form (Br and BrO) compared to a much lower percentage for chlorine. Bromine in the form of bromine monoxide (BrO) interacts with chlorine monoxide (ClO), without sunlight and atomic oxygen, to destroy ozone in the lower stratosphere where ozone concentrations are naturally higher than in the upper region[10] (Equation 1.9).

Thus the bromine loading is of major importance and it has been of interest to attain a value which represents the relative conversion between bromine-catalysed ozone destruction and chlorine-catalysed ozone destruction. Solomon et al.[11] suggest a conversion

between bromine and chlorine of close to 40, ie. an atom of bromine ultimately causes 40 times more destruction of ozone than an atom of chlorine.

Using man-made bromine under Montreal Protocol 3 conditions, an equivalent chlorine loading was calculated using this conversion factor of 40. Natural bromine has been omitted as it is reasonable to assume that this is in equilibrium with the natural chlorine loading, and therefore does not contribute to anthropogenically enhanced ozone destruction. The equivalent chlorine loadings derived from the bromine loading model are added to the reference level of the chlorine loading model, and are shown in Figure 8.15 and Table 8.4.

The results of this study show that the combined effect of the chlorine and bromine loading has a marked impact, producing an equivalent peak chlorine loading of 4.23 ppb (compared to the reference level of 3.80 ppb) in the same year, namely 1994. The effect on the 2 ppb date is less, with an extension to the year 2057 from 2053. This highlights the importance of bromine as an ozone depleting entity because, despite bromocarbon production only comprising less than 5% of chlorocarbon production, equivalent chlorine from bromocarbons contributes over 11% to peak chlorine.

8.4.10 Sensitivity of the Chlorine Loading to the Value of the Conversion Factor.

Unfortunately, due to the complex interactions occurring between chlorine and bromine in a multitude of photochemical conditions on a global scale, the value of this conversion factor is not easy to derive, and is therefore subject to a large degree of uncertainty. Albritton and Watson[5] calculate it to be between 20 and 100 (best estimate is 40), compared to a value of about 30 (and uncertainty ranging from 10 to 50) given by Prather and Watson,[9] and a range between 30 and 120 in WMO 1991.[2] We apply a conversion factor of 20, 30 and 50 and show the results in Figure 8.16 (together with the x40 used in Section 8.4.9) and Table 8.4.

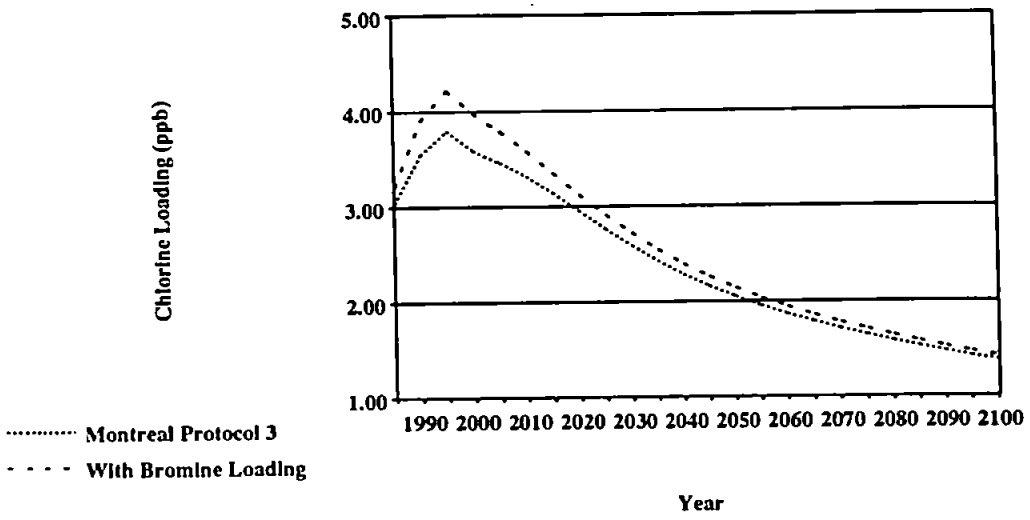

Figure 8.15 The sensitivity of the total chlorine loading to the combined effects of bromine- and chlorine-catalysed ozone destruction.

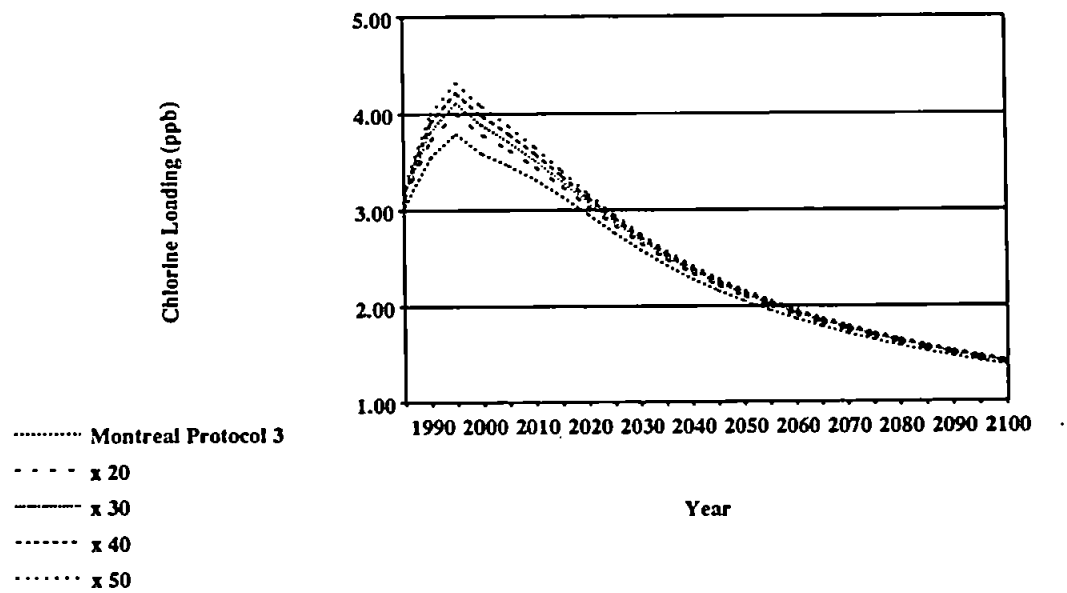

Figure 8.16 The sensitivity of the total chlorine loading to uncertainty in the conversion factor used to convert the bromine-catalysed chemistry into a chlorine equivalent.

Table 8.4 Results of combined chlorine and bromine loading models.

Study Section	Variable	Forcing Factor	Change on Peak Chlorine in Reference Scenario (%)	Year of Peak Chlorine (years)	Change in 2 ppb Date (years)
8.4.9	Br to Cl Conversion	x40	+11.3	-	+4
8.4.10	Uncertainty in Conversion Factor	x20	+5.5	-	+2
		x30	+8.4	-	+3
		x50	+14.2	-	+6

Using these estimates of the conversion factor raises the peak chlorine loading by 0.21 ppb, 0.32 ppb and 0.54 ppb for a x20, x30 and x50 conversion respectively. If peak chlorine is calculated for the higher estimates given above of x100 and x120, then peak chlorine is raised by 1.08 ppb and 1.29 ppb to 4.88 ppb and 5.09 ppb respectively. These represent respective increases of 28.4% and 33.9% on the reference level. Although a factor relating bromine-catalysed ozone destruction with that of chlorine is useful, it can only be of limited worth in the light of such a large range of uncertainty.

8.5 General Conclusion

In terms of an absolute estimation of future bromine loadings, the results of this model are limited because of the large uncertainties associated with the data used within it, particularly lifetimes of the bromocarbons (Section 8.4.1). Clearly, estimates of these parameters with a smaller degree of uncertainty would reduce this problem.

However, in terms of the relative ability for various forcing factors to influence the bromine loading, the model is informative. The delay coefficients, based on the work of McCulloch,[6] have a greater affect on the profile of the bromine loading curve than the delay coefficients employed in the chlorine loading model (Section 8.4.2), although the loading is not sensitive to the exact form that these delays take (Sections 8.4.5 and 8.4.6).

Generally any cutbacks in the use of halons is an advantage (Sections 8.4.3 and 8.4.8) but last minute measures will have a minimal affect on both the peak bromine loading and the 2100 level, because most of the halon which has been produced will have already reached the environment (Section 8.4.7).

The potential for bromine to destroy ozone is illustrated by converting it into an equivalent chlorine loading, and assessing its relative impact (Section 8.4.9). However, this bromine to chlorine conversion factor has an inherently large uncertainty making such a factor of only limited use (Section 8.4.10). The ability of bromine to catalyse ozone

destruction confirms the need to remove the halons by the end of 1993 whereas the removal of man-made methyl bromide, unless undertaken shortly, will have a negligible affect on reducing the peak bromine loading achieved in 1994 (Section 8.4.4).

Appendix 1 Flow correction spreadsheets used in analysis of raw flow times.

There follows a list of the Supercalc 5.0 spreadsheet files which are contained on the disk at the back of this thesis and an explanation of what they contain;

134FLO35, 134FLO50, 134FLO70, 134FLO90, 134FLO110, 134FLO130 give Dean and Reynolds numbers, mean capillary pressures and corrected flow times for HFC 134a at 308.15 K, 323.15 K, 343.15 K, 363.15 K, 383.15 K and 403.15 K respectively.

123FLO35, 123FLO50, 123FLO70, 123FLO90 give Dean and Reynolds numbers, mean capillary pressures and corrected flow times for HCFC 123 at 308.15 K, 323.15 K, 343.15 K and 363.15 K respectively.

124FLO10, 124FLO35, 124FLO50, 124FLO70, 124FLO90, 124FLO110, 124FLO130 give Dean and Reynolds numbers, mean capillary pressures and corrected flow times for HCFC 124 at 283.15 K, 308.15 K, 323.15 K, 343.15 K, 363.15 K, 383.15 K and 403.15 K respectively.

39FLO35, 39FLO50, 39FLO70, 39FLO90, 39FLO110, 39FLO130 give Dean and Reynolds numbers, mean capillary pressures and corrected flow times for MP 39 at 308.15 K, 323.15 K, 343.15 K, 363.15 K, 383.15 K and 403.15 K respectively.

REG134, REG123, REG124 and REG39 contain the slip flow regression analyses for each of the sample gases HFC 134a, HCFC 123, HCFC 124 and MP 39 respectively.

Appendix 2 Examples of magnitude of correction terms used in calculation of the corrected flow time from the raw flow time.

Sample Gas	Temperature /K	Pressure Code	Pointers	K_b	K_{bl}	K_h	Combined Correction
HFC 134a	308.15	FV_6BV_6	8-9	1.006745	0.9836505	0.9992104	0.989503
			9-10	1.006397	0.9842676	0.9993121	0.989883
			10-11	1.005778	0.9854006	0.9994826	0.990581
			11-12	1.004923	0.9870586	0.9996962	0.991617
	383.15	FV_4BV_4	7-8	1.003468	0.9816083	0.9994187	0.984440
			8-9	1.003255	0.9824340	0.9995078	0.985147
			9-10	1.003099	0.9830511	0.9995701	0.985674
			10-11	1.002822	0.9841841	0.9996748	0.986641
HCFC 123	323.15	FV_7BV_{13}	9-10	1.006732	0.9823443	0.9993713	0.988336
			10-11	1.005525	0.9848836	0.9995932	0.989922
			11-12	1.003861	0.9885529	0.9998358	0.992207
	343.15	FV_3BV_8	6-7	1.007877	0.9732530	0.9989729	0.979912
			7-8	1.007121	0.9752677	0.9991971	0.981424
			8-9	1.006425	0.9771616	0.9993860	0.982836
			9-10	1.005922	0.9785635	0.9995123	0.983878
HCFC 124	283.15	FV_7BV_{14}	8-9	1.011286	0.9811451	0.9991549	0.991380
			9-10	1.010247	0.9825477	0.9993096	0.991931
			10-11	1.008395	0.9850880	0.9995521	0.992913
			11-12	1.005835	0.9887588	0.9998171	0.994346
	403.15	FV_1BV_2	3-4	1.006077	0.9666995	0.9992261	0.971821
			4-5	1.005754	0.9680801	0.9993264	0.972995
			5-6	1.005483	0.9692500	0.9994068	0.973986
			6-7	1.005182	0.9705680	0.9994924	0.975102
MP 39	343.15	FV_7BV_{13}	9-10	1.001547	0.9951320	0.9996181	0.996291
			10-11	1.001270	0.9958321	0.9997529	0.996850
			11-12	1.000888	0.9968438	0.9999002	0.997629
	363.15	FV_7BV_{13}	8-9	1.001400	0.9947454	0.9995937	0.995733
			9-10	1.001272	0.9951320	0.9996683	0.996067
			10-11	1.001044	0.9958321	0.9997854	0.996658

Appendix 3 Examples of slip flow correction plots for each of the sample gases.

The following diagrams illustrate the associated standard error of the y-intercept as $\pm 1\sigma$.

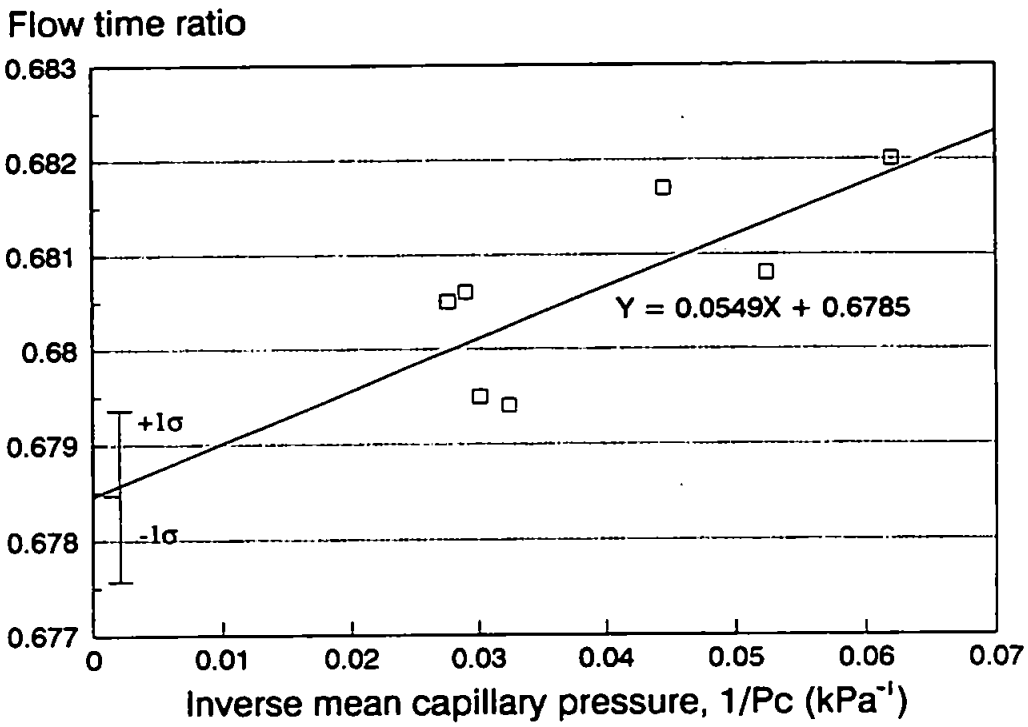

Figure A3a Slip flow correction plot for HFC 134a at 323.15 K. Error bar indicates the standard error associated with the value of the y-intercept.

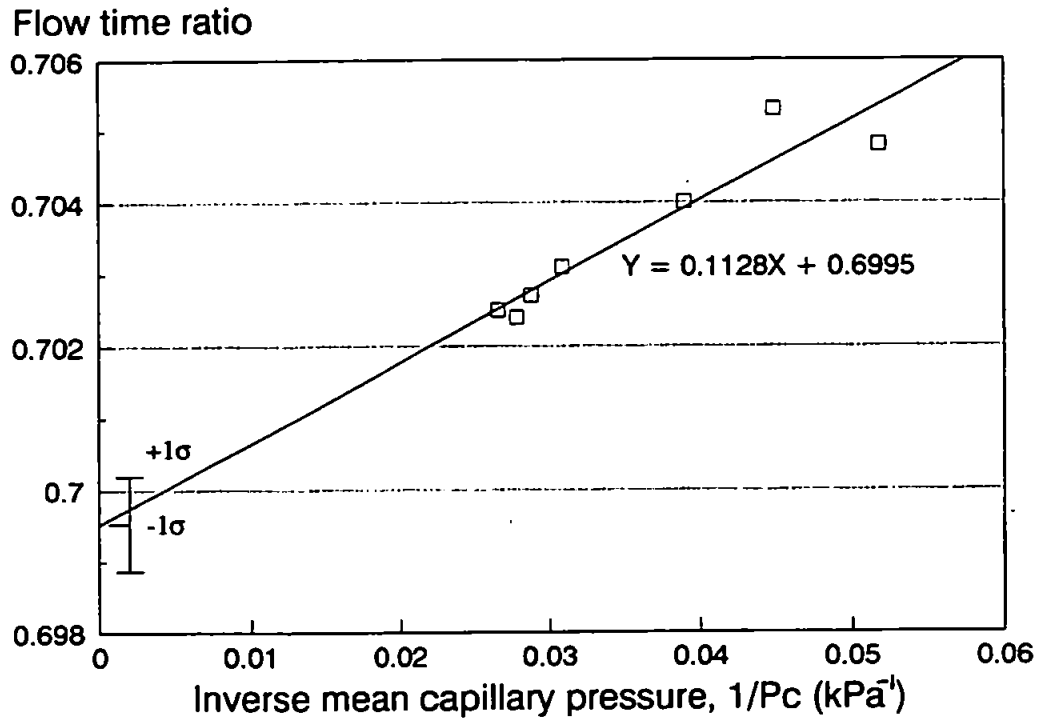

Figure A3b Slip flow correction plot for HFC 134a at 383.15 K. Error bar indicates the standard error associated with the value of the y-intercept.

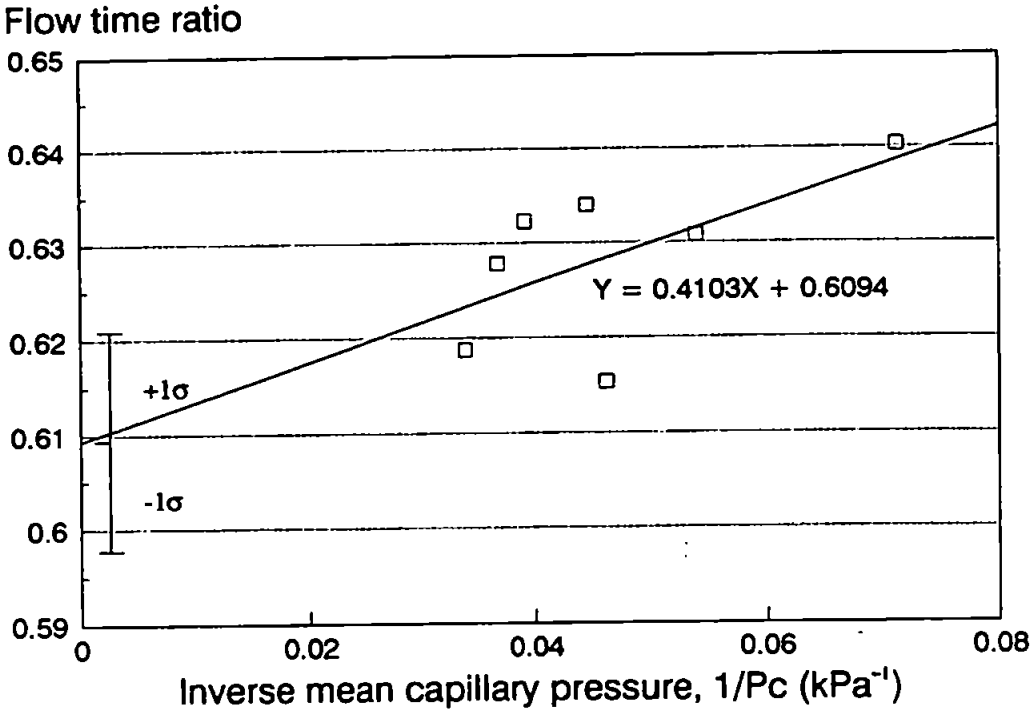

Figure A3c Slip flow correction plot for HCFC 123 at 308.15 K. Error bar indicates the standard error associated with the value of the y-intercept.

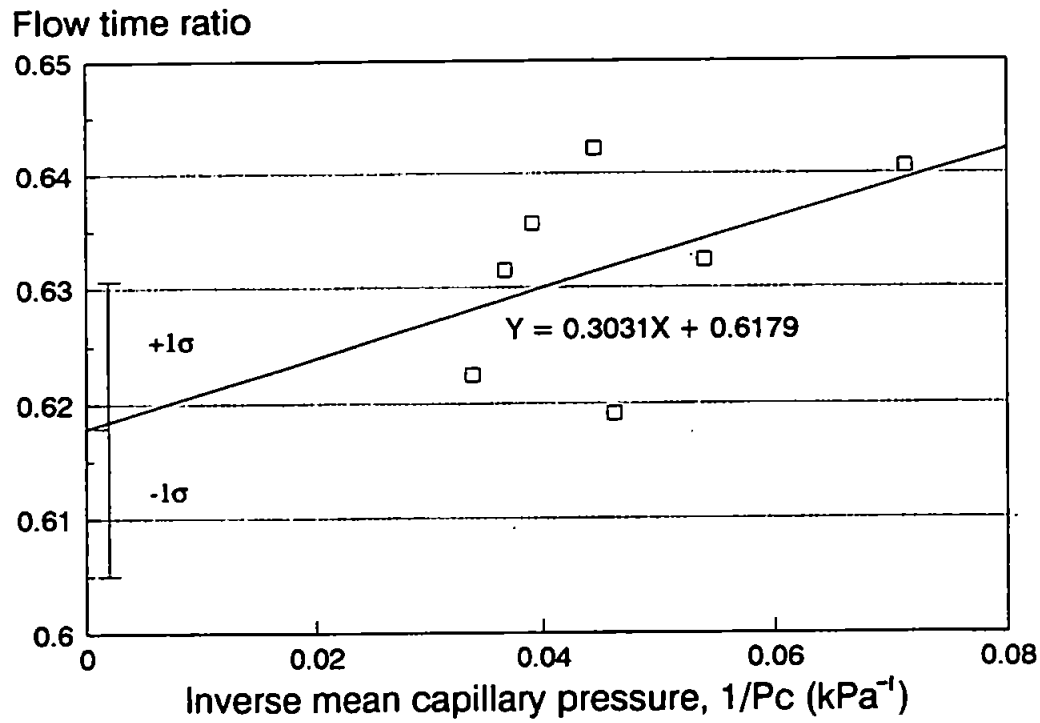

Figure A3d Slip flow correction plot for HCFC 123 at 323.15 K. Error bar indicates the standard error associated with the value of the y-intercept.

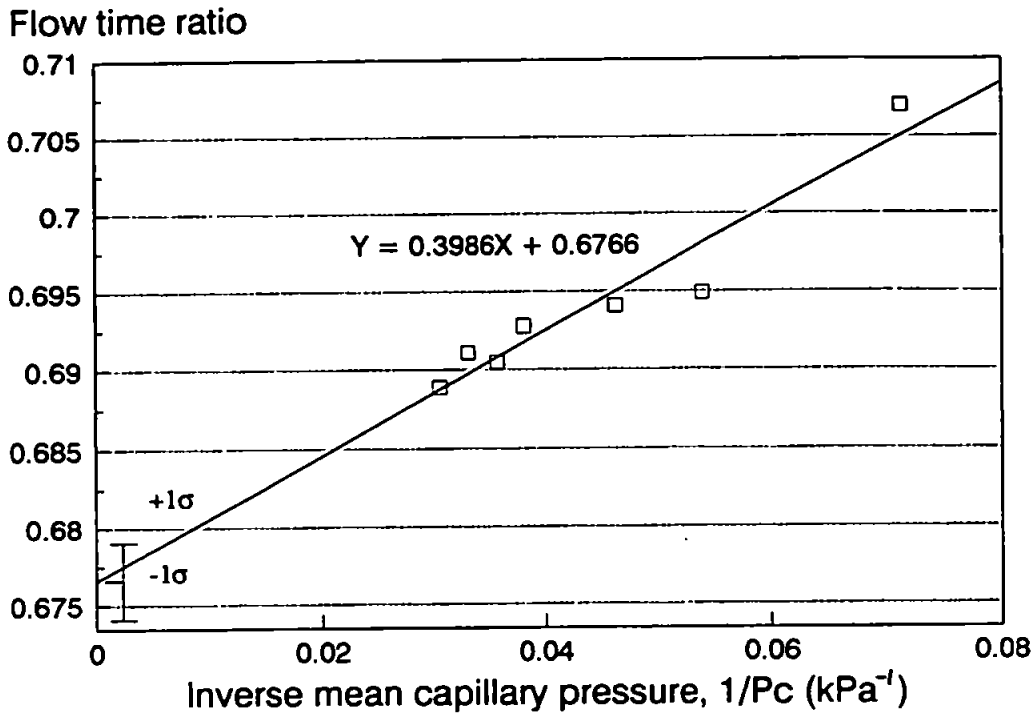

Figure A3e Slip flow correction plot for HCFC 124 at 343.15 K. Error bar indicates the standard error associated with the value of the y-intercept.

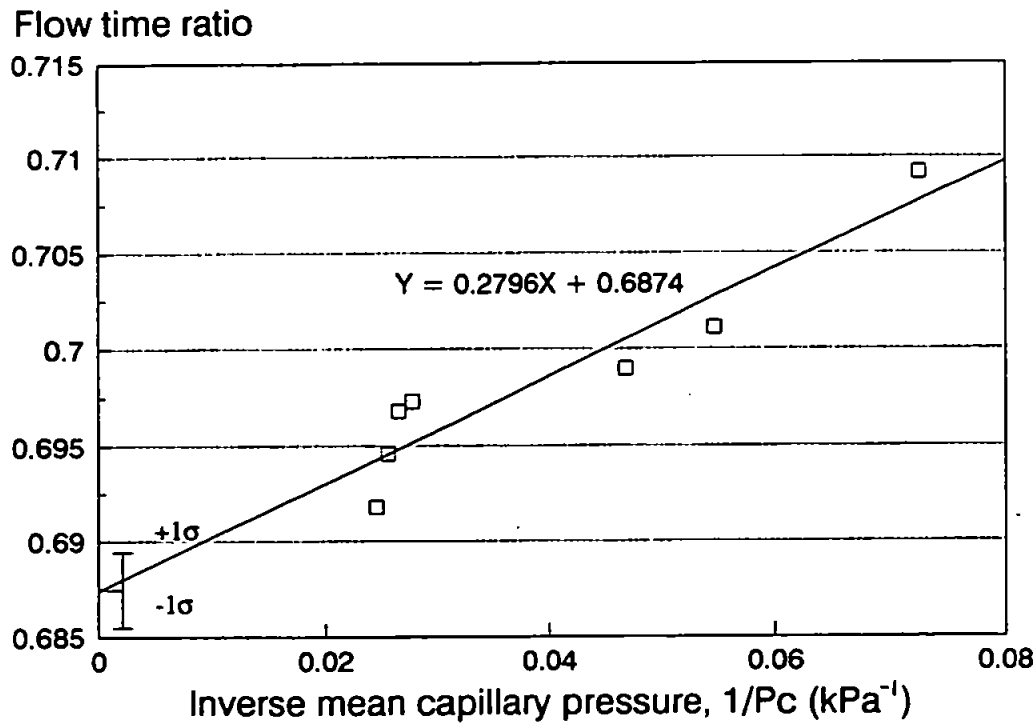

Figure A3f Slip flow correction plot for HFC 124 at 383.15 K. Error bar indicates the standard error associated with the value of the y-intercept.

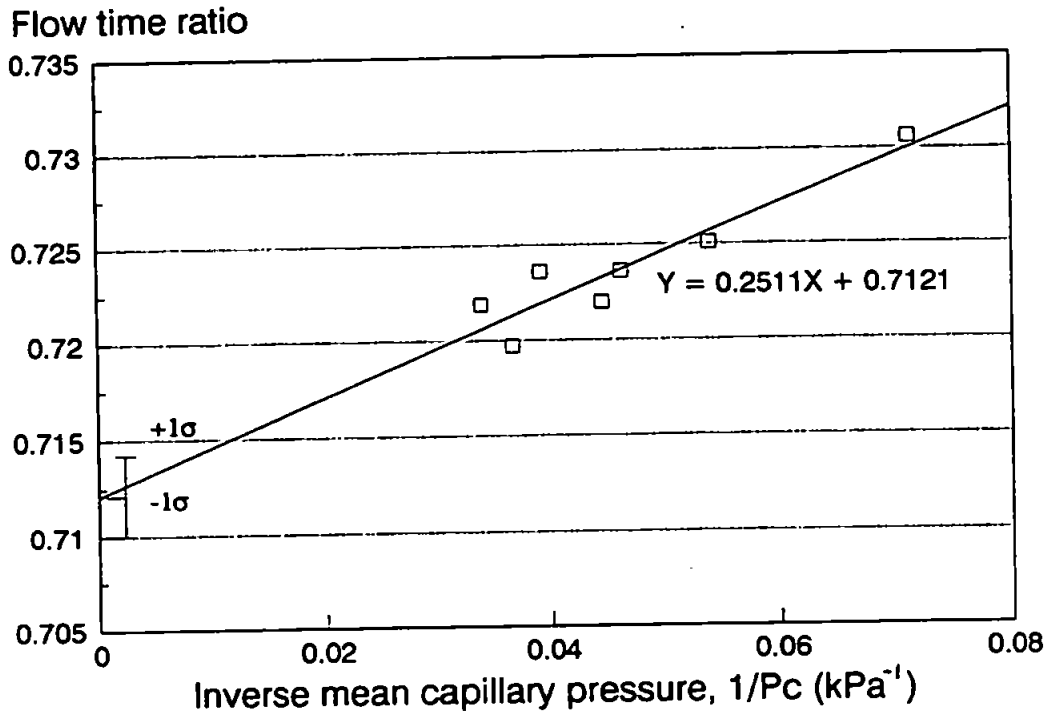

Figure A3g Slip flow correction plot for MP 39 at 323.15 K. Error bar indicates the standard error associated with the value of the y-intercept.

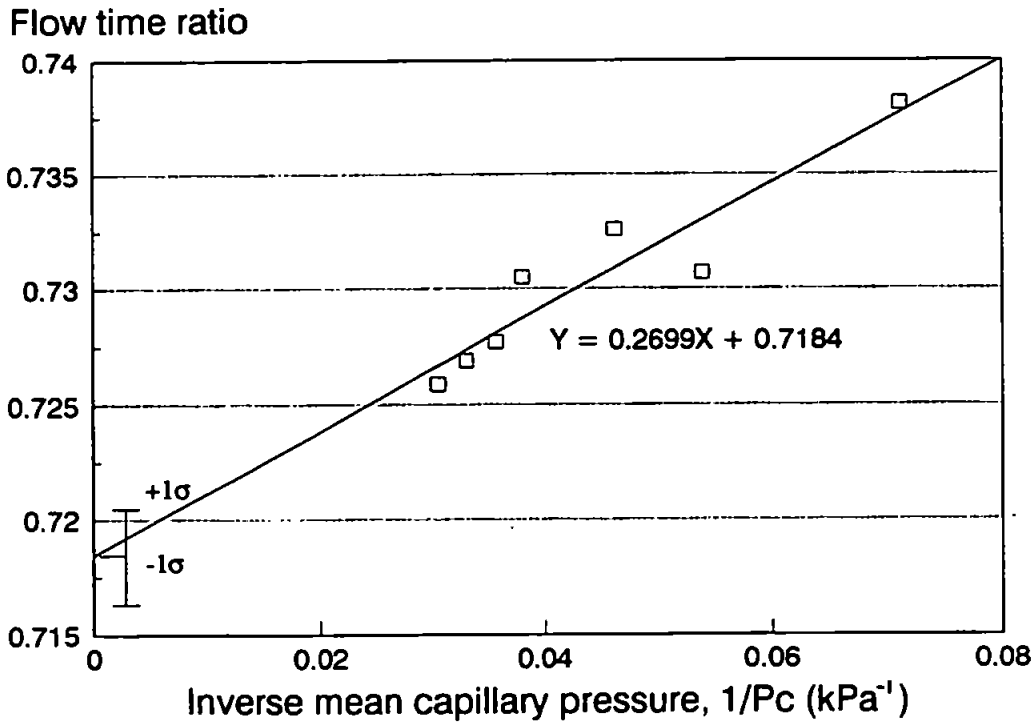

Figure A3h Slip flow correction plot for MP 39 at 343.15 K. Error bar indicates the standard error associated with the value of the y-intercept.

Appendix 4a Experimental flow times for HFC 134a.

Temperature /K	Mean front vessel pressure /kPa	Mean back vessel pressure /kPa	Mean capillary tube pressure /kPa	Mean HFC 134a flow time /s	Mean nitrogen flow time /s	Flow time ratio
308.15	55.359	11.557	33.458	311.703	461.894	0.6748
	52.022	12.368	32.195	320.395	475.476	0.6738
	45.947	13.805	29.867	1175.749	1748.763	0.6723
	37.127	15.840	26.483	1888.603	2811.552	0.6717
	38.560	6.418	22.489	1601.886	2379.754	0.6731
	29.739	8.452	19.096	2694.879	3991.347	0.6752
	22.107	10.153	16.130	4184.443	6200.972	0.6748
323.15	60.829	11.424	36.127	448.778	659.468	0.6805
	56.338	12.536	34.437	332.479	488.498	0.6806
	53.001	13.347	33.174	340.874	501.680	0.6795
	46.927	14.785	30.856	1248.173	1837.239	0.6794
	38.560	6.418	22.489	1760.043	2581.900	0.6817
	29.739	8.452	19.096	2954.379	4339.417	0.6808
	22.107	10.153	16.130	4589.290	6729.095	0.6820
343.15	62.340	12.934	37.637	482.720	700.155	0.6894
	57.848	14.046	35.947	357.308	518.641	0.6889
	54.511	14.857	34.684	365.645	531.391	0.6881
	48.437	16.295	32.366	1333.672	1940.338	0.6873
	41.731	9.589	25.660	1706.271	2479.663	0.6881
	32.910	11.623	22.267	2801.134	4072.010	0.6879
	25.278	13.234	19.301	4242.100	6160.538	0.6886
363.15	68.547	13.181	40.864	331.199	476.137	0.6956
	63.784	14.379	39.081	515.868	741.821	0.6954
	59.292	15.491	37.392	381.110	548.553	0.6948
	55.956	16.302	36.129	388.761	560.697	0.6934
	41.731	9.589	25.660	1899.365	2724.168	0.6972
	32.910	11.623	22.267	3119.361	4472.153	0.6975
	25.278	13.324	19.301	4726.858	6765.493	0.6987
383.15	62.340	12.934	37.637	597.247	850.129	0.7025
	57.848	14.046	35.947	441.061	627.916	0.7024
	54.511	14.857	34.684	453.025	644.691	0.7027
	48.437	16.295	32.366	1650.657	2347.520	0.7031
	41.731	9.589	25.660	2109.941	2997.095	0.7040
	32.910	11.623	22.267	3469.016	4918.243	0.7053
	25.278	13.324	19.301	5248.191	7445.863	0.7048
403.15	76.448	13.720	45.084	270.884	381.515	0.7100
	73.699	14.433	44.066	192.133	270.564	0.7101
	70.593	15.227	42.910	385.278	542.808	0.7098
	65.831	16.425	41.128	597.620	843.062	0.7089
	41.731	9.589	25.660	2328.728	3269.747	0.7122
	32.910	11.623	22.267	3820.841	5364.600	0.7122
	25.278	13.324	19.301	5785.704	8113.946	0.7131

Appendix 4b Experimental flow times for HCFC 123.

Temperature /K	Mean front vessel pressure /kPa	Mean back vessel pressure /kPa	Mean capillary tube pressure /kPa	Mean HCFC 123 flow time /s	Mean nitrogen flow time /s	Flow time ratio
308.15	49.405	9.782	29.593	749.552	1211.270	0.6188
	43.802	10.743	27.272	630.984	1005.126	0.6278
	39.654	11.455	25.554	727.205	1150.038	0.6323
	32.142	12.744	22.443	3879.985	6120.203	0.6340
	39.654	3.619	21.637	621.404	1009.713	0.6154
	32.142	4.907	18.525	2819.708	4469.815	0.6308
	21.287	6.769	14.028	8138.404	12710.06	0.6403
323.15	49.405	9.782	29.593	819.642	1316.679	0.6225
	43.802	10.743	27.272	691.532	1095.044	0.6315
	39.654	11.455	25.554	796.489	1253.092	0.6356
	32.142	12.744	22.443	4280.050	6664.790	0.6422
	39.654	3.619	21.637	679.493	1097.620	0.6191
	32.142	4.907	18.525	3078.873	4868.172	0.6324
	21.287	6.769	14.028	8864.988	13837.66	0.6406
343.15	55.366	10.189	32.778	532.908	867.626	0.6142
	49.405	11.212	30.309	949.143	1501.258	0.6322
	43.802	12.174	27.988	808.526	1259.906	0.6417
	39.654	12.886	26.270	938.841	1458.930	0.6435
	39.654	3.619	21.637	761.100	1219.476	0.6241
	32.142	4.907	18.525	3455.355	5402.873	0.6395
	21.287	6.769	14.028	9956.204	15344.07	0.6489
363.15	59.266	11.658	35.462	288.196	460.036	0.6265
	55.366	12.327	33.847	626.739	982.261	0.6381
	49.405	13.351	31.378	1115.343	1722.218	0.6476
	43.802	14.312	29.057	966.826	1476.444	0.6548
	39.654	3.127	21.390	844.098	1342.686	0.6287
	32.142	4.415	18.279	3833.468	5910.524	0.6486
	21.287	6.277	13.782	10750.84	16388.76	0.6560

Appendix 4c Experimental flow times for HCFC 124.

Temperature /K	Mean front vessel pressure /kPa	Mean back vessel pressure /kPa	Mean capillary tube pressure /kPa	Mean HCFC 124 flow time /s	Mean nitrogen flow time /s	Flow time ratio
283.15	49.405	15.396	32.401	797.711	1194.369	0.6679
	43.802	16.356	30.079	698.488	1046.788	0.6673
	39.654	17.067	28.360	862.008	1292.407	0.6670
	43.802	2.411	23.106	533.529	802.906	0.6645
	39.654	3.121	21.387	589.346	883.549	0.6670
	32.142	4.407	18.274	2597.515	3893.977	0.6671
	21.287	6.265	13.776	7231.302	10815.37	0.6686
308.15	49.405	9.782	29.593	818.881	1211.626	0.6759
	43.802	10.743	27.272	679.511	1005.416	0.6759
	39.654	11.455	25.554	778.948	1150.375	0.6771
	32.142	12.744	22.443	4150.449	6122.003	0.6780
	39.654	3.619	21.637	682.138	1010.010	0.6754
	32.142	4.907	18.525	3023.971	4471.129	0.6763
	21.287	6.769	14.028	8728.810	12713.80	0.6866
323.15	49.405	9.782	29.593	906.451	1316.335	0.6886
	43.802	10.743	27.272	750.721	1094.757	0.6857
	39.654	11.455	25.554	862.346	1252.764	0.6884
	32.142	12.744	22.443	4589.555	6663.048	0.6888
	39.654	3.619	21.637	757.152	1097.333	0.6900
	32.142	4.907	18.525	3354.362	4866.899	0.6892
	21.287	6.769	14.028	9674.500	13834.04	0.6993
343.15	55.366	10.189	32.778	597.682	867.596	0.6889
	49.405	11.212	30.309	1037.539	1501.205	0.6911
	43.802	12.174	27.988	869.9571	1259.862	0.6905
	39.654	12.886	26.270	1010.647	1458.879	0.6928
	39.654	3.619	21.637	846.445	1219.433	0.6941
	32.142	4.907	18.525	3754.172	5402.683	0.6949
	21.287	6.769	14.028	10847.63	15343.53	0.7070
363.15	59.266	11.658	35.462	319.173	460.212	0.6935
	55.366	12.327	33.847	681.084	982.636	0.6931
	49.405	13.351	31.378	1195.279	1722.876	0.6938
	43.802	14.312	29.057	1030.128	1477.008	0.6974
	39.654	3.127	21.390	933.093	1343.200	0.6947
	32.142	4.415	18.279	4115.357	5912.785	0.6960
	21.287	6.277	13.782	11496.53	16395.03	0.7012
383.15	66.813	14.776	40.794	415.439	600.528	0.6918
	62.728	15.476	39.102	502.579	723.584	0.6946
	59.266	16.069	37.668	381.273	547.171	0.6968
	55.366	16.737	36.052	823.345	1180.711	0.6973
	39.654	3.121	21.387	1042.632	1491.605	0.6990
	32.142	4.407	18.274	4608.708	6573.569	0.7011
	21.287	6.265	13.776	12878.86	18160.91	0.7092
403.15	66.813	14.805	40.809	452.259	644.590	0.7016
	62.728	15.506	39.117	548.657	779.585	0.7038
	59.266	16.101	37.683	415.888	587.769	0.7076
	55.366	16.770	36.068	899.337	1271.394	0.7074
	39.654	3.127	21.390	1134.166	1606.055	0.7062
	32.142	4.415	18.279	5013.880	7073.322	0.7088
	21.287	6.277	13.782	14025.54	19579.45	0.7163

Appendix 4d Experimental flow times for MP 39.

Temperature /K	Mean front vessel pressure /kPa	Mean back vessel pressure /kPa	Mean capillary tube pressure /kPa	Mean MP 39 flow time /s	Mean nitrogen flow time /s	Flow time ratio
308.15	49.405	9.782	29.593	868.563	1211.626	0.7168
	43.802	10.743	27.272	719.794	1005.416	0.7159
	39.654	11.455	25.554	829.286	1150.375	0.7208
	32.142	12.744	22.443	4402.311	6122.003	0.7190
	39.654	3.619	21.637	725.436	1010.010	0.7182
	32.142	4.907	18.525	3205.312	4471.129	0.7168
	21.287	6.769	14.028	9181.470	12713.80	0.7222
323.15	49.405	9.782	9.593	950.386	1316.335	0.7219
	43.802	10.743	27.272	787.900	1094.757	0.7197
	39.654	11.455	25.554	906.577	1252.764	0.7236
	32.142	12.744	22.443	4810.725	6663.048	0.7220
	39.654	3.619	21.637	794.031	1097.333	0.7236
	32.142	4.907	18.525	3519.389	4866.899	0.7231
	21.287	6.769	14.028	10107.73	13834.04	0.7306
343.15	55.366	10.189	32.778	629.799	867.596	0.7259
	49.405	11.212	30.309	1091.256	1501.205	0.7269
	43.802	12.174	27.988	916.908	1259.862	0.7277
	39.654	12.886	26.270	1065.804	1458.879	0.7305
	39.654	3.619	21.637	893.446	1219.433	0.7326
	32.142	4.907	18.525	3947.899	5402.683	0.7307
	21.287	6.769	14.028	11325.57	15343.53	0.7381
363.15	59.266	11.658	35.462	339.882	460.212	0.7385
	55.366	12.327	33.847	723.670	982.636	0.7365
	49.405	13.351	31.378	1272.099	1722.876	0.7384
	43.802	14.312	29.057	1089.171	1477.008	0.7374
	39.654	3.127	23.355	891.813	1219.904	0.7311
	32.142	4.415	21.637	991.162	1343.217	0.7379
	21.287	6.277	18.525	4387.478	5943.561	0.7382
383.15	66.813	14.776	40.794	436.818	600.811	0.7270
	62.728	15.476	39.102	529.970	723.926	0.7320
	59.266	16.069	37.668	401.422	547.430	0.7332
	55.366	16.737	36.052	865.348	1181.269	0.7325
	39.654	3.121	21.387	1096.509	1492.310	0.7347
	32.142	4.407	18.274	4822.699	6576.677	0.7333
	21.287	6.265	13.776	13435.32	18169.50	0.7394
403.15	66.813	14.805	40.809	480.525	644.725	0.7453
	62.728	15.506	39.117	582.650	779.749	0.7472
	59.266	16.101	37.683	440.612	587.892	0.7494
	55.366	16.770	36.068	951.289	1271.660	0.7480
	39.654	3.127	21.390	1198.030	1606.392	0.7457
	32.142	4.415	18.279	5279.064	7074.805	0.7461
	21.287	6.277	13.782	14698.57	19583.56	0.7505

Appendix 5 Derivation of the 'Factor' term.

Assuming a compound X has a relative molecular mass (RMM) of 115.

$$1 \text{ kt of X} = 10^9 \text{g} = \frac{10^9}{115} \text{ moles} \quad \text{(No of moles = Weight / RMM)}$$

No of molecules per mole = 6.023×10^{23}, thus X has

$$\frac{10^9}{115} \times 6.023 \times 10^{23} \text{ molecules}$$

Assuming there are 10^{44} molecules in the troposphere;

$$\text{Concentration} = \frac{10^9 \times 6.023 \times 10^{23}}{115 \times 10^{44}} \frac{\text{molecules}}{\text{molecules in the troposphere}}$$

Expressed as ppt;

$$\text{Concentration} = \frac{10^9 \times 6.023 \times 10^{23} \times 10^{12}}{115 \times 10^{44}} \frac{\text{ppt}}{\text{kt}}$$

$$= \frac{6.023 \times 10^{44}}{115 \times 10^{44}} = 0.052 \text{ ppt/kt}$$

$$\text{Factor} = 1 / 0.052 = 19.23 \text{ kt ppt}^{-1}$$

The factors used for each of the halocarbons in the chlorine and bromine loading models are shown in Tables 6.6 and 6.7 respectively.

Appendix 6 List of chlorine and bromine loading model spreadsheet filenames.

MOD9.wkx - Basic chlorine loading model.

MOD5.wkx - Chlorine loading model with the effect of use of halocarbons by developing countries.

MOD4.wkx - Chlorine loading model with emphasis on the sensitivity of the chlorine loading to the flux equation.

MODBRIAN.wkx - Basic bromine loading model.

List of References

Chapter 1

1. R P Wayne, *Proceedings of the Royal Institution of Great Britain*, 1990, 13.

2. P Phillips, *SSR*, 1990, **71 (256)**, 15.

3. M B McElroy and R J Salawitch, *Science*, 1989, **243**, 763.

4. M B McElroy, R J Salawitch, S C Wofsy and J A Logan, *Nature*, 1986, **321**, 759.

5. R S Stolarski, *Scientific American*, 1988, **258 (1)**, 20.

6. J C Farman, B G Gardiner and J D Shanklin, *Nature*, 1985, **315**, 207.

7. F S Rowland, *American Scientist*, 1989, **77**, 36.

8. D J Hofmann, S J Oltmans, J M Harris, S Solomon, T Deshler and B J Johnson, *Nature*, 1992, **359**, 283.

9. R Stolarski, R Bojkov, L Bishop, C Zerefos, F Staehelin and J Zawodny, *Science*, 1992, **256**, 342.

10. *New Scientist*, 1992, **28th November**, 16.

11. D W Fahey, K K Kelly, S R Kawa, A F Tuck, M Loewenstein, K R Chan and L E Heidt, *Nature*, 1990, **344**, 321.

12. R A Cox and G D Hayman, *Nature*, 1988, **332**, 796.

13. M J Molina, T L Tso, L T Molina and F C Y Wang, *Science*, 1987, **238**, 1253.

14. M A Tolbert, M J Rossi, R Malhotra and D Golden, *Science*, 1987, **238**, 1258.

15. S B Moore, L F Keyser M T Leu, R P Turco and R H Smith, *Nature*, 1990, **345**, 333.

16. B G Levi, *Physics Today*, 1988, **July**, 17.

17. F Arnold, T Bührke and S Qiu, *Nature*, 1990, **348**, 49.

18. R B Symonds, W I Rose and M H Reed, *Nature*, 1988, **334**, 415.

19. *New Scientist*, 1992, **29th February**, 20.

20. F M Schaart, C Garbe and C E Orfanos, *Der Hautarzt*, 1993, **44**, 63.

21. D Concar, *New Scientist*, 1992, **16th May**, 23.

22. G Pitari, G Visconti and M Verdecchia, *J. of Geophys. Res.*, 1992, **97 (D8)**, 8075.

23. T A Day, T C Vogelmann and E H DeLucia, *Oecologia*, 1992, **92**, 513.

24. H O Spauschus, *Rev. Int. Froid*, 1990, **13**, 73.

25. WMO (World Meteorological Organization), Scientific assessment of ozone depletion: 1991, global ozone research and monitoring project. Report no. 25, WMO, Geneva 1992.

Chapter 2

1. A Townsend; An investigation of the thermophysical properties of gases and gas mixtures; PhD thesis, Polytechnic South West, 1989.

2. I N Hunter; The viscosity of gaseous mixtures; DPhil thesis, Oxford University, 1989.

3. G C Maitland, M Rigby, E B Smith and W A Wakeham, *Intermolecular Forces - Their Origin and Determination*, Clarendon Press, Oxford, 1981.

4. A R H Goodwin and M R Moldover, *J. Chem. Phys.*, 1990, **93(4)**, 2741.

5. A R H Goodwin and M R Moldover, *J. Chem. Phys.*, 1991, **95(7)**, 5236.

6. M Rigby, E B Smith, W A Wakeham and G C Maitland, *The Forces between Molecules*, Clarendon Press, Oxford, 1986.

7. R A Buckingham, *Proc. Roy. Soc.*, 1938, **A168**, 378.

8. G C Maitland, Symposium on Transport Properties of Fluids and Fluid Mixtures, issued by National Engineering Laboratory, East Kilbride, Glasgow, 1979.

9. W H Stockmayer, *J. Chem. Phys.*, 1941, **9**, 398.

10. B Schramm, J Hauck and L Kern, *Ber. Bunsenges. Phys. Chem.*, 1992, **96(6)**, 745.

11. P Clancy, D W Gough, G P Matthews, E B Smith and G C Maitland, *Molecular Physics*, 1975, **30(5)**, 1397.

12. G C Maitland, V Vesovic and W A Wakeham, *Mol. Phys.*, 1985, **54**, 301.

13. J Kestin, S T Ro and W A Wakeham, *Physica*, 1972, **58**, 165.

14. Y Abe, J Kestin, H E Khalifa and W A Wakeham, *Ber. Bunsenges. Phys. Chem.*, 1979, **83**, 271.

15. J Kestin, S T Ro and W A Wakeham, *J. Chem. Phys.*, 1972, **56**, 5837.

16. R Tillner-Roth and H D Baehr, *J. Chem. Thermodynamics*, 1992, **24**, 413.

17. L A Weber, *Int. J. of Thermophys.*, 1989, **10(3)**, 617.

18. L A Weber, *J. Chem. Eng. Data*, 1990, **35**, 237.

19. E A Mason and L Monchick, *J. Chem. Phys.*, 1962, **36**, 1622.

20. L Monchick and E A Mason, *J. Chem. Phys.*, 1962, **35**, 1676.

21. J A Bearden, *Phys. Rev.*, 1939, **56**, 1023.

22. L Bruschi, M Santini and G Torzo, *J. Phys. E: Sci. Instrum.*, 1984, **17**, 312.

23. E Vogel, *Ber. Bunsenges. Phys. Chem.*, 1984, **88**, 997.

24. J B H Hooglands, H R Van Den Berg and N J Trappeniers, *Physica*, 1985, **134A**, 169.

25. I N Hunter, G Marsh, G P Matthews and E B Smith; *Int. J. Thermophysics*, 1993 (in press).

26. A Hobley, G P Matthews and A Townsend, *Int. J. of Thermophysics*, 1989, **10(6)**, 1165.

27. J Kestin and W A Wakeham, *Ber. Bunsenges. Phys. Chem.*, 1979, **83**, 573.

28. D E Diller, *Physica*, 1983, **119A**, 92.

29. H Nabizadeh and F Mayinger, Proceedings of The 12th European Conference on Thermophysical Properties, 24th - 28th September, 1990, Vienna, Austria.

30. M Takahashi, C Yokoyama and S Takahashi, Proceedings of The 30th High Pressure Conference of Japan 1989.

31. M Takahashi, C Yokoyama and S Takahashi, Proceedings of The 11th Japan Symposium on Thermophysical Properties 1990.

32. R A Dawe, *Rev. Sci. Instrum.*, 1973, **44(9)**, 1231.

33. J R Partington, *An Advanced Treatise on Physical Chemistry*, Vol 1, 1949.

Chapter 3

1. A Townsend; An investigation of the thermophysical properties of gases and gas mixtures; PhD thesis, Polytechnic South West, 1989.

2. I N Hunter; The viscosity of gaseous mixtures; DPhil thesis, Oxford University, 1989.

3. I N Hunter, G Marsh, G P Matthews and E B Smith; *Int. J. Thermophysics*, 1993 (in press).

4. R L Rusby, R P Hudson, M Durieux, J F Schooley, P P M Steur and C A Swenson; *Metrologia*, 1991, **28**, 9.

5. R A Dawe,; *Rev. Sci. Instrum.*, 1973, **44(9)**, 1231.

6. Eurotherm, 3-term controller type 810 reference manual; Eurotherm Ltd, Faraday Close, Durrington, Worthing, Sussex BN13 3PL.

Chapter 4

1. *Chemistry in Britain*, August 1991, 694.

2. E Vogel; *Ber. Bunsenges. Phys. Chem.*, 1984, **88**, 997.

3. I A Barr, G P Matthews, E B Smith and A R Tindell; *J. of Phys. Chem.*, 1981, **85**, 3342.

4. D W Gough, G P Matthews and E B Smith; *J. of the Chem. Soc., Faraday Trans. 1*, 1976, **72**, 645.

5. G C Maitland and E B Smith; *J. of Chem. and Eng. Data*, 1972, **17(2)**, 150.

6. G C Maitland and E B Smith; *The Viscosities of Eleven Common Gases: A Critical Compilation*, Oxford, 1971.

7. R A Dawe and E B Smith; *J. of Chem. Phys.*, 1970, **52**, 693.

8. H L Johnston and K E McCloskey; *J. of Chem. Phys.*, 1940, **51**, 4156.

9. J H Dymond and E B Smith; *The Virial Coefficients of Pure Gases and Mixtures - A Critical Compilation*, Clarendon Press, Oxford, 1980.

10. B Schramm, J Hauck and L Kern, *Ber. Bunsenges. Phys. Chem.*, 1992, **96(6)**, 745.

11. R Tillner-Roth and H D Baehr, *J. Chem. Thermodynamics*, 1992, **24**, 413.

12. L A Weber, *J. Chem. Eng. Data*, 1990, **35**, 237.

13. A R H Goodwin and M R Moldover, *J. Chem. Phys.*, 1991, **95(7)**, 5236.

14. H Nabizadeh and F Mayinger; Proceedings of the 12th European Conference on Thermophysical Properties, 24th - 28th September, 1990, Vienna, Austria.

15. ASHRAE; *The Thermophysical Properties of Refrigerants*, ASHRAE, New York, 1976.

16. H Nabizadeh and F Mayinger; *Int. J. of Thermophysics*, 1989, **10(3)**, 701.

17. M Takahashi, C Yokoyama and S Takahashi; Proceedings of the 30th High Pressure Conference of Japan, 1989.

18. M Takahashi, C Yokoyama and S Takahashi; Proceedings of the 11th Japan Symposium on Thermophysical Properties, 1990.

19. Y Tanaka and S Matsuo; *Thermophysical Properties of Environmentally Acceptable Fluorocarbons HFC 134a and HCFC 123*, Japanese Association of Refrigeration, Tokyo, Japan, 1990.

20. R Krauss and K Stephan; Submitted to *Int. J. of Thermophysics*, 1993.

21. M Takahashi, C Yokoyama and S Takahashi, *J. Chem. Eng. Data*, 1987, **32**, 98.

Chapter 5

1. R C Reid, J M Prausnitz and T K Sherwood, *The Properties of Gases and Liquids*, McGraw-Hill Book Co., USA, 1977.

2. H Nabizadeh and F Mayinger, Proceedings of The 12th European Conference on Thermophysical Properties, 24th - 28th September, 1990, Vienna, Austria.

3. B Schramm, J Hauck and L Kern, *Ber. Bunsenges. Phys. Chem.*, 1992, **96(6)**, 745.

4. G C Maitland, M Rigby, E B Smith and W A Wakeham, *Intermolecular Forces* -

Their Origin and Determination, Clarendon Press, Oxford, 1981.

5. J Kestin and W A Wakeham, *Ber. Bunsenges. Phys. Chem.*, 1979, **83**, 573.

6. D C Dowdell and G P Matthews, *J. Chem. Soc. Faraday Trans.*, 1993, **89(19)**, 3545.

7. G P Matthews; The thermophysical properties of simple gases and their mixtures; DPhil thesis, Oxford University, 1976.

8. P Clancy, D W Gough, G P Matthews, E B Smith and G C Maitland, *Molecular Physics*, 1975, **30(5)**, 1397.

9. J Kestin, S T Ro and W Wakeham, *Physica*, 1972, **58**, 165.

10. C W Meyer and G Morrison, *J. Chem. Eng. Data*, 1991, **36**, 409.

11. C W Meyer and G Morrison, *J. Phys. Chem.*, 1991, **95**, 3860.

12. M Takahashi, C Yokoyama and S Takahashi, Proceedings of The 30th High Pressure Conference of Japan 1989.

13. M Takahashi, C Yokoyama and S Takahashi, Proceedings of The 11th Japan Symposium on Thermophysical Properties 1990.

14. Japanese Association of Refrigeration, *Thermophysical Properties of Environmentally Acceptable Fluorocarbons HFC 134a and HCFC 123*, Tokyo, Japan, 1990.

15. M Rigby, E B Smith, W A Wakeham and G C Maitland, *The Forces between Molecules*, Clarendon Press, Oxford, 1986.

16. R Tillner-Roth and H D Baehr, *J. Chem. Thermodynamics*, 1992, **24**, 413.

17. L A Weber, *Int. J. of Thermophys.*, 1989, **10(3)**, 617.

18. L A Weber, *J. Chem. Eng. Data*, 1990, **35**, 237.

19. A R H Goodwin and M R Moldover, *J. Chem. Phys.*, 1990, **93(4)**, 2741.

20. A R H Goodwin and M R Moldover, *J. Chem. Phys.*, 1991, **95(7)**, 5236.

21. ASHRAE, Thermophysical Properties of Refrigerants, *ASHRAE Journal*, 1976.

22. M Takahashi, C Yokoyama and S Takahashi, *J. Chem. Eng. Data*, 1987, **32**, 98.

Chapter 6

1. WMO (World Meteorological Organization), Scientific assessment of ozone depletion: 1991, global ozone research and monitoring project. Report no. 25, WMO, Geneva 1992.

2. M J Prather and R T Watson, *Nature*, 1990, **344**, 729.

3. SORG (Stratospheric Ozone Review Group), Stratospheric ozone 1990. Report for the Dept of the Environment and the Meteorological Office. HMSO, London, 1990.

4. WMO (World Meteorological Organization), Scientific assessment of ozone depletion: 1989, global ozone research and monitoring project. Report no. 20, WMO, Geneva, 1990.

5. D A Fisher, C H Hales, D L Filkin, M K Ko, N Kak Sze, P S Connell, D J Wuebbels, I S A Isaksen and F Stordal, *Nature*, 1990, **344**, 508.

6. AFEAS, 1992; Production, sales and atmospheric release of CFC 11 and CFC 12 through 1990. AFEAS, The West Tower, Suite 400, 1333 H Street N.W., Washington D.C. 20005.

7. AFEAS, 1992; Production, sales and atmospheric release of CFC 113, CFC 114 and CFC 115 through 1990. AFEAS, The West Tower, Suite 400, 1333 H Street N.W., Washington D.C. 20005.

8. AFEAS, 1992; Production, sales and atmospheric release of HCFC 22 through 1990. AFEAS, The West Tower, Suite 400, 1333 H Street N.W., Washington D.C. 20005.

9. D A Fisher and P M Midgley, *Atmospheric Environment*, 1993, **27A(2)**, 271.

10. P M Midgley, *Atmospheric Environment*, 1989, **23(12)**, 2663.

11. D L Albritton and R T Watson, Report for the United Nations Environment Programme on behalf of contracting parties to the Montreal Protocol, 1992.

12. P H Gamlen, B C Lane, P M Midgley and J M Steed, *Atmospheric Environment*, 1986, **20(6)**, 1077.

13. Du Pont draft report; Du Pont, Wilmington, Delaware, USA, 1993 *(in press)*.

14. A McCulloch, *Atmospheric Environment*, 1992, **26A(7)**, 1325.

15. S Solomon, M Mills, L E Heidt, W H Pollock and A F Tuck, *J. of Geophys. Res.*, 1992, **97(D1)**, 825.

16. J S Hoffman, *Ambio*, 1990, **19(6,7)**, 329.

17. *Chemistry in Britain*, August, 1991, 694.

18. Du Pont, Environmentally acceptable refrigerants from Du Pont, SUVA - Tomorrow's standard today, Du Pont de Nemours Int. SA, Le Grand Saconnex, Geneva, Switzerland, 1991.

19. M G J den Elzen, R J Swart and J Rotmans, *The Science of the Total Environment*, 1992, **113**, 229.

20. J H Butler, J W Elkins, B D Hall, S O Cummings and S A Montzka, *Nature*, 1992, **359**, 403.

21. A Rosemarin, *Ambio*, 1990, **19(6,7)**, 280.

22. WMO (World Meteorological Organization), Scientific assessment of ozone depletion: 1985, global ozone research and monitoring project. Report no. 16, WMO, Geneva, 1986.

23. M A K Khalil, S A Edgerton and R A Rasmussen, *Environ. Sci. Technol.*, 1983, **17(9)**, 555.

24. H B Singh, L J Salas, H Shigeishi and E Scribner, *Science*, 1979, **203**, 899.

25. O C Zafiriou, *J. of Marine Res.*, 1975, **33**, 75.

26. S L Manley and M N Dastoor, *Limmol. Oceanography*, 1987, **32**, 709.

27. D B Harper, J T Kennedy and J T G Hamilton, *Phytochemistry*, 1988, **27(10)**, 3147.

28. T Y Palmer, *Nature*, 1976, **263**, 44.

29. S Tassios and D R Packham, *J. of Air Pollution Control*, 1985, **35**, 41.

30. R A Rasmussen, L E Rasmussen, M A K Khalil and R W Dalluge, *J. of Geophys. Res.*, 1980, **85**, 7350.

31. P R Edwards, I Campbell and G S Milne, *Chemistry and Industry*, 1982, 619.

Chapter 7

1. M J Prather and R T Watson, *Nature*, 1990, **344**, 729.

2. J C Farman, B G Gardiner and J D Shanklin, *Nature*, 1985, **315**, 207.

3. WMO (World Meteorological Organization), Scientific assessment of ozone depletion: 1991, global ozone research and monitoring project. Report no. 25, WMO, Geneva 1992.

4. H O Spauschus, *ASHRAE Journal*, 1991, **February**, 23.

5. P R Reed and H O Spauschus, *ASHRAE Journal*, 1991, **February**, 40.

6. *Chemistry in Britain*, 1991, **December**, 1105.

7. J L Boot, *Int. J. Refrig.*, 1990, **13**, 100.

8. K Marts and J Howard, *Journal of the IES*, **Sept./Oct.**, 34.

9. S K Fischer and M McFarland, *MRS Bulletin*, 1992, **March**, 39.

10. C Kroeze and L Reijnders, *The Science of the Total Environment*, 1992, **111**, 1.

11. Du Pont draft report; Du Pont, Wilmington, Delaware, USA, 1993 *(in press)*.

12. M G J den Elzen, R J Swart and J Rotmans, *The Science of the Total Environment*, 1992, **113**, 229.

13. J H Butler, J W Elkins, B D Hall, S O Cummings and S A Montzka, *Nature*, 1992, **359**, 403.

14. AFEAS, 1992; Production, sales and atmospheric release of CFC 11 and CFC 12 through 1990. AFEAS, The West Tower, Suite 400, 1333 H Street N.W., Washington D.C. 20005.

15. AFEAS, 1992; Production, sales and atmospheric release of CFC 113, CFC 114 and CFC 115 through 1990. AFEAS, The West Tower, Suite 400, 1333 H Street N.W., Washington D.C. 20005.

16. AFEAS, 1992; Production, sales and atmospheric release of HCFC 22 through 1990. AFEAS, The West Tower, Suite 400, 1333 H Street N.W., Washington D.C. 20005.

17. D A Fisher and P M Midgley, *Atmospheric Environment*, 1993, **27A**(2), 271.

18. A McCulloch, *Atmospheric Environment*, 1992, **26A(7)**, 1325.

19. P M Midgley, *Atmospheric Environment*, 1989, **23(12)**, 2663.

20. WMO (World Meteorological Organization), Scientific assessment of ozone depletion: 1985, global ozone research and monitoring project. Report no. 16, WMO, Geneva, 1986.

21. J D Peak and R M Harrison, *Environmental Technology*, 1992, **13**, 867.

22. P H Gamlen, B C Lane, P M Midgley and J M Steed, *Atmospheric Environment*, 1986, **20(6)**, 1077.

23. C Brühl and P J Crutzen, *Ambio*, 1990, **19 (6,7)**, 293.

24. R L McCarthy, F A Bower and J P Jesson, *Atmospheric Environment*, 1977, **11**, 491.

25. SORG (Stratospheric Ozone Review Group), Stratospheric ozone 1990. Report for the Dept of the Environment and the Meteorological Office. HMSO, London, 1990.

26. P R Edwards, I Campbell and G S Milne, *Chemistry and Industry*, 1982, 619.

27. D B Harper, J T Kennedy and J T G Hamilton, *Phytochemistry*, 1988, **27(10)**, 3147.

28. C A Moore, *Ambio*, 1990, **19 (6,7)**, 320.

29. H Ahmadzai and T Hedlund, *Ambio*, 1990, **19 (6,7)**, 341.

30. A Rosencranz and R Milligan, *Ambio*, 1990, **19 (6,7)**, 312.

31. N Myers (ed.), The Gaia atlas of planet management, Pan Books, London, 1985.

32. *New Scientist*, 1990, **30th June**, 39.

33. *New Scientist*, 1989, **11th February**, 28.

34. Alliance for Responsible CFC Policy, Realistic policies on HCFCs needed in order to meet global ozone protection goals, **June, 1990**, 2011, "I" Street N.W., Washington, DC 20006.

Chapter 8

1. J B Burkholder, R R Wilson, T Gierczak, R Talukdar, S A McKeen, J J Orlando, G L Vaghjiani and A R Ravishankara, *J. of Geophys. Res.*, 1991, **96 (D3)**, 5025.

2. WMO (World Meteorological Organization), Scientific assessment of ozone depletion: 1991, global ozone research and monitoring project. Report no. 25, WMO, Geneva 1992.

3. SORG (Stratospheric Ozone Review Group), Stratospheric ozone 1990. Report for the Dept of the Environment and the Meteorological Office. HMSO, London, 1990.

4. S Penkett, B Jones, B Rycroft and D Simmons, *Nature*, 1985, **318**, 550.

5. D L Albritton and R T Watson, Report for the United Nations Environment Programme on behalf of contracting parties to the Montreal Protocol, 1992.

6. A McCulloch, *Atmospheric Environment*, 1992, **26A(7)**, 1325.

7. J H Butler, J W Elkins, B D Hall, S O Cummings and S A Montzka, *Nature*, 1992, **359**, 403.

8. *Chemistry in Britain*, 1993, **May**, 382.

9. M J Prather and R T Watson, *Nature*, 1990, **344**, 729.

10. M B McElroy, R J Salawitch, S C Wofsy and J A Logan, *Nature*, 1986, **321**, 759.

11. S Solomon, M Mills, L E Heidt, W H Pollock and A F Tuck, *J. of Geophys. Res.*, 1992, **97(D1)**, 825.